TECHNISCHE UNIVERSITÄT MÜNCHEN

Lehrstuhl und Versuchsanstalt für Wasserbau und Wasserwirtschaft

Transient bedload transport of sediment mixtures under disequilibrium conditions

An experimental study and the development of a new dynamic hiding function

Nikolaos P. Efthymiou

Vollständiger Abdruck der von der Fakultät für Bauingenieur- und Vermessungswesen der Technischen Universität München zur Erlangung des akademischen Grades eines

Doktor-Ingenieurs

genehmigten Dissertation.

Vorsitzender: Univ.-Prof. Dr. rer. nat. Kurosh Thuro

Prüfer der Dissertation:

1. Univ.-Prof. Dr.-Ing. Peter Rutschmann
2. Univ.-Prof. Dr.-Ing. Theodor Strobl, i. R.
3. Prof. Abdallah J. Hussein Malkawi, Ph.D.,
   Jordan University of Science & Technology, Jordanien

Die Dissertation wurde am 06.12.2011 bei der Technischen Universität München eingereicht und durch die Fakultät für Bauingenieur- und Vermessungswesen am 14.05.2012 angenommen.

Για τον πατέρα μου

To my father

"As you set out for Ithaka
hope the voyage is a long one,
full of adventure, full of discovery.
Laistrygonians and Cyclops,
angry Poseidon—don't be afraid of them:
you'll never find things like that on your way
as long as you keep your thoughts raised high,
as long as a rare excitement
stirs your spirit and your body.
Laistrygonians and Cyclops,
wild Poseidon—you won't encounter them
unless you bring them along inside your soul,
unless your soul sets them up in front of you."

C. P. Cavafy, Ithaka

Abstract

This study deals with the investigation of the temporal evolution of the phenomenon of static armoring. Thereby, experiments with objective the precise mapping of the temporal and spatial variability of fractional transport rates as well as of the grain size distribution of bed surface were performed. The coupling of these experimentally acquired data and their further analysis enables the development of a new transport model that allows an accurate reproduction of the observed transport processes. The model that has been herein developed requires, in contrast to previous models, the consideration of the median grain diameter of both the bed surface as well as of the substrate. Using various data sets from the literature, the predictive capability of the developed model was validated. The good agreement between model predictions and measurements confirmed the applicability of the model under different boundary conditions.

Zusammenfassung

Die Arbeit befasst sich mit der Untersuchung der zeitlichen Entwicklung des Phänomens der statischen Deckschichtbildung. Hierzu wurden Grundlagenversuche zur genauen Abbildung der zeitlichen und räumlichen Variabilität der fraktionierten Transportraten, sowie der Kornzusammensetzung der Sohloberfläche durchgeführt. Die Kopplung dieser Daten und ihre weitere Auswertung ermöglicht die Entwicklung eines neuen Transportmodels, das mit großer Genauigkeit die beobachteten Transportprozesse reproduzieren kann. Das hier entwickelte Modell impliziert, im Gegensatz zu bisherigen Modellen, die Berücksichtigung des mittleren Korndurchmessers sowohl der Deckschicht als auch der Unterschicht. Anhand verschiedener Datensätze aus der Literatur wurde die Prognosefähigkeit des entwickelten Models validiert. Die gute Übereinstimmung der Berechnungs-ergebnisse mit den Messungen bestätigt die Anwendbarkeit des Modells unter unterschiedlichen Randbedingungen.

Περίληψη

Το αντικείμενο της εργασίας είναι η διερεύνηση της χρονικής εξέλιξης του φαινομένου της στατικής θωράκισης του πυθμένα. Για το λόγο αυτό έγιναν πειράματα με στόχο τον προσδιορισμό της χρονικής και χωρικής μεταβλητότητας της στερεομεταφοράς και της κοκκομετρίας της επιφάνειας του πυθμένα. Η σύζευξη αυτών των δεδομένων και η περαιτέρω ανάλυση τους επίτρεψε την εξέλιξη ενός νέου μοντέλου, το οποίο είναι σε θέση να αναπαραγάγει τις διαδικασίες στερεομεταφοράς με ακρίβεια. Το μοντέλο που προτείνεται , σε αντίθεση με τα υπάρχοντα, λαμβάνει υπ' όψιν τόσο τη μέση διάμετρο της επιφάνειας του πυθμένα όσο και του υποστρώματος. Η ποιότητα των προβλέψεων του μοντέλου πιστοποιήθηκε βάση διάφορων σετ δεδομένων από τη βιβλιογραφία. Η συμφωνία μεταξύ των προγνώσεων και των μετρήσεων επιβεβαίωσε την καταλληλότητα εφαρμογής του μοντέλου υπό διαφορετικές οριακές συνθήκες.

Acknowledgements

The dissertation that you hold is the final result of my work at the Lehrstuhl und Versuchsanstalt für Wasserbau und Wasserwirtschaft of the Technische Universität München. This study would not have been possible without the support of a large number of people. At this point I would like to express my deepest gratitude to all of them. Herzlichen Dank! Thank you! Ευχαριστώ!

My work was partly funded by Deutscher Akademischer Austaush Dienst (DAAD) and the State Scholarships Foundation of Greece (IKY). My personal gratitude to these foundations for the scholarships granted.

My Doktorvater Prof. Dr. Peter Rutschmann provided all the necessary means for the successful realization of this research project. The trust that he showed and the academic freedom that he gave allowed me to develop own research directions and to build a sound scientific self-confidence. The understanding and patience that he showed when I had to interrupt the writing of the dissertation in order to accomplish my military service is greatly appreciated. Finally, the granted funds for the reconstruction and automatization of the employed experimental facilities made possible the experimental investigation, which is the core of the present work.

Univ. Prof. (em) Dr.-Ing. Theodor Strobl gave me the opportunity to join his team at the Institute at the end of 2004. His persistence on the praxis oriented aspect of my work helped greatly in delineating the ocean of thoughts. To a large extent this work owes its finalization to his moral support, encouragement and motivation. Finally, I feel deeply indebted because he has been a father figure to me showing always interest not only on my academic development but on my personal life too.

I express my gratitude to Univ. Prof. Dr.-Ing. Abdallah I. Husein Malkawi for his engagement in the examination committee and the hospitality that he offered during my stay at the Jordan University of Technology in Irbid, Jordan. I would also like to thank Prof. Dr. rer. nat Kurosh Thuro for chairing the examination procedure.

I had the privilege to conduct research at the Oskar von Miller Institute in Obernach, Bayern, the laboratory that facilitated the research activities of famous Engineers like Oskar von Miller, Hunter Rouse and Jost Knauss among others. Without the help and support of the technical staff of the laboratory this work would not have been realized. The support of the director of the laboratory director, Dr.-Ing. Arnd Hartlieb, is greatly appreciated for his willingness to discuss any requests or questions.

The support of Univ. Prof. Dr.-Ing Uwe Stilla, who provided the software, that was used for the estimation of bed surface gradation by means of image analysis, as well as the help of Dipl.-Ing. Ludwig Högner who introduced me to the potential capabilities of the program is gratefully acknowledged.

Table of contents

1.   Introduction

1.1   Need of sediment transport predictions in river engineering

People attempt to alter the natural course and behavior of rivers with use of hydraulic structures since the ancient years, e.g. Knauss (1996), Strobl & Zunic (2006). The goals of these manmade interventions involve the management of water resources for drinking and irrigation purposes, the protection against floods in order to gain land for agriculture and settlement, the creation of new ways for the trade of products and the production of energy, e.g. from water mills in the roman empire and from hydro-power plants nowadays.

Planning and dimensioning of hydraulic structures requires a combination of many engineering disciplines. These may concern sediment transport, which can be defined as the understanding of the laws governing the movement of solid grains that constitute the river bed, due to gravity and the forces acting on the sediment which are caused by the flow of water. The understanding and consideration of sediment transport processes is necessary, because every technical intervention disturbs the established state of equilibrium and the river morphology evolves toward a new equilibrium profile, which will be determined by the new hydraulic and sedimentological conditions.

A river reach is in equilibrium when the sediment which is supplied during a sufficient long but finite period from the catchment area is transported downstream without important erosion or deposition, conserving in that way a stable morphology. The quantity of sediment that the river is able to transport is called sediment transport capacity. This parameter is defined by the river's bed geometry and texture, i.e. slope, depth, width and boundary roughness, which determine the shear stress that acts on the river bed as well as the grain size of bed material. The width of the river, roughness, bed slope and depth of flow, as well as the amount and composition of sediment supply are the four interdependent variables of the hydraulic system. A change in any of these interdependent variables is compensated by a change in the others until a new equilibrium is established.

A graphical illustration of the interrelations among those variables is depicted by the stable channel balance which was published by E. W. Lane in 1955 and is shown in fig. 1.1.

2
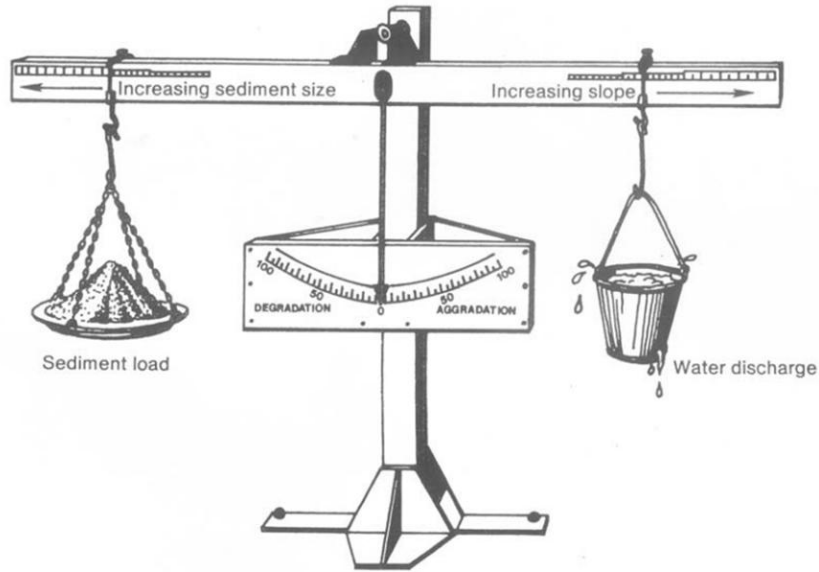
Fig.1.1   Stable channel balance (From Lane, 1955)

It must be mentioned that the term "sediment load" expresses the difference between the amount of sediment supplied to the reach and the transport capacity. The value of that parameter will determine whether the channel will aggrade or degrade. Changing the bed slope, the channel width, the water depth or the roughness will alter the sediment transport capacity. When transport capacity becomes less than the sediment supply, then the reach will aggrade until the established bed slope will force the transport capacity to become equal to sediment supply.

Predicting the new morphological equilibrium that will be established after the completion of the hydraulic engineering work is essential in order to assure the structural stability and functionality of the construction. Furthermore it is necessary in order to assess the environmental impacts e.g. lowering of underground water table in case of bed degradation or deprivation of habitat characteristics in river delta biotope. The quantification of change in river morphology requires reliable and accurate estimates of the bed-load discharge under certain hydraulic conditions, something that has been and still is the topic of extensive research.

1.2   Development of bed-load equations

The sediment transport capacity can be estimated by an empirical functional relation between bed-load transport rate and parameters which describe the forces acting on the grains by the flow and the ability of the bed material to resist entrainment, for example discharge or most commonly used average shear stress. An example of such a function is illustrated in fig. 1.2.
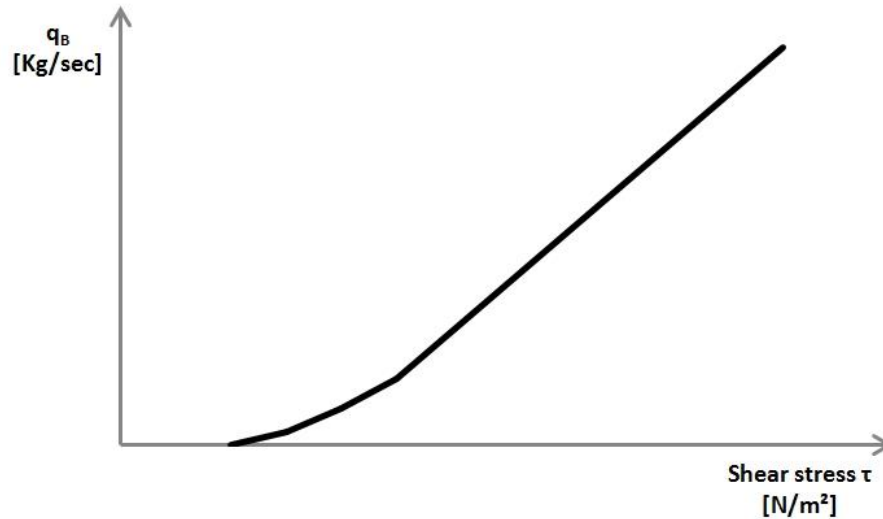
Fig. 1.2   Graphical plot of simplified bed-load transport function

Milestones in the sediment transport research can be considered to be the pioneering work of Du Boys (1879) who was the first who tried to correlate the shear stress to the amount of grains transported by water based on theoretical considerations motivated by observations at Rhone River.   The foundation of the first organized hydraulic engineering laboratories especially in German speaking countries gave a boost for new developments in area of sediment transport. Shields (1936) and Meyer Peter & Müller (1948) published their works on motion threshold and transport capacity respectively, which are widely accepted and used till today.

The first equations were based on data sets which were obtained from experiments with uniform bed material. The experiments were and still are conducted with the following procedure. Sediment is supplied at the upstream end of a laboratory flume either by a technical feed with a constant predefined rate under a constant discharge or by recirculating the grains that exit the flume. The sediment leaving the flume is collected and weighed. When the transport rate of sediments leaving the flume is equal to the one entering it is assumed that a state of equilibrium has been established. The bed slope and water depth are measured and their product is correlated to the measured bed-load discharge. Although the experiments are carried out with uniform bed material, the resulting equations are used also for the case of non-uniform bed material, which is almost always the case in nature. In that case the equations are applied with use of a median diameter which characterizes the composition of the sediment mixture. This method implies that the grain size distribution of the transported material is identical to the one of the parent bed material.

Soon it was recognized that the assumption of identity between bed-load and parent bed material composition does not hold always. Especially in the case of gravel bed

rivers, which are characterized by a wide bed material grain size distribution and large bed slopes. The bed surface of these rivers is typically armored, meaning that a coarser protective layer is positioned over the underlying, finer bed material (fig. 1.3). This armor layer has important implications relevant to sediment transport processes which need to be considered during the estimation of bed-load transport rate. The coarser bed surface regulates the availability for transport of the grains, while at the same time it protects the bed from further erosion during lower discharges.

Fig. 1.3   Coarser armor layer on the bed surface of River Wharfe, UK (Courtesy of Ian Reid, taken from Powell (1998))

It has been widely reported by many researchers that the composition of bed-load varies with the imposed shear stress. It is found that the transported material has the same grain size distribution with the parent bed material during high flow events, while during lower discharges the transported bed material is significantly finer than the parent bed material (e.g. Ashworth & Fergusson (1989)). Another important observation was that regardless of the magnitude of the shear stress acting on the bed, all grain sizes are contained in the composition of transported material (Günther (1971), Gessler (1965)). The finer grain classes are over-presented in the transported material, meaning that there are differences among the relative mobility of the various grain classes. This fact was modeled by integrating a correction function into the bed-load equations. The role of this function was to modify the excess shear stress acting on each grain class. The term excess shear stress is used to describe the difference between average shear stress acting on the bed and the required shear stress for entrainment into motion of a grain with specific size and weight.

H. A. Einstein (1950) was the first to publish a method which allowed for the calculation of the transport capacity of each grain class separately, with use of a hiding function which was integrated in the transport formula, while at the same time Harrison (1950) carried out the first systematic investigations on the phenomenon of coarsening of the bed surface. Egiazaroff (1965) provided a sound theoretical background for the use of hiding functions. Ashida & Michue (1971) used a similarity collapse over grain size based on a reference shear stress for expressing the fractional transport rates with a unique functional relationship. Parker et al. (1982) introduced the concept of equal mobility that provided a mechanism which linked the bed-load grain size distribution with the observed by many researchers coarsening of bed surface. Proffitt & Sutherland (1983) were perhaps the first who associated the transport rates of each grain class with the grain size distribution of bed surface instead of parent bed material, creating that way a surface-based transport model for sediment mixtures. Parker (1990) and Wilcock & Crowe (2003) presented surface-based transport models which incorporated the similarity collapse of the fractional transport rates as well as the concept of equal mobility, which were based on comprehensive data sets from field and laboratory measurements respectively.

1.3   Motivation of the present study

The goal of the large channelization projects at the beginning of the previous century was to increase the conveyance of the rivers in order to mitigate the flood risk. The straightening of the rivers had as a consequence an increase of the bed slope, which in turn raised the river's sediment transport capacity. A subsequent degradation tendency was generated that way which was desired, because higher flood discharges could be routed. In order to dimension the new river cross-section profile, the river engineer had to predict the new equilibrium bed slope that would be established after channelization. This task was accomplished with the application of one of the early transport formulas which were derived from experiments with uniform bed material. This approach was adequate, because it has been observed that on the long term the composition of transported material tends to be similar to the grain size distribution of the parent bed material (Parker et al. (1982)).

The river engineer nowadays is confronted with more complex questions than in the past. He needs to make as accurate predictions of the river bed morphology evolution as possible, even under non-steady flow events or under constrained sedimentological boundary conditions, which are generated by man-made intervention in the river course, e.g. the construction of sediment barriers or human activities that are

associated with a change of the land uses and subsequently an alteration of sediment supply in a river reach. Furthermore, he needs to estimate not only the final equilibrium bed slope and elevation but the intermediate transient stages as well, especially during unsteady flow events. In this way the river engineer is able to improve the flood protection and mitigate thus the risk of loss of life as well as the interruption of economic activity. Thus, the river engineer should be able to estimate not only the final equilibrium condition but also the temporal and spatial variation of river bed morphology until the establishment of the new equilibrium. In addition, he must be able to predict the transient changes that take place during unsteady flow events regardless of whether the new equilibrium has been established or not.

An example of human intervention and the associated problems seeking for an answer from the river engineer is given below. The construction of dams interrupted the sediment transport continuity in most of the rivers. Downstream of dams the clear water flow in order to saturate its transport capacity causes an erosion process which in the worst case scenario amplifies the already existing degradation tendency which was triggered by river channelization. In order to counteract these negative impacts, new sediment management techniques have been developed. These techniques aim at the re-establishment of the sediment transport continuity as well as the better operation of hydro power plants. Two widely employed methods for mitigation of the negative effects of sediment continuity interruption are either reservoir flushing (fig. 1.4) or excavation of material that is accumulated in the reservoir of the hydraulic construction and transportation downstream of the dam (Fig.1.5).

Fig. 1.4   Bed surface downstream of Eisenbahnerwehr after flushing activity
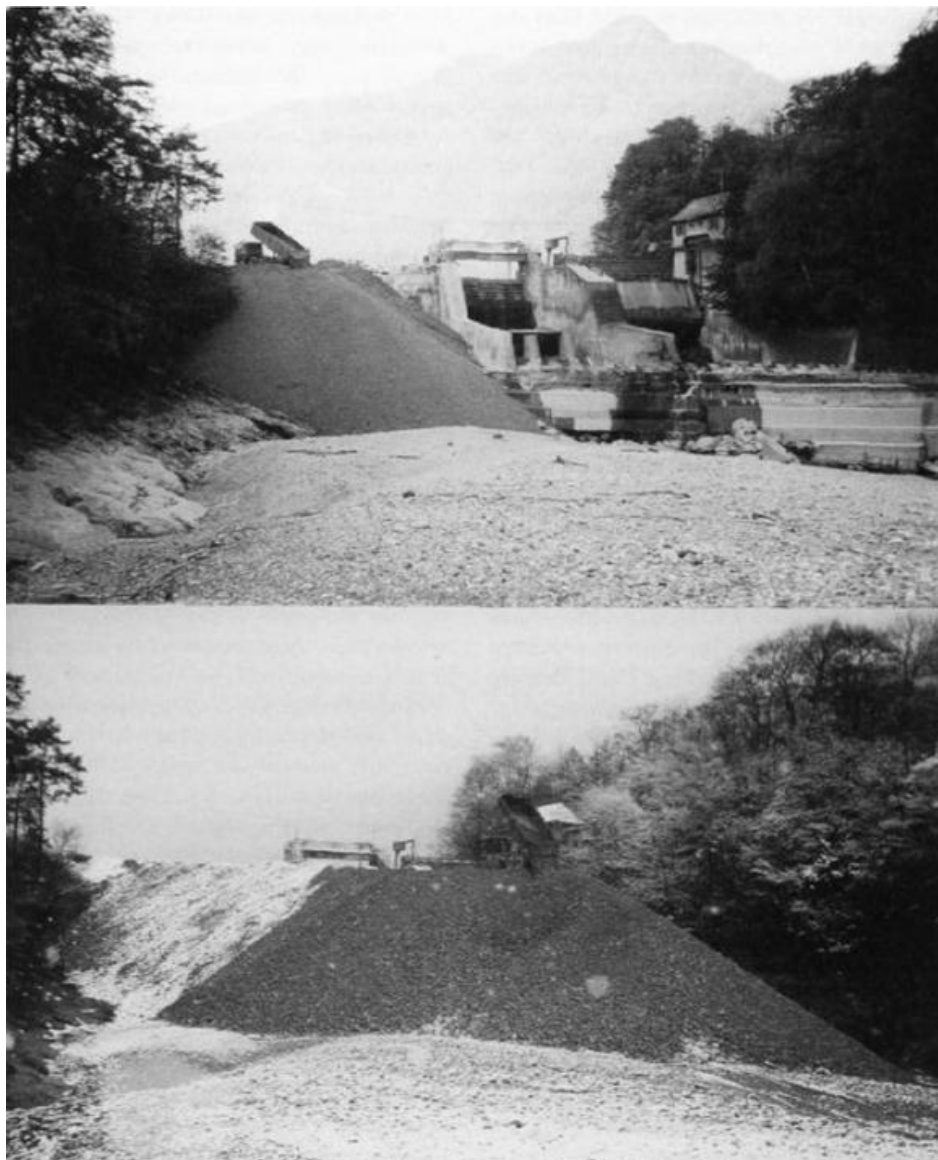
Fig. 1.5 Supply of fine material downstream of Kiblinger Sperre (River Saalach) (Courtesy of LfU, Schaipp)

These techniques are very expensive and therefore they need to be carefully planned because they can lead to unwanted aggradation of the river bed when the supplied amount of sediments is larger than the amount that the river is able to transport. In addition, the supplied material is usually finer than the parent bed material and therefore it affects the composition of the bed surface downstream of the hydraulic construction dramatically. Thus the river engineer is called to plan these activities by choosing the appropriate total mass and grain size distribution of material that will be given downstream of the dam. In this way the observed bed degradation tendency will not deteriorate, the fish habitat environment will enhance and the additional sediment supply will be transported further downstream without causing bed aggradation that will increase the flood risk.

Answering such questions becomes much more complicated in gravel-bed rivers, i.e. rivers that are characterized by a bed material that is described by a wide grain size distribution with particles that belong both to the sand size range and to the gravel size range. The reason for the increased complexity in predicting the behavior of these rivers is that an additional parameter, apart from grain size of parent bed material and bed slope, is associated and strongly interrelated to the finally established equilibrium condition. That is, the development of a distinct, coarser than the substrate surface layer, the so called bed armor.

Two examples that show the effect of grain size distribution of armor layer in sediment transport processes during unsteady flow events are given below. Reid et al. (1985) carried out continual bed-load measurements in a gravel-bed channel in a period of two years. The analysis of the recordings revealed a pattern of bed-load transport that varied from flood to flood. When floods followed each other closely bed-load occurred predominantly during the rising limb of the hydrograph than during the recession limb. Contrary, isolated floods which followed long low flow periods were characterized by substantial bed-load on the recession and lower on the rising limb. The variability in the direction of the hysteric loop of the bed-load response relative to flow hydrograph was attributed to the organization of the bed surface. When the time interval between two floods was short, the bed material did not consolidate sufficiently and thus could be entrained on the rising limb of the hydrograph more easily. On the other hand when the bed had enough time to consolidate bed-load was confined to the recession limb of the hydrograph, as the bed had to loosen up first.

The importance of stress history effects on bed-load transport during subsequent high flow events was illustrated also by Haynes & Pender (2007). They conducted experiments which were comprised of two phases. In the first phase, which was called antecedent stress history period, an armor layer under varying shear stresses and antecedent durations was created. In the second phase, which was called stability test, a larger shear stress which remained the same for all experiments was applied on the armored bed. The purpose of the experiments was to investigate the influence of the antecedent stress history on the residual stability of the bed which was characterized by its response during the stability test. The experimental results showed that the antecedent stress history condition played an important role in the observed transport processes during the stability test. The total mass of bed-load during the stability test reduced with the increasing time that the bed had at its disposal to create an armor layer. This means that an armor layer created by a prolonged antecedent period is more stable. In addition increasing the antecedent shear stress magnitude led to larger mass of total bed-load transport during the stability test, showing a reduction of bed stability. They interpreted this behavior in terms of two counteracting mechanisms

which control the stability of an armor layer. These two mechanisms concern the rearrangement of grains of all sizes into a more stable and imbricated structure. Coarser grains were repositioned into a more stable position and the fines fulfilled the interstices among them and packed into a tighter configuration. The second mechanism was the compositional change through the winnowing of the fines which acted destabilizingly as it was the reason for larger exposure of the coarse grains to fluid forces.

The above examples show the effect of the phenomenon of vertical sorting on transport processes in gravel-bed rivers, especially during unsteady flow events. Consequently, it is easily concluded that the simulation quality of river morphology evolution during unsteady flow events in gravel-bed rivers depends considerably (along with correct estimation of exerted shear stress) on taking into account the effect of armor layer composition and its corresponding transient changes on transport rate and composition of bed-load. The interrelation among bed surface gradation, exerted flow strength and fractional transport rates has been the subject of intensive research at least in the last 30-40 years. However, relatively recently, Diplas & Shaheen (2005) mentioned:

"…the development of a reliable bed load transport formula, valid for a wide range of gravel-bed conditions remains an elusive goal."

The development of numerical models that solve the basic equations of flow and sediment transport by means of arithmetic analysis methods, allow for calculation of bed-load transport rates and subsequently bed morphology evolution with very high temporal and spatial discretization, something that would not be possible with manual calculations. Thus, the river engineer posses a tool that is a basic requirement for the prediction of non-equilibrium sediment transport processes. However the potential that has been created by the increased computing capacity and the development of more effective numerical algorithms is not fully exploited due to the not yet complete understanding of the physical laws that govern the processes of sediment transport of non-uniform bed material, something that becomes even more difficult considering the variability that is exhibited by the streams on the field.

Bui & Rutschmann (2006) applied a 3 dimensional numerical model in order to simulate the experiments of Yen and Lee (1995) on transport processes in alluvial curved channels with non-uniform bed material under unsteady flow and zero sediment feed conditions. The comparison of calculated results and experimental measurements revealed the necessity for implementation of a non-equilibrium parameter into the model in order to obtain a better agreement between numerical

simulation and experimental observations. The non-equilibrium parameter reduced to a certain pattern the fractional bed-load discharge that was calculated by the transport formula that was incorporated in the model, altering thus the spatial distribution of the initially estimated transport rates. Bui & Rutschmann (2006) demonstrated that the need for this modification was larger with increasing unsteadiness of the imposed flow hydrograph.

Short summary

The evolving even more complicated problems that the river engineer nowadays is called to encounter, include the prediction of sediment transport processes under conditions of disequilibrium. These are triggered either by constraint sediment supply or by unsteady hydraulic boundary conditions or of course both. Performing such predictions is even more difficult in the case of gravel-bed rivers due to the non-uniformity of bed material and the impact on sediment transport processes of the distinct armor layer that has been observed to develop on bed surface. The development of numerical models provide a tool in the hands of an engineer, that allows him to perform the required large number of calculations that are necessary for simulation of non-equilibrium transport. However, our not yet complete understanding of the processes that take place during non-equilibrium transport in gravel-bed rivers, is introduced in the empirical bed-load formulas that are employed by the numerical models, affecting thus the quality of simulation. Therefore, it is necessary to investigate systematically the disequilibrium transport processes of sediment mixtures and attempt to describe the observed transient changes mathematically by means of a bed-load predictor, especially developed for this purpose.

1.4 Subject, objectives and practical application of the present study

1.4.1 Subject

The subject of the present study is the investigation of the formation procedure of a coarse armor layer on the surface of an initially unarmored bed, under zero sediment feed conditions and relatively low exerted shear force that remains constant throughout the process of bed surface transformation. The investigated bed material is a sediment mixture, characterized by high sand content and wide grain size distribution, showing thus a slight bimodality. Analysis of substrate samples that were taken on the field has shown that this type of bed material is met frequently in gravel-bed rivers. The term

"relatively low exerted shear force" means that the imposed shear stress during the experiments is able to entrain and set into continuous motion particles of all grain classes contained in the bed material but is not sufficient to cause transport of particles of different sizes at the same rate (when the fractional content of each individual grain class is ignored). Therefore, the transport mode can be characterized as preferential, i.e the transport rate of particles with small diameter will be higher than the transport rate of coarse fractions (when the fractional content of each individual grain class is ignored).

The examined case is a clear example of bed-load transport of sediment mixtures under disequilibrium. It was mentioned that equilibrium transport is denoted by equivalence between the mass discharge of sediment entering and leaving a given river reach with finite length during a finite time period. In the case examined herein, the entering bed-load discharge is zero. However the imposed flow strength is large enough to cause the preferential transport of fine relative to coarse particles. Thus, the exiting bed-load discharge is larger than zero and therefore deviates from the equilibrium transport rate which is zero due to the upstream constraint sedimentological boundary condition. The preferential transport of fines will have as result the coarsening of bed surface due to reduction of fractional content of small grain classes and the subsequent increase of fractional content of coarse grain sizes. The progressive coarsening of bed surface will have in turn as result the better protection of fines that remain on bed surface (because they will have an increased possibility to find shelter in the wake of a coarser particle). At the same time the, associated with bed surface coarsening increased bed roughness will render the transport of coarse particles even more difficult. For these two reasons the observed fractional transport rates will be continuously reduced, approaching thus asymptotically the equilibrium which is defined as condition of zero transport. The armor layer that will progressively evolve is called static armor layer, where the term static finds its etymology in ancient Greek and means "still", i.e. the bed surface has obtained a coarse enough structure that prohibits any particle movement under the given imposed flow intensity.

1.4.2 Objectives

The phenomenon of static armoring has been investigated by many researchers in the past e.g. Harrison (1950), Gessler (1965), Günther (1971), Chin et al. (1994) among others. These investigations focused mainly on the prediction of the fully developed armour layer grain size distribution as a function of the imposed shear stress and

composition of parent bed material. The term "fully developed armor layer" describes the condition of the bed surface which doesn't allow any further erosion under a given constant shear stress. These methods are characterized as single step methods according to Paris (1991) because they allow for a deterministic prediction of the final armor layer composition. A second possibility is the simulation of the evolution of a static armor layer with use of the basic equations of flow and sediment transport. This method is called multi step and requires the employment of a numerical model. Therefore an equation that can describe the hiding-exposure effects that determine the fractional transport rates is required. So far the equations that have been used for this purpose have been developed by data sets that were obtained from experiments where a state of equilibrium has been established. However the formation of static armor layers is clearly a transient process under disequilibrium which is unsteady over time and space.

The above considerations define the two objectives of the present study. The first objective is to document the transient changes that take place during the transformation of a rich in fines bed surface into an armored one. This includes investigation of the changes in bed geometry, bed surface composition and fractional transport rates not only at the end or at the beginning of the phenomenon but throughout the formation process as well as along the flume. Thus, the first objective of the present study is a detailed documentation of the spatial and temporal variation of fractional transport rates, bed surface composition and bed geometry during the under investigation case of disequilibrium transport.

The second objective of the present study is the investigation of the interrelationships among observed bed surface grain size distribution, total transport rate, composition of transported material and imposed shear stress at different stages of the phenomenon of formation of a finally static armor layer. It was previously mentioned that the progressive coarsening of bed surface is associated with modification of the mobility of individual grain classes. Thus the measured at a given time point values of fractional transport rates will be related to the associated grain size distribution of bed surface and imposed flow strength. The final product of this correlation will be a transport model that will be able to reproduce the observed transient changes with accuracy. The proposed surface based transport model will be able to take into account the progressively changing hiding/exposure conditions that the armor layer offers to particles of different absolute size.

1.4.3 Practical application

The present study focuses on the transient changes that occur during progressive armoring of a bed material with high sand content under constraint sediment feed conditions. The declining abundance of sand grains on bed surface has as result the transformation of the initially matrix supported (sand content > 30 %) bed surface to framework supported (sand content < 15 %) bed surface. A new dynamic hiding function is proposed, which when incorporated in an appropriate transport model renders the model able to predict with high accuracy the temporal and spatial variation of fractional transport rates as a function of grain size distribution of bed surface and parent bed material (the term that renders the hiding function dynamic, as the degree of armoring is taken into consideration when compared to other already published hiding functions) and exerted shear stress. Thus, when the proposed function is implemented in a numerical model, the latter should require less tuning in order to simulate with accuracy the transport of fine sediment over a coarse bed surface.

In engineering praxis it will be frequently asked to plan activities like reservoir flushing or transfer and deposition of sediment that settled in the reservoir downstream of the dam, in order to mitigate the negative impacts of dam construction on river morphology. The proposed model was derived from measurements of fractional transport rates directly coupled to the actual grain size distribution of bed surface when the latter was transformed from matrix to framework supported. Thus the model is suitable for the prediction of transient changes of bed surface under a given sediment supply (defined by the total supply rate and composition) or for the prediction of the composition and transport rate of the material that can be transported over a given armor layer. In the first case the model will help in choosing for example the appropriate sediment supply that will reduce the erosion tendency and will not endanger the fish habitat. In the second it will help in predicting the impact of a change of land uses in watershed and subsequently of sediment supply on bed stability.

1.5 Flowchart of research activities and outline of the work

Literature review on relationship between bed surface composition and fractional transport rates as observed in experiments when the condition of equilibrium transport had already been established	Chapter 2
Literature review of investigations on static armor layers	Chapter 3
Literature review on derivation of bed-load predictors with focus on published surface based transport models	Chapter 4
Formulation of the subject and objectives of the present study and determination of the employed methodology.	Chapter 1
Preliminary experiments & development of method for estimation of armor layer grain size distribution by means of processing of plan view photos of bed surface	
Experimental investigations	Chapter 5

1st objective

Analysis of row data and determination of bed surface grain size distribution fractional transport rates and exerted shear stress at different time intervals and measuring stations	6.2 - 6.6	Chapter 6
Determination of temporal and spatial variation of fractional grain mobility	6.7	

1st objective	Comparison of experimental results with results of relative studies published in the past	6.8.2	
2nd objective	Justification of the necessity of the employment of a surface based transport model for the accurate simulation of non-equilibrium bed-load transport of non-uniform bed material	6.8.1	Chapter 6
	Association of observed variation of grain mobility with the required variation pattern of fractional reference shear stress that a hiding function should be able to predict	6.8.3	
	Association of the observed variation of mobility of individual grain classes and consequently reference shear stress with the hiding/exposure effects by means of optical observations during the experimental runs and theoretical considerations (physical mechanism that governs the observed transient changes)	6.8.4	
	Determination of reference shear stress of individual fractions by means of experimental results, by plotting fractional grain mobility against dimensionless fractional shear stress.	7.2	Chapter 7
	Comparison of the empirically determined variation pattern of fractional reference shear stress (based on experimental measurements) with the variation pattern that was conceived from theoretical considerations	7.2	

2nd objective	Development of dynamic hiding function from values of reference shear stress that were determined from measurements performed in the present study for a given sediment	7.3.1 - 7.3.2	
	Theoretical considerations on the behavior of different types of sediment mixtures in case of non-equilibrium transport under the same sedimentological and hydraulic boundary conditions.	7.3.3.1	Chapter 7
	Modification of the previously developed hiding function with use of appropriate data from recent studies of Wilcock in order to be adjusted also to other sediment mixtures	7.3.3.2	
	Similarity collapse of measured fractional transport rates during the present study and the study of Wilcock et al. (2001) with use of the predictions of the proposed hiding function.	7.4.1	
	Determination of the function that expresses adequately the variation of fractional mobility with excess shear stress for the data sets of both studies.	7.4.2	
2nd objective	Validation of the proposed transport model by comparison of model predictions with experimental measurements from studies that were not taken into consideration during the development of the model.		Chapter 8

2.   Influence of vertical segregation of a coarse surface layer on transport of sediment mixtures

The influence of bed material gradation on sediment transport processes has been the subject of numerous research studies. These studies have revealed various patterns of bad material sorting at different spatial and temporal scales. The most important of these patterns are downstream fining and vertical segregation of bed material. The present chapter reviews studies regarding the development of a coarse surface layer on the bed surface of a gravel-bed river. Its importance on the establishment of an equilibrium transport condition is analyzed along with the inter-relationships that exist between composition of bed surface, flow strength and particle size distribution of bed-load.

2.1   Bed surface coarsening as a mechanism related to establishment of equilibrium bed-load transport

2.1.1   Definition of state of equilibrium

If we consider a river reach to be a transporting system, then it is in a state of equilibrium when the sediment supplied at the upper end leaves from the downstream end at the same rate. When the supplied sediment is transported further downstream under a given flow, without net deposition or erosion and subsequently alteration of bed geometry, it means that this is the amount of sediments per unit time that the flow is able to transport and is called sediment transport capacity.

If the material that is contained in the system as well as the input material is uniform, meaning that it can be characterized by a single grain size d, then the required identity refers necessarily to the input and output total transport rate.

$$q_{b\ in} = q_{b\ out} \qquad\qquad \text{Eq. (2.1)}$$

where: $q_{b\ in}$ is bed-load discharge entering the system
$q_{b\ out}$ is bed-load discharge leaving the system

If the sediment supply or the material contained in the riverbed however, is a mixture of grains with different sizes, then the identity between entering and leaving transport rate must apply to every grain class that is contained in the sediment mixture. In that case the condition of equilibrium is described by the equation.

$$q_{bi\ in} = q_{bi\ out}.$$
<div align="right">Eq. (2.2)</div>

where: $q_{bi\ in}$ is bed-load discharge of ith grain class entering the system

            $q_{bi\ out}$ is bed-load discharge of ith grain class leaving the system

The previous equation can be recast

$$q_{bT\_in}\ p_{in}(i) = q_{bT\_out}\ p_{out}(i)$$
<div align="right">Eq. (2.3)</div>

where: $p_{in}(i)$ is fractional content of ith grain class in the mixture entering the system

            $p_{out}(i)$ is fractional content of ith grain class in the mixture leaving the system

The identity of fractional transport rates of individual grain classes means that the total bed-load discharge that is supplied to the system will be equal to the total bed-load discharge leaving. Therefore, according to eq. 2.3, in the state of equilibrium the grain size distribution of the sediment entering the system will be exactly the same as the grain size distribution of the sediment leaving the system.
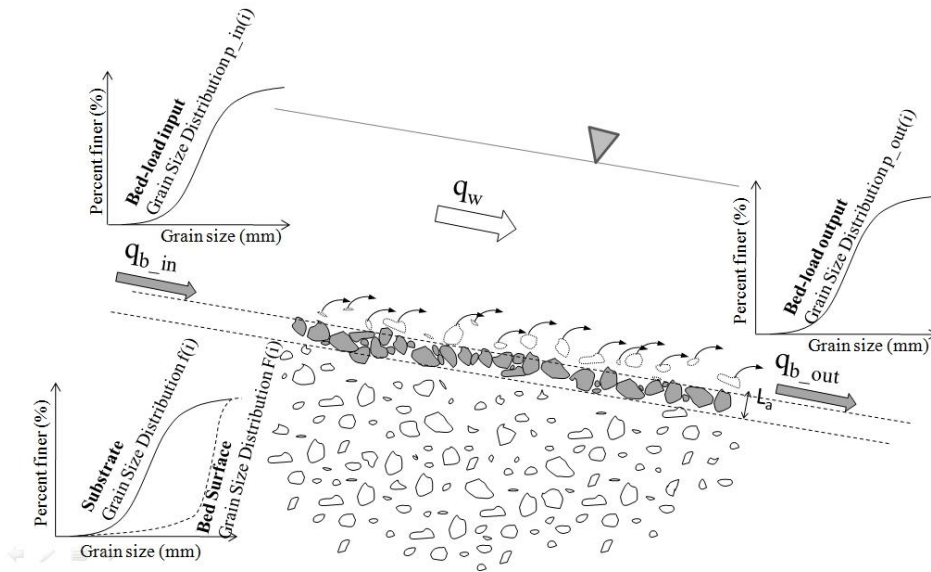
Fig. 2.1   Definition sketch of the condition of equilibrium for transport of non uniform sediments

The condition of equilibrium for the case of sediment mixtures can be divided into two cases. If the grain size distribution of the transported material is identical to the grain size distribution of the parent bed material, i.e. p(i) = f(i) and the transport takes place at a constant rate, then according to Parker et al. (1982a) and Parker & Klingeman (1982) this equilibrium condition is called condition of equal mobility. If the grain size distribution of the transported material is different from the grain size distribution of

the bed material, then according to Parker & Wilcock (1993) the condition of equilibrium is defined as partial transport.

2.1.2   Mechanism of establishment of an equilibrium condition

When the transport under equilibrium is interrupted e.g. because of a change in the water discharge or in the sediment supply or in the geometry of the river reach, then a new equilibrium must be established. The bed-load transport that takes place during the process of establishment of a new equilibrium condition that will satisfy the new boundary conditions is called non-equilibrium transport.

In the simplified case of uniform sediment, when the equilibrium is disturbed, the system will adjust its bed slope in order to establish a new hydraulic condition, e.g. Lane (1955). The new flow regime will finally exert the required shear stress which can cause the entrainment and transport of the necessary number of grains per unit time in order to assure that the flux of sediments entering the river reach is also leaving the downstream end.

If the material contained in the system as well as the supplied material is poor sorted, meaning that it is a sediment mixture which contains particles with a wide range of grain sizes, something that is almost always the case especially in gravel-bed rivers, then the process of establishment of a new equilibrium is much more complicated and not so clear yet. In that case the system might adjust not only its bed slope in order to establish a new, appropriate flow condition, but the grain size distribution of surface layer too, in order to achieve the identity between entering and leaving fractional bed-load transport rate. The development of a distinct surface layer with thickness L_a about the d_{90} particle size contained in the parent bed material (e.g. Petrie and Diplas (2000)) has been observed in almost all gravel-bed rivers. The grain size distribution with density function F(i) of the armor layer is relatively coarser and better sorted in comparison with the underneath lying bulk material, which can be described by the density function f(i) (see fig. 2.1). The presence of this surface layer has been recognized to be a fundamental feature of gravel-bed rivers, as are dunes in sand bed rivers (Parker et al. (1982 a)).

As it will be later shown, when a grain is contained into a sediment mixture, its mobility depends not only on the mass of the grain and the exerted drag force by the flow but also on the sheltering that its surrounding can offer. The change of composition of bed surface might increase the exposure to the flow field or provide a more effective shelter in between larger immobile particles for the coarse and fine

grains respectively, e.g. Einstein (1950), Eggiazziarof (1965), affecting that way the grain mobility. Therefore, the coarsening of bed surface that alters the grain size distribution of the sediment mixture that is subjected to the flow attack, consequently affects the mobility of the different grain classes. Parker & Klingemann (1982) called this mechanism for the adjustment of fractional mobility "microscopic hiding" and is illustrated in fig. 2.2a. Furthermore, the alteration of bed surface grain size distribution can regulate the availability for transport of the grains of different grain sizes. Parker et al. (1982a) and Parker & Klingemann (1982) showed that the coarsening of the bed surface renders the larger (smaller) grains with intrinsic lower (higher) mobility, due to their greater (smaller) inertia, over-presented (under-presented) on the bed surface and subsequently (reduced) the possibility of entrainment is increased, providing that way an additional mechanism for the establishment of equilibrium. This mechanism was called "macroscopic hiding" by the authors and is described in fig. 2.2b.
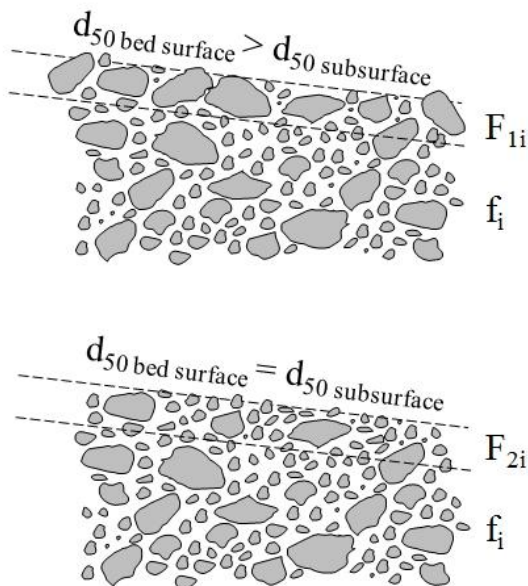
Fig. 2.2a   Microscopic hiding   **Fig. 2.2b**   Macroscopic hiding

(coarsening of bed surface results in larger grains being more exposed to the flow and fine grains being better sheltered)

(coarsening of bed surface results in larger grains being overrepresented on the bed surface and fine grains being underrepresented)

2.1.3   Patterns of vertical sorting in gravel bed-rivers

The above described phenomenon of vertical sorting, i.e. the development of a distinct bed surface layer that is relatively coarser than the underlying substrate, has been

identified in numerous investigations in laboratory as well as field studies. An important discrimination has been done through the characterization of the coarse surface layer. When the bed surface coarsens due to an imbalance between sediment supply and bed-load transport capacity of the flow, then the bed surface layer is called static armor layer (e.g. Sutherland (1987)). When bed surface coarsening is observed despite sufficient sediment supply to cover the transport capacity of the flow, then the coarse surface layer is called pavement or mobile armor (e.g. Parker et al. (1982a).

Suitable conditions for the development of static armor layers are met downstream of a dam or at lake outflows. In that case the sediment supply is usually less than the ability of the stream to transport bed-load and therefore the deficit between supply and transport capacity has to be covered by erosion from the bed itself. However, during low or moderate flows, the exerted drag force is incompetent to transport all grains at equal transport rates, regardless of their size. As a result the fine grains are preferentially transported at higher proportion than the coarser particles and a subsequent coarsening of the bed surface takes place, due to the reduction of the fractional content of fines on the bed surface and the increase of the proportion of the coarse grains. The grains that remain on the bed surface are immobile as the flow is not able to set them into motion and therefore the term static is used in order to describe the resulting armor layer. When the sediment supply is further reduced, the balance of the sediment load is provided with a larger degree of coarsening until an ultimate degree of bed surface coarsening is reached. This mechanism has been called downstream winnowing by Gomez (1984) and is shown in fig. 2.3.
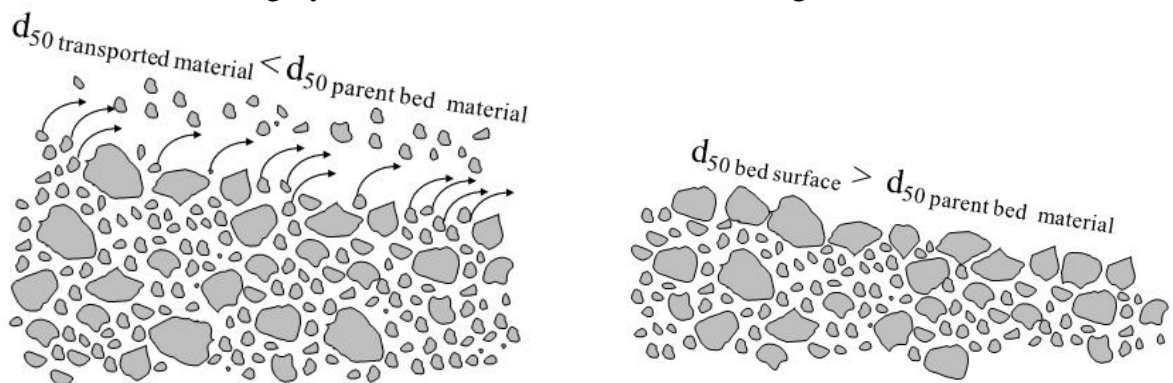
Fig. 2.3 Explanation sketch for mechanism of downstream winnowing

Contrary to static armoring, mobile armoring is observed even when the sediment supply is equal to the transport capacity of the flow. It is also observed during high flows that are able to transport all available grains at rates that preserve equality among the grain size distribution of transported material and parent bed material. In that case the coarsening of the bed surface can be attributed to the segregation of finer grains into the subsurface, by falling through the crevices created by the larger

particles of the bed surface. When a large grain is dislodged, small grains might fall into the hole where the large grain was initially located. Due to the increased shelter that fine grains find in their new position their probability of re-entrainment is reduced and in that way the equation of mobility of grains with different grain sizes is assured. Parker & Klingemann (1982) and Diplas & Parker (1992) called this process vertical winnowing and is described in fig. 2.4. The mechanism of vertical winnowing resembles the mechanical shaking of a container filled with a mixture of multisized particles, a phenomenon called the "Brazil nuts effect" that was described by Rosato et al. (1987). Herein, the smaller particles fill in the transient gaps that open beneath the larger particles and a geometrical rearrangement that dislocates the large particles to the top of the container takes place. According to Parker et al. (1982b) the pavement can coexist with transport of all grain sizes because motion is sporadic. Therefore, at a given time only a small proportion of the grains lying on the bed surface is in motion and a continuous exchange between bed-load and pavement takes place.
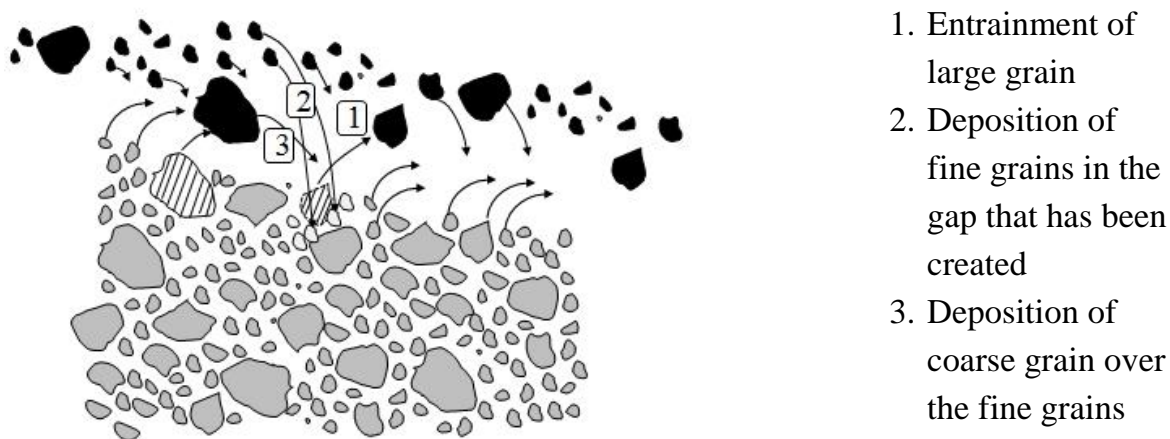
1. Entrainment of large grain
2. Deposition of fine grains in the gap that has been created
3. Deposition of coarse grain over the fine grains

Fig. 2.4   Explanation sketch for mechanism of vertical winnowing

It could be stated that the main distinction between static and mobile armor is that the former is associated with an immobile bed while the latter with an active surface layer (Parker & Klingemann (1982), Jain (1990)). The distinction between static and mobile armor refers to the final stage when the equilibrium has been achieved. In the case of static armoring the equilibrium refers to a state of no motion. The sediment supply is zero and therefore the bed surface must obtain a coarser composition so as to resist to the exerted drag force of the flow, in order to prevent from erosion which could cause an imbalance between supply and transport, allowing that way the establishment of equilibrium of zero transport. If the system is fed with sediment, then the bed surface coarsens in order to create the conditions that will allow for all grain sizes to be entrained and deposited with the same rate. Thus, an equilibrium condition is established which is described by the equality between the fractional transport rates entering and leaving the system.

2.2 Transport concepts for graded bed material

Soon it was recognized that the mobility of a grain of a given size that belongs to a multisized population is not the same with the mobility that the grain would have if it belonged to a population that contained particles of the same size only. Researchers have documented the transport processes of sediment mixtures and have proposed different scenarios regarding the inter-relationship of fractional mobility among grains of different size belonging to the same sediment mixture. These concepts are the theoretical background upon which the development of transport capacity predictors is based.

2.2.1 Equal mobility

The concept of equal mobility was introduced by Parker & Klingeman (1982) and Parker et al. (1982a). The concept was derived from measurements of fractional transport rates during flows above the critical discharge for the break-up of armor layer in Oak Creek, USA and further supported by laboratory experimental investigations conducted by Parker et al. (1982b). The analysis of the field data showed that the shear stress at which the grains of individual fractions are transported at a set low dimensionless transport rate does not vary significantly with grain size. Moreover, the dimensionless fractional transport rates could be collapsed reasonably well into a single transport curve. Based on these observations, Parker and his co-workers formulated two hypotheses, which were called later by Parker & Toro-Escobar (2002) the weak and the strong form of the equal mobility statement.

According to the weak form, the formation of a mobile armor enables the transport of the coarser half of the mean annual gravel load to be at the same rate as the finer half. The coarser bed surface is required because the coarser gravel fractions are intrinsically less mobile than the finer gravel fractions. The lower mobility of the coarser fractions is compensated by their overrepresentation on bed surface, which in turn increases the possibility for entrainment. Thus, an equalization of mobility among the grain fractions is achieved. The difference in mobility between the fractions is smaller as flow strength increases and therefore the armor layer tends to diminish with increasing flow intensity.

According to the strong form of the concept of equal mobility, the grain size distribution of the average annual yield of gravel bed-load is similar to the grain size distribution of the gravel content of the subsurface bed material. This assumption is not meant to apply to every flow but rather to a time averaged flow, which is

responsible for the stream morphology after many hydrographs. As far as individual flows of constant discharge are concerned, Parker et al. (1982) have stated that a gradual coarsening of the bed-load should be expected with increasing stage.

Parker & Toro-Escobar (2002) have clearly pointed out that the concept of equal mobility does not imply that the grains contained in a sediment mixture possess the same mobility. What the concept suggests is that there is a tendency toward equalization of mobility among grain fractions, which is achieved by means of hiding effects that compensate for the weight effects and the coarsening of bed surface which in turn compensates for the remaining mobility differences. Furthermore the concept of equal mobility does not imply that all grains are entrained at the same critical shear stress. It by-passes the problem of threshold of motion for sediment mixtures with the use of a reference shear stress that corresponds to a set low value of dimensionless bed-load transport rate instead of a critical shear stress that corresponds to zero bed-load transport.

The condition of equal mobility is met under two circumstances. The first occurs when the sediment supplied to the system has the same composition with the bed material. In that case the condition of equal mobility is imposed on the system by the sediment feed regardless of the flow strength. If the bed-load transport is determined solely by the flow and the sediment within the system, then the condition of equal mobility is met by high shear stresses when all the grain classes that are contained in the bed material are in motion.

2.2.2 Selective transport

The concept of equal mobility challenges the approach of selective transport, which is based on the classical work of Shields (1936) on incipient motion. According to this concept, the critical shear stress of a given grain class is directly proportional to particle size. That means that particle weight is the principal force restricting movement. Therefore, larger particles are intrinsically less mobile than smaller particles due to their greater inertia and require higher shear stresses to entrain them. This implies that finer particles will be preferentially entrained by a flow exerting a competent shear stress to the bed surface. This concept has been used in studies regarding flow competence, in an attempt to evaluate velocities and bed stresses during flood events from the grain size of the largest transported particle, e.g. Komar (1987), Komar & Li (1988).

The concept of selective transport has been used as the conventional explanation for

the development of armor layers. By assuming a wide range in critical shear stresses of individual grain fractions, the finer particles are winnowed from the bed when a flow is competent to transport them and thus the bed surface becomes coarser, e.g. Gomez (1983). Gomez (1984) named this mechanism as "downstream winnowing" which requires the larger fractions to remain immobile.

It is well known that the dimensionless critical shear stress approaches a constant value of 0,045 for large values of particle Reynolds number. In that case the critical shear stress can be written as a function of grain size as follows.

$$\tau_c = 0{,}045 \frac{\rho_s - \rho}{\rho} g d \qquad \text{Eq. (2.4)}$$

where: τ_c is critical shear stress
        ρ_s is sediment density
        ρ is water density
        g   is gravitational acceleration
        d   is grain size of bed material

The fig. 2.5 shows a plot of eq. 2.4 in a log-log diagram that illustrates the linear trend between critical shear stress τ_c in Pascal and grain size d in mm. According to the concept of selective transport if the shear stress exerted on the bed takes a value of 4 Pa for example, then the grains that are larger than 5,55 mm will remain immobile on the bed surface, while the grains with diameter smaller than 5,55 mm will be entrained. A direct implication is that the composition of the bed-load will be truncated in relation to the composition of bed material.
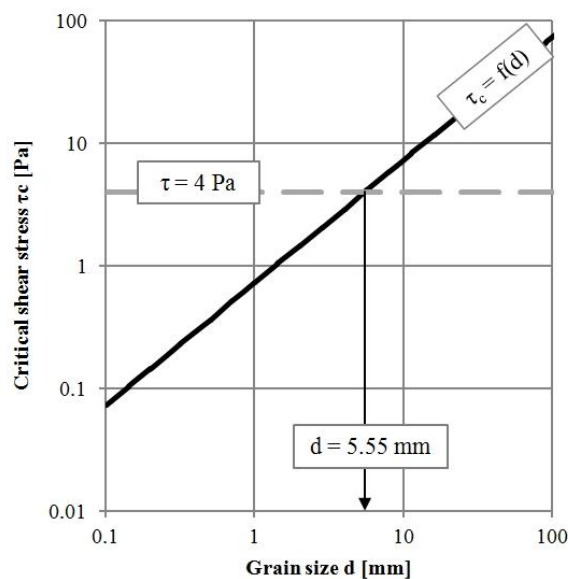
Fig. 2.5   Estimation of the critical shear stress under the assumption of rough turbulent flow for a grain of a given size

However, experimental studies concerning static armoring have shown that such armor layers are coarser than the parent bed material, but their grain size distribution is not truncated compared to the corresponding size distribution of the subsurface, e.g. Gessler (1965). Furthermore, the material that is entrained and transported downstream during the formation of static armor layers contains all the fractions that are present in the parent bed material, e.g. Tait et al. (1992). These observations reveal that selective transport due to preferential entrainment of fine particles cannot describe the related processes accurately.

2.2.3   Partial transport

Based on optical observations through the sidewalls of a flume Wilcock & McArdell (1993), suggested that for a given flow strength a proportion of the surface grain population that belongs to a given size fraction may remain immobile during a transport event, while the remainder of the grain population is entrained regularly. The authors termed this condition partial transport. A similar distinction between active and inactive grain populations has been made by Drake et al. (1988) after an analysis of motion picture film of graded material transport.

Wilcock & McArdell (1997) further investigated the state of partial transport by measuring the proportion of grains that remained immobile over the duration of experiments with different flow strengths. In order to locate and count the immobile grains they used a series of bed photographs that were taken during the flume runs. Thus, they provided a direct demonstration of partial transport and described its variation with time, flow strength and grain size. Moreover, they combined the determined proportions of active grains for each fraction with the corresponding fractional transport rate. Thus, they demonstrated how partial transport affected fractional transport rates.

Wilcock & McArdell (1997) showed that grains of a single size are entrained over a range of bed shear stresses. Their experimental results show that the portion of grains that are mobilized, changes within this range of shear stresses. As flow strength increases, the population of immobile grains that remain at their initial location during the flow event is reduced. In addition they showed that the range of shear stress between no transport and full mobilization is the same for all grain sizes. The necessary flow strength for entrainment of half of the grains in a size fraction increases with grain size.

The authors correlated partial transport with the commonly observed decrease of

transport rate with grain size. They found that the transport rates of the fully mobilized fractions were independent of grain size and larger than the transport rates of coarser partially entrained grain fractions. Fully mobilized fractions are those that all the surface grains that belong to this size class are entrained. Contrary, the correlation of the observations on partial transport with the measured fractional transport rates revealed a consistent decline of transport rate with reducing proportion of mobilized grains.

Partial transport has been documented also on the field with use of magnetically tagged stones by Haschenburger & Wilcock (2003).

The condition of partial transport is met only by low to moderate flow strengths when the bed-load transport is adjusted by the prevailing flow and sediment conditions in the system. Another prerequisite is the sufficient mobility variability among individual grain sizes of the sediment mixture.

2.3 Methods for investigating bed-load transport of heterogeneous bed material

In our effort to understand the laws that govern bed-load transport in gravel-bed rivers we have two tools. The first one is coupled observations and measurements of flow, transport rate, and bed material (surface and subsurface) composition in the field. The second tool is experimental investigations under controlled conditions in the laboratory. The experimental studies in the laboratory can be performed with two different sediment flume operation configurations. The first one is the sediment feed mode and the second is the recirculating mode. The two different operational modes are illustrated in fig. 2.6a and b respectively.
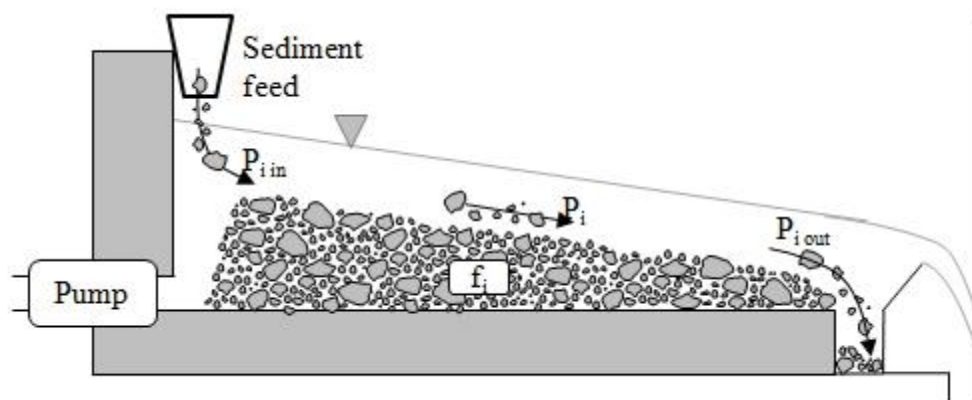
Fig. 2.6a Sediment feed flume configuration
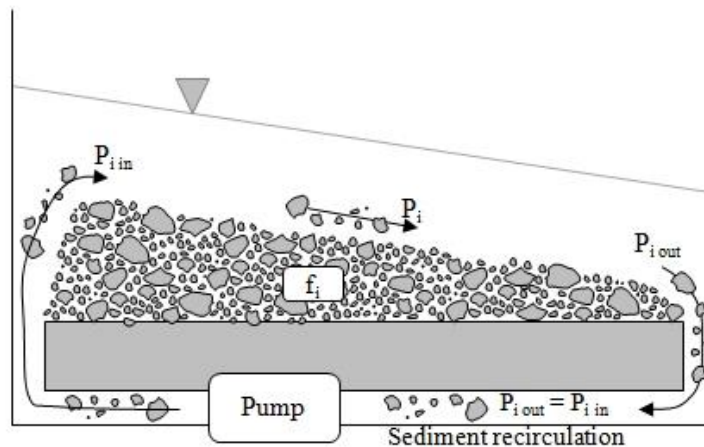
Fig. 2.6b Sediment recirculation flume configuration

In the sediment feed configuration, water discharge and sediment feed rate and composition are set by the flume operator. The flow depth, bed slope and bed surface grain size distribution are free to adjust and will evolve until a condition of equilibrium transport will be established. In the recirculating configuration water discharge and flow depth are set by the flume operator and bed slope and surface size distribution as well as bed-load transport rate and composition are free to adjust by evolving toward equilibrium.

Guy et al. (1967) demonstrated that in the case of unisize bed material, the two flume configurations will force the establishment of the same equilibrium, which in turn will be independent of the initial conditions. In the case of graded bed material however, the two flume operation configurations might establish two different equilibrium conditions. According to Parker & Wilcock (1993) the reason is that in the recirculating mode the constraints of water discharge and flow depth are not sufficient to determine the final equilibrium that will be achieved. The latter will depend also on the initial bed slope and grain size distribution of the bed material.

The two different operation modes of sediment flumes answer two different questions. The sediment feed flume addresses the question: what is the bed's response to a change in the sediment feed rate? On the other hand the recirculating configuration answers the question: what is the response of the fractional transport rates to a change in the bed slope or the bed material?

Wilcock & Southard (1989) and Parker & Wilcock (1993) have pointed out that the two different equilibrium conditions that might be obtained from the two standard configurations of sediment flume operation for the same bed material, can eventually lead to different transport functions. These transport relations will be directly comparable only if the fractional transport rates are scaled by fractional content on bed

surface. Finally, experiments conducted in recirculating flumes approach better the behavior of gravel bed rivers over short time and space scales, for example during flood events. In contrast, experiments in sediment feed flumes approach better the field case for longer time scales, i.e. decades to centuries with averaged water and sediment supply.

2.4   Adjustments between bed-load and bed surface texture

It is widely accepted that the adjustment of bed surface composition is a necessary mechanism for the establishment of equilibrium transport of non-uniform material. Furthermore, field observations and experimental studies in the laboratory have shown that the grain size distribution of the bed-load might be finer than the bed material that is contained in the subsurface at flow events of low and medium intensity. Results of investigations on the adjustment of bed surface to different conditions of sediment supply and flow strength are presented herein. Additionally how bed-load size distribution changes with varying shear stress is also shown along with findings regarding the inter-relationship between bed-load and bed surface gradation.

2.4.1   Composition of transported material

2.4.1.1 Field studies

Measurements of fractional bed-load transport rates in gravel-bed rivers have revealed that the composition of the transported material can vary widely with flow strength. Jackson & Beshta (1982) sampled bed-load transport in a small sand and gravel bedded channel characterized by a sequence of pools and riffles. They categorized bed-load transport events into two individual phases. During Phase I moderate flow dominated and mainly transport of sand-sized material over the stable armored bed took place. The transported material was considerably finer than the bed material. Phase II corresponded to bed-load transport occurring during higher flow events, that enabled the entrainment of riffle armor. The bed-load transport of phase II proved to be non-uniform in the downstream direction and unsteady over time at a constant discharge. Nonetheless, the transported material was appreciably coarser compared to the transport occurring during Phase I.

Kuhle (1992) published the results of field measurements of fractional bed-load transport rates at Goodwin Creek, a gravel-bed river with width of 20,7 m, slope of 0,0033 and bed subsurface material mean grain size of 8,3 mm. The bed material of

the investigation area was characterized by a bi-modal grain size distribution with prominent modes in the sand and gravel size ranges respectively. The comprehensive data set consisted of 488 samples taken with a modified Heley Smith bed-load sampler, during 21 transport events. He observed, likewise Jackson & Beshta (1982) that during low flows the grain size distribution of transported material was considerably finer than the bed subsurface material. With increasing bed shear stress bed-load became coarser and its size distribution tended to become identical to that of subsurface bed material. Fig. 2.7 shows the composition of transported material during six different flow events at Goodwin Creek. The figure is a reproduced after the originally published results.
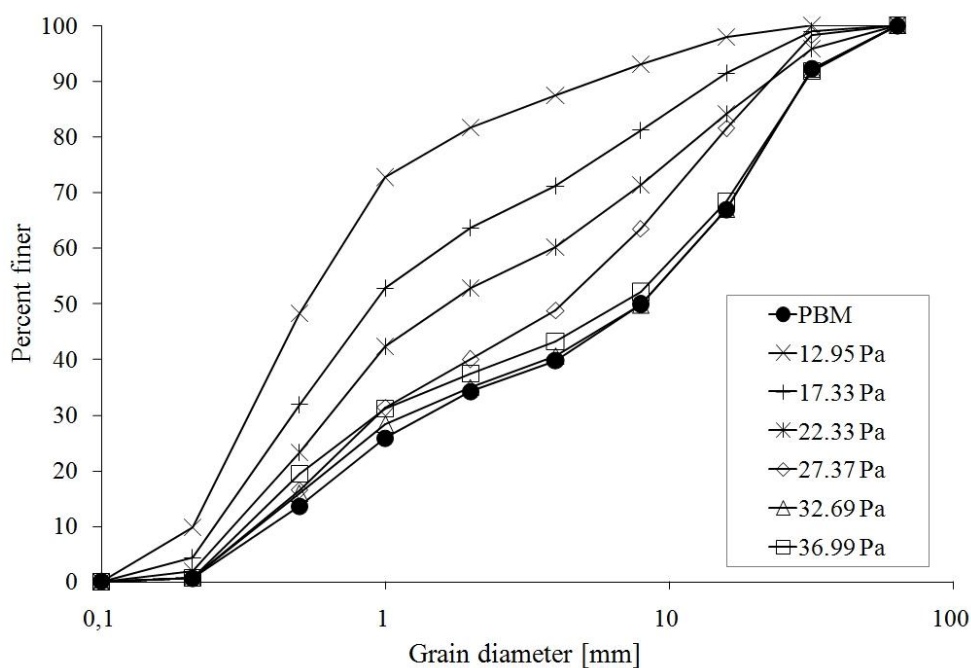
Fig. 2.7   Variation of grain size distribution of transported material with varying shear stress (from Kuhnle (1992))

Wilcock & DeTemple (2005) showed that the fractional bed-load transport rates measured in Oak Creek, a steep, small, with flume-like geometry gravel-bed stream exhibited a systematic coarsening of bed-load with bed shear stress. This behavior was recognized also by Parker et al. (1982a) who first analyzed the Oak Creek data set that was collected by Milhous (1973). In their classical work it is stated that higher shear stresses are associated with larger mean bed-load grain sizes, demonstrating thus a systematic deviation from fractional transport similarity. Therefore they proposed an empirical method for predicting bed-load composition, which included three different transport functions for grains of three different size ranges, in order to achieve a better fit to the field data.

Diplas (1987) published a reanalysis of the Oak Creek data set and also suggested, that the median grain size of bed-load became gradually coarser as flow strength increased approximating the grain size distribution of subsurface material. Furthermore he suggested that the bed-load coarsens when the normalized Shields stress φ_{50}, defined as the ratio of dimensionless shear stress to reference shear stress of d_{50} of subsurface, increases from the value of 0,6 to the value of 1,2. At the upper limit of $\varphi_{50} = 1,2$ the transported material becomes identical to the subsurface material, meaning that the condition of equal condition with regard to subsurface has been reached.

Similar observations on increase of mean bed-load grain size with flow strength have been made and reported also by Ferguson et al. (1989), Church et al. (1991) and Carling (1988).

The previous studies have shown a progressive coarsening of transported material with flow strength. Parker et al. (1982a) have suggested that this dependence of bed-load grain size upon flow intensity appears to result in a mean annual bed-load composition approximating that of the subsurface bed material. Lisle (1995) studied the grain size distribution of the material transported over a long period of time in 13 natural gravel-bedded channels. The main motivation was to investigate whether the subsurface bed material has the same particle size distribution with the longterm averaged bed-load, an approximation that is the basis of the concept of equal mobility. The comparison between bed-load and subsurface bed material composition was based on a collection of field data from previous studies of other researchers and the author, e.g. Smith et al. (1993), Carling (1989) and Lisle (1989) among others.

In most cases the bed-load samples were taken over short and widely spaced time intervals. In order to obtain a representative long-term average bed-load size distribution from the measurements, Lisle (1995) weighted grain size distribution of individual bed-load samples by transport rate and frequency of corresponding water discharge (when the latter was available). With this averaging method he removed the bias of sampling bed-load disproportionally to the frequency of occurrence of discharges. A comparison between averaged grain size distribution of bed-load and composition of substrate bed material composition at fourteen different reaches showed that in six out of thirteen natural gravel bed channels that were studied, the average particle size of bed-load transport over a period of years was finer than that of the subsurface bed material. This result shows that the main hypothesis of equal mobility does not hold always. The ratio of median bed material grain size to median bed-load grain size decreased to unity with increasing drainage area, bank-full discharge, dimensionless stream power and bed material sorting.

2.4.1.2 Laboratory investigations

Wilcock & Southard (1988), Wilcock (1992) and Wilcock & McArdell (1993) also observed a coarsening of bed-load with increasing flow intensity during studies of sediment mixtures transport under equilibrium condition in recirculating flumes. The finer and coarser grain sizes were underrepresented in the composition of transported material at smaller flows and subsequently the transported material was finer than the bulk mix of parent bed material. As flow strength increased the transported material composition tended to become identical to the parent bed material grain size distribution, approaching that way the condition of equal mobility.

2.4.1.3 Effect of increased sand supply on gravel transport rates

Curran & Wilcock (2005) investigated the effect of sand supply on fractional transport rates in a series of flume experiments. They kept the water discharge, water depth and gravel supply rate constant and used different sand feed rates from run to run. Theoretically, the overall increase of sediment being supplied to the flume should lead to an increase in transport capacity, which could be accomplished by an increase in the bed slope. This would be the case if the grain size of the increased supply was kept constant, according to the widely accepted approach of Lane (1955). However, in the experiments of Curan & Wilcock (2005) the sediment supply not only increased but became finer too, as the increase in transport rate was due to a feed of larger amounts of sand, while the gravel feed rate was kept constant. The main focus of the experiments was to document the response of the bed to a progressively increased and finer sediment supply.

The experiments were separated into two segments. During the first phase the sediment feed was identical to the bed material. The second phase commenced as soon as a steady state was established. During that phase the sand feed rate was increased, resulting in an overall increase and a simultaneous fining of the sand-gravel mixture supply. This phase was terminated when a new equilibrium condition had been established. Some of the experiments were supplemented with a third segment, during which the rate and composition of sediment feed was returned to the initial values of the first segment, so as to be verified that the altered rate and grain size distribution of the sediment supply was responsible for the bed response.

The channel bed responded to the larger total sediment supply of the second segment by increasing the sand content on the bed surface and reducing the bed slope. The channel slope reduction took place by bed degradation which was realized by

evacuation of a wedge of sediment that was thicker in the upstream direction. As the sand supply increased from run to run the bed surface sand content and bed slope reduction was consistently bigger. The observed behavior reveals that the variation of sediment feed composition resulted in a change of the fractional mobility. As the sediment mixture became finer, it became more mobile too and consequently it could be transported by the available flow by a smaller shear stress. This is evident in the behavior of gravel fractions. The gravel feed rate was kept constant in the first and the second experimental phases. This gravel transport rate could be transported by a lower shear stress when the sand content of the mixture increased.

The experiments of Curran & Wilcock (2005) are supported by the results of previous studies conducted by Jackson & Beschta (1984), Ikeda & Iseya (1988) and Hassan & Church (2000) that provided indications regarding the increase of gravel fractions mobility due to an increased sand supply. Ikeda (1984) suggested that the increased mobility of gravel can be attributed to three phenomena. These concern the lower drag of gravel particles and higher near-bed flow velocity due to a hydraulic smoothing of the bed by sand, the reduction of friction angle and finally the lack of locations on the bed surface, where the particles could be caught in the wakes of protruding grains.

Venditti et al. (2010) found that the mobility of gravel fractions can be increased also due to addition of suitably finer gravel and not just sand. Furthermore, the authors verified the mechanism that was proposed by Ikeda (1984), based on measurements of near-bed velocity and turbulence. Based on their experimental results they suggested that the grain ratio together with the abundance of finer sediment should be used for the estimation of critical shear stress during bed-load calculations.

2.4.2   Composition of bed surface

Flume experiments and field observations have indicated that the heterogeneity of particle sizes in gravel-bed channels provides a capacity for adjusting to changes in sediment supply or flow strength through changes in the particle size distribution of the surface layer.

2.4.2.1 Investigations in sediment feed flumes

Laboratory investigations in flumes with sediment feed with constant composition identical to that of the parent bed material as upper sedimentological constraint have shown the bed surface grain size distribution to be coarser at low flows and to become

progressively finer as flow strength increases approaching the composition of the subsurface material at sufficiently high shear stress values. These observations are in corroboration with the assumption of Parker et al. (1982) that at high transport rates the coarse grain fraction does not need to be overrepresented on the bed surface because the mobility difference between coarse and fine grain sizes is reduced or even disappears.

Dietrich et al. (1989) carried out experiments in a sediment feed flume. The water discharge and composition of sediment supply in the upstream end of the flume was the same for all experiments, while the transport rate of sediment supply was reduced among the experimental runs. The material used as sediment supply was the same with the bed material initially placed in the flume. The researchers waited until the feed rate matched the measured bed-load discharge at the downstream end of the flume and the water surface slope stabilized. At that time, when equilibrium transport had been achieved, they determined the bed surface grain size distribution by measuring the diameter of grains that were located under fixed points, determined by an overlaid grid. At high bed-load discharge of 1740 g/min m the median grain size of the bed surface was equal to the median grain size d_{50} (3,7 mm) of the load within measurement error. The reduction of sediment feed rate in the following two experimental runs was reduced to 610 and 170 g / min m respectively. This reduction of feed rate was associated not only with a reduction of the water surface slope which was responsible for a lower total bed shear stress and subsequently a lower transport capacity, but with a coarsening of bed surface as well (4,3 mm and 4,7 mm respectively). In total, a 90% reduction in feed rate had as result 32% coarsening of bed surface.

Kuhnle (1989) carried out experiments in a sediment feed flume similar to those previously described, characterized by constant sediment supply and identity between supply, bed-load and bed material composition. He also demonstrated that the mobile bed armor gradually diminished with increasing bed shear stress and hence, increasing bed-load discharge. In the experimental run with the highest feed rate however, the measured median grain size of bed surface was finer than the median grain size of the parent bed material, something that was not observed in the experiments of Dietrich et al. (1989).

Suzuki & Kato (1991) and Suzuki & Hano (1992) also arrived at the conclusion of inverse relation between bed grain size and transport rate, arrived also by conducting experiments with the same procedure. A progressive fining of the bed surface was associated with an increase in transport rate. In addition, they showed that the geometric deviation of the grain size distribution of the sediment mixture (or degree of

uniformity) comprising the initially placed and supplied into the flume material, affected the magnitude of the observed changes in bed surface composition with flow strength. A bed material with a wide grain size distribution, meaning large geometric deviation could achieve a larger degree of coarsening at low flows, becoming finer than the parent bed material when compared to a bed material with small geometric deviation.

Further support for the progressive coarsening of the bed surface as response to the reduction of bed-load transport or equivalent flow strength was provided by the experimental investing ation of Lisle et al. (1993). Finally, field observations that are presented by Lisle et al. (2000) and Lisle & Madej (1992) imply that the adjustments of bed surface texture in local scale within a gravel-bed stream, can be attributed to local variation of boundary shear stress within the under investigation reach.
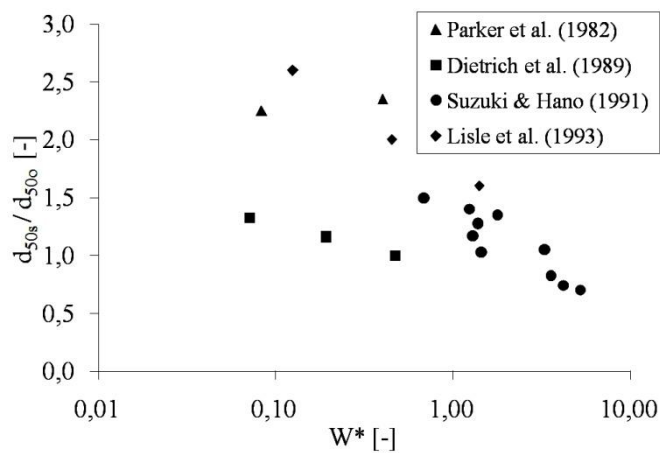
Fig. 2.8 Observations in sediment feed experiments of changes in degree of bed surface coarsening with varying transport rate, when the transported material has the same size distribution with the subsurface material (graphical illustration of experimental results obtained in four different studies)

2.4.2.2 Investigations in recirculating flumes

 All the works that were described above, were limited by the constraint of identity between the grain size distribution of material in transport and grain size distribution of parent bed material or sub-surface material. However, this identity does not occur in the whole spectrum of flows when it is not imposed by the sediment supply boundary condition at the upper end of the reach. If the bed-load is finer than the parent bed material then the bed surface texture adjustment is more complicated and not so clear yet.

Wilcock et al. (2001) investigated the influence of sand content in the bed material on the grain size distribution of the transported material and on the composition of the armor layer by means of an experimental study in a recirculating flume. By adding different proportions of a sand mixture to a gravel mixture, they prepared five different sand-gravel mixtures with sand content 6, 14, 21, 27 and 34 % respectively. They placed these mixtures in a recirculating flume and carried out nine or ten experimental runs with different water discharges with each one of them. They found out that an increase in shear stress was associated with a coarsening of the transported material and an increase of the total transport rate. Furthermore the bed surface grain size distribution showed little or no coarsening with increasing shear stress, over a wide range of flow conditions. This behavior was observed for all sand-gravel mixtures that were used in the experiments. This observation casted doubts on the classical approach that armor layers break-up or weaken during high flows which are associated with large transport rates. This behavior is plotted in fig. 2.9 which shows the observed degree of bed surface armoring against dimensionless transport rate in all experiments of Wilcock et al. (2001).
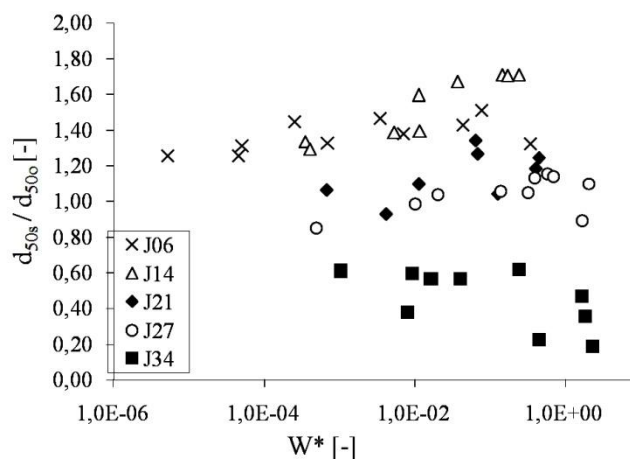
Fig. 2.9   Observations in recirculation experiments of changes in degree of bed surface coarsening with varying transport rate, for five sediment mixtures with different sand content (based on the results of Wilcock et al. (2001)

2.4.2.3 Field measurements

The weakening of armor layer with increasing shear stress or sediment supply is also supported by measurements in ephemeral streams where conditions of extreme high Shields stresses are encountered. Powell et al. (2001) and Laronne et al. (1994) have observed the absence of a coarser surface layer in such ephemeral channels. In addition Laronne & Reid (1993) report the presence of a surface layer that is finer than the subsurface bed material in Nahal Yatir, Israel. In this ephemeral stream, shear

stresses as high as 13 times the critical shear stress during floods have been reported. Finally, the field data of Powell et al. (2001) verify the progressive coarsening of transported material with flow strength and the approximation of equal mobility conditions at high shear stresses. Reid et al. (1996) have tested bed-load equations against a field data set obtained during flash floods. They found that the Meyer-Peter Müller equation performed well. The good performance of MPM equations was attributed to the large supply and absence of coarser armor layers that characterize channels in desert and semi desert environments contrary to perennial rivers that are met in humid zones.

Simon & Thorne (1996) have reported that the eruption of Mount St. Helens resulted in large-scale channel instabilities. These instabilities caused channel adjustments in flow energy and hydraulic properties. They reported that the reduced sediment supply was associated with bed surface coarsening. The authors tried to predict the new stable channel geometry, however their attempts were unsuccessful. This was attributed to the limited ability of the transport equations to predict the energy slope accurately, as the used equations could not account for the transport of sand material over the coarser armor layer, leading that way to an underprediction of the inflow transport rates.

Unfortunately the difficulty of collecting data concerning the bed surface composition during high flows in the field has prohibited us from providing a sound answer to the question of persistence of armor layers during active bed conditions. Andrews & Erman (1986) have published the only field data on bed surface composition during high flows. They conducted measurements in Sagehen Creek, USA during low flow as well as during a snowmelt storm which mobilized most of the available gravel sizes. They found that the median grain size of the bed surface at low flow was 58 mm and during the peak of the flood hydrograph it was 46, when the median grain size of the subsurface was 30 mm, providing that way an evidence of armor layer persistence during active bed conditions.

2.4.3 Interrelationship between bed-load composition and bed surface composition

Wilcock & DeTemple (2005) have arrived to an important conclusion regarding the interrelationship between the composition of bed-load and that of bed surface. They noticed that the main result of experiments conducted in sediment feed flumes was that when the transport rate declines while the composition of transported material is constant and equal to that of parent bed material, the bed surface coarsens (see fig. 2.8). Contrary, recirculating experiments have showed that when the bed-load

discharge is reduced, the grain size distribution of the bed surface becomes slightly coarser or does not change at all (fig. 2.9), while the bed-load becomes finer. The combination of these two observations leads to the conclusion that regardless of the upstream sediment boundary condition the composition of the transported material coarsens in relation to the composition of bed surface with increasing transport rate. This is illustrated in fig 2.10 a and b , where the values of the ratio of median particle size of transport to median particle size of bed surface against dimensionless transport rate from experiments in sediment feed and recirculating flumes are plotted.
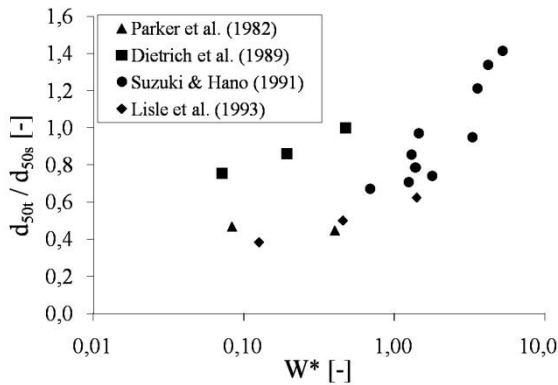
Fig. 2.10a Ratio d_{50tr}/d_{50s} as determined in sediment feed experiments
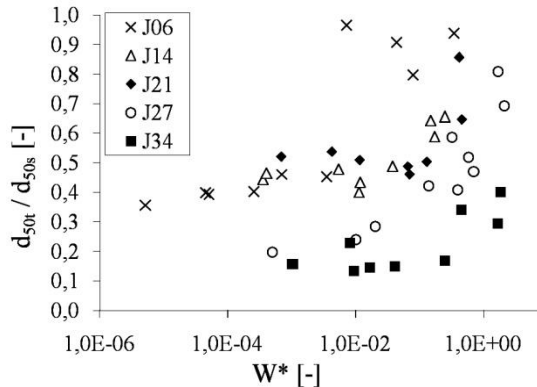
Fig. 2.10b Ratio d_{50tr}/d_{50s} as determined in recirculating experiments

The drawing of fig. 2.10a was based on experimental results of four different previously published studies. Fig. 2.10b was based on the experimental results contained in Wilcock et al. (2001).

Whiting & King (2003) used an extensive data set obtained from field measurements in 12 streams in Idaho, USA in order to investigate which grain fractions were supply limited and which were limited due to incompetent flow. The comprehensive data set was published by King et al. (2004) and contained measurements of flow discharge, fractional bed-load transport rates, grain size distributions of surface and subsurface bed material as well as bed slope, cross-sectional geometry and water depth. The measured flows ranged from below mean annual up to flood events with recurrence interval of minimum seven years. The degree of bed surface armoring (defined as the ratio of median grain size of bed surface to median grain size of subsurface material) varied between 1,7 and 10,2.

Whiting & King (2003), based on the bed-load and flow discharge measurements, also estimated the long-term averaged grain size distribution of transported material, following the method that was initially proposed by Lisle (1995). They found that the ratio D* of median particle size of subsurface material to median particle size of transport- and frequency-weighted bed load was in all channels larger than one. That

means that in all cases the transported material was finer than the subsurface, something that is a violation of the equal mobility concept. An important aspect of the work of Whiting & King (2003) is that they showed that the value of the ratio D* showed a consistent increase with the degree of bed surface armoring. This observation can be interpreted as an indication of bed-load coarsening with weakening armor layers.

2.5   Chapter Summary

If the bed material contains grains of different sizes, i.e. the bed material is non-uniform, then, in comparison to the unisize case, an additional parameter is involved with the establishment of equilibrium bed-load transport. This additional parameter is the grain size distribution of bed surface. It is described as "additional" because contrary with the case of uniform bed material which is characterized only by the grain size d, that remains always the same regardless of the exerted flow strength, in the case of sediment mixtures the composition of bed surface varies under different sedimentological or hydraulic boundary conditions. Thus, the transport capacity depends not only on the exerted flow strength but on the composition of bed surface too. Accordingly, when the transport rate and composition of sediment supply remains constant (determining thus the transport capacity), the equilibrium condition is established by means of bed slope adjustment as well as evolution of an appropriate surface armor layer.

Parker and co-workers gave an explanation for this vertical segregation between surface armor layer and subsurface bed material that is observed in almost all gravel-bed rivers. The intrinsically lower mobility of coarse grains (relative to the mobility of fine grains) is compensated by their over-representation on bed surface. Thus by means of armor layer development particles of different size tend to become equally mobile. However, equal mobility among individual grain classes means that the composition of transported material is identical with the composition of parent bed material. This constrain of the concept of equal mobility is however contradicted by observations on the field as well as in the laboratory especially during low flows. The behavior of preferential transport of fines during low flow events is better explained by the concept of selective transport. However this concept presents its own shortcomings. For example many researchers have observed that the armor layers (in both cases of mobile and static armor layers respectively) contain all grain classes that are met in the substrate material. This phenomenon contradicts the selective transport theory. The concept of partial transport that has been based on experimental work performed by Wilcock and co-workers and has been verified also by field

measurements, provides a theoretical framework that is able to explain the observed changes in grain size distribution of bed surface and transported material respectively.

Nonetheless, the interplay among the three interdependent variables, i.e. the exerted flow strength, the bed surface gradation and the corresponding transport capacity (which includes the fractional transport rate of each individual grain class and consequently the composition of transported material) is not clear yet. Experimental studies with sediment feed configuration have focused mainly on the variation of bed surface with flow strength and/or transport rate. Summarizing the main results of previous research activities on this subject it can be said:

- The bed surface coarsens when the imposed flow strength becomes smaller (and consequently when the transport rate is also reduced). Contrary at high flows the bed surface tends to become identical with (or even slightly finer than) the substrate material. This observation is valid when the transported material has the same composition with the parent bed material.

- Field measurements have shown that the transported material is finer than the substrate bed material during low flow events. When the exerted shear stress increases, bed-load becomes coarser (approaching thus the composition of parent bed material).

- The sand content in bed-load and/or bed surface affects considerably the mobility of gravel grain classes. The particles belonging in gravel size range become more mobile when the sand content in sediment load and subsequently on bed surface increases.

- The previous observations as well as recent field measurements and experimental studies show that coarser armor layers are associated with fining of the transported material.

Non-equilibrium bed-load transport of sediment mixtures concerns the transient processes that define the response of the system to a change of one of the above variables (i.e. exerted flow strength, composition and transport rate of sediment load and bed surface gradation). The prediction of non-equilibrium bed-load transport is based on a quasi-equilibrium approach. After a temporal and spatial discretization, it is assumed that within each finite space element and during each time step a condition of equilibrium transport prevails. Therefore, the employed bed-load predictor should be able to reproduce with the highest possible accuracy the inter-relationship among these three variables, in order to provide adequate predictions during the intermediate stages of non-equilibrium processes.

3. Investigations on static armoring

Non-equilibrium bed-load transport of sediment mixtures is the core of the present study. The formation process of a finally static armor layer, i.e. the transformation of an initially unarmored bed surface to a stable armor layer is a case of non-equilibrium bed-load transport under zero sediment supply. The main results of previous experimental studies on the phenomenon of static armoring are reported in this chapter. The early research activities regarding this phenomenon focused mainly on the final equilibrium condition, i.e. the grain size distribution of the static armor layer and the equilibrium bed slope. These two parameters can define the critical shear stress of graded bed material and therefore are necessary during the design of stable channels. Additionally, some researchers have documented the transient changes in bed-load transport rate and composition that occur during progressive coarsening of bed surface under constraint sediment feed. These results are also reviewed and reported herein.

3.1 Investigations of Harrison

The first perhaps systematic investigation on the phenomenon of static armoring has been carried out by Harrison (1950). He conducted three series of experimental runs with different sediment mixtures. After establishing an equilibrium transport condition in his experiments he cut-off the sediment supply and observed the following coarsening of the bed surface. A parallel degradation along the flume took place in all experiments. The observed erosion stopped when a static armor layer had developed for the two coarser sediment mixtures that were used. When the bed consisted of the third mixture, which was finer than the other, the observed coarsening of the bed surface was not sufficient to stop the erosion.

3.2 Investigations of Gessler

Gessler (1965 & 1970) published his investigation on incipient motion of the graded bed material. His study was based on the argument that the problem of the grain entrainment is closely related to the process of self-stabilization that is observed in alluvial channels with poor sorted sediment, since both of these two conditions refer to a situation where the individual grains are not being removed from the bed. Gessler conducted experiments - similar to those of Harrison - that aimed in the determination of the armor layer composition under different Shields stresses. From the obtained

armor layer grain size distribution F_i he estimated the probability that an individual grain will remain on the bed surface although it has been subjected to the attack of the flow. Finally, based on the assumption that shear stress fluctuations are normally distributed over time, he found the probability that in a given flow the shear stress exerted to an individual grain will be smaller than the critical shear stress of that grain.

Gessler made some important observations on the development of static armor layers. He also observed a parallel degradation during his experiments as Harrison did. Furthermore, he found that the armor layer as well as the material that had been eroded during the formation of the armor coat contained all grain classes present in the parent bed material that was initially placed in the flume. This observation counteracts the concept of selective entrainment because according to the latter only the grains that are small enough under certain flow strength can be entrained and transported downstream. Therefore, the eroded material should only contain the grains which are smaller than the boundary defined by the imposed shear stress and the fractions that can be transported should be exhausted from the developed armor layer.

The eroded material was always finer that the parent bed material used in the experiments. The composition of the eroded material became coarser with increasing flow strength as the composition of the armor layer did too. Gessler published a plot of the measured composition of eroded material in experimental run 1.5 (see fig. 3.1) that shows that the eroded material became slightly finer as the time evolved and the bed surface became coarser. The theoretical approach that he followed was, however, based on the assumption that the grain size distribution of the transported material does not change over time. Therefore, he used an averaged over time grain size distribution estimated from samples of material collected at the downstream end of the flume.
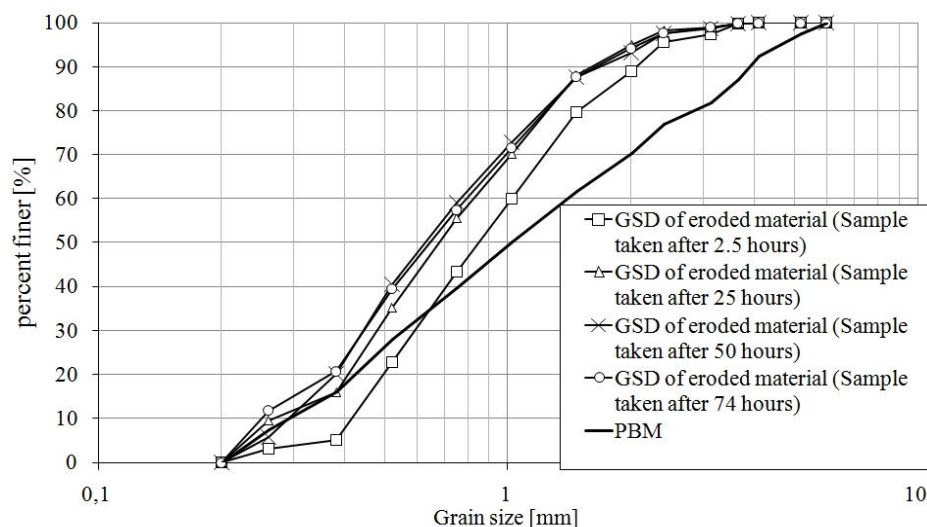
Fig. 3.1: Composition of eroded material in one of Gessler's experiments in different time points (from Gessler (1965))

Based on observations from experimental investigations on transient degradational processes conducted by Willi (1966), regarding rotational erosion, Gessler assumed that a static armor layer might develop when the shear stress is lower than a specific upper limit. This shear stress boundary - according to the theoretical considerations of Gessler - could be calculated with use of the critical dimensionless shear stress related to the maximum grain size contained in the parent bed material mixture. If the applied shear stress is lower than this threshold value then the bed can stabilize by means of a parallel degradation, i.e. without change of the bed slope and a coarsening of the bed surface. If the applied shear stress is higher than the above threshold, then only the coarsening is not sufficient to stabilize the bed and therefore a reduction of the bed slope is also necessary and will result in a reduction of the bed shear stress that will allow a self-stabilization of the bed in conjunction to the bed surface coarsening. Theoretically, the bed surface coarsening should attain its maximum value at this threshold value of shear stress.

3.3   Investigations of Günter

Günter (1971) continued the work of Gessler on incipient motion of sediment mixtures. Based on the theoretical considerations of Gessler he tried to determine the critical hydraulic boundary that would allow a self-stabilization of the river bed by achieving the maximum possible degree of surface coarsening. In his experiments, Günter used a bed from a sediment mixture that initially had a large slope while at the same he fixed the bed elevation at the downstream end of the flume. The experiments were conducted with zero sediment feed. With this arrangement Günter assured that the imposed shear stress would be large enough in order to avoid a parallel degradation and that rotational erosion would take place. The idea was that the slope and consequently the bed shear stress would be reduced until the coarsening of the bed surface which would be sufficient to protect the bed from further erosion. This way, it would establish an equilibrium of zero transport that would have been imposed by the boundary condition of zero sediment supply. The experimental configuration that was employed by Günter is shown in fig. 3.2.
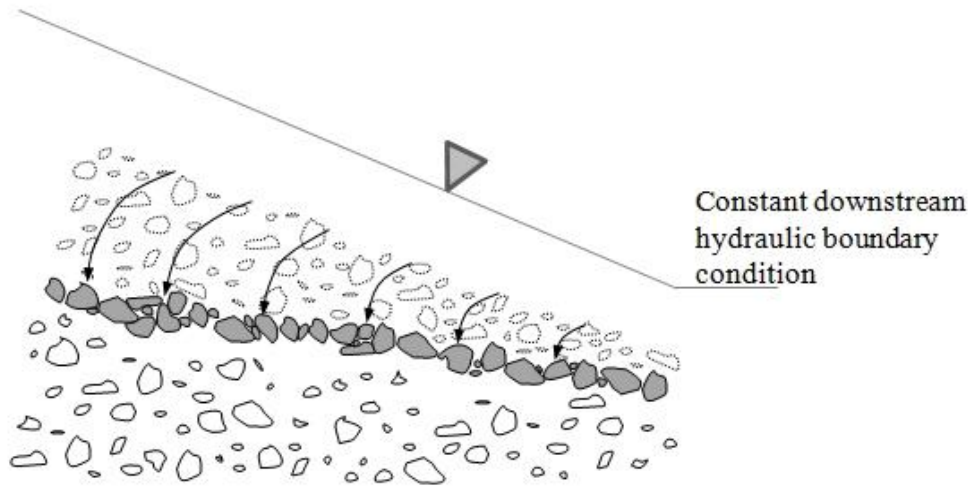
Fig. 3.2   Experimental configuration employed in Günter's study

The bed shear stress at the end of each experiment was estimated by the product of bed slope with water depth and was considered to be equal to the critical shear stress of the sediment mixture. Based on his experimental results, Günter found that the critical dimensionless shear stress of a sediment mixture could be calculated by

$$\tau*_{cdms} = \tau*_{ce} \left(\frac{d_{mo}}{d_{ms}}\right)^{0,33}$$
Eq. (3.1)

where: $\tau*_{cdms}$ is the dimensionless critical shear stress related to median diameter of bed surface

$\tau*_{ce}$ is the dimensionless critical shear stress for uniform bed material (equal to 0,047 according to MPM)

d_{mo} is the median grain size of armor layer on bed surface

d_{ms} is the median grain size of parent bed material

The above equation can be written equivalent as

$$\tau*_{cdmo} = \tau*_{ce} \left(\frac{d_{ms}}{d_{mo}}\right)^{0,67}$$
Eq. (3.2)

where: $\tau*_{cdms}$ is the dimensionless critical shear stress related to median diameter of parent bed material

According to eq. 3.1 the dimensionless critical shear stress related to d_m of the bed surface will be lower than the corresponding dimensionless critical shear stress of a uniform bed material with the same grain size as the bed surface dm. This can be attributed to the fact that a grain that belongs to the armor layer will be entrained rather easier when it is positioned on a finer sediment mixture than on a uniform subsurface.

Günter further investigated the composition of the eroded material during his experiments. He observed that at the beginning of his experiments the transported material was finer than the parent bed material. As time evolved and the bed surface coarsened the transported material tended to have the same grain size composition as the subsurface. This observation shows that the change of bed surface grain size distribution allowed the transport of the bed subsurface material even by a lower shear stress from the initial.

3.4　　Investigations of Chin

Chin et al. (1994) presented the results of an experimental investigation on the influence of parent bed material composition and exerted shear stress by the flow on the phenomenon of bed surface coarsening. In terms of their study, they verified the findings of Gessler (1965) and Günter (1971). They carried out nine series of experiments each with different sediment mixtures from the parent bed material. Every series of experiments consisted of three to six runs, each of them with different flow strength. The main objectives of the experimental plan was to observe the mechanism that governs the phenomenon of bed surface coarsening in order to find the relationship between the degree of bed surface coarsening and the exerted shear stress on the bed and to determine the maximum shear stress that allowed a self stabilization of the bed.

Optical observations made during the experiments revealed that a scour hole was created in front of the larger particles due to the increased exposure to the flow. This scour hole was usually filled with large or medium sized grains that slid in there. Some of the fine grains that were entrained during the formation of the scour hole were deposited at the rear of large particles. The mechanism caused a rearrangement of the surface particles that resulted in a reduced exposure of the larger grains and a better sheltering of the fine grains that remained on the bed surface. The proposed mechanism is similar to the mechanism that was described by Raudkivi (1990) in order to explain the observed embedment at gravel-bed rivers. The clusters that were created that way consisted of particles of all sizes that supported one another while the largest grain functioned like an anchor stone. Due to erosion in the periphery of individual clusters the latter were gradually disintegrated and the process of a new cluster formation was initiated when the anchor stone moved downstream to a new stable location. Thus, the writers attributed the development of armor layers to a continuous process of formation and disintegration of grain clusters. This process is observed more sporadically as the bed surface becomes coarser. Finally, the proposed

mechanism explains the presence of all grain sizes contained in the parent bed material on the armor layer as well as in the eroded material.

Chin et al. (1994) found that the degree of bed surface coarsening, which can be defined as the ratio of a characteristic grain size of the bed surface grain size distribution to the same characteristic grain size of parent bed material, depends mainly on the maximum grain size contained in the parent bed material. In agreement to Gessler (1965) they found that the grain size distribution of the armor layer becomes progressively coarser with increasing flow strength and reaches the maximum degree of coarsening at a specific upper limiting value of exerted shear stress as implied by Günter (1971). The armor distribution skew towards the right with increasing flow strength until the median particle size d_{50s} of the bed surface became approximately equal to 1,8 times, the maximum diameter contained in the parent bed material. Therefore, it can be written

$$\frac{d_{max}}{d_{50s(\text{max})}} = 1,8 \qquad\qquad \text{Eq. (3.3)}$$

where: d_{max} is the coarsest grain size contained in the parent bed material and at the same time in the armor layer

$d_{50s(\text{max})}$ is the d_{50} of the coarsest armor layer that can be developed by a given sediment mixture (when the exerted shear stress by the flow reaches a certain upper limit value)

The above relationship might be used to describe the coarsest armor layer that was developed at the upper limiting shear stress condition, together with the observation that the geometric standard deviation of the fully developed armor layer was equal to 1,5. A further corollary that supports the use of the above value of geometric standard deviation for the fully developed armor layer is that this value of σ_g corresponds to an upper limit of criteria used to distinguish uniform and non-uniform sediment.

Schöberl (1991) discussed that the above equation contradicts the observation of dependence between the grain size distributions of the parent bed material and the coarsest armor layer that the former can develop, which was made by Günter (1971). Furthermore, he commented that this dependence is also obvious in the experimental data of Chin et al. (1994), although ignored. A detailed inspection of the data revealed that the value of the ratio was not constant and equal to 1,8, but decreased from 1,9 to 1,5 depending on the composition of the parent bed material. According to eq. (3.3) two different parent bed material - the grain size distribution of which has as coarsest boundary the same maximum grain size - will develop two identical armor layers attaining the same degree of uniformness (if the ratio $d_{max}/d_{50s(\text{max})}$ is considered to be a

surrogate of the geometric standard deviation σ_g). Although the grain size distribution of armor layers obtained from many studies shows that the armor layers tend to become as uniform as possible, they do not always attain the same degree of uniformity.

Furthermore, similar to Günter, Chin et al. also investigated the upper boundary of shear stress that allows the development of an armor layer that will be stable and protect the underlying subsurface material from further erosion. Therefore, they observed the evolution of erosion with time during each experimental run. When the erosion depth asymptotically approached a limiting value after a finite time period, it was assumed that a stable armor had developed and therefore the imposed shear stress was below the critical shear stress boundary. When the bed degradation continued even after many hours from the time experiment had began, they assumed that under the given shear stress the bed could not become stable and therefore the imposed shear stress exceeded the critical boundary. By interpolation between the higher observed shear stress that led to a stable armor layer and the lowest shear stress that had not allowed a self stabilization of the bed they estimated the maximum shear stress that allowed the development of a stable armor layer.

Based on their own data, as well as those obtained by studies of Günter (1971) and Baker (1986), Chin et al. (1994) found that the limiting dimensionless shear stress for a self-stabilization of a river-bed can be determined by the following equation.

$$\frac{\tau*_{cdms}}{\tau*_{ce}} = \frac{\tau*_{cdms}}{0{,}05} = \left(0{,}4\left(\frac{d_{50s(max)}}{d_{50o}}\right)^{-0{,}5} + 0{,}6\right)^2 \qquad \text{Eq. (3.4)}$$

where: d_{50o} is the median grain of parent bed material

Taking into account eq. (3.3), according to which $d_{max}/d_{(50s)max}$ becomes insensitive to shear stress near the limiting condition and equal to 1,8 eq. (3.4) can be written in the following equivalent form

$$\frac{\tau*_{cdms}}{\tau*_{ce}} = \frac{\tau*_{cdms}}{0{,}05} = \left(0{,}4\left(\frac{d_{max}}{1{,}8d_{50o}}\right)^{-0{,}5} + 0{,}6\right)^2 \qquad \text{Eq. (3.5)}$$

The ratio of maximum grain size d_{max} to median grain size d_{50o} indirectly expresses the degree of nonuniformity of the parent bed material, being a surrogate of geometric standard deviation.

3.5 Investigations of Schöberl

Schöberl (1979) conducted also an experimental investigation on the self-stabilization process of beds with graded material. According to his approach a limiting slope exists, at which the bed cannot be further degraded due to the presence of an armor layer that has attained its maximum degree of coarseness.

The limiting slope can be calculated by

$$S = 0{,}305 \frac{\rho_s - \rho}{\rho} \frac{\varepsilon}{\alpha_g} \left(\frac{1}{F_d}\right)^2 \qquad \text{Eq. (3.6)}$$

where: ρ_s is the density of sediment
        ρ is the density of water
        ε is the relative roughness number
        α_g is a parameter determined by the grain size distribution of parent bed material
        F_d is parameter defined as particular Froude number

The parameter α_g is used to describe the shape of the grading curve of the parent bed material and is given by

$$a_g = \left(\frac{d_{90o}}{d_{50o}}\right)^{1/3} \left(\frac{d_{mo}}{d_{50o}}\right)^{1/2} \qquad \text{Eq. (3.7)}$$

F_d is a parameter, which is defined by Schöberl (1992) as particular Froude number. It is calculated by

$$F_d^2 = \frac{v^2}{g\left(\frac{\rho_s - \rho}{\rho}\right) d_{ms(\max)}} \qquad \text{Eq. (3.8)}$$

where: v   is the maximum permissible flow velocity according to the steepest possible slope
        $d_{ms(\max)}$ is the average diameter of the mature armour layer (coarsest armour layer that the parent bed material can develop), when the sieve analysis is based on an areal sample of bed surface

The relative roughness number is defined by

$$\varepsilon = \frac{d_{ms(\max)}}{h} \qquad \text{Eq. (3.9)}$$

where: h   is the depth of flow

The median grain size of the armor layer at the limiting shear stress condition $d_{50s(max)}$ can be estimated by

$$p_{d50s(\text{max})} = 0,5 + 0,475(1 - d_{90*})^{0,24d_{90*}}$$
Eq. (3.10)

where: $p_{d50s(max)}$ is the relative weight of the original distribution that corresponds to the median grain size of the armor layer at the limiting shear stress condition $d_{50s(max)}$

The dimensionless parameter d_{90*} is given by

$$d_{90*} = \frac{d_{90}}{d_{max}}$$
Eq. (3.11)

The equation proposed by Schöberl for the estimation of limiting slope and consequently the estimation of critical shear stress at the condition of maximum coarsening takes into account the influence of relative roughness as well as Froude number that has been neglected in the previous investigations. Contrary to the relation of Chin et al. (1994) the criterion of Schöberl (1979) predicts a variability of the critical condition, with the product of the parameters α_g and F_d playing the controlling factor.

3.6 Investigations on the formation process of armor layers

The studies presented so far have mainly focused on the hydraulic and sediment conditions under which the bed surface becomes coarser as well as on the development of a predictive relation between the grain size distribution of the final armor layer and the grain size distribution of the parent bed material.

3.6.1 Temporal variation of total transport rate during evolution of armor layers

Lamberti & Paris (1992) and Tait et al. (1992) published the results of two studies regarding the transient changes that take place during the process of formation of armor layers. Relevant observations have been made during the experimental investigations of Proffitt (1980) and Mosconi (1988). They carried out experiments under sediment starved feed conditions with different sediment mixtures as initial parent bed material. The amount of transported sediment consistently diminished with progressive coarsening of the bed surface, as expected. The continuous measurements,

however, revealed two distinct phases in the temporal variation of the bed-load transport rate. During the initial phase the transport rate remained approximately constant or increased to a peak value. During the second phase the transport rate declined for more than one magnitude of orders. This pattern, which characterizes the temporal variation of bed-load transport rate during the formation process of a finally static armor layer, is illustrated in fig. 3.3. This figure shows the variation of the total transport rate with time as observed during an experimental run performed by Tait (1992).
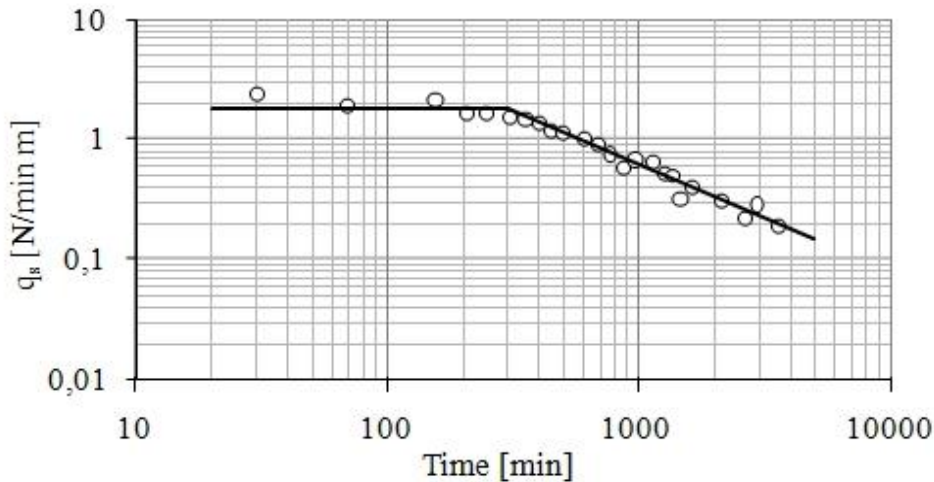
Fig. 3.3   Temporal variation of total bed-load transport rate during experimental run 3 performed by Tait et al (1992)

Tait et al. (1992) showed that the duration of the initial phase of constant transport rate depends on the bed shear stress and on the grain size distribution of the parent bed material. An increase of the exerted drag force on the bed resulted in an onset of the bed-load discharge decline sooner. Similarly, experiments carried out with finer parent bed material led to shorter duration of the first phase. Tait et al. (1992) concluded that the higher fractional content of the fine tail of grain size distribution resulted in a larger amount of grains that could be easily entrained, so the initial phase was prolonged. Mosconi (1988) also made the same observation and called the first phase "armor layer disintegration phase" during which the coarser material is eroded from the surface layer. Mosconi called the second phase "evolution phase". During the second phase, the transport rate diminished rapidly as time progressed. Proffitt (1980) found that the decline of the total transport rate can be described by a power relation of the form:

$$q_{bT} = at^b \qquad\qquad \text{Eq. (3.12)}$$

where: q_{bT} is total bed-load discharge per unit width

t   is time

a and b   are parameters for curve fitting

In the above relation parameter b expresses how fast the reduction of the total transport rate takes place during the formation of a static armor layer and therefore it should be closely associated to the changes that take place on the bed surface gradation. Although a power functional relation could be fitted to the experimental results of all relevant studies, no correlation with flow strength or parent bed material composition is reported in the literature.

3.6.2　Spatial variation of total transport rate during evolution of armor layers

Mosconi (1988) also investigated the spatial variation of fractional transport rates during the formation of an armor layer and found that fractional rates increased slightly in the downstream direction. The increase of q_{bi} with distance was of the same magnitude of order with that reported in the present study. Thus, the experimental results of Mosconi are in agreement with the results of the present study. In fig. 3.4 the total transport rates measured at four different time intervals during Mosconi's experimental run 3-2, against distance from flume inlet are plotted. In the same figure the fitted power functions and their equations are shown. The exponents of the fitted power functions that express a measure of spatial variation of bed-load discharge varied with time in his experiments with a certain pattern. In the early stages they were characterized by low values that approached zero, meaning that bed-load transport did not vary along the flume. As time progressed the value of the exponents increased, approaching unity. This means that transport rate increased linearly with distance.
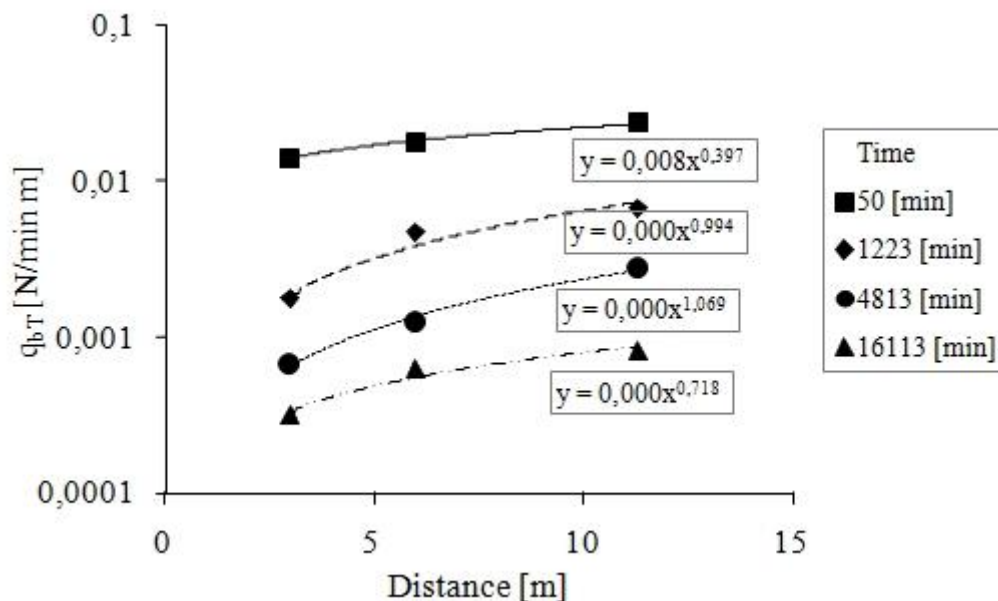
Fig. 3.4　Spatial variation of total bed-load, during experimental run 3.2, in investigation of Mosconi (1988)

A reverse solving of Exner mass continuity equation shows that parallel degradation requires a linear variation of bed-load with distance. Thus, the observed spatial variation of bed-load discharge in the study of Mosconi is in good agreement with the measurements of bed surface elevation during ongoing experiments that reveal a parallel degradation with minor bed slope changes. The parallel degradation was also observed and reported by Harrison (1950), Gessler (1961) and Pender (2001) who performed experiments with the same configuration.

3.6.3 Temporal variation of characteristic grain size of transported material during evolution of armor layers

Lamberti & Paris (1992) and Tait et al. (1992) also presented results regarding the temporal variation of the bed-load composition during the formation of static armor layers. A reduction of the characteristic grain size of the transported material was observed during the experiments in both studies. Tait et al. (1992) documented the development of the modal grain size of the bed-load over time, i.e. the grain size that is most populous by weight. The bed-load initially consisted of rather coarse material. As time progressed the transported material became progressively finer. The measurements also revealed strong fluctuations of the modal grain size. They attributed this phenomenon to a periodic release of waves of coarse material. These waves occurred due to winnowing of the fine material located around the larger particles and the time intervals between them increased with diminishing bed-load discharge.

The same behavior was also observed during the experiments that were conducted by Lamberti & Paris (1992). They investigated also the transient changes in bed-load transport that take place during the formation of a static armor layer. They performed 11 experiments with the same arrangement as the one employed in the present study. During the experiments the authors took several samples of transported material at different time intervals in order to determine the temporal variation of its grain size distribution. In addition, the published experimental results showed a consistent reduction of median grain size of transported material with progressive bed surface coarsening. They presented the temporal variation of d_{50} of the transported material which is shown in fig. 3.5. The median grain size of the bed-load decreased with time during all experiments.
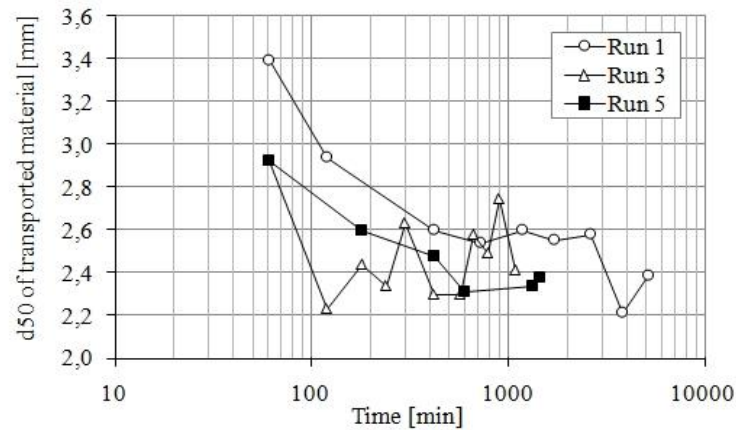
Fig. 3.5 Temporal variation of eroded material's median grain size during experimental runs 1, 3 and 5 performed by Lamberti & Paris (1992)

Fig. 3.6 presents the ratio of d_{50} of the last sample of transported material to d_{50} of the first sample that was taken in each experiment of Lamberti & Paris against dimensionless shear stress related to median grain size of parent bed material τ^*_{d50o}. The values of the plotted ratio are always smaller than one, meaning that the transported material at the end was always finer than the transported material at the beginning of each experiment. Additionally, the plotted values show a clear falling trend with increasing τ^*_{d50o}, which means that the fining was larger as the exerted flow strength increased.
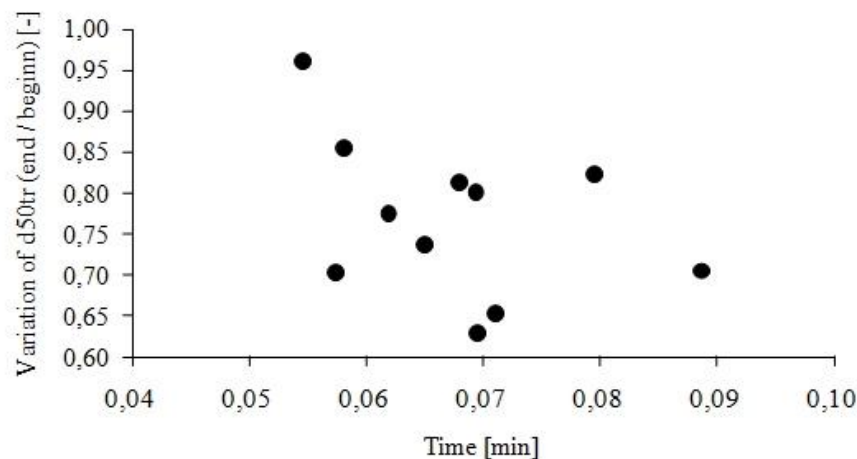
Fig. 3.6 Difference in d_{50} of samples of transported material taken at the end and at the begin of each experiment in the study of Lamberti & Paris (1992)

The experiments of Haynes & Pender (2007) on the influence of antecedent stress history on stability of graded beds were separated into two phases. The first phase was identical with the experiments performed in the present study. By applying different water discharges for various flow durations under zero sediment feed conditions the authors created different armor layers. In the second phase, the stability of the previously created armor layer was tested by applying a water discharge, which was higher than the antecedent and remained constant in all experimental runs. Ockelford

(2011) expanded the study of Haynes & Pender by performing similar experiments with different bed materials. These two investigations are very interesting because they demonstrate the influence of grain size distribution of bed surface on the response during a subsequent higher flow event. Haynes & Pender found that the transported material collected at the end of the first phase of their experiments was finer than the parent bed material and that the fining was progressively larger with increasing antecedent shear stress.

Gessler (1965) also presented a diagram with the measured grain size distributions of the eroded material during one of his experiments. A progressive fining of the bed-load is apparent there too although Gessler did not take it into account and only used the averaged over time values in his analysis. The pattern of progressive fining of transported material during the evolution procedure of an armor layer has been documented also by Pender et al. (2001)

3.7   Chapter summary

The early investigations on the phenomenon of static armoring focused on the final equilibrium condition. This condition is characterized by the established bed slope and the grain size distribution of bed surface when under a given flow no transport takes place. Thus the main objective of these studies was the development of formulas for the prediction of these two parameters. The ability of accurate predictions of the equilibrium bed slope and gradation of bed surface enhanced considerably the designing of stable channels.

Later on, researchers documented the transient changes that take place during the formation of coarse surface layer under sediment starved conditions, i.e. the evolution procedure of a finally static armoring layer. Thus, they provided a description of bed-load transport driven by disequilibrium under the given boundary conditions that lead to the formation of a static armor layer. The main findings are summarized herein.

- The total transport rate declined with progressive coarsening of bed surface.
- The temporal variation of bed-load discharge was segmented into two clearly distinct phases.
- The transported material became progressively finer as the final equilibrium condition of no transport was approached.

These findings will be compared with the experimental results of the present study in order to check their compatibility.

4. Review of bed-load transport predictors

It sounds logical that a predictive model for bed-load transport should be derived from the equations of motion (Navier-Stokes) for turbulent sediment transporting flow. However, the problems of turbulence closure as well as the complexity and the stochastic character of the physics of particle transport in turbulent shear flow haven't allowed a fundamental solution to the problem yet, despite the progress that has been achieved e.g. Diplas (2008), Grünzner (2009). The common approach that is currently employed focuses on the formulation of a mathematical framework, which can describe the sediment transport processes rationally. It usually involves a number of equations, which contain some adjustable parameters that are determined by fitting the equations on data sets of sediment transport rate measurements obtained in the field or in the laboratory.

4.1 Bed-load transport models for uniform bed material

The first transport models were derived from data sets that were obtained from experimental investigations performed with uniform bed material. It is useful to present the theoretical background of these models because it remains the same to a large extent for the latest bed-load predictors of non-uniform bed material, as well.

4.1.1 Dimensional analysis for bed-load transport of uniform bed material

In terms of this framework it is assumed that the bed-load discharge depends on a number of variables that represent the forces acting on the bed due to the flow, the properties of the fluid and finally the properties of the particles that are contained in the bed material. These variables are shown in fig. 4.1.
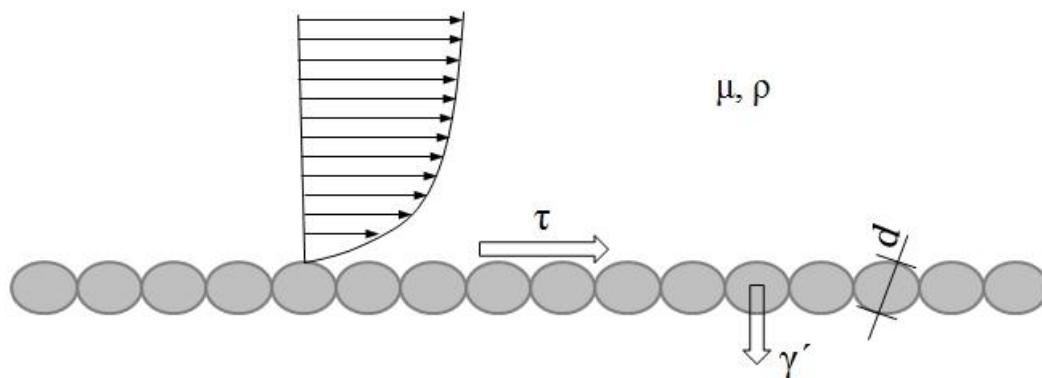
Fig. 4.1 Variables that affect bed-load transport of uniform bed material

In the literature are found different sets of parameters that define the steady and uniform two-dimensional two-phase motion for the case of uniform bed material, e.g. Yalin (1992), Southard (2006). Wilcock (2004) carries out the dimensional analysis with the set of controlling parameters contained on the right side of eq. 4.1 for the case of flow over uniform granular bed material.

$$q_b = f(\tau, h, d, \rho_s, \rho, \mu, g)$$ Eq. (4.1)

where: q_b is bed-load transport rate

 f denotes a functional relation

 τ is boundary shear stress

 h is flow depth

 d is grain size of bed material

 ρ_s is sediment density

 ρ is fluid density

 μ is viscosity of the fluid

 g is gravitational acceleration

Shear stress τ and flow depth h represent the forces that act on the bed due to the flow of water. Grain size d and sediment density ρ_s describe the granular material that forms the bed. Water density ρ and water viscosity μ represent the properties of water. Acceleration of gravity g influences the flow of water as well as the movement of sediment particles.

According to Wilcock (2004) eq. (4.1) is reduced to the following dimensionless functional relation.

$$q_b^* = f\left(\tau^*, Re^*, s, \frac{d}{h}\right)$$ Eq. (4.2)

Where:

q_b^* is the dimensionless bed-load transport rate or Einstein transport parameter

$$q_b^* = \frac{q_b}{\sqrt{(s-1)gd^3}}$$ Eq. (4.3)

τ^* is dimensionless shear stress or Shields parameter

$$\tau^* = \frac{\tau}{(s-1)\rho gd}$$ Eq. (4.4)

Re^* is the particle Reynolds number

$$Re^* = \frac{\sqrt{(s-1)gd^3}}{\mu/\rho} \qquad\qquad \text{Eq. (4.5)}$$

and s is the submerged specific gravity of sediment

$$s = \frac{\rho_s}{\rho} \qquad\qquad \text{Eq. (4.6)}$$

Eq. (4.2) has four parameters on the right hand side instead of seven and at the same time it holds all the information that is contained in eq. (4.1). It can be further reduced under some conditions. Eq. (4.2) can be applied only in the case of flow of water over particles with quartz density. The flow depth must be a few times greater than the grain diameter d. Finally, the grains cannot be very small. For example, they must be coarser than e.g. 0,2 mm. These conditions are almost always fulfilled in the case of gravel-bed rivers. Therefore, the last three parameters in the bracket of eq. (4.2) can be dropped and the equation can now be written

$$q_b^* = f(\tau^*) \qquad\qquad \text{Eq. (4.7)}$$

The transport functions are usually written in the following form

$$q_b^* = a(\tau^* - \tau_c^*)^b \qquad\qquad \text{Eq. (4.8)}$$

where: τ_c^* is dimensionless critical shear stress

The dimensionless critical shear stress τ^*_c is a threshold value that represents the required dimensionless shear stress for the entrainment of the grains. It will be further analyzed in a following chapter. The term within the bracket in eq. (4.8) expresses the excess shear stress that is responsible for the bed-load transport.

4.1.2   Examples of transport formula for uniform bed material

Parameters a and b are obtained from fitting the above functional relation on data sets of transport rate measurements coupled with the corresponding dimensionless shear stress.

For example the Meyer-Peter & Müller transport formula is written

$$q_b^* = 8(\tau^* - \tau_c^*)^{3/2} \qquad\qquad \text{Eq. (4.9)}$$

The above expression of the M-PM formula is simplified as the terms for the wall and bed-form shear stress correction have been neglected.

4.2   Bed-load transport models for sediment mixtures

Meyer-Peter and Mueller (1948) carried out experiments not only with uniform bed material but with sediment mixtures as well, during their pioneering work. They suggested that the total bed-load transport rate in the case of poor sorted bed material could be predicted with the direct application of the transport formula that they published with the use of geometric mean grain size of the sediment mixture. The use of a representative grain size for the prediction of total bed-load transport rate was suggested by Engelund and Hansen (1972) too. An implication of this methodology was that it was assumed that the grain size distribution of the transported material was identical to the grain size distribution of the parent bed material. Further research on bed-load transport of sediment mixtures has shown that the identity between transported and bed material composition does not always hold, especially during low flows, e.g. Jackson and Beschta (1982), even under equilibrium conditions. Although the above mentioned methodology was practical as it only required the knowledge of a representative grain size regarding the bed material, was not able to follow the observed changes in the grain size distribution of the bed-load transport. Leopold (1992) showed that it could lead to under-predictions of the transport rate for the fine grain classes, which could be significantly larger than the transport rate of gravel grain fractions. Therefore, more sophisticated models, which were able to predict the transport rate of individual grain fractions, were formulated.

4.2.1 Dimensional analysis for bed-load transport of sediment mixtures

If the bed material is a sediment mixture which contains different grain sizes di with fractional content of f_i then eq. (4.1) it can be recast as

$$q_{bi} = f\left(\tau, h, \rho_s, \rho, \mu, g, d_i, d_m, \sigma_g\right)$$ Eq. (4.10)

where: q_{bi} is bed-load transport rate per unit width per unit fraction content
         d_i is diameter of particles belonging to i^{th} grain class
         d_m is mean size of grains belonging to the sediment mixture
         σ_g is standard deviation of sediment mixture grain sizes

With the application of the dimensional analysis, eq. (4.10) is reduced to the following dimensionless form.

$$q_{bi}^* = f\left(\tau_i^*, Re_i^*, s, \frac{d}{h}, \frac{d_i}{d_m}, \sigma_g\right)$$ Eq. (4.11)

Where:

f denotes a functional relation

q^*_{bi} is the dimensionless bed-load transport rate per unit width per unit fraction content

$$q_{bi}^* = \frac{q_{bi}}{f_i\sqrt{(s-1)gd_i^3}}$$ Eq. (4.12)

f_i in eq. (4.12) can represent the fraction content of ith grain class either in the surface layer or in the subsurface.

τ^* is dimensionless shear stress or Shields parameter, which may contain the parameter d_i

$$\tau_i^* = \frac{\tau}{(s-1)\rho g d_i}$$ Eq. (4.13)

Re_i^* is the particle Reynolds number corresponding to i^{th} grain class

$$Re^* = \frac{\sqrt{(s-1)gd_i^3}}{\mu/\rho}$$ Eq. (4.14)

Under the assumptions of large particle Reynolds numbers in order to assure that the flow is hydraulically rough and large flow depth relative to the grain size it is justified to reduce further eq. (4.11) to

$$q_{bi}^* = f\left(\tau_i^*, \frac{d_i}{d_m}, \sigma_g\right)$$ Eq. (4.15)

By dividing both sides of eq. (14) by $\tau_i^{*3/2}$ an equivalent form can be obtained.

$$W_i^* = f_1\left(\tau_i^*, \frac{d_i}{d_m}, \sigma_g\right)$$ Eq. (4.16)

W^*_i is a second dimensionless expression for bed-load transport rate per unit width per unit fraction content such that

$$W_i^* = \frac{q_{bi}^*}{\tau_i^{*3/2}} = \frac{(s-1)gq_{bi}}{f_i u_*^3}$$ Eq. (4.17)

f_1 denotes a functional relation, which is given by

$$f_1 = \frac{f}{\tau_i^{*3/2}}$$

Eq. (4.18)

Eq. (4.16) has the advantage of setting the parameter of grain size d_i only on the right hand side of the equation, as the parameter W_i^* does not contain d_i by definition. In this way, it is easier to investigate the influence of grain size on fractional bed-load transport.

To summarize, the previous analysis shows that the transport rate for each grain class can be calculated by a functional relation that requires as independent variables the imposed shear stress, the grain size of the grain class, a mean grain size for the sediment mixture and the arithmetic standard deviation of the sediment mixture.

4.2.2 Similarity hypothesis

According to eq. (4.15) or eq. (4.16) the fractional dimensionless bed-load transport rate is a function of not only τ_i^* but of the ratio d_i/d_m too. That means that the function which relates q_{bi}^* to τ_i^* may differ with grain size. In order to investigate whether a single universal function that can describe the variation of W_i^* with τ_i^* for all grain sizes exists, the measured values of W_i^* or q_{bi}^* are plotted against the corresponding τ_i^* as it is shown on the right hand side of fig. 4.2. By normalizing both the dependent and independent variables of W_i^* and τ_i^* respectively, with appropriate scaling factors W_r^* and τ_{ri}^*, it is investigated whether a consistent collapse of the normalized pair of measurements on a unique curve can be pursued.
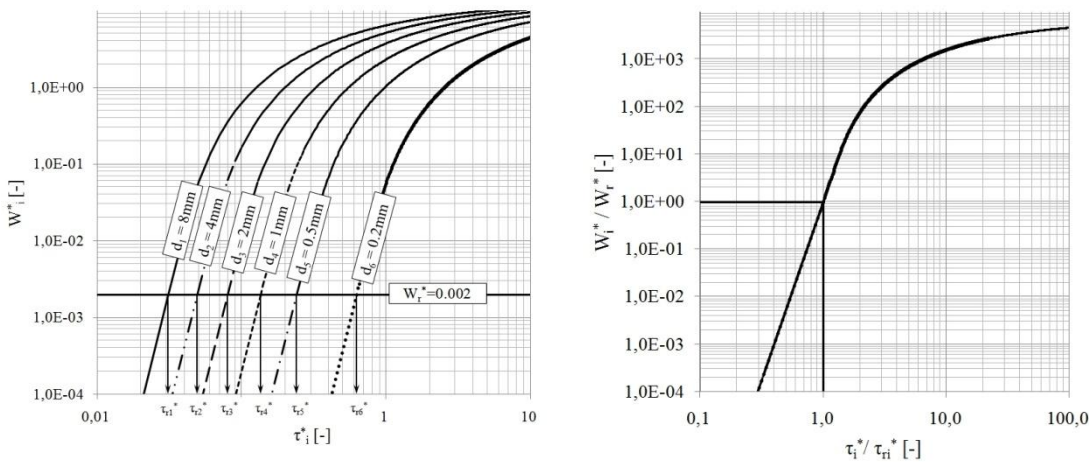
Fig. 4.2 Plot of fractional transport curves and similarity collapse into one universal curve after normalization (reproduction after corresponding figure in Parker (2008))

The idea of normalizing the dimensionless shear stress with a reference value, was initially introduced by Ashida & Michiue (1972) and has proven to be a valuable tool in the analysis of fractional bed-load transport. Parker (1990), Wilcock & McArdell (1993), Wilcock (1997) and Wilcock & Crowe (2003) have showed that the variation of W^*_i with τ^*_i, when the former is related to the fractional content of bed surface, can be sufficiently approximated for all grain classes by a unique function of the form.

$$\frac{W^*_i}{W^*_r} = G\left(\frac{\tau^*_i}{\tau^*_{ri}}\right)$$

Eq. (4.19)

τ^*_{ri} is a reference value of the fractional dimensionless shear stress at which W^*_i becomes equal to a standard predefined value W^*_r, which should account for transport that is slightly above the threshold condition of incipient motion.

Parker et al. (1982a) showed that a definite tendency toward similarity existed when the dimensionless transport rate W^*_i was related to the fractional content of the substrate material. The authors used this tendency to develop a transport function which only required the d_{50} of the substrate bed material as input data. However, the authors stated that the assumption of perfect similarity provided a useful first approximation. In the same paper they published a method which incorporated a deviation from the similarity which was necessary to describe the tendency of the bed-load to coarsen with increasing flow intensity. This deviation from similarity suggested three different transport functions for three different grain size ranges.

Diplas (1987) reanalysed the field data of Oack Creek, which were used for the derivation of the Parker et al. (1982) model and used a different similarity approach in order to obtain a better approximation. By plotting the related to substrate values of W^*_i against τ^*_i and fitting curves of the form $W^*_i = a_i (\tau^*_i)^{mi}$ he found that the exponent m_i exhibited a consistent increase with d_i. The use of a new similarity parameter that incorporated this dependence on d_i led to a better collapse of the measurements on a single curve. Diplas (2005) used the same methodology to obtain a better similarity collapse for the experimental data of Proffitt (1980).

4.3   Incipient motion of uniform bed material

The question of incipient motion of grains due to forces acting on them by the flow of water has been a topic of intense research for 80 years. It has wide applications to numerous engineering problems like the design of stable channels, the protection against scour, the prediction of sedimentation upstream and the degradation

downstream of a dam and assessment of aquatic habitat among others. The main objective was to determine the necessary shear stress for entraining a grain that lies still on the bed surface into motion. This threshold value is called critical shear stress. The determination of the critical shear stress is based on the classical work of Shields (1936) according to which

$$\tau_c^* = \frac{\tau_c}{\rho(s-1)gd} = f(Re^*) \qquad\qquad \text{Eq. (4.20)}$$

where: τ_c^* is dimensionless critical shear stress

τ_c is critical shear stress for entrainment of grain

d   is diameter of grain

f   denotes function

Re^* is boundary Reynolds number related to grain size d

Shields conducted an experimental investigation in order to determine the critical shear stress and subsequently its dimensionless counterpart which was defined by dimensional analysis. He found τ_c by plotting the measured transport rates against the corresponding shear stresses and extrapolating the resulting curve to zero transport. Fig. 4.3 is the originally published diagram which was derived from Shields experimental results as well as the results of previous investigations on transport of uniform bed material. Shields demonstrated that τ_c^* of uniform grains varies with boundary Reynolds number Re^*. At high boundary Reynolds numbers, rough turbulent flow prevails, something that is always the case in gravel bed rivers, In that case τ_c^* is independent of Re^* and equal to 0,06. The choice of the value of 0,06 was supported by a single data point. Miller et al. (1977), Yalin & Karahan (1979), Meyer-Peter & Mueller (1948) found that in the area of rough turbulent flow τ_c^* is equal to 0,045-0,047. Buffington & Montgomery (1997) published a comprehensive analysis of the studies regarding incipient motion that have been published during the last 80 years. They showed that much of the scatter is owed to biases introduced by the employment of different investigative methodologies.
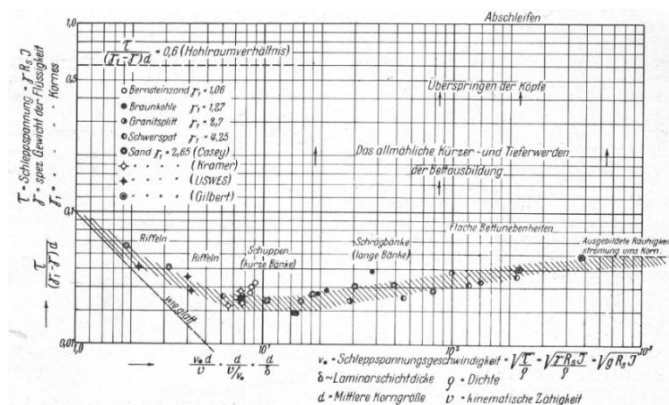
Fig. 4.3   Shields curve, as it was originally published (from Shields (1936))

In order to explain the physical meaning of critical dimensionless shear stress an oversimplified mechanical model will be employed. The following analysis is taken by Malcherek (2006). The model consists of a grain resting on two similar grains and is graphically illustrated in fig. 4.4. The forces that act on the spherical sediment particle are drawn on the same figure.
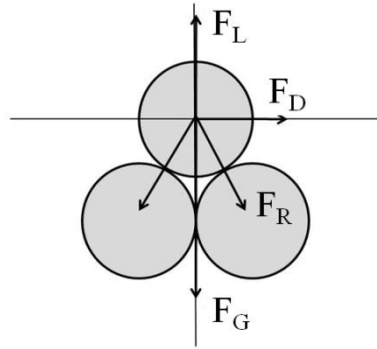
Fig. 4.4 Equilibrium of forces acting on sediment particle resting on two similar grains

The forces that act on the sediment particle by the flow of water are:

The submerged weight F_G given by

$$F_G = \frac{1}{6}(\rho_s - \rho)\pi g d^3$$

Eq. (4.21)

where: ρ_s is density of sediment

The Coulomb resistance force F_R, given by

$$F_R = C_1 F_G$$

Eq. (4.22)

where: C_1 is constant, which is function of the angle of repose of the granular material

The lift force F_L, given by

$$F_L = C_2 \tau_B d^2$$

Eq. (4.23)

where: C_2 is constant

The drag force F_D, given by

$$F_L = C_3 \tau d^2$$

Eq. (4.24)

where: C_3 is constant, which is a function of boundary Reynolds number

A grain is in a state of incipient motion when the following condition is satisfied:

$$M_o = M_R$$

where: M_o is overturning moment due to to F_D and F_{Rx}
   M_R is resisting moment due to F_L and F_G

By substituting eq. (4.21) – (4.24) to eq. (4.25)

$$(F_L - F_L)\frac{d}{2}\sin\varphi = F_D\frac{d}{2}\cos\varphi$$

$$\left[(\rho_s - \rho)g\frac{\pi d^3}{6} - C_2\tau_c d^2\right]\sin\varphi = C_3\tau_c\frac{\pi d^2}{4}\cos\varphi$$

$$\tau_c = \frac{2}{3}\frac{\pi\tan\varphi}{C_3\pi + 4C_2\tan\varphi}(\rho_s - \rho)gd$$

$$\theta_c = \frac{2}{3}\frac{\pi\tan\varphi}{C_3\pi + 4C_2\tan\varphi}$$

Eq. (4.26)

where: φ is the angle of repose of the granular material

Although this relation is practically useless due to the over-simplified mechanical model and the number of undefined variables it shows that the dimensionless critical shear stress is a function of the shape and the packing arrangement of the particles on the bed surface. When the bed material is uniform, the packing arrangement is independent of the grain size and therefore the grains start moving at the same dimensionless critical shear stress regardless of their size.

4.4   Incipient motion of sediment mixtures

In the case of uniform bed material of grain size d it was shown by many researchers that the dimensionless critical shear stress τ^*_c is equal to 0,045 for rough turbulent flow and consequently the grains start moving at shear stress equal to $\tau_c = \tau^*_c$ $(\rho_s - \rho)gd$. In the case of sediment mixtures the problem of incipient motion can be postulated as follows: If the bed consists of a mixture of grains with sizes d_i and geometric mean size d_m will the sediment mixture behave as if the bed consisted of a uniform granular material with grain size d_m?

4.4.1 Absolute and relative grain size effects on incipient motion of sediment mixtures

If the grains of size d_i behaved as though they were surrounded only by grains of the same size as themselves, that would mean that regardless of their size d_i, the grains would start moving at the same dimensionless critical shear stress $\tau^*_{ci} = \tau^*_{cm} = 0,045$, with τ^*_{ci} denoting the critical Shields parameter of grain with size d_i and τ^*_{cm} denoting the critical Shields parameter of grain with size d_m equal to the geometric mean size of the sediment mixture. Subsequently, the grains with size d_i would require a shear stress equal to $\tau_{ci} = \tau^*_{cm} (\rho_s - \rho)gd_i$ in order to be entrained. That means that the critical shear stress would increase linearly with grain size or in other words, the smaller grains would start moving at a lower shear stress compared to the coarse grains. This scenario can be characterized as grain-independent because the grain behavior is not affected by its surroundings (independence). It is more difficult for the large grains to be entrained because of the larger mass and thus the larger weight.

However, the behavior of the grains that belong in a sediment mixture and especially those grains that are located on the bed surface layer and are attacked by the flow are influenced by the degree of sheltering that their surroundings offer. The coarse grains are more exposed because they protrude more into the flow while the fine grains can find shelter behind coarse grains and in this way they reduce their exposure to the drag force of the flow. This behavior is illustrated in fig. 4.5 where the packing arrangement of a grain of size d_i is compared to the case of sediment mixture and the unisize case. It can be assumed that the coarse grains are more exposed to the flow when they belong to a sediment mixture than if they belonged to a uniform bed material. On the contrary, the fine grains are better sheltered in the environment of a sediment mixture than in the environment of a uniform bed material. The above described effects on the packing arrangement of grains with different sizes due to the grain size gradation are called hiding effects.
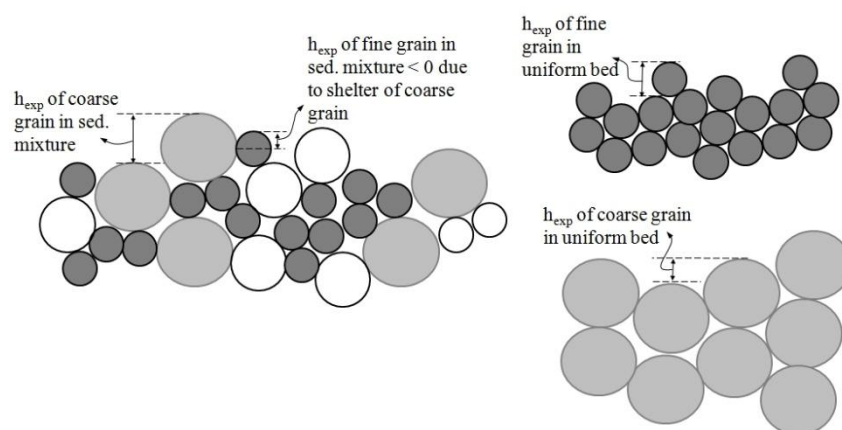
Fig. 4.5 Packing arrangement of particles of the same size when they belong to a sediment mixture or to a uniform bed material

By combining the behaviors that were described in the two previous paragraphs it is concluded that the larger grains are intrinsically harder to be entrained because of their mass. However, this difficulty is compensated by the hiding effects that render them more exposed to the drag force of the flow than what they presumably would be if they belonged to a uniform grain population of the same size. On the other hand, the fine grains, by their nature, require a low critical shear stress in order to start moving because of their small weight. The better shelter they find in a sediment mixture (because of the presence of larger grains) makes their entrainment more difficult than what it would be if they belonged to a uniform population of the same grain size. Therefore, the hiding effects reduce the difference in the necessary shear stress for entrainment of grains of different size that belong to the same mixture. If the hiding effects totally eliminate the difference among the required critical shear stresses of grains of different grain size, then all the grains that comprise the sediment mixture will start to move simultaneously if the imposed boundary shear stress exceeds a threshold value. In that case the sediment mixture would behave as a uniform bed material of the grain size equal to the geometric mean size d_m of the mixture. The critical shear stress of the mixture would be determined by d_m and the dimensionless critical shear stress τ^*_{cm} related to d_m. This condition is called by Parker condition of equal threshold.

The two extreme conditions of grain independence and equal threshold that were described above can be described mathematically in the following way. By the condition of grain independence the particles start moving at the same dimensionless critical shear stress, regardless of their size. Therefore, it can be written

$$\tau^*_{ci} = \tau^*_{cm} \ or \ \frac{\tau^*_{ci}}{\tau^*_{cm}} = 1 \qquad \text{Eq. (4.27)}$$

where: τ^*_{ci} is dimensionless critical shear stress related to grain size d_i
τ^*_{cm} is dimensionless critical shear stress related to geometrical mean grain size d_m

Equivalent, eq. (4.27) can be written

$$\frac{\tau_{ci}}{\rho(s-1)gd_i} = \frac{\tau_{cm}}{\rho(s-1)gd_m}$$

$$\frac{\tau_{ci}}{\tau_{cm}} = \frac{d_i}{d_m} \qquad \text{Eq. (4.28)}$$

where: τ_{ci} is critical shear stress of particle with size d_i
τ_{cm} is critical shear stress of particle with size d_m

By the condition of equal threshold the grains are entrained at the same treshold value of shear stress, regardless of their grain size and thus it can be written

$$\tau_{ci} = \tau_{cm} \ or \ \frac{\tau_{ci}}{\tau_{cm}} = 1 \qquad\qquad \text{Eq. (4.29)}$$

Equivalent eq. (4.29) can be written

$$\tau_{ci}^* \rho \ (s-1)gd_i = \tau_{cm}^* \rho \ (s-1)gd_m$$

$$\frac{\tau_{ci}^*}{\tau_{cm}^*} = \left(\frac{d_i}{d_m}\right)^{-1} \qquad\qquad \text{Eq. (4.30)}$$

Eq. (4.27) and (4.30) now can be written

$$\frac{\tau_{ci}^*}{\tau_{cm}^*} = \left(\frac{d_i}{d_m}\right)^{-m} \qquad\qquad \text{Eq. (4.31)}$$

Similarly eq. (4.28) and (4.29) can be writen

$$\frac{\tau_{ci}}{\tau_{cm}} = \left(\frac{d_i}{d_m}\right)^{1-m} \qquad\qquad \text{Eq. (4.32)}$$

Eq. 4.31 and 4.32 when m takes value 0, 1 and 0,8 are plotted in fig. 4.6 with straight, dashed and dotted lines respectively. It can be considered that m reflects the influence of hiding effects on the behavior of the sediment mixture regarding incipient motion. The parameter m takes the value of 0 for the case of grain independence and becomes equal to 1 for the condition of equal threshold. A value between 0 and 1 would mean that due to the hiding of the difference of critical shear stress among different grain classes is reduced but is not totally eliminated. A value closer to 1 means that the hiding is important and the difference in the required shear stress for entrainment among the various grain sizes is small.
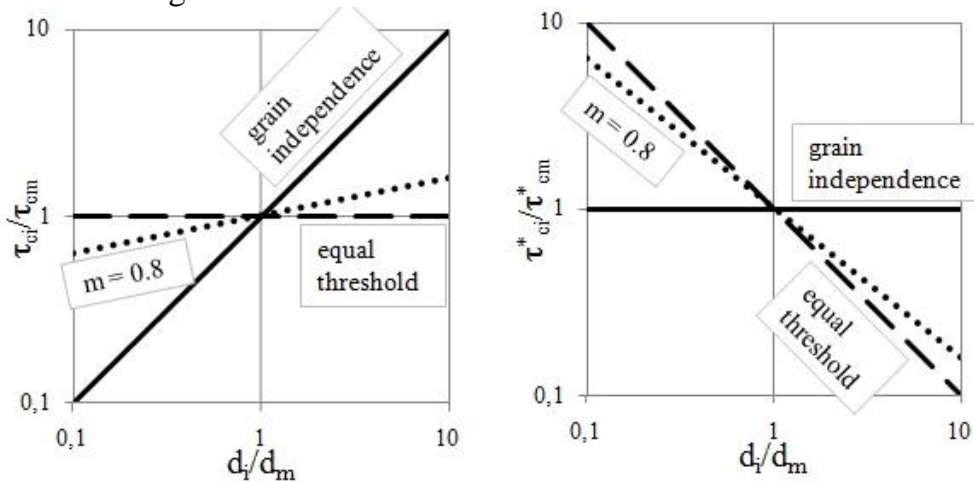
Fig. 4.6 Plot of eq. (4.31) and (4.32) for m = 0, 0,8 and 1

4.4.2   Hiding effects for different types of bed material

The question that arises is which of the above mentioned behaviors is observed in the sediment mixtures that are found in natural gravel-bed rivers. Wilcock (1993) showed that the critical shear stress in unimodal and weakly bimodal sediment mixtures does not change with grain size. Examples of such sediment mixtures are a mixture that contains grain in the size range between sand and pea gravel, or a mixture only with grains of different sizes in the gravel size range and a small content of sand. All grains that are contained in such a sediment mixture are entrained at the same shear stress. The value of the critical shear stress depends on a characteristic grain size like d_{50}. Thus, the critical shear stress of individual grain fractions of a not too widely sorted sediment mixture do not exhibit significant variation and can be estimated with the use of the Shields curve and the corresponding median grain size d_{50} of the sediment mixture. Wilcock & Southard (1988) showed that the condition of equal threshold holds for a wide range of grain size distributions like lognormal, skewed or rectangular as long as they are unimodal or weakly bimodal.

However, further investigations on the condition of incipient motion for a wide range of sediment mixtures showed that in some cases the grain size affects the required shear stress for entrainment significantly. Wilcock (1992) showed that in sand-gravel sediment mixtures with high sand content the fractional critical shear stress might increase with grain size. This behavior was observed for bimodal sediment mixtures, i.e. mixtures, the grain size distribution of which has a prominent mode in the gravel size range and another mode in the sand size range. Nevertheless, not all bimodal mixtures showed this size of selective behavior. When the gravel mode was significantly larger than the sand mode the sand grains started moving at lower shear stress than the gravel grains. Wilcock (1992) concluded that the condition of equal threshold stops to hold when the two modes are separated in size by a factor smaller than a boundary which lies between 2,8 and 8. This finding was in agreement with previous investigations of Misri et al. (1984) who also investigated the incipient motion of bimodal sediment mixtures.

The reference shear stress values for different sediment mixtures that were found in the comprehensive investigations of Wilcock and his co-workers as well as in the Shields curve are plotted in fig. 4.7. The mixtures MC-50, FC-50, FC-70 were bimodal and differed in terms of distance between the two modes of the distribution i.e. MC-50 and FC-50 and sand content i.e. FC-50 and FC-70. The other mixtures were unimodal and differed in terms of median diameter, i.e. $d_{50\_FUNI} < d_{50\_MUNI} < d_{50\_CUNI}$ and degree of sorting, i.e. $\sigma_{g\_1\Phi} > \sigma_{g\_1/2\Phi} > \sigma_{g\_MUNI}$.
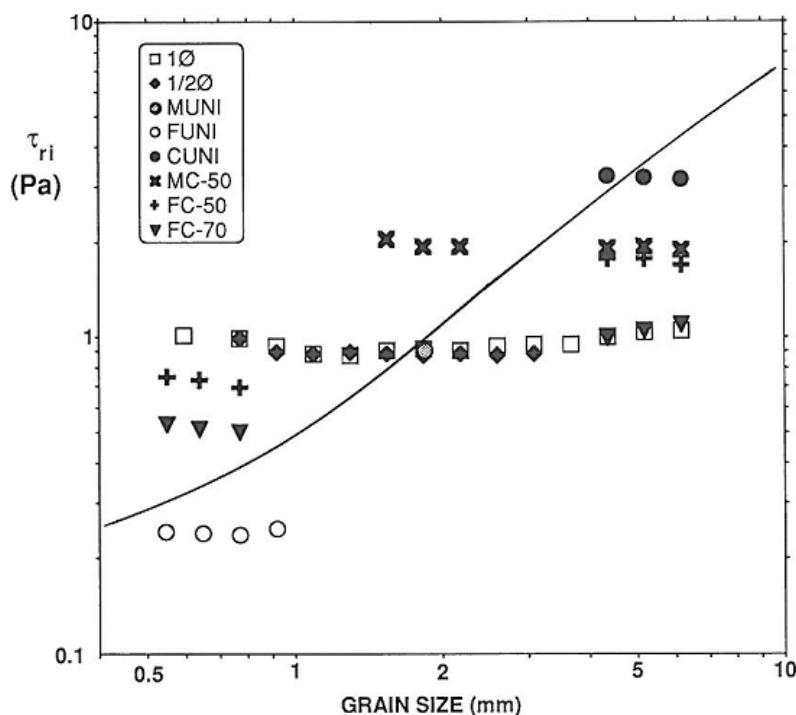
Fig. 4.7 Fractional reference shear stress for different types of sediment mixtures (from Wilcock (1992))

The reference shear stress did not vary with the grain class size or with the degree of sorting. It only varied with median grain size for the unimodal sediment mixtures that were tested as well as for the mixture MC-50, which was weakly bimodal. The value of the reference shear stress for these mixtures could be approximated by the Shields curve for grain size equal to the median grain size of the mixtures. On the contrary, the reference shear stress of the sand grains was smaller than the reference shear stress of the gravel grains for the two strongly bimodal sediment mixtures, i.e. FC-50 and FC-70. Furthermore, the sand content affected the critical shear stress of both modes. Larger sand content resulted in a reduction of the gravel reference shear stress until the later approached the value that was observed for unimodal mixtures. At the same time, the reference shear stress of the sand size range became smaller too, approaching the value that is given by the Shields criterion for uniform sand bed material with grain size equal to the median diameter of the sand mode.

The above described behavior was also observed during measurements of fractional bed-load transport rates in the field at different gravel-bed streams.

The above observations as well as field measurements, which showed that a deviation from the concept of equal mobility was apparent in many bed streams, motivated further investigations for clearing out the influence of sand content on incipient motion threshold. Wilcock & McArdell (1993) and Wilcock et al. 2001 carried out experiments with poorly sorted bimodal sediment mixtures with varying sand content.

4.5 Surface based transport models

4.5.1 Equation of Proffitt & Sutherland (1983)

Proffitt & Sutherland developed a transport equation based on observations from experiments on armouring of non-uniform bed materials. The methodology that they applied was to adapt for use with poor sorted sediment mixtures the Ackers & White (1973) and the Paintal (1971) transport formula, which were based on data from experiments with uniform bed material. Therefore they integrated a correction parameter, which alters the fractional mobility in order to take into account the hiding-exposure effects that characterize the transport of sediment mixtures. The role of the correction was to force the existing transport formula to return the measured transport rate for each fraction during the experiments. A similar approach was used by Day (1980). The main innovation was that they related the dimensionless fractional shear stress to the dimensionless fractional transport rate. The latter was found by scaling the measured transport rate by the fractional content of the bed surface and not by the fractional content of the parent bed material. In this way, they developed the first surface based bed-load transport model.

The model of Paintal after the correction of Parker & Sutherland is written:

$$g_{bi}^* = F_i f(\varepsilon_i \tau_i^*)$$

Eq. (4.33)

where:
g_{bi}^* is dimensionless weight transport rate per unit width
F_i is content of ith grain class in bed surface material
ε_i is correction of fractional Shields stress
τ_i^* is Shields stress related to i^{th} grain class

The dimensionless fractional transport rate is calculated by the following equations:

$$g_{bi}^* = \frac{p_i g_b}{\gamma_i d_i [(s-1)g d_i]^{1/2}}$$

Eq. (4.34)

where:
p_i is content of ith grain class in transported material
g_b is total weight transport rate per unit width
γ_s is specific weight of the sediment
d_i is the mean size of the ith grain class
s is the submerged specific gravity of sediment
g is gravitational acceleration

The exposure correction ε_i for each grain fraction is approximated by the following relation:

$$\varepsilon_i = \begin{cases} 1{,}00\left(\dfrac{d_i}{d_u}\right)^{0{,}51}, & 0{,}6 < \dfrac{d_i}{d_u} < 10 \\[3mm] 1{,}16\left(\dfrac{d_i}{d_u}\right)^{0{,}81}, & \dfrac{d_i}{d_u} < 0{,}6 \end{cases} \qquad \text{Eq. (4.35)}$$

where: d_u is scaling grain size

The scaling grain size d_u expresses the mean size of the grain class for which the calculated g_{bi} by the original transport formula is equal to the transport rate which was measured during the experiment and therefore no exposure correction is required. The scaling grain size can be calculated by equation 4.36.

$$\frac{d_u}{d_{50}} = \begin{cases} 1{,}1, & \tau_{50}^* < 0{,}035 \\ -51{,}13\tau_{50}^* + 2{,}89, & 0{,}035 \le \tau_{50}^* < 0{,}04 \\ -11{,}00\tau_{50}^* + 1{,}32, & 0{,}04 \le \tau_{50}^* < 0{,}055 \\ 0{,}7, & \tau_{50}^* \ge 0{,}055 \end{cases} \qquad \text{Eq. (4.36)}$$

where: d_{50} is d_{50} of bed surface material

τ^*_{50} is dimensionless shear stress related to d_{50} of bed surface material

The hiding function that Proffitt & Sutherland proposed increases the mobility of the coarser material when compared to the mobility of the uniform bed material of the same size. At the same time, it reduces the mobility of the fine bed material in comparison to the mobility of a uniform bed material of the same grain size. This is done by altering the value of the imposed shear stress.

4.5.2   Transport formula of Wilcock & Crowe (2003)

Wilcock & Crowe presented a surface based transport model for sand and gravel mixtures, which was based on a large data set obtained by a plethora of experiments with five different sediment mixtures. The experiments were conducted in a recirculating flume and offered a comprehensive record of coupled measurements of the bed surface grain size distribution and the fractional bed-load transport rates for a range of different flows. The measurements were carried out when a condition of equilibrium was established. The model development was based on the concept of similarity collapse over the fractional bed-load transport rate that was introduced by

Ashida & Michiue (1971). The shame method was successfully used by Parker & Klingemann (1982) for the development of a substrate based transport model which was derived solely from field data. The similarity collapse is founded on the assumption that a unique function exists. This function can reproduce the variation of the fractional dimensionless transport rate with a scaled parameter which expresses the intensity of flow for each grain class.

The transport model of Wilcock & Crowe is written as follows.

$$W_i^* = F_i f\left(\frac{\tau}{\tau_{ri}}\right)$$
Eq. (4.37)

where: W^*_i is the Einstein bed-load parameter, i.e. the dimensionless volumetric transport rate per unit width

   F_i is fractional content of ith grain class in bed surface material

   τ is average bed shear stress

   τ_{ri} is reference shear stress related to i[th] grain class

The Einstein bed-load parameter is defined by

$$W_i^* = \frac{(s-1)g q_{bi}}{u_*^3}$$
Eq. (4.38)

where: s   is ratio of sediment to water density

   q_{bi} is fractional volumetric bed-load transport per unit width

   u_* is shear velocity

Shear velocity is given by the well known equation

$$u_* = \sqrt{\frac{\tau}{\rho}}$$
Eq. (4.39)

The reference shear stress is a surrogate for the fractional critical shear stress τ_{ci} and was experimentally determined by finding the shear stress τ at which the scaled by proportion on the bed surface F_i volumetric transport rate of the ith grain class W^*_i corresponds to a small but measurable reference value W^*_r. This definition was given by Parker et al. (1982a and b) and Wilcock (1988), who set as reference value of W^*_i the W^*_r=0,002. Wilcock & Crowe used the experimental data to develop a new hiding function for predicting the fractional reference shear stress which is given by eq. 4.40.

$$\frac{\tau_{ri}}{\tau_{rs50}} = \left(\frac{d_i}{d_{s50}}\right)^b \qquad \text{Eq. (4.40)}$$

where: τ_{rs50} is reference shear stress related to d_{50} of bed surface material

d_{s50} is d_{50} of bed surface

b is parameter for determining the variation of τ_{ri} with relative grain size d_i/d_{50s}

The exponent b of the hiding function is given by

$$b = \frac{0,67}{1 + exp\left(1,5 - \dfrac{d_i}{d_{s50}}\right)} \qquad \text{Eq. (4.41)}$$

The reference shear stress of d_{50} of bed surface was found that decreased when the sand content on the bed surface increased, something that was for first time integrated into a transport model. The functional relation between τ_{rs50} and sand content that described better the experimental data was

$$\tau^*_{rs50} = 0,021 + 0,015exp(-20F_s) \qquad \text{Eq. (4.42)}$$

$$\tau_{rs50} = \tau^*_{rs50}(s - 1)\rho g d_{s50} \qquad \text{Eq. (4.43)}$$

where: τ^*_{rs50} is the dimensionless reference shear stress related to d_{50} of bed surface material

F_s is the sand content on bed surface

The hiding function of Wilcock & Crowe is similar to other hiding functions (previously published) in terms of reducing the mobility of fine grain sizes and increasing the mobility of coarse grain sizes relative to the case of uniform bed material of the same grain size. However, the reduction of τ^*_{rs50} with increasing sand content on the bed surface introduces a nonlinearity between the sand content and the transport rate, which allows the incorporation of the effect of sand content on transport rate of coarser grain fractions into the model.

The transport function that better fitted the experimental measurements and expresses the functional relation that is denoted with f in equation 5 was the following.

$$W_i^* = \begin{cases} 0{,}002 \left(\dfrac{\tau}{\tau_{ri}}\right)^{7,5}, & \dfrac{\tau}{\tau_{ri}} < 1{,}35 \\[4mm] 14 \left(1 - \dfrac{0{,}894}{(\tau/\tau_{ri})^{0,5}}\right)^{4,5}, & \dfrac{\tau}{\tau_{ri}} \geq 1{,}35 \end{cases} \qquad \text{Eq. (4.44)}$$

The selected function has a similar form with the transport function of Parker (1990). Furthermore, it forces W_i^* to approach a constant value asymptotically, when the imposed shear stress is high, something that was initially stated by Yalin (1972).

4.5.3 Transport formula of Parker (1990)

Parker et al. (1982) presented a substrate based transport model which was derived solely from the field data for Oak Creek, Oregon USA. The model was based on the observation that the grain size distribution of the average annual yield of transported gravel is similar to the grain size distribution of the gravel of the substrate. At the same time, the bed surface is coarser from the substrate and the transported bed material. Parker & Toro-Escobar (2002) called the previous assumption as the "weak form" of equal mobility. The assumption of equal mobility was the motivation for referring the dimensionless transport rate to the grain size distribution of the sub-pavement. However, the condition of equal mobility does not always hold and therefore the substrate based model of Parker et al. should be applied only to near equilibrium mobile-bed conditions. In order to account of selective sorting processes driven by disequilibrium, Parker (1990) transformed the substrate based model into a surface based transport model, which was able to predict fractional gravel bed-load transport in proportion to the content of each grain class on the bed surface.

The Parker surface based transport model takes the form

$$W_i^* = 0{,}00218 F_i G\left[\omega \varphi_{sg0} g_o \left(\frac{d_i}{d_{sg}}\right)\right] \qquad \text{Eq. (4.45)}$$

where: W_i^* is the Einstein bed-load parameter, which is given by eq. (4.17)

     G denotes functional relation

     ω is straining function for adaptation to mixtures of arbitrary composition

     φ_{sg0} normalized dimensionless shear stress referred to d_{sg} of bed surface

     g_o denotes hiding function

     d_{sg} is the geometric mean size of the bed material in the bed surface

The geometric mean size of the bed surface material is calculated by the following equation

$$d_{sg} = \sum F_i \, ln d_i$$

Eq. (4.46)

The parameter φ_{sg0} expresses the intensity of the flow and is defined as

$$\varphi_{sg0} = \frac{\tau^*_{sg}}{\tau^*_{rsg}}$$

Eq. (4.47)

where: τ^*_{sg} is the dimensionless bed shear stress related to d_{sg} of bed surface material

τ^*_{rsg} is the reference dimensionless bed shear stress related to d_{sg} of bed surface material

τ^*_{sg} is given by the equation

$$\tau^*_{sg} = \frac{\tau}{\rho(s-1)gd_{sg}}$$

Eq. (4.48)

The dimensionless reference bed shear stress related to d_{sg} of bed surface material was found to be

$$\tau^*_{rsg} = 0,0386$$

Eq. (4.49)

The hiding function g_o is written

$$g_o\left(\frac{d_i}{d_{sg}}\right) = \left(\frac{d_i}{d_{sg}}\right)^{-0,0951}$$

Eq. (4.50)

The straining parameter ω is determined by

$$\omega = 1 + \frac{\sigma_\varphi}{\sigma_{\varphi 0}}(\omega_0 - 1)$$

Eq. (4.51)

where: σ_φ is the standard deviation of the surface material on the φ-scale

ω_0 and $\sigma_{\varphi 0}$ are functional relations of the form $\omega_0 = \omega_0(\varphi_{sg0})$ and $\sigma_{\varphi 0} = \sigma_{\varphi 0}(\varphi_{sg0})$ which are defined in fig.4.8
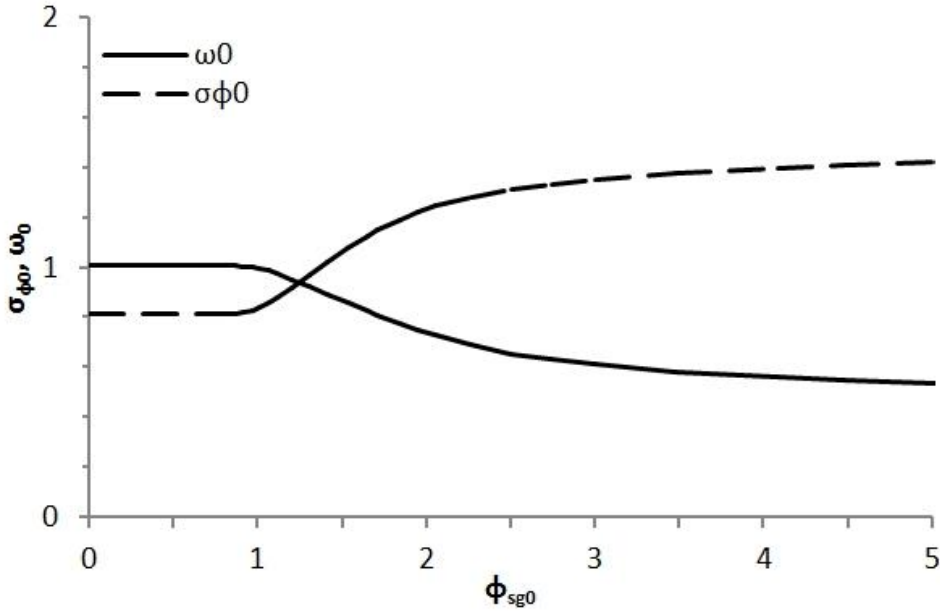
Fig. 4.8 Plot of ω_0 and $\sigma_{\varphi 0}$ as function of φ_{sg0}

The standard deviation of the surface material σ_φ is estimated by

$$\sigma_\varphi^2 = \sum \left[\frac{\ln(d_i/d_{sg})}{\ln(2)} \right]^2 F_i \qquad \text{Eq. (4.52)}$$

The function G is given by

$$G(\varphi) = \begin{cases} 5474 \left(1 - \dfrac{0,853}{\varphi}\right)^{4,5} & \varphi > 1,59 \\ exp[14,2(\varphi - 1) - 9,28(\varphi - 1)^2] & 1 \le \varphi \le 1,59 \\ \varphi^{14,2} & \varphi < 1 \end{cases} \qquad \text{Eq. (4.53)}$$

where: φ is a dummy variable equal to the argument in the brackets of eq.(13)

The hiding function that is integrated into the model differs from the classical approach of Einstein (1950) because it adjusts the mobility of each grain class relative to the mobility of the grain class with size equal to the geometric mean of the bed surface material. On the contrary, the hiding function of Einstein and those that followed the same concept adjust the mobility of each grain class of a sediment mixture relative to the mobility that the grains of the same size would have if they belonged to a unisize bed material instead of a sediment mixture.

It must be noted that the transport model of Parker is only suitable for the determination of the fractional bed-load transport rates within the gravel size range. By

the calculation made with this formula the composition of the bed surface must be renormalized by excluding the sand fractions proportion. The mean size d_{sg} as well as the arithmetic standard deviation σ_φ of the bed material in the surface layer must be computed by the renormalized fractions F_i. Parker decided to exclude the sand fractions from the analysis that he used for developing the model because during flow events with high gravel transport rates it is common for the sand to be transported in suspension. However, he states that sand is not always transported suspended even during high flows while during low flows it is transported as bed-load.

4.5.4   Transport model of Hunziker (1995)

Hunziker (1995) and Hunziker & Jäggi (2002) published a surface based transport model for fractionwise calculation of bed-load transport. The model was based on the transport function of Meyer-Peter & Müller (1948) and the concept of equal mobility. An important aspect of the work of Hunziker is the re-evaluation of the classical transport function of Meyer-Peter & Müller. He was based on the work of Jäggi (1984) who showed that the original equation was derived from data which were overcorrected by the applied bedform correction. Hunziker applied a more appropriate method in order to account for the bedform roughness and after a regression analysis on the corrected data he obtained a modified version of the M-PM equation which is given by

$$q_b^* = 5(\tau_{mo}^* - 0{,}05)^{3/2} \qquad\qquad \text{Eq. (4.54)}$$

where: τ_{mo}^* is a dimensionless shear stress related to mean size of substrate

The difference with the original equation, which is given by eq. (1) is that the multiplying coefficient of the term of excess shear stress changed from 8 to 5 and the critical dimensionless shear stress τ_c^* changed from 0,047 to 0,05. Furthermore, when a bedform roughness correction is required then the method of Yalin and Scheuerlein (1988) should be applied instead of the parameter $(k_s/k_r)^{1,5}$ that is suggested in the original paper. Wong & Parker (2006) presented a similar analysis of the data that were used for the derivation of the original M-PM formula and proposed a modification too.

The transport model of Hunziker (1995) is given by the following equations

$$q^*_{bdms,i} = F_i 5(\varphi_i(\tau'^*_{ms} - \tau^*_{cm}))^{3/2}$$

Eq. (4.55)

where: $q^*_{bdms,i}$ is fractional dimensionless bed-load transport rate related to mean grain size of bed surface

F_i is fractional content of ith grain class in bed surface

φ_i denotes the hiding correction

τ'^*_{ms} is the corrected for side wall effects and bedform drag dimensionless shear stress related to mean grain size of bed surface

τ^*_{cm} is the critical dimensionless shear stress related to mean grain size of bed surface

The fractional dimensionless bed-load transport rate parameter $q^*_{bdms,i}$ is given by

$$q^*_{bdms,i} = \frac{q_{bi}}{\sqrt{(s-1)gd^3_{ms}}}$$

Eq. (4.56)

where: q_{bi} is the volumetric fractional bed-load transport rate per unit width

d_{ms} is the mean grain size of bed surface

The hiding function was calibrated with data from experiments for mobile as well as static armoring conducted by Suzuki and Kato (1991), Suzuki and Hano (1992) and Günter (1971). The necessary correction for taking into account the hiding effects is given by the following power equation

$$\varphi_i = \left(\frac{d_i}{d_{ms}}\right)^{-a}$$

Eq. (4.57)

where: τ^*_{mo} is a dimensionless shear stress related to mean size of substrate

The parameter α that is incorporated in the hiding function is given by

$$a = 0,11\tau'^{*-1,5}_{ms} - 0,3$$

Eq. (4.58)

For the calculation of the critical dimensionless shear stress referred to the mean grain size of the bed surface the equation that was developed by Günter (1971) is used

$$\tau^*_{cms} = \tau^*_{ce}\left(\frac{d_{mo}}{d_{ms}}\right)^{0,33}$$

Eq. (4.59)

where: τ^*_{ce} is the critical dimensionless shear stress for incipient motion for uniform bed material

d_{mo} is the mean grain size of the parent bed material

4.6 Chapter summary

The theoretical background of bed-load predictors is presented in this chapter. The theoretical considerations upon which was based the development of the early transport models for uniform bed material are initially presented. The further developments of this concept in order to account for graded bed material are subsequently reported. Special attention is given to the condition of threshold of motion both for uniform bed material as well as for sediment mixtures. The physical mechanism of hiding is explained and the influence of relative grain size effects on incipient motion is described. Additionally, the derivation of hiding functions, i.e. functions that serve to predict the critical shear stress of particles belonging in a multisized population is given. Finally, the previously published surface based transport models are presented in detail. The literature review focused on this type of bed-load predictors because it is widely accepted that these models are suited for prediction of transient changes during ongoing bed-load transport events driven by disequilibrium.

5.   Experimental apparatus and procedure

The experiments described herein were performed in the laboratory Oskar von Miller of the Department of Hydraulic and Water Resources of the Faculty of Civil Engineering and Surveying of Technische Universität München, Germany. The laboratory is located in Obernach in Oberbayern.

5.1   Experimental program

The objective of the experiments was to document the transient transport processes that occur during the formation of a static armor layer. Hence, continuous measurements of fractional transport rates at different locations along the flume were required. These measurements would allow for a complete description of the phenomenon only if they were coupled with the changes in bed surface grain size distribution taking place over time and space.

Three series of experiments were performed, each one of them with the same parent bed material and initial bed slope but different test reach lengths. Thus, the fractional transport rates were measured at three different locations, with distance 4, 8 and 12 m from the upstream end of the erodible bed respectively. The spatial variation of bed-load transport was determined this way. The grain size distribution of the bed surface was estimated at regular time intervals during on-going experiments, at three different locations along the flume by means of a non-intrusive method. Each series contained five experimental runs. The experimental runs were performed with varying flow intensity. The flow strength was regulated by adjusting the water discharge from run to run. The five runs of each experimental series were conducted with water discharges of 70, 80, 100, 120 & 150 l/s respectively

Thus, the desired data set of coupled observations of bed-load transport and bed surface texture was obtained from a total count of 15 experiments.

5.2   Experimental set-up

Herein the experimental apparatus arrangement is described. The used materials are also delineated and their employment is justified.

5.2.1 Flume

The experiments were conducted in a flow recirculating flume with rectangular cross-section. A schematic illustration of the flume is shown in fig. 5.1. In the sketch the water circulation system has been drawn oversimplified and will be described in a following paragraph.
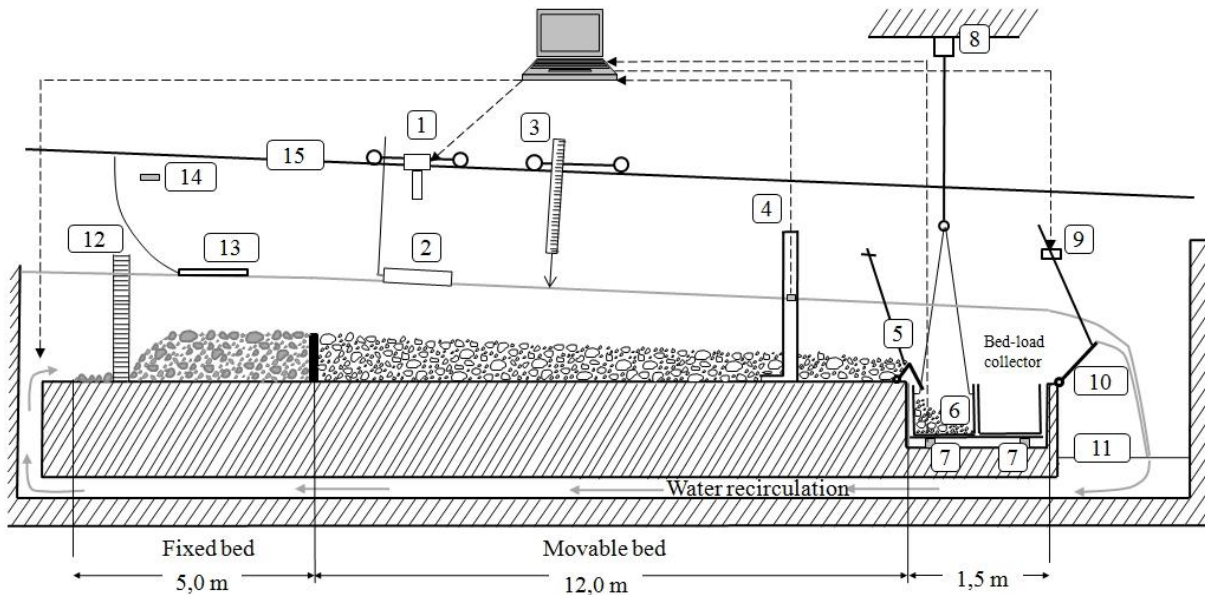
1. Camera
2. Plexiglass plate
3. Point Gauge
4. Waterlevel measurement
5. Adjustable downstream end of movable bed
6. Bed-load collector
7. Sensors for weight measurement
8. Crane for removing the bed-load collector
9. Engine for teil weir movement
10. Tail weir for regulation of water level
11. Grid
12. Straitening tubes
13. Polystyrene plate
14. Emergency switch
15. Running rails

Fig. 5.1 Schematic illustration of the flume that was used in the experiments

The flume has a width of 0,5 m, height of 0,7 m and length of 20 m. The left side wall as we look in the downstream direction is made of concrete and has been painted with acrylic paint in order to obtain a hydraulically smooth surface. The wall at the right side is made of plexiglass allowing for direct optical observations of the transport processes during the experiments. Running rails extending along the length of the flume were located on the top of the side walls (notated with 1 in Fig. 5.1). As the flume could not be tilted by mechanical means, its slope was adjusted by the running rails. The slope of the running rails was set by screw gauges located at each side of the flume with a distance of 0,5 m from each other.

Two carriages were moving on the running rails along the flume. A point gauge was mounted on the first moving carriage. The point gauge was used for the determination of water and bed surface profiles. A digital camera was mounted on the second moving carriage for taking plane view photos of the bed surface. The photographs were used later for the estimation of bed surface particle size distribution during the experiments. Also, the external lighting instrumentation was adjusted on the same carriage in order to enhance the lighting conditions. Finally, a plate of plexiglass with adjustable vertical position was mounted on the same cart.

The water level was measured continuously with an electronic device that was installed 1 m before the downstream end of the erodible bed. The measurements were recorded automatically at the central computer and where coupled with the module for controlling and setting the tail weir position.

The water level in the flume was controlled by a tail weir located at the downstream end of the flume. The position of the tail weir could be adjusted either manually or through a computer. The water returned to the sump after being discharged over the tail gate.

A low weir was located at the downstream end of the movable bed in order to protect the latter from uncontrolled erosion during the filling of the flume. The height of the weir was adjusted manually. As soon as the flume was filled with water the height of the weir was adjusted to be 1 cm lower than the bed surface in order to allow sediment and water to pass over it and be collected in the bed-load trap. During the experiments the weir height was further lowered so as not to disturb the bed geometry development by stabilizing the bed slope.

An upstream portion of the flume bed was artificially roughened to induce the full development of a turbulent boundary layer before encountering the loose sediment bed. Therefore a length of 5 m directly downstream of the straightening tubes was covered with a 16 mm diameter immobile sediment. The sediment was mixed with a small amount of cement and then placed on a roughened surface and dried. In order to obtain measurements of the fractional transport rates for different lengths of the erodible bed the upstream immobile bed was extended progressively further downstream reducing thus, the length of the test reach. Thus, the fixed bed had a length of 5, 9 and 13 m for the three experimental series respectively.

The material that was eroded during the experiments was caught at the bed-load collector placed at the downstream end of the erodible bed. The collector had a length of 1,5 m in order to be able to catch all the transported material. The bed-load trap consisted of two boxes placed on a plate that was mounted on three electronic sensors

that measured continuously the accumulative submerged weight of the caught material. On the roof of the hall a crane was installed to lift and remove easily the bed-load collector when an inspection of the weight measurement device installations was required.

The flow-meter and the water level measuring device communicated with the central computer and their measurements were recorded continuously. The position of the tail gate was also recorded automatically. The position of the tail gate was automatically adjusted until the wished water surface elevation was established. Finally, the photo camera was controlled through the computer unit. In this way it was assured that the camera was not moved when the snapshots were taken, that no shading effects were caused due to the presence of the user, and the settings could be more easily controlled.

5.2.2   Water cirquit

The flume was equipped with two pumps having a capacity of 150 and 600 l/s respectively. In the present study only the small pump was used, with the exception of some days during which the water discharge of 150 l/s was not sufficient to cover the needs of the experiments conducted simultaneously in the laboratory hall. In that case, either both or only the large pump was activated.

Water was drawn by the pump from the sump with a volume of 9 m^3 that was located below the flume. Water passed through a supply pipe into a head tank before passing over the erodible bed. At the flume outlet water passed over an adjustable tailgate, returned to the sump, and recirculated. The valve that regulated the actual discharge was remotely controlled by the central PC.

5.2.3   Bed material

Three main considerations determined the choice of the sediment mixture that was used as parent bed material in the experiments that are herein described. First, the bed material should be poorly sorted with enough coarse material to allow for the development of a coarse static armor layer. Second, the chosen sediment mixture should represent sufficiently the subsurface bed material that is observed in gravel bed rivers in the field. Finally, the employed sediment mixture should contain grains coarse enough to prevent from significant suspension and to ensure their transport as bed-load. Generally, the used sediment should provide a mechanistic model of a typical gravel-bed river.

5.2.3.1 Grain size distribution of employed sediment mixture

The chosen bed material contained grains with size from 0,2 mm to 16 mm. The grain size distribution of the employed bed material is given in table 5.1 and is graphically illustrated in fig. 5.2. Thus, the bed material that was used in the experiments is a sediment mixture that contains both sand and gravel particles. The sand grains are characterized by sizes from medium till coarse sand. The gravel particles that are contained in the employed sand-gravel mixture range from fine gravel till medium gravel.

Table 5.1   Grain size distribution of employed sediment mixture

Grain size [mm]	0,2-0,5	0,5-1,0	1,0-2,0	2,0-4,0	4,0-8,0	8,0-16,0	16,0-32,0
Mean fractional grain size [mm]	0,32	0,71	1,41	2,83	5,66	11,31	22,63
Fractional content [%]	9,51	10,65	17,37	14,38	14,42	32,67	1,00
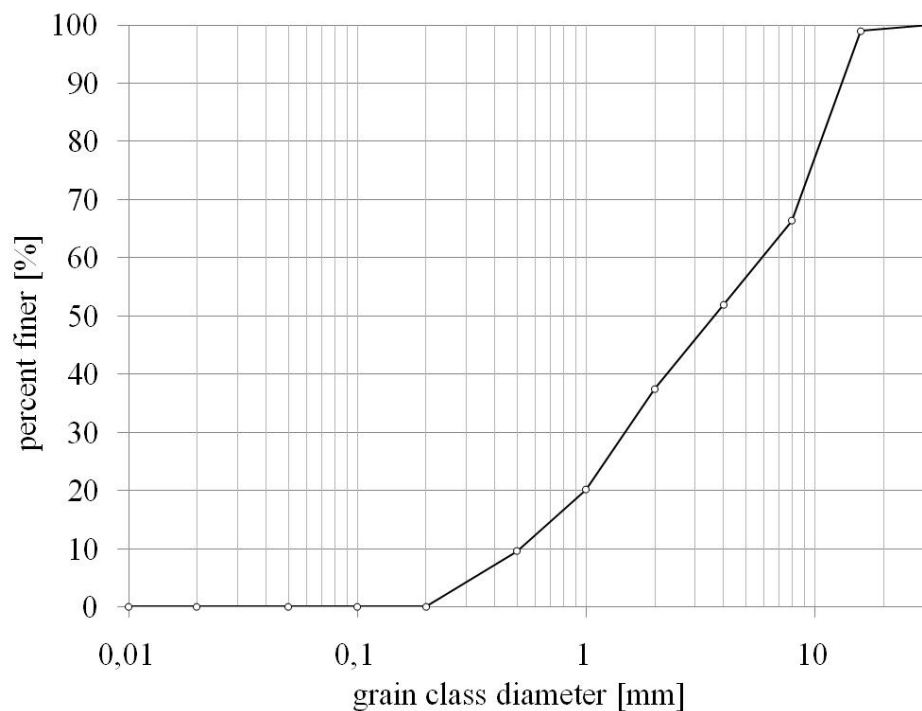
Fig. 5.2   Grain size distribution of employed sediment mixture

The characteristic grain sizes as well as the geometric standard deviation and the sand content are shown in table 5.2.

Table 5.2   Statistical properties of the employed sediment mixture

Median grain size d_{50}	Arithmetic mean size d_m	Geometric mean size d_g	d_{84}	d_{16}	Geometric standard deviation	Sand Content
[mm]	[mm]	[mm]	[mm]	[mm]	[-]	[%]
3,65	5,83	3,12	11,64	0,76	1,74	37,53

The arithmetic mean size d_m is given by the equation that was proposed by Meyer-Peter & Mueller (1948)

$$d_m = \sum_{i=1}^{n} f_i \, d_i \qquad \text{Eq. (5.1)}$$

where:
f_i is fractional content of ith grain class
d_i is mean grain size of ith grain class

The geometric mean size d_g of the used bed material is calculated by

$$ln(d_g) = \sum_{i=1}^{n} f_i ln(d_i) \qquad \text{Eq. (5.2)}$$

The geometric standard deviation σ_g is calculated by

$$\sigma_g = 2^{\sum_{i=1}^{n} f_i \log_2(d_i)} \qquad \text{Eq. (5.3)}$$

5.2.3.2 Control for suspension

The criterion for onset of significant suspension proposed by Bagnold (1966) was used for the determination of the smallest grain size that could be transported as bed-load under the given flow conditions. The criterion is based on the logical consideration that the settling velocity characterizes the forces that are opposite to the turbulent entraining forces acting on the grain. It is formulated as follows

$$\frac{u_*}{w_s} \geq a \qquad \text{Eq. (5.4)}$$

where: w_s is grain settling velocity

        u_* is shear velocity

        a   constant that takes a value near unity

A plethora of formulas have been proposed so far for the calculation of settling velocity of natural sediments, for example, Graf (1971), Zanke (1977), Dietrich (1982), van Rijn (1984), Cheng (1997), Ahrens (2000) among others. In the present study, the grain fall velocity was estimated with the use of Dietrich's equation (1982) because the incorporated analysis is the most comprehensive in terms of the data set that was used for the derivation of the equation.

The grain fall velocity w_s can be found by the following equation

$$w_s = \left(\frac{(\rho_s - \rho)}{\rho} \, g \, v \, w_* \right)^{1/3} \qquad \text{Eq. (5.5)}$$

where: w_* is dimensionless grain settling velocity

        ρ_s is sediment density

        ρ is water density

        g   is gravitational acceleration

The dimensionless settling velocity w_* is obtained from

$$w_* = R_3 10^{R_1 + R_2} \qquad \text{Eq. (5.6)}$$

where: R_1 is parameter accounting for the effect of grain size and density

        R_2 is parameter accounting for the effect of grain shape

        R_3 is parameter accounting for the effect of grain roundness

The parameter R_1 is calculated by

$$R_1 = -3{,}76715 + 1{,}92944(\log D_*) - 0{,}09815(\log D_*)^2 \\ - 0{,}00575(\log D_*)^3 + 0{,}00056(\log D_*)^4 \qquad \text{Eq. (5.7)}$$

where: D_* is dimensionless grain size

The dimensionless grain size D_* is given by

$$D_* = \frac{(\rho_s - \rho)}{\rho} \frac{g}{v^2} d^3$$

<div align="right">Eq. (5.8)</div>

where: v   is kinematic viscosity of the fluid

d   is grain size

The parameter R_2 is given by

$$R_2 = \log\left(1 - \frac{1 - CSF}{0,85}\right) - (1 - CSF)^{2.3}\tanh(\log D_* - 4,6)$$
$$+ 0,3(0,5 - CSF)(1 - CSF)^2(\log D_* - 4,6)$$

<div align="right">Eq. (5.9)</div>

where: CSF   is the Corey shape factor

The shape factor CSF that was introduced by Corey (1949) is estimated by

$$CSF = \frac{c}{\sqrt{ab}}$$

<div align="right">Eq. (5.10)</div>

where: a   is the longest axis of the particle

b   is the intermediate axis of the particle

c   is the shortest axis of the particle

The CSF factor varies between 0 and 1. The smaller its value the flatter is the particle. When the value of the factor cannot be estimated from direct measurements and no other information on shape is available, Jimenez & Madsen (2003) recommended using a shape factor value of 0,7 for natural worn sediments.

Finally the parameter R_3 is found by

$$R_3 = \left[0,65 - \left(\frac{CSF}{2,83}\tanh(\log D_* - 4,6)\right)\right]^{\left(1 + \frac{3,5 - P}{2,5}\right)}$$

<div align="right">Eq. (5.11)</div>

where: P   is the Powers value of roundness

The roundness parameter P can take values from 0 for perfectly angular particles to 6 for perfectly round grains. Dietrich (1982) and Jimenez & Madsen (2003) recommended a value of 3,5 for naturally shaped grains.

In fig. 5.3 the values of the ratio of shear velocity to settling velocity are plotted against the grain size for different values of shear velocity. The individual curves represent a value of shear velocity. The range of shear velocities used in the diagram is representative of the flows used in the experiments. In Fig. 5.3 it is evident that the ratio of shear velocity to grain fall velocity approaches the value of 1 for grain sizes in the range of 0,25 mm to 0,4 mm depending on the shear velocity value.
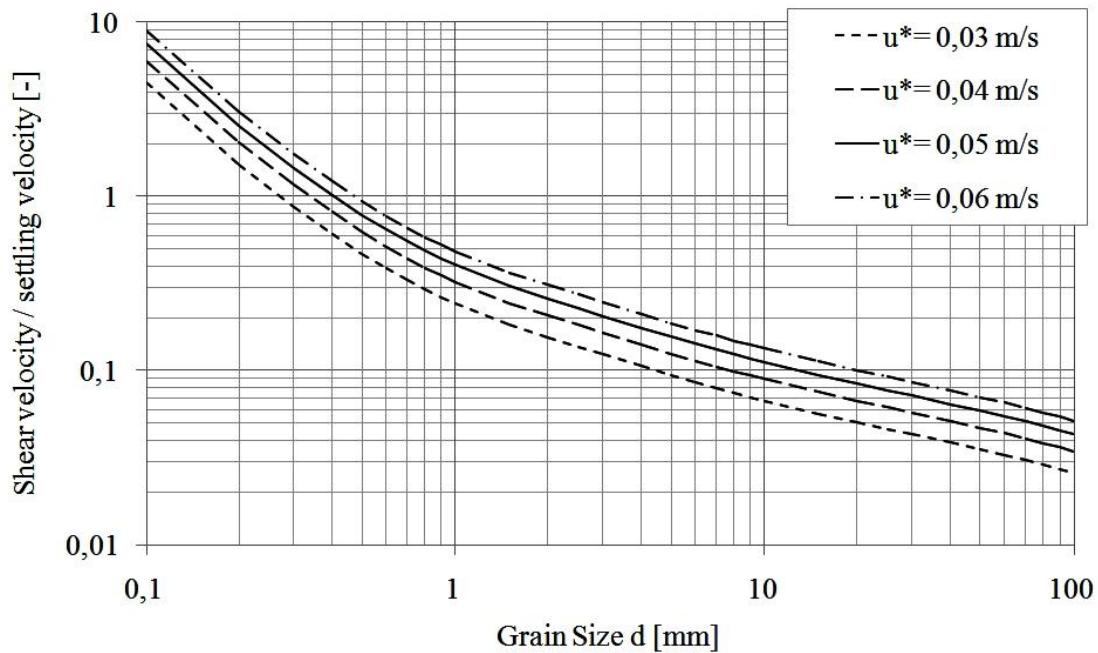
Fig. 5.3 Variation of ratio shear velocity / settling velocity with grain size and shear velocity

Based on the above analysis, the diameter of 0,2 mm was chosen as the cutoff grain size of the employed sediment mixture. This decision was supported by preliminary experimental runs, where no suspension was observed even when high shear stress was exerted on the bed. This can be attributed to the fact that there is no arbitrary division between bed-load and suspended load (Parker et al. (1982b). Finally, the major constraint that affects the decision regarding the cutoff size of the fine end of the used grain size distribution is the efficiency of the bed-load collector. The unusually long trap that was used in the experiments assured that no grains that would occasionally go into suspension would pass over it. This was verified by the observation that the second box of the bed-load trap (see fig. 5.1) was always empty, which means that the whole amount of transported material was caught in the first basket. Therefore, it can be stated with certainty that no error was introduced in the measurement of the total load.

5.2.3.3 Ability of the parent bed material to develop a coarser surface layer

Based on the considerations that were presented in the above paragraph, the sediment mixture that was used in the experiments contained grains with size that ranged between 0,2 mm and 16 mm. Dietrich (1997) gave a summary of the criteria that have been proposed regarding the ability of a non-uniform bed material to allow for the development of a coarser armor layer on its surface. These criteria usually involve the relation between the maximum grain size and the particle size distribution of the sediment mixture. The criteria that have been proposed for this purpose are presented in table 5.3.

Table 5.3 Criteria regarding the ability of sediment mixture to allow the development of a coarse surface layer (from Dittrich (1998))

Author	Criterion	
Gessler (1965)	$$\sigma = \frac{d_{84}}{d_{50}} > 2$$	Eq. (5.12a)
Little & Mayer (1976)	$$\sigma_g = \sqrt{\frac{d_{84}}{d_{16}}} \geq 1,3$$	Eq. (5.12b)
Chin (1985)	$$\sigma = \frac{d_{84}}{d_{50}} \geq 1,5$$ $$\text{and } \frac{d_{max}}{d_{50s}} \geq 1,8$$	Eq. (5.12c)
Schöberl (1981)	$$\sigma_g = \sqrt{\frac{d_{84}}{d_{16}}} \geq 1,35,$$ $$\frac{d_{90}}{d_{50}} \geq 1,55$$ $$\text{and } \frac{d_{ms}}{d_{50}} > 1,05$$	Eq. (5.12d)

Where: d_{max} the largest grain size contained in the sediment mixture
d_{50s} the median grain size of the armor layer
d_{ms} the arithmetic mean grain size of the armor layer

The employed grain size distribution satisfied all the criteria that were proposed in the literature. Therefore, it was deemed suitable for the purpose of the experimental investigation.

5.2.3.4 Comparison with natural sediments

A comparison of the grain size distribution of the employed sediment mixture with field data from four gravel bed rivers in Bayern showed that the used bed material was representative of the conditions that are met in the field. The comparison is shown in Fig. 5.4 and shows that the grain size distribution of the employed material (is always the line on the left side of each figure) can describe sufficient the conditions that are met in typical gravel bed rivers.
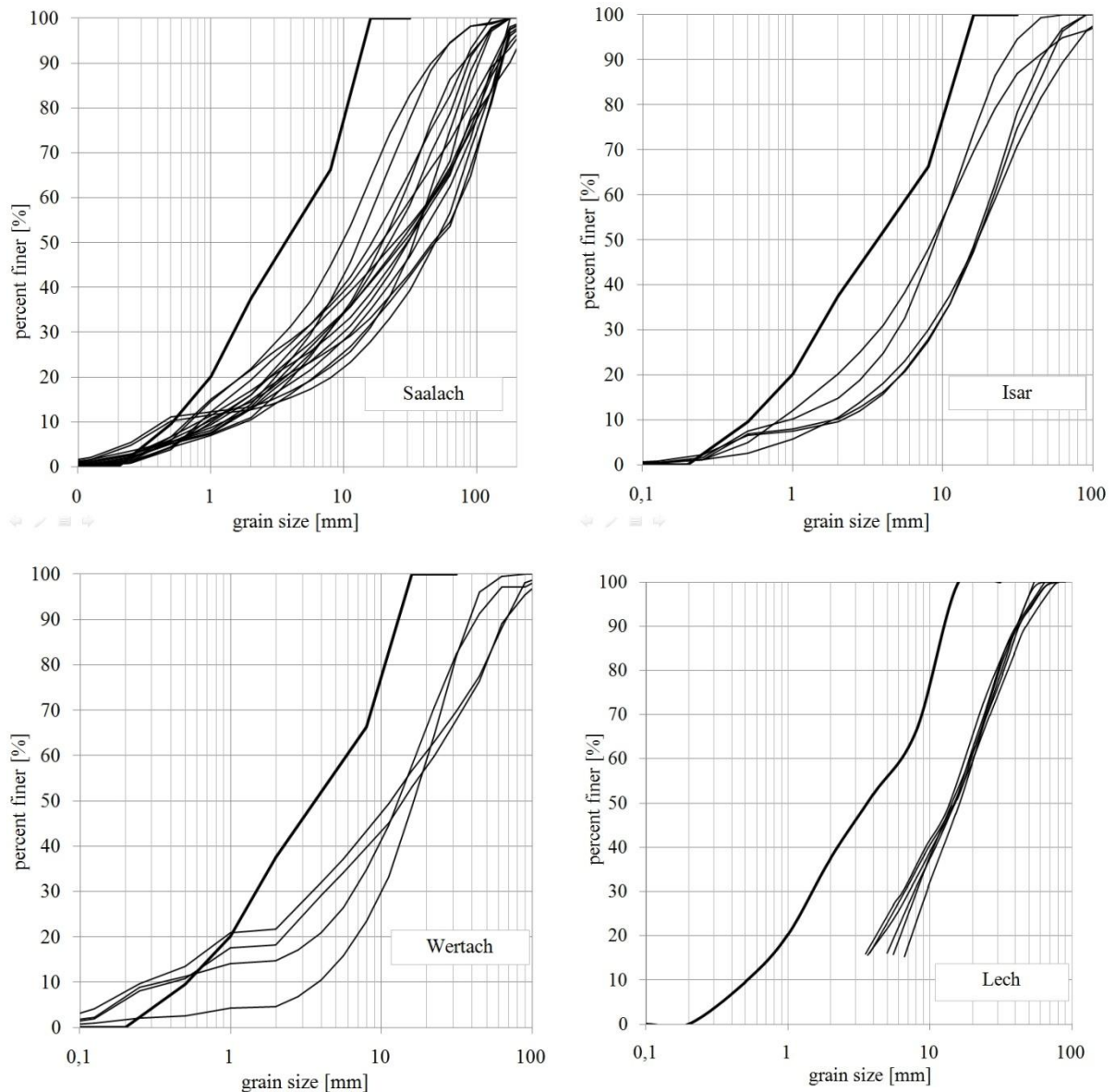
**Fig. 5.4** Comparison of employed material's composition with samples of subsurface bed material taken at 4 different gravel bed rivers in Bayern

These four rivers were characterized from bed slopes that varied between 0,001 and 0,005. Hence, the chosen bed slope was within the range that is met in field conditions.

The purpose of the experiments was to provide a mechanistic model of a typical gravel

bed river. The employed material was 5 to 10 times finer than the substrate bed material that is found in this typical gravel bed rivers in Bayern. Within this geometric scale range carrying out the typical similitude analysis for Froude models it was found that the maximum imposed flow strength was equivalent with flood events of the magnitude of HQ2 or a little bit higher. Thus the imposed flow conditions were suitable for the investigation of the bed surface changes during low flow events.

5.3 Measurement techniques and data analysis

The measured variables included:

- Water discharge
- Transported bed-load rate and grain size distribution at three different locations along the flume
- Bed surface topography
- Water depth and water surface slope
- Bed surface composition

5.3.1 Measurement of water discharge

The water discharge was measured by an electronic flowmeter that was located in the return pipe. The accuracy of the discharge measurements was ±0,1 l/s for the pump that was used during the experiments.

5.3.2 Determination of bed surface profiles

The bed surface elevation was measured along the center line of the flume at 0,5 m intervals with the use of a scaled point gauge. The accuracy of the measurements was ± 0,1 mm. At each station, the elevation was determined at 5 different locations that lied within a narrow zone with a width of 10 cm. Two of these locations were occupied by coarse grains with a diameter larger than 4 mm. The remaining three measurements were taken at locations occupied by fine grains, with diameter between 0,2 and 1 mm. The employed method for the determination of bed surface elevation is illustrated in Fig. 5.5. The mean bed elevation was calculated as the weighted average of the individual point measurements, taking into consideration the area coverage of fine and coarse fractions respectively.

The longitudinal bed slope was estimated by fitting a linear equation on the averaged bed elevation measurements. The measurements were repeated at regular time intervals during the experiments, in order to document the temporal variation of bed geometry.
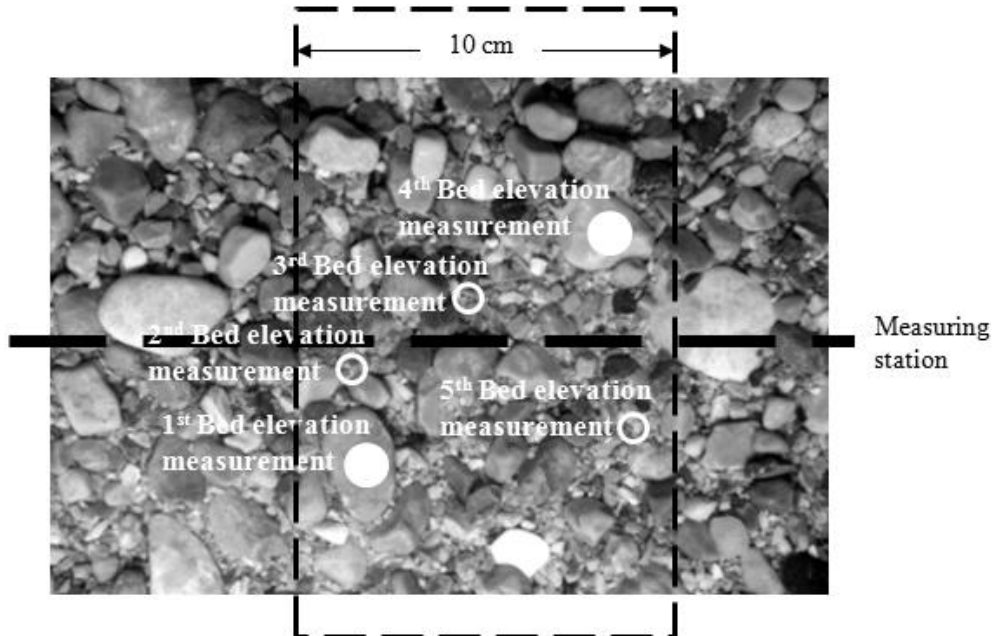
Fig. 5.5   Employed method for the determination of bed surface elevation. Solid white circles and open white circles represent measurements of elevation at locations that were occupied by coarse and fine grains respectively. The measurements where conducted within a zone, approximately 10 cm wide, along the centerline of the flume

5.3.3   Determination of water surface elevation

The water surface elevation along the flume was determined by measurements conducted with a point gauge mounted on a movable carriage. The measurements were repeated at regular time intervals during the experiments, in order to assure the existence of normal flow conditions. The water level fluctuated over time. Therefore, the vertical position of the gauge was adjusted until its end was half the time over the water and half the time below the water surface, when observed for a sufficient long time period of 10 seconds. The measurements of the point gauge were subsequently corrected for the slope of the running rails. The measurements were taken at 1 m intervals along the flume and were accurate to ± 0,1 mm.

Furthermore, continuous measurements of the water level were conducted and recorded in the control unit with use of a float which moved along a displacement transducer. This measuring device was located 16 m downstream of the flume inlet

and 1m upstream from the bed-load collector. The continuous water level measurements were accurate to ± 0,01 mm. The agreement between the measurements of the electronic device and the point gauge was very good. The slope of the water surface was estimated by fitting a linear equation with regression analysis to the measurements.

5.3.4   Estimation of bed shear stress

The experiments were performed under normal flow conditions and, hence, the average boundary shear stress can be calculated by the product of hydraulic radius and energy slope.

$$\tau_b = \gamma_w r_h J$$ Eq. (5.12)

where: γ_w is specific weight of water
r_h is hydraulic radius
J is energy slope

In case of a wide open channel the above equation can be recast by replacing hydraulic radius r_h with water depth h without introduction of significant error in the estimation of bed shear stress.

As in most laboratory open-channel flows over loose beds, the roughness factor of the side-walls differed from the roughness of the bed. Therefore shear stress was not uniformly distributed over the cross-section. Furthermore, the value of the width to depth ratio varied from 2 to 4 and therefore the side wall effects should be eliminated by means of a proper side wall correction of the estimated average bed shear stress. The experimental runs were characterized by the absence of bed forms. Therefore, the use of a drag-partition model was not required in order to estimate the skin friction portion of the total bed shear stress.

5.3.4.1 Common assumptions of side-wall correction procedures

In order to calculate the effective shear stress that is actually exerted on the bed, the following equation can be used.

$$\tau_b = \gamma_w r_{hb} J$$ Eq. (5.13)

where: r_{hb} is hydraulic radius associated with the loose bed

Several methods have been proposed in the literature for this necessary correction in order to eliminate side-wall effects. The most widely applied are the following:

- Einstein's method (1934).
- Vanoni & Brooks' method (1957)
- Williams' method (1970)

The side-wall correction methods are commonly based on the following assumptions:

- The cross-section area can be divided into two sub-areas. The first one is producing shear on the bed and the other on the walls. The boundaries between these two sections are surfaces of zero shear and, thus, they will not be accounted for at the determination of the sub-area wetted perimeter. Thus, in case of rectangular cross-section with width b and water depth h, the wetted perimeter of the bed section p_b is equal to the bed width b and the wetted perimeter of the wall section p_w is equal to water depth h.
- The mean velocity in the two sections v_w and v_b is the same and equal to the mean velocity in the cross-section v_m.
- A flow equation can be applied separately to each section as if it were a channel by itself.
- The walls and bed have different roughness; however it remains constant within each of the two sections.

5.3.4.2 Vanoni & Brooks (1957) approach

Vanoni and Brooks (1957), based on the above assumptions, presented a method for the elimination of side-wall effects. The main difference with the Einstein's approach is that instead of the Manning-Strickler flow equation they applied the Darcy-Weisbach equation. Furthermore, they simplified the procedure for finding the wall friction factor f_w. Instead of determining the value of f_w with an auxiliary calculation, they published a figure where the wall friction factor was related to the ratio of R/f. This simplification was based on the fact that side-walls are practically hydrodynamically smooth and therefore the relative roughness can be eliminated as one of the variables. Hence for smooth walls, f_w will be a function only of the Reynolds number for the wall sub-area R_w. A schematic illustration of the parameters that are used during the estimation of effective bed shear stress is given in fig. 5.6
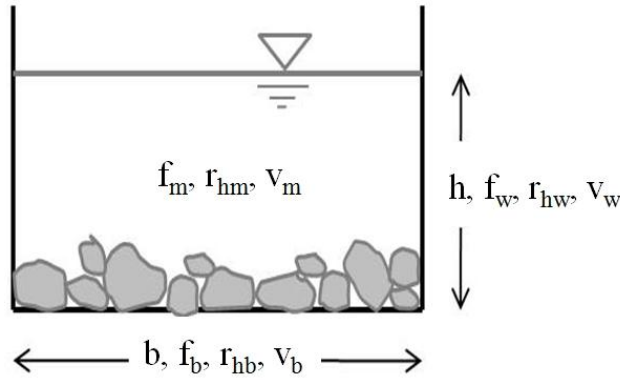
Fig. 5.6 Schematic illustration of parameters related with the sidewall correction

Writing the Darcy-Weisbach equation for the complete cross-section as well as for the two sub-areas of bed and wall respectively, we obtain

$$
\left.
\begin{aligned}
g r_{hm} J &= \frac{f_m}{8} v^2 \\
g r_{hb} J &= \frac{f_b}{8} v^2 \\
g r_{hw} J &= \frac{f_w}{8} v^2
\end{aligned}
\right\}
\Rightarrow \frac{r_{hw}}{f_w} = \frac{r_{hb}}{f_b} = \frac{r_{hm}}{f_m}
\qquad \text{Eq. (5.14)}
$$

where:

f_m is Darcy-Weisbach friction factor for the whole cross section

f_w is Darcy-Weisbach friction factor for the wall sub-area

f_b is Darcy-Weisbach friction factor for the bed sub-area

r_{hm} is the whole cross-section hydraulic radius

r_{hw} is the wall hydraulic radius

r_{hb} is the bed hydraulic radius

Assuming that the mean velocity remains the same in the two sections and by writing the Reynolds number for the wall and the whole cross-section the following expression for the Reynolds number associated with the wall section is obtained

$$
\left.
\begin{aligned}
Re_w &= \frac{4 v_w r_{hw}}{v} \\
Re_m &= \frac{4 v_m r_{hm}}{v} \\
v_m &= v_w
\end{aligned}
\right\}
\Rightarrow Re_w = Re_m \frac{r_{hw}}{r_{hm}}
\qquad \text{Eq. (5.15)}
$$

where:

Re_m is Reynolds number for the whole cross-section

Re_w is Reynolds number for the wall sub-area

v_m is velocity in the whole cross section

v_w is velocity in the wall sub-area

By combining eq. 5.14 and 5.15 we obtain

$$\frac{Re_w}{f_w} = \frac{Re_m}{f_m}$$

Eq. (5.16)

Thus the value of the ratio R_w/f_w can be found directly but neither R_w nor f_w individually. In order to determine f_w, Vanoni & Brooks presented a diagram with a graphical illustration of the Karman-Prandtl resistance equation for turbulent flow in smooth pipes. Thus, the value of f_w was estimated as function of R_w/f_w. Cheng (2005) fitted a curve on the graphic that was presented by Vanoni & Brooks. The curve is given by the following equation

$$f_w = \left[20\left(\frac{Re_w}{f_w}\right)^{0,1} - 39\right]^{-1}$$

Eq. (5.17)

Gessler (1965) applied the Karman-Prandtl equation for the calculation of wall related friction factor f_w.

$$\frac{1}{\sqrt{f_w}} = 2log\frac{4v_m r_{hw}}{v}\frac{\sqrt{f_w}}{2.5}$$

Eq. (5.18)

where: v   is kinematic viscosity of the fluid

Gessler suggested using the equation that was proposed by Blasius for calculation of wall friction factor if the Reynolds number associated with the wall sub-area is smaller than 100000. The equation of Blasius is the following

$$f_w = \frac{0,316}{Re_w^{1/4}}$$

Eq. (5.19)

The main advantage of the above equation is that it contains explicitly the term f_w and accordingly the iterations for finding this term can be avoided.

By replacing the term of hydraulic radius with the ratio of wetted area A to wetted perimeter p into the Darcy-Weisbach flow equation; and taking into account the geometrical requirement that sum of the area of wall and bed sub-areas respectively equals the area of the whole cross-section, i.e. $A = A_b+A_w$ as well as the assumption of equality of flow velocity in the different sections, the following expression is obtained:

$$
\left.\begin{array}{l}
A_m = \dfrac{p_m f_m v_m^2}{8gJ} \\[2mm]
A_m = \dfrac{p_m f_m v_m^2}{8gJ} \\[2mm]
A_m = \dfrac{p_m f_m v_m^2}{8gJ} \\[2mm]
v_b = v_w = v_m \\[1mm]
A_m = A_b + A_w
\end{array}\right\} \Rightarrow p_m f_m = p_b f_b + p_w f_w \Leftrightarrow f_b = \dfrac{p_m}{p_b} f_m - \dfrac{p_w}{p_b} f_w \quad \text{Eq. (5.20)}
$$

where: A_m is wetted area associated with the whole cross-section

A_w is wetted area associated with the wall

A_b is wetted area associated with the bed

p_m is wetted perimeter associated with the whole cross-section

p_w is wetted perimeter associated with the wall

p_b is wetted perimeter associated with the bed

For rectangular channels of width b and depth h, the wetted parameters p_m, p_b, p_w are respectively:

$$p_m = b+2h$$

$$p_b = b$$ Eq. (5.21)

$$p_w = 2h$$

eq. 5.20 can now be further simplified

$$f_b = f_m + \frac{2h}{b}(f_m - f_w) \qquad \text{Eq. (5.22)}$$

By substituting f_b into eq. 5.14 the hydraulic radius associated with the bed sub-area r_{hb} is determined, allowing thus for the estimation of the effective bed shear stress τ_b from eq. 5.13.

5.3.5   Determination of total and fractional bed-load transport rates

The total bed-load transport rate was estimated by measuring continuously over time the accumulative submerged weight of the material caught at the bed-load trap that was installed at the downstream end of the erodible bed. The dimensions of the bed-load trap were dictated by geometrical constraints imposed by the flume itself and the need to catch the fine end of the material transported as bed-load. A plate was based

on three force transducers that communicated with the central computing unit. The accuracy of the employed sensors for weight measurement was according to the manufacture ± 50 gr. Two removable boxes were placed on that plate and collected the transported material.

In order to eliminate the considerable high frequency noise in the transducers output voltage signal, the latter was passed through a filter. The relation between submerged weight of the empty bed-load trap plus the collected sediments and the voltage signal of the force transducers was linear. A calibration procedure was used to relate the voltage output to weight. The submerged weight was measured for a period of three to four seconds and then this value was displayed and saved in a data file on the computer. Fluctuation of the water surface or sediment impacts on the floor of the trap did not affect the measurements.

The bed-load trap was emptied as soon as a sufficient amount of sediment for a reliable sieve analysis had been accumulated. The smallest bed-load sample taken, weighted at least 1 kg. The sample of the transported material was then air dried at 105 $^{\circ}$C for 24 hours and then a typical sieve analysis at 1 phi sieve intervals was performed in order to obtain the particle size distribution of bed-load transport.

5.3.6   Estimation of bed surface composition

5.3.6.1 Introduction

The determination of bed material grain size distribution requires the following three steps:

1. Collection of a representative sample of the bed material,
2. Division of the sample into size classes or assignment of particle sizes
3. Finding the frequency of occurrence of each grain class

Each step can be performed with the employment of several methods. A short summary of the available methods is presented in table 5.4.

Table 5.4   Available methods for finding the particle size distribution of bed material

Methods for collection of sample	Methods for assignment of grain sizes	Methods for finding frequency of occurrence
a) Volumetric sampling	a) Sieve analysis	a) Distribution by weight
b) Grid sampling i.e. pebble counts	b) Diameter of sphere with equal volume	b) Distribution by number
c) Areal sampling	c) Measurement of b-axis with caliper or rule	
d) Transect or line sampling	d) Measurement of b-axis on photographs	

The four sampling methods and the two methods for determining the frequency of occurrence of each grain class, when combined, result in eight different procedures for the analysis of bed material. These procedures, in turn, are called volume by weight (abbreviated v-w), volume by number (v-n), grid-by-weight (g-w), grid-by-number (g-n) and so on. The choice of the appropriate procedure depends on the bed material composition as well as the population type (i.e. bed-load, surface or subsurface material) that needs to be analyzed. For example, to obtain the particle size distribution of the subsurface bed material or bed-load transport, a volume-by-weight procedure should be applied. However, a description of the bed surface is possible only with the use of a surface oriented procedure e.g. an area-by-weight or grid-by-number procedure, depending on the size of the grains that are contained in the armor layer. Furthermore, the choice of the adhesive that will be used in case of areal sampling depends on the range of grain sizes that are contained in the surface layer.

One major problem is that different procedures of grain size analysis produce varying results, even if they are applied to the same bed material. For example, a grid-by-number analysis will yield a finer grain size distribution than an area-by-weight analysis, although both of these methods are referred to the same sediment population. Moreover, the bed-load and subsurface material composition are found by a customary

bulk sieve analysis, i.e. a volume-by weight grain size analysis. In order to couple observations of bed surface texture with fractional bed-load transport rates of a given parent bed material, the corresponding particle size distributions must be equivalent and directly comparable. Therefore, it is necessary to convert results of non-equivalent grain size analysis methods into their equivalents of volume-by-weight procedure.

In the following sections the employed methods for determining the particle size distribution of the bed surface are described. Additionally, the required conversions between non-equivalent grain size analysis methods are presented.

5.3.6.2 Employed grain size analysis methods

The composition of the surface bed material was determined with use of three different methods for grain size analysis, depending on the phase of the experiment. The employed methods are summarized in table 5.5.

Table 5.5   Employed methods for the determination of bed surface grain size distribution in the present study

Time	Sampling method	Assignment of grain sizes	Frequency of occurrence	Notation
$t = 0$ Initial bed surface GSD	Volumetric	Sieve analysis	Distribution by weight	Volume by weight (v-w)
Intermediate stages	Grid sampling	Measurement of intermediate b-axis on photographs	Distribution by number	Grid by number (g-n)
$t = t_{end}$ Final bed surface GSD	Areal	Sieve analysis	Distribution by weight	Area by weight (a-w)

The initial grain size distribution of bed surface was considered to be identical to that of parent bed material. Therefore, the grain size distribution was found by customary bulk sieve analysis. A predetermined volume of bed material was sampled at three different locations along the flume. Subsequently, the sample was air dried in 105 ^{o}C

for 24 hours and sieved for five minutes. The frequency of occurrence of each grain class was expressed as the percentage by weight of the sample remaining between two consequent square mesh sieves.

During ongoing experiments a photographic non-intrusive method was used for the evaluation of bed surface composition. The sample was created by selecting the grains lying beneath the nodes of a grid that was superimposed on plan view photos of bed surface taken during the experiments. The frequency of occurrence of each grain class was found by means of a numerical sieving procedure. It was expressed as the percentage by total count of sampled particles falling into the size interval between two consequent square mesh sieves. Thus, this method for grain size analysis can be characterized as grid-by-number method.

At the end of the experimental runs in the series with test reach length of 12 m the flume was dried and afterwards three area samples of surface grains were collected at three different locations with the use of wax as adhesive material. Subsequently, the sampled grains were separated from the wax and dried. The grain size distribution was found by sieve analysis of the dried material. The frequency of occurrence of each grain class was expressed as the percentage by weight of the sample falling into the size interval between two consequent square mesh sieves. Thus, this method for grain size analysis can be characterized as area-by-weight method.

Just before the end of each experiment, when the flume was still filled with water and just before collecting the area sample after the flume had been dried, the bed surface was photographed and the image analysis method was used in order to determine the armor layer grain size distribution. The comparison of the photos taken under dry and wet flume conditions assured that the flow of water did not affect the reliability of the image analysis method. Finally, the grain size distribution of the armor layer at the end of the experimental run that was obtained from image analysis was compared to that obtained from area sampling, after the latter was converted to its volume-by-weight equivalent. The fact that the results of the two methods were in agreement showed that the image analysis gave reliable results.

5.3.6.3 Determination of bed surface composition by image analysis and discussion on equivalence with volume-by-weight methods

In order to document the temporal evolution of bed surface composition without interrupting the experiment and disturbing locally the structure of the bed surface by sampling, a non-intrusive method was necessary. Therefore, the grain size distribution

was obtained by taking plan view pictures of the bed surface, which were further processed to obtain the grain size distribution.

The photographs needed to be clicked while the bed was still under water. In order to overcome the difficulties which are to be seen in Fig. 5.7 a plexiglass sheet mounted on a carriage providing flexibility of adjustment of its vertical position was lowered till it slightly grazed the water surface. There was no obvious effect of the near bed flow affecting the armoring process, thus facilitating the mode to obtain sharp images of the bed surface.
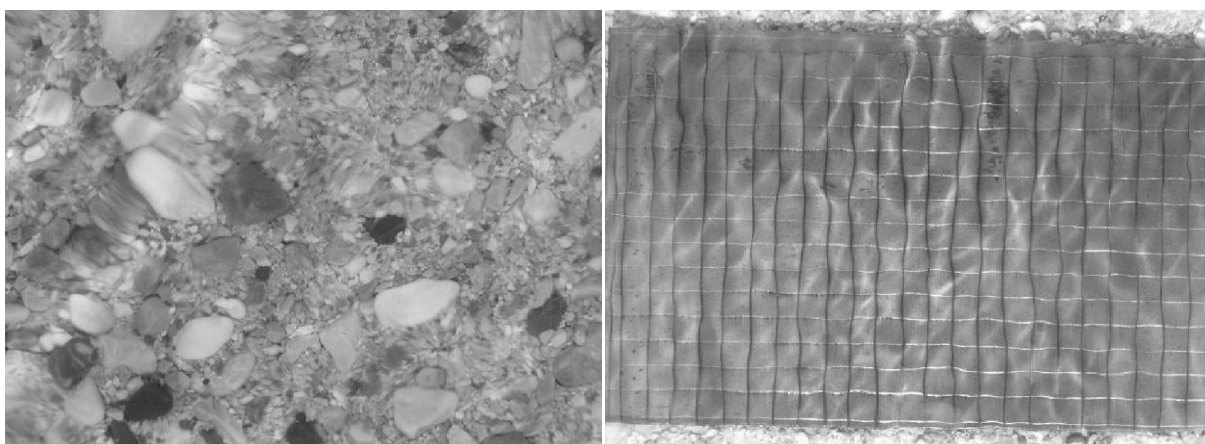
a: Blurring due to the flow   b: Distorsion of objects due to light effects

Fig.5.7   Problems that occurred when trying to photograph the bed surface through water (from Efthymiou & Rutschmann (2009))

The snaps were taken using a Canon EOS 450D camera with a 12,2 Megapixel sensor and a Tamron 18-200/3,5-6,3 lens. The camera was placed 50 cm above the bed surface, resulting in image pixel dimensions of 0,032 mm of real length. Care was taken to keep the camera's optical axis orthogonal to the bed surface in order to minimize tilt distortion. Two external lighting sources were arranged symmetrically to the camera position in order to achieve uniform luminosity and to minimize the shading effects during image collection.

The images of the bed were processed with the software Hdevelop v. 8.0.2 developed by the company MVTec software GmbH, Munich, Germany. The aim of the processing was to segment the picture into different regions consisting of single grains. Therefore a procedure was developed, which allowed for an automated identification of grain boundaries, based on the difference between neighboring pixels color intensities, and subsequent image segmentation. The applied segmentation method is presented by Efthymiou & Rutschmann (2009). Due to the lack of a contrasting background, heterogeneity in grain lithology, texture and shape as well as the packing

arrangement, the automated identification of individual particles was a difficult task. Therefore a manual correction of erroneous segmented regions was necessary in order to achieve the best possible results.

Subsequently, a grid was established over the surface and the virtual grains and the corresponding segmented regions lying beneath the nodes were sampled. The distance between the grid nodes was chosen to be 1,8 cm which was larger than the maximum grain diameter of the mixture. Moreover, the grid was positioned in such a way over the photograph, so that no grains which were cut by the photo boundaries were selected. This grid dimensions and positioning led to a sample of approximately 120 grains in every photo. Wolman (1954) in his classical work about grid sampling recommended the use of samples consisting of 100 grains. Hey and Thorne (1983) suggest that samples as small as 40 stones are sufficient.

The sampled grains were assigned into size intervals by means of a numerical sieving procedure. Ellipses were fitted onto segmented regions and the lengths of the two main axes were measured. The fitted ellipses had the same second moment as the regions. Butler et al. (2001) used the same method and argued that the estimated length of the intermediate axis when estimated by ellipse fitting is similar to that measured directly by a rule. The finding was verified by similar measurements in the current study. The assumption was made that the visible small axis of the 2 dimensional ellipse corresponds to the intermediate or b principal axis of the 3 dimensional ellipsoid. The above described procedure is equivalent with picking up the grain and measuring the b-axis with a caliper or a ruler. Consecutively the caliper determined axis was converted to its equivalent square sieve opening with eq. 5.23, which is given by Church et al. (1987).

$$\frac{D}{b} = \frac{1}{\sqrt{2}} \sqrt{\left[1 + \left(\frac{c}{b}\right)^2\right]} \qquad \text{Eq. (5.23)}$$

where: D   is square sieve opening [m]
        b   is caliper determined b-axis [m]
        c   is length of c-axis

In order to estimate the flatness of the grains, 30 grains of each fraction were identified on an image and then collected and measured with a ruler. For the coarser fractions an average flatness index c/b of 0,55 was found, where 'c' and 'b' are the small and intermediate axes lengths respectively. For particles smaller than 2 mm the measurements were less accurate, however they were more spherical and therefore a ratio c/b =1 was used for estimating the length of the small axis. Then the ellipses were

distributed to classes with respect to their corrected b-axes. The above described technique provides a measure of size that is equivalent to conventional sieving. The ratio of number of grains belonging to each size interval to the total count of sampled grains was used for expressing the frequency of occurrence of each grain class.

Discussion on the equivalence of particle size distributions obtained by grid-by-number and volume-by-weight methods

The above described method, which can be abbreviated as grid by number (g-n), was used because it is widely inferred that the particle distribution obtained by this procedure is equivalent and subsequently comparable with the corresponding distribution obtained by the volume by weight standard procedure. Nevertheless, Fracarollo & Marion (1995) claimed that the grid by number distribution which is obtained from image analysis of plan views of the bed surface is identical to the surface by area distribution, which in turn needs to be converted to its equivalent volume by weight distribution. They stated that the problem goes back to the definition of grid sampling. Theoretically, the grains that are located underneath the grid nodes should be collected, even if they lie deeper in the void or interstice between larger grains, as long as they are visible. Practically it is not possible to collect a grain through the small voids of the surface layer by using one's finger. In addition Hey & Thorne (1983) stated that it is common practice to neglect sampling these grains and instead picking up the nearest particles. This common operator error introduces a bias which renders the volume by weight distribution equivalent with the grid by number distribution, as initially stated by Kellerhals & Bray (1971). However, when the grid sampling is performed by image analysis this operational error is absent and consequently the obtained grid by number distribution is equivalent to the surface by area distribution instead of the volume by weight.

In order to overcome this difficulty and make the procedure of grid sampling after image analysis equivalent with grid sampling in field conditions there were two options. The first one was to convert the surface by area distribution obtained by image analysis to its equivalent volume by weight distribution with use of eq. 5.24 a-c which was published by Fraccarollo & Marion (1995).

$$p_{i,\infty} = p_{i,0}\left(1 + \frac{p_{v,0}}{D_i \sum_{j=1}^{N} \frac{p_{j,0}}{D_j}}\right)$$ Eq. (5.24 a)

$$p_i^{s-a} = p_{i,\infty} - \frac{(1-\delta_{Ni})p_{i,0}}{2} + \frac{1}{2}\sum_{j\ 1}^{i\ 1} \frac{p_{j,0}p_{i,\infty}}{\left(1 - \sum_{k=1}^{j} p_{k,\infty}\right)}$$ Eq. (5.24 b)

$$p_i^{s-a} = p_{i,\infty}\left(1 + \sum_{j=1}^{N} \frac{p_{j,0}}{2}\right) - \frac{p_{i,0}}{2}$$ Eq. (5.24 c)

where: p_i^{s-a} is percentage of ith fraction in surface by area frequency distribution

$p_{i,0}$ is percentage of total volume occupied by particles of the ith fraction

$p_{i,\infty}$ is porosity

D_i mean sieve diameter for the ith grain-size fraction

N   number of grain-size fractions

δ Kronecker operator (it is assumed that $D_i > D_j$ when j>i)

Eq. 5.24b should be applied in case of matrix-supported arrangement of the bed surface, while Eq. 5.24 c in case of framework-supported arrangement. The problem regarding the expressions proposed by Fraccarollo and Marion (1995) is that the inverse problem is mostly of interest. This means that provided that the surface by area distribution p_i^{s-a} is known by the image analysis, the equivalent volume by weight distribution $p_{i,0}$ must be found. However, the system of equations they proposed is nonlinear with respect to the volumetric parameters $p_{i,0}$ and therefore doubtful whether they can analytically be inverted and provide a unique solution, as stated by Diplas & Crowder (1997). Fraccarollo & Marion (1997) commented that in the event of the reverse problem they found the solution numerically, by trial and error. The latter, however, is burdensome when a large number of grain-size classes is found. Notwithstanding, the most important problem is that the grains lying deeper in the voids of the bed surface must be correctly attributed to their relevant grain size, in order to obtain the best possible surface by area distribution. This is possible only in laboratory investigations when particles of different colors are used; even in that case the outcome is doubtful due to shading effects. If no colored particles are used, as in the current study, then the use of the above set of equations will lead to erroneous results. The second option was to try to transfer the procedure of grid sampling as it is carried out on the field to the case of image analysis.

5.3.6.4 Conversion of area-by-weight grain size distribution to equivalent volume-by-weight

At the end of each experiment an area sample of the bed surface was taken with use of wax as adhesive. After the separation of the grains from wax the sample was dried and the particle size distribution was found with sieving. This procedure led to an area-by-weight sample which needed to be converted to its equivalent volume-by-weight sample. Kellerhals & Bray (1971) based on their voidless cube model proposed the following formula for the conversion of an area-by-weight distribution to an equivalent volume-by-weight distribution.

$$p(V - W)_i = Cp(A - W)_i \overline{D}_i^{-1} \qquad \text{Eq. (5.25)}$$

where: $p(V\text{-}W)_i$ is percentage of ith fraction obtained from volume-by-weight

$p(A\text{-}W)_i$ is percentage of ith fraction obtained from area-by-weight

C is constant found by integrating Eq. 5.25

The integration of eq. 5.25 gives

$$\int_{\overline{D}_{min}}^{\overline{D}_{max}} p(V - W)_i \overline{D}_i \ d\overline{D}_i = C \int_{\overline{D}_{min}}^{\overline{D}_{max}} p(V - W)_i \overline{D}_i \ d\overline{D}_i \qquad \text{Eq. (5.26 a)}$$

$$E_V[\overline{D}_i] = C \qquad \text{Eq. (5.26 b)}$$

or alternatively

$$E_A\left[\overline{D}_i^{-1}\right]^{-1} = C \qquad \text{Eq. (5.26 c)}$$

where: $E_V[\overline{D}_i]$ is the arithmetic mean diameter of the volumetric sample

$E_A\left[\overline{D}_i^{-1}\right]$ is the arithmetic mean diameter of the areal sample

However, further investigations, for instance Ettema (1984), showed that the aforementioned conversion procedure when applied to gravels from stratified and armored deposits, overcompensates for the sampling differences by biasing the finer fractions. This means that the converted area-by-weight distribution will be finer than the one obtained from volumetric analysis of the same material. Gomez (1983) and Anastasi (1984) proposed substituting the conversion parameter which is expressed by the exponent at the end of eq. 5.26a with a value of -0,5 instead of -1. Diplas and Sutherland (1988) pointed out that the major shortcoming of the Kellerhals & Bray cube model is the absence of voids. They introduced a modified cube model which included voids accounting for a 33% porosity and thus was more representative of

fluvial sediments. Based on experiments with river gravels in combination with the newly introduced modified cube model they suggested the use of an exponent with value of -0,47 for converting area-by-weight samples to volume-by-weight samples when sampling takes place with use of wax as an adhesive.

Fehr (1987a and 1987b) proposed a method based on transect line sampling for the determination of bed surface grain size distribution. In order to mitigate the bias of erroneous sampling of fine particles when the fluvial deposits contain particles within a wide range of grain sizes, Fehr suggested a methodology for the correction of the initially obtained grain size distribution and the conversion to its volume by weight equivalent. Considering that the line sampling provides a representative sample of particles sizes between medium gravel and small boulders while for grains finer than 2 mm a representative sample can be obtained by means of an area-based method (e.g. with use of an adhesive), Fehr proposed the adjustment of the distribution derived from line sampling with a Fuller curve. Thus a new cumulative frequency distribution for the fine part of the line sample is created and the bias due erroneous sampling of fine particles is removed. The above described method offers a very fast and effective method for the determination of a volume-by-weight equivalent grain size distribution of bed surface, which suitable for field investigations especially for sand-coarse gravel mixtures. However, in the present study the range of grain sizes contained in the employed sediment mixture was considerably smaller, while the high resolution of the photos taken allowed a clear distinction even of medium sand grains. Therefore, the results of the pebble count on a grid overlying on a plan view photo of bed surface was considered to be representative of the fine counterpart.

Diplas & Fripp (1992) demonstrated that the value of the conversion parameter depends on the penetration depth of the adhesive, which in turn depends on adhesive viscosity as well as porosity, sorting and fine content of the bed material. In a framework-supported deposit which contains predominantly coarse material (fines are less than 20%-25%) the coarse grains are sampled areally, while the finer grains are sampled volumetrically when wax is used as adhesive material. In the case of a coarse framework supported sediment mixture the conversion factor was found to be -0,5, while for fine framework-supported sediment mixtures the conversion factor varied between -0,5 for the coarse fractions and 0 for the finer particles. These results showed that in that case a two-exponent approach should be used. The authors, however, suggested that in most cases the use of a single value of -0,47 can lead to a sufficient areal-to-volumetric conversion as long as the percentage of fines in the mixture is rather small. For a matrix-supported deposit which contains a considerable amount of fines (fines more than 30%), both fine and coarse grains will be sampled areally, as the abundance of fine sediment prevented the deep penetration of the adhesive. This

renders it a truly areal sample for which the established by Kellerhals & Bray conversion factor of -1 is valid. In order to overcome the difficulties regarding the choice of the suitable conversion factor in eq. 5-25a Marion & Fraccarollo (1997) proposed a conversion procedure where the penetration depth will be calculated from the area and weight of the sample and consequently will be used to compute the volume-by-weight particle size distribution. The procedure consists of the following equations:

$$W_{tot} = \sum_{j=1}^{N} W_j = \gamma A_s \frac{(1 - p_{v,0})}{\sum_j p_j^{a-w}/(D_s + D_i/2)} \qquad \text{Eq. (5.27 a)}$$

$$p_{i,0} = \frac{p_i^{a-w}(1 - p_{v,0})}{(D_s + D_i/2) \sum_{j=1}^{N} \dfrac{p_j^{a-w}}{D_s + D_i/2}} \qquad \text{Eq. (5.27 b)}$$

where: W_{tot} is the total weight of the areal sample
       W_i is weight of the ith fraction in the area sample
       γ is specific weight of the sediments
       A_s is sampling area
       $p_{v,0}$ is porosity
       p_i^{a-w} is fraction of the ith fraction in the area-by-weight distribution
       N is number of grain-size fractions
       D_s is wax penetration depth
       D_i is mean sieve diameter for the ith fraction
       $p_{i,0}$ is fraction of the ith fraction in the volume-by-weight distribution

Eq. 5.27a can be solved iteratively by trying different values of the penetration depth until the calculated total weight of the areal sample is equal to the measured. The size of the D_{50} particle can be used as starting value for D_s.

In Fig. 5.8 the median grain size of the armor layer determined by means of the grid-by-number size analysis procedure, performed on plan view photos of the armor layer taken at the end of each experiment against the median grain size of the same armor layer that was determined by means of the area-by-weight grain size analysis is plotted. The 15 points refer to samples taken at the end of five experiments (the series of experiments with test reach length of 12 m), at three different locations along the flume. The grain size distribution obtained by the area-by-weight method was converted to its equivalent volume-by-weight particle size distribution by using the

Diplas & Sutherland (1988) method (open circles in fig. 5.8) and the Marion & Fraccarollo (1997) method (black x). A value 0f -0,47 was used as exponent in the conversion with Diplas & Sutherland (1988). The comparison shows a satisfactory agreement between the results obtained by the two different grain size analysis methods when the conversion of Diplas & Sutherland (1988) is applied. On the contrary, the conversion of Marion & Fraccarollo (1997) led to an over-estimation of the median grain size of the armor layer when compared to that obtained by the grid-by-number procedure.
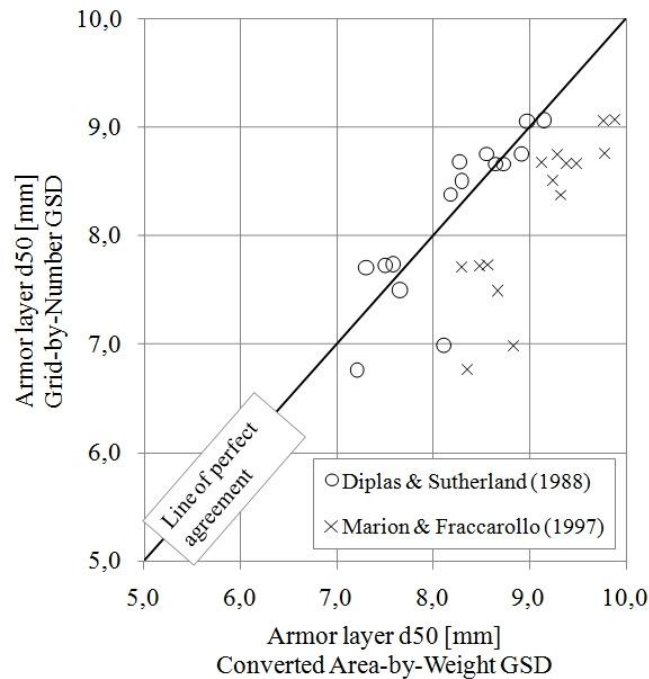

Fig. 5.8 Comparison between median grain sizes of armor layer obtained by gird-by-number and area-by-weight grain size analysis methods. The area-by-weight grain size distribution has been converted to its volume-by-weight equivalent with use of two different conversion methods reported in the literature

The good agreement between the two different analysis methods, increased the reliability of the results of the image analysis procedure that was employed to document the temporal variation of the grain size distribution of the armor layer.

6.   Experimental results & discussion

6.1   Introduction

In the present chapter the results of the experiments are presented. As previously stated, the experiments focused on the investigation of the spatial and temporal evolution of the phenomenon of static armoring under varying shear stresses. The experimental results concern:

- the variation of total as well as fractional bed-load transport rates during the experiments and along the working length
- the evolution of bed geometry
- the development of bed surface grain size distribution

During the experiments the measurements were undertaken at three different locations along the flume. Thus, a detailed insight into the transport processes that take place during the formation of armor layers was gained. These measurements reveal the unsteadiness of bed-load discharge both in time and space. Furthermore, each grain class behaves differently on the one hand, due to size effects and on the other, due to variation of bed surface composition. Herein an effort is made to present the main trends that were observed in the experiments with the intention of providing a better understanding of the mechanism that governs the phenomenon of static armoring. The main focus lies on the recognition of systematic patterns which characterize the transient changes of fractional transport rates. These will be further interrelated to grain size distribution of bed surface.

6.2   Bed elevation development and hydraulic properties of experimental runs

The elevation of bed surface was measured regularly during ongoing experiments. The documentation of transient changes in bed surface geometry and water table was necessary, in order to estimate the shear stress that was exerted on bed. Fig. 6.1 shows the set of bed surface elevation measurements taken during the experimental run that was performed with flow discharge 70 l/s and length of movable bed 12 m. The initial thickness of the bed was 10 cm in a dry condition. However, after the initial wetting the bed thickness was found to be always slightly smaller and therefore the initial condition in fig. 6.1 is taken to be the straight line with elevation 0,097 m azl. Two sets of original measurements taken a few minutes after the inception of the experiment and after closing the water discharge are also illustrated in fig. 6.1 with

solid rectangular and round symbols. The intermediate measurements are represented by straight lines that were fitted to original measurements with linear regression. The bed elevation measurements are normalized by the original slope of 0,0015. Thus, a horizontal line in fig. 6.1 corresponds to bed surface with average slope of 0,0015 in reality.
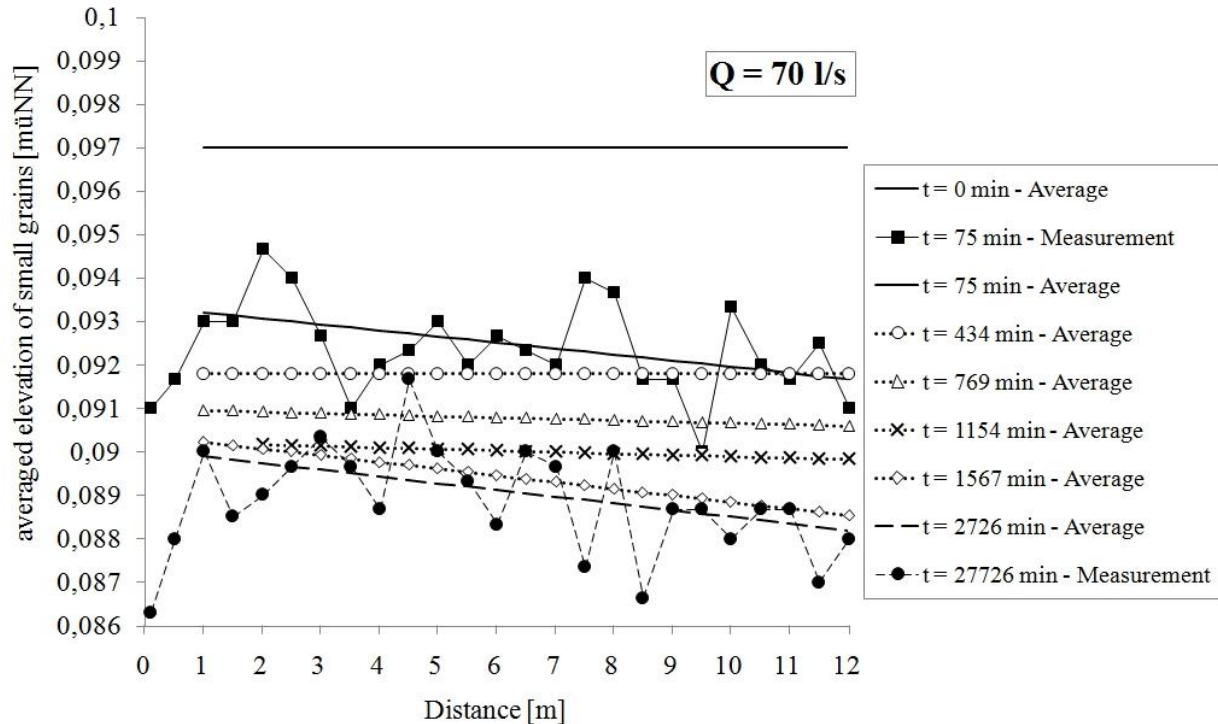

Fig. 6.1 Data set of bed surface elevation development, as observed during experimental run performed with flow discharge 70 l/s and working length 12 m

An almost parallel degradation was observed during all experimental runs and the average bed slope varied slightly. The water depth was kept constant during ongoing experiments by adjusting the water level to the measured average bed surface elevation. Hence, the exerted shear on bed did not change considerably during the formation of armor layer. Bed degradation occurred faster in the early stages of each experiment and slowed down as time progressed, being thus directly associated to the observed bed-load transport rates. A small scour hole developed in the upstream area of movable bed. The scour hole had a length of about 1 m and did not expand in the downstream direction throughout the experiments. The maximum depth varied with flow discharge between 2-3 mm when water discharge was 70 l/s to something less than 1 cm when the imposed flow rate was 150 l/s. Accordingly, the developed scour hole affected only locally the flow field. As expected, the observed bed degradation was larger when the imposed flow rate increased. Nonetheless, the pattern of parallel degradation was met in all of the experiments regardless of flow strength. In fig. 6.2 the variation with time of bed elevation is shown in three different locations along the

flume. The diagram contains measurements taken during experiments performed with 70, 100 and 150 l/s.
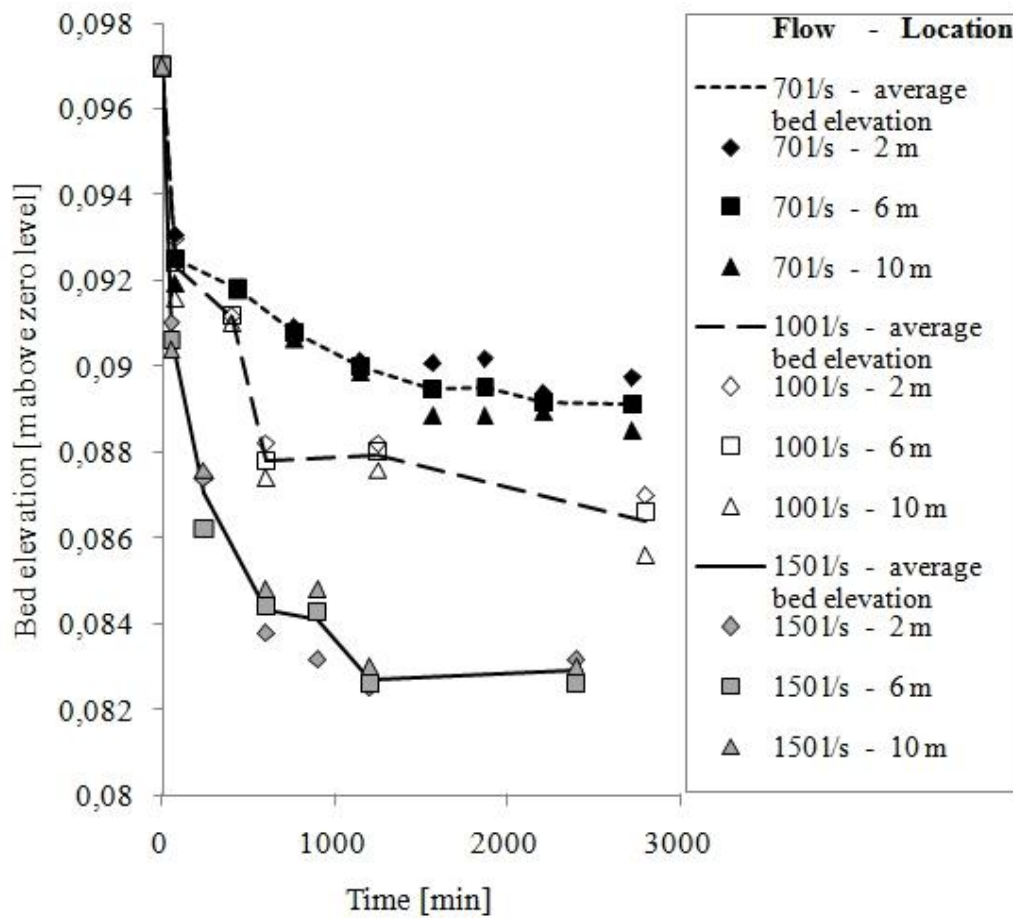

Fig. 6.2 Variation with time of bed elevation in three different locations, as observed in experiments performed with 70, 100 and 150 l/s

The hydraulic conditions of each experimental run are summarized in table 6.1. The run annotations that start with A signify an individual experimental series containing five runs that were performed with length of the erodible bed of 4 m and varying water discharges. The annotations B1-B5 and C1-C5 signify experimental runs that were conducted with length of sediment bed 8 and 12 m respectively. The flow depth was kept constant throughout the experiments by adjusting periodically the downstream hydraulic boundary condition according to the measured bed degradation. The flow depth was measured along the flume in order to verify the prevalence of normal flow conditions during the experimental runs.

Table 6.1   General hydraulic properties of experimental runs

Run	Sediment bed length [m]	Water discharge [l/s]	Flow depth [m]	Slope [-]	Shear stress [Pa]
A1	4	70	0,190	0,0015	2,00
A2	4	80	0,230	0,0014	2,29
A3	4	100	0,268	0,0016	3,05
A4	4	120	0,298	0,0016	3,24
A5	4	150	0,340	0,0016	3,44
B1	8	70	0,190	0,0015	2,00
B2	8	80	0,230	0,0015	2,50
B3	8	100	0,265	0,0015	2,75
B4	8	120	0,297	0,0016	3,22
B5	8	150	0,342	0,0016	3,48
C1	12	70	0,191	0,0016	2,20
C2	12	80	0,232	0,0014	2,32
C3	12	100	0,270	0,0016	3,09
C4	12	120	0,295	0,0015	2,91
C5	12	150	0,338	0,0016	3,40

The bed slope for each individual experimental run that is given in Table 6.1 was determined from plots of measured bed elevation at different time intervals (similar with fig. 6.1). In order to estimate the bed slope, a linear trend-line was fitted to the local measurements of average bed elevation at different cross-sections along the flume. The first upstream section of the movable bed with length of 1 m, where the scour hole developed was neglected. Hence, the bed slope was determined by the measured bed elevations of cross-sections 1-4 m, 1-8m and 1-12m when the length of the sediment bed was 4, 8 and 12 m respectively.

The shear stress values that are given in the last column of Table 7.1 correspond to the effective shear stress exerted to the bed after the elimination of the side wall effects. The bed shear stress was estimated by applying the side wall correction method that was proposed by Vanoni & Brooks and is described in chapter 5.3.4.2. Due to the lack of bed forms during the experiments the estimation of the skin friction portion out of total bed shear stress was not necessary.

6.3   Total bed-load discharge

The weight of the transported material collected in the bed-load trap, which was located at the downstream end of the flume, was continuously measured during all experiments. Thus, the total bed-load transport rate was calculated. The total transport rate was measured at three different locations during the experiments that were conducted with 70 and 150 l/s respectively. The rate is plotted in Fig. 6.3. As expected, the total bed-load discharge diminished as time proceeded due to progressive coarsening of bed surface. The measurement of bed-load at three different locations revealed an increase of transport rate in the downstream direction. Finally, increasing the imposed flow strength resulted in higher bed-load transport rates.
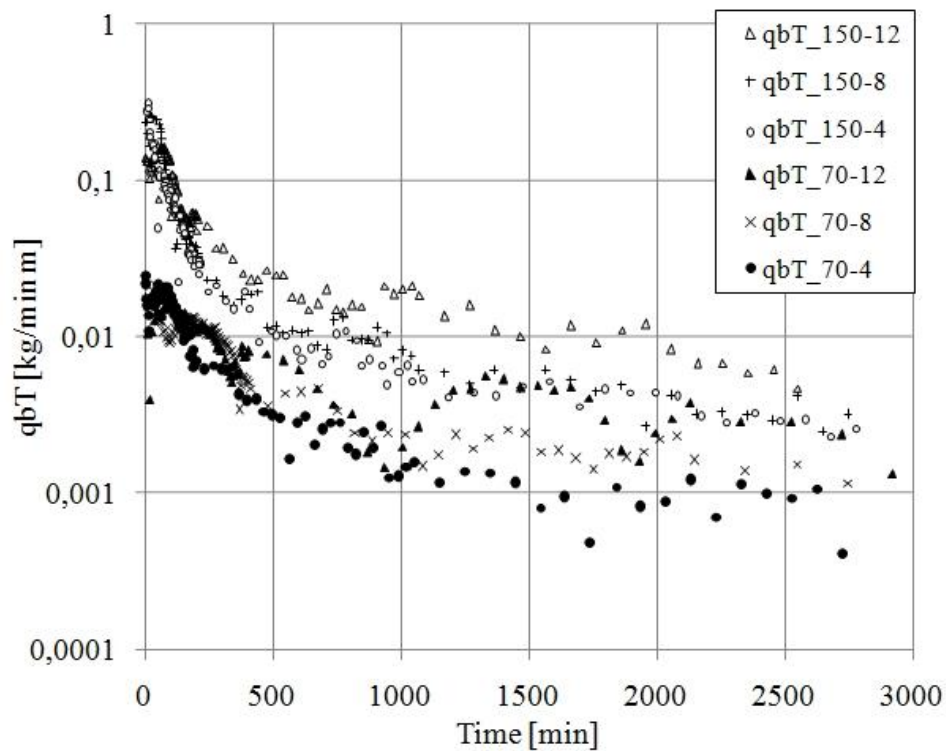

Fig. 6.3   Measured total transport rate during experiments with 70 and 150 l/s at 4, 8 and 12 m respectively

6.3.1   Temporal variation of total bed-load discharge

In all of the experiments the temporal evolution of sediment transport rate could be approached by two distinct phases. At the beginning of each experimental run and for a short time period, the bed-load discharge was constant. After this time period, the duration of which varied with flow strength, the total transport rate started to gradually decrease with time. This observation confirms results of previous studies e.g. Tait et al. (1992), Mosconi (1988) and Paris (1991).

The duration of the initial phase was determined by plotting total transport rate against time in log-log diagram. A characteristic plot of this type is shown in fig. 6.4. In this figure the total transport rate that was measured in the experimental run conducted with water discharge of 120 l/s and movable bed length of 4m is plotted. The end of the initial phase has been represented by a solid black line at 50 minutes.
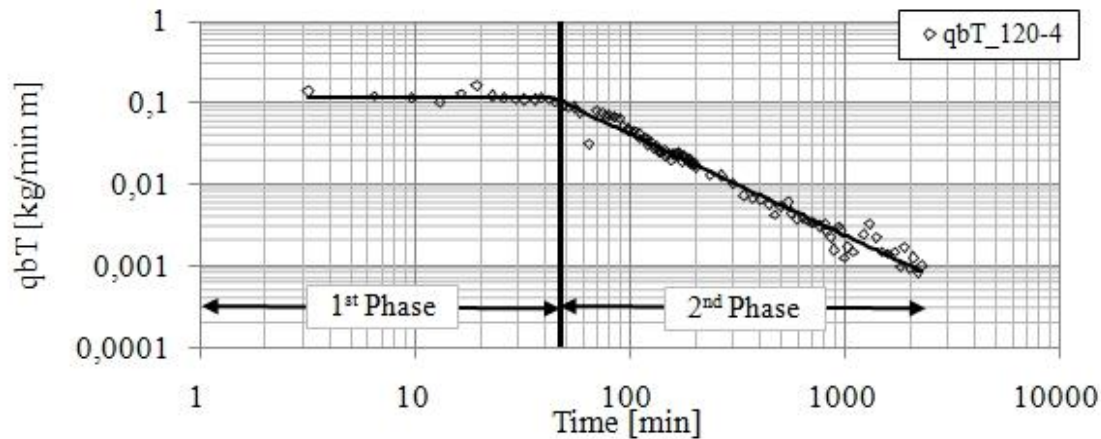

Fig. 6.4 Typical log-log plot of total transport rate against time

The estimated durations of the first phase are shown in fig, 6.5. The duration of the initial phase showed a consistent reduction with increasing flow strength. Furthermore, the onset of transport rate decline does not occur at the same time along the flume. The phase of the initial constant bed-load transport has a shorter duration when closer to the flume inlet. Tait et al. 1988 showed that the duration of the initial phase also depends on the composition of the parent bed material. As the parent bed material coarsened the duration of the initial phase became shorter.
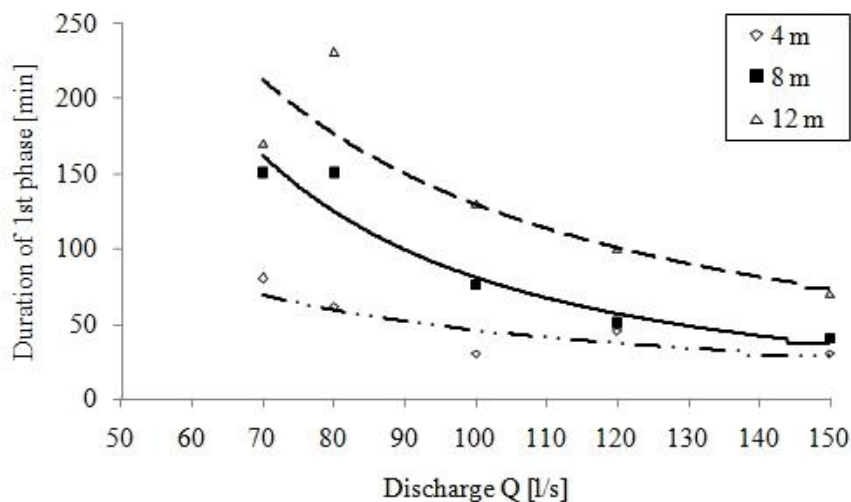

Fig. 6.5 Duration of 1st phase (constant transport rate) against discharge and distance from flume inlet

After the first phase of constant transport rate the bed-load discharge started to decline with time. A power relation could describe adequately the temporal variation of total

bedload transport rate. In fig. 6.4 the corresponding power relation is represented by the solid thin black line. The fitted lines were described by equations of the form:

$$q_{bT} = a_1 \cdot t^{n1} \qquad \qquad \text{Eq. (6.1)}$$

where: q_{bT} is total bed-load discharge

   t is time

   a_1 , n_1 are constants for each run

The determined values of exponent n of the fitted equations are plotted in Fig. 6.6. The value of this parameter expresses the rate of change with time of the measured transport rates. The negative values reflect that the transport rates diminished as time progressed. The smaller the value of exponent n, the more rapid the decline of sediment transport rate with time. The plot of the determined values shows no specific tendency for increase or reduction with flow strength. The values of exponent n varied between -0,7 and -1,1.   Despite the large scatter, a tendency for reduction with decreasing distance from the flume inlet is apparent, within the aforementioned range of values. This means that the measured total transport rate declined more slowly as the distance from flume inlet increased.
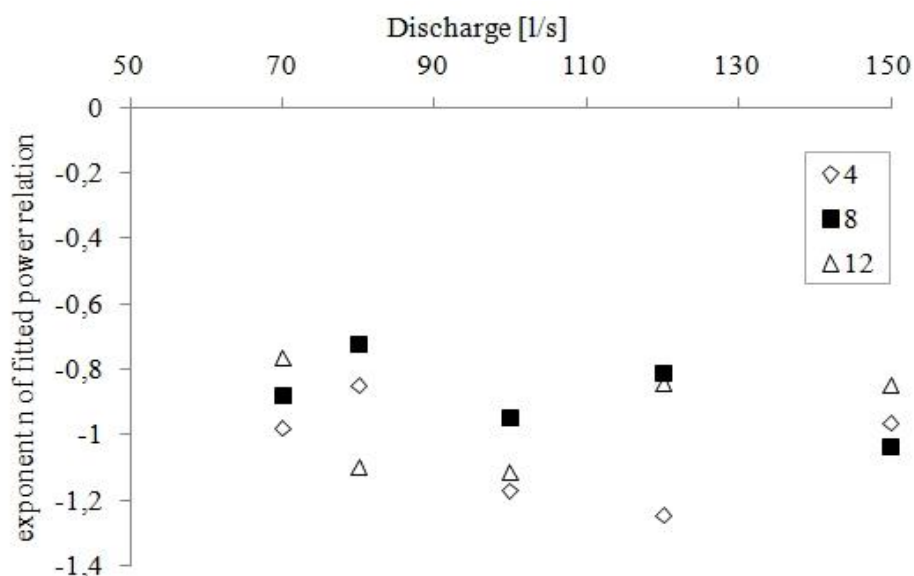

Fig. 6.6   Observed rate of transport rate reduction with time, expressed as the exponent of a fitted power relation

The measured transport rates diminished over two magnitudes of order during each run. By the end of each experiment the bed-load transport was approximately 1% of the initial transport rate. For example during the experiment which was carried out with a discharge of 150 l/s and working length of 4 m the measured transport rates ranged from 0,2 kg/min m to 0,002 kg/min m. This decrease of the transport rates is caused by the reduction of the dimensionless shear stress because of the coarsening of the bed surface.

6.3.2 Spatial distribution of total bed-load transport rates

The comparison of measured values of total transport rate at different locations along the flume showed that during the first minutes of all experiments the transport rate did not vary with distance along the flume. However, in forthcoming stages the earlier onset of transport rate decline at cross-sections closer to the flume inlet had as result that the transport rate appeared to increase with distance. The spatial distribution of total bed-load discharge at various intermediate stages along the flume is shown in Fig. 6.7 when the water discharge was set to 150 l/s. The point symbols represent measurements of total transport rate taken at distance of 4, 8 and 12 m from flume inlet respectively, while solid lines represent power relations fitted to the experimental data.
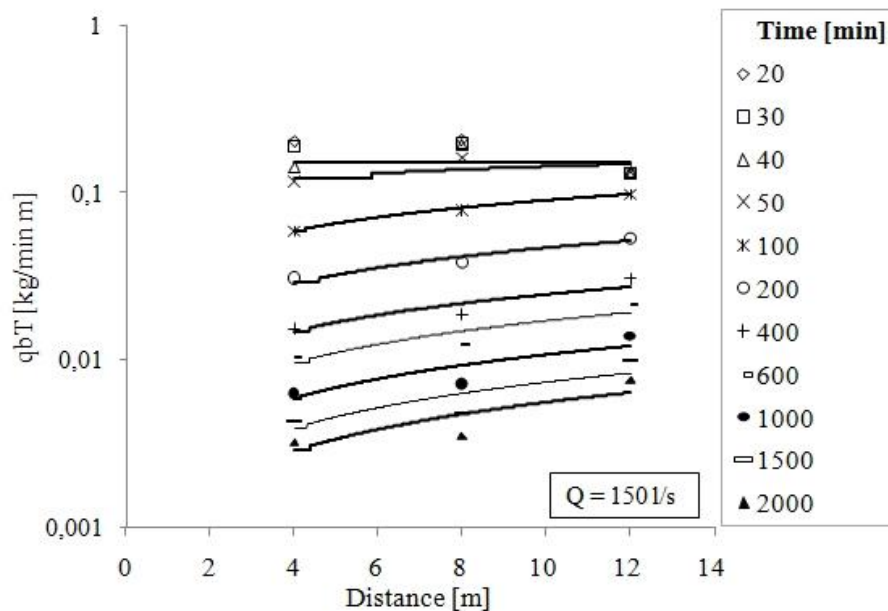

Fig. 6.7 Spatial distribution of measured total transport rates in the experiments with 150 l/s

The previous figure reveals that during the first minutes, when the bed surface had a high sand content, the amount of bed material that the flow could transport was extracted from the first meters of the flume length and then was transported over the bed surface until it was trapped in the bed-load collector. As time proceeded the line that connects the measurements obtains a positive slope, which reveals the increase of transport rate with distance.

The spatial variation of bed-load transport rates can be adequately described by an equation of the form:

$$q_{bT} = a_2 \cdot x^{n2} \qquad \qquad \text{Eq. (6.2)}$$

where: x is distance from the flume inlet

   a_2 , n_2 are constants for each run

Fig. 6.8 shows a plot of the values of exponent n_2 which were obtained from a regression analysis of the experimental measurements in intermediate stages during the experiments. This parameter expresses the variation of bed-load transport rate with distance. A value near one means that the transport rate increases linearly with increasing distance. On the contrary, a value close to 0 means that the transport rate remains constant along the flume. There seems to be no correlation with the flow strength but the form of the curves reveals an increase of the value of the exponent n over time after the initial phase when it takes values around 0. As bed surface coarsening proceeds the value of exponent n_2 approaches a value of 1.
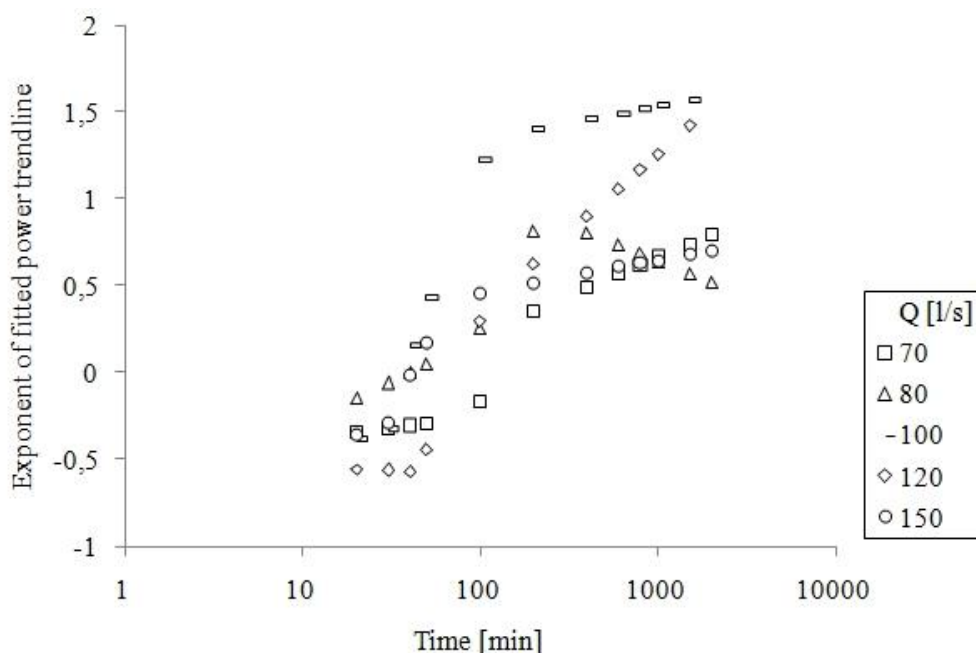

Fig. 6.8   Observed increase of transport rate with distance, expressed as the exponent of a fitted power relation

6.3.3   Variation of total bed-load discharge with flow strength

The measured bed-load transport rates increased with increasing flow strength as shown in Fig. 6.9, where the ratios of measured transport rates to the transport rate of the experiment with the lowest discharge are plotted.

It is evident that at the beginning of each run, when the bed was not armored, variations of the imposed shear stress caused large differences in the measured transport rates. By the end of each experiment, when the static armor layer was almost fully formed, the same variation of imposed shear stress caused much smaller variation of the observed transport rates. For example, at the beginning of the run with 150 l/s the transport rate was about 13 times higher than the measured transport rate at the

beginning of the run with 70 l/s. After 2000 minutes the transport rate in the run with 150 l/s was about 4 times higher than the corresponding transport rate of the run with 70 l/s. This observation leads to the conclusion that the armor layer becomes coarser with increasing flow strength. The ratio of the observed transport rates is proportional to the ratio of the dimensionless shear stresses. Fig. 6.9 shows that this proportionality is dynamic over time due to the coarsening of the bed surface. Taking into account that the average shear stress did not change over time and the fact that higher flow strength was associated with larger reduction of the value of this ratio, this behavior can only be attributed to the formation of a coarser armor layer at the end of the experiment with 150 l/s
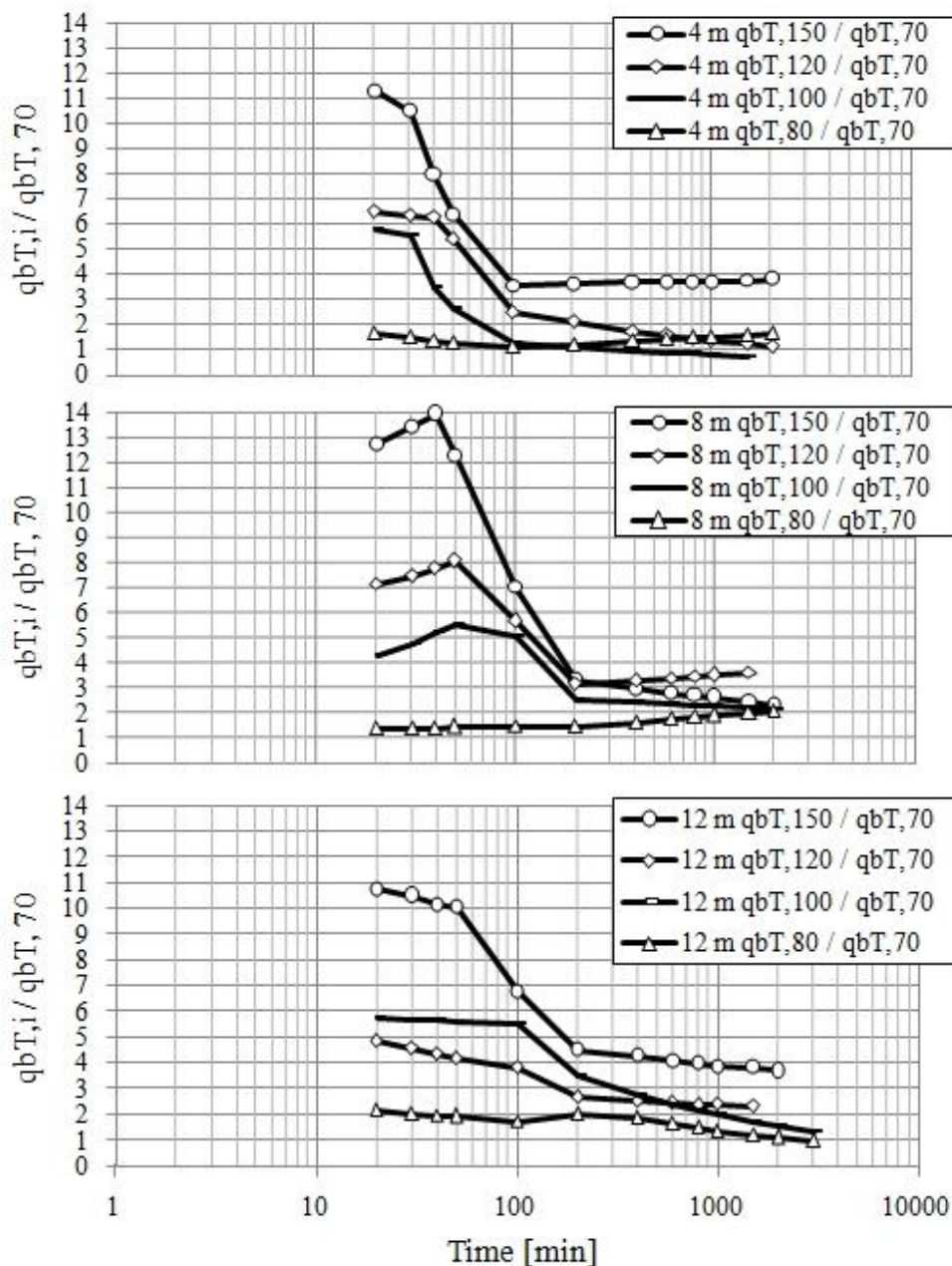

Fig. 6.9 Spatial distribution of measured total transport rates in experiments with 150 l/s

6.4   Composition of transported material

The transported material was collected at the end of the flume in a bed-load trap. The trapped sediment was removed from the bed-load collector as soon as a sufficient amount had gathered which would allow for a reliable sieve analysis. Subsequently the samples of transported material were air dried and a custom sieve analysis was performed in order to determine the corresponding grain size distribution. The composition of transported material allowed for the estimation of fractional bed-load transport rates. Fig.6.10 shows the temporal variation of d_{50} of transported material.
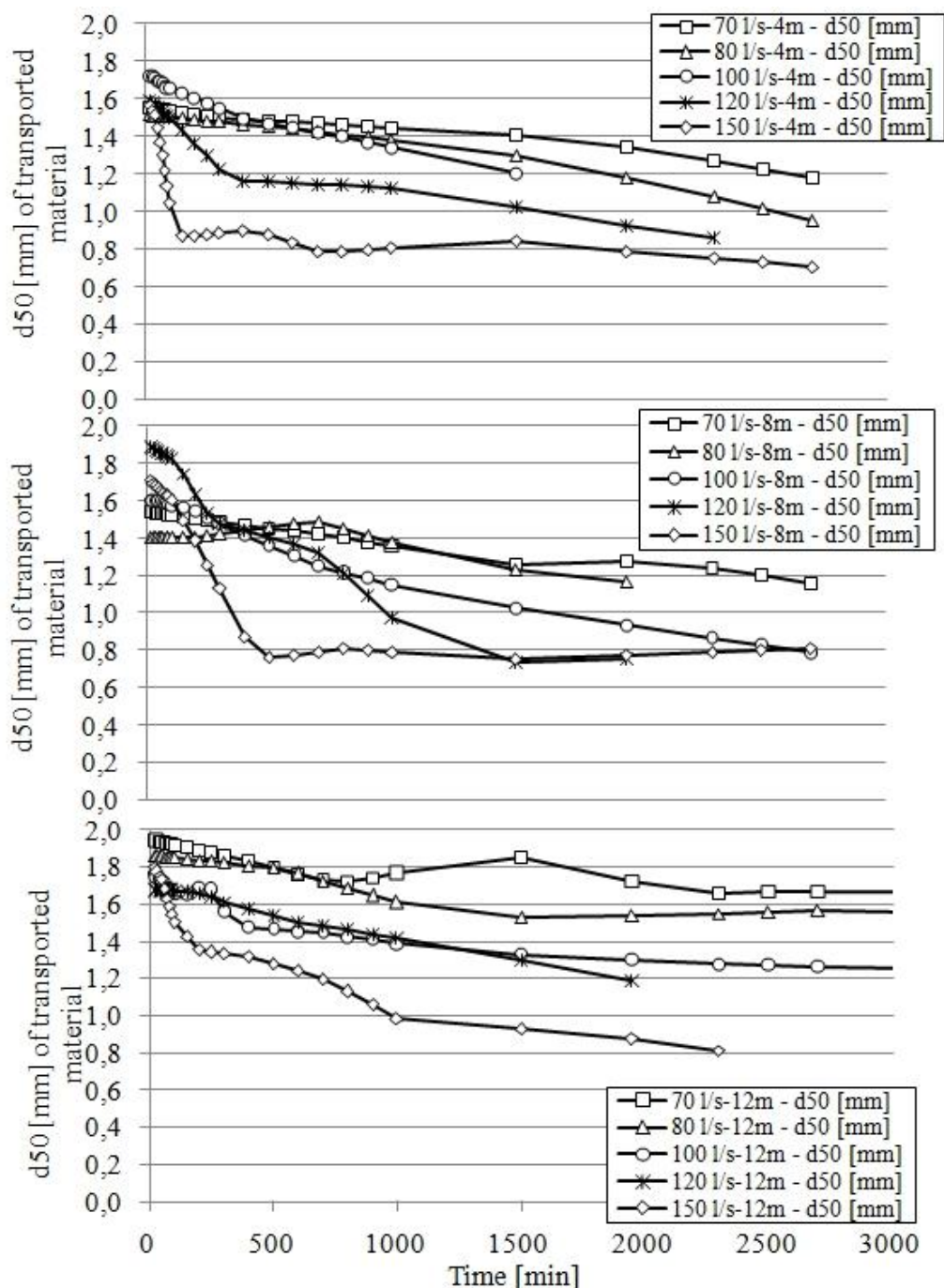

Fig. 6.10   Variation of median diameter of transported material with time

It is evident that in all experiments the transported bed material became finer as time progressed and bed surface coarsened. The decline of median diameter of material in transport occurred faster and was more prominent with increasing flow strength as well as reducing distance from the flume inlet. The observed fining of transported material can be attributed to the change of composition of bed surface which regulates the availability of the grains that can be entrained by the flow.

A more detailed analysis reveals a systematic adjustment of the composition of transported material over time. Fig. 6.11 shows the temporal variation of fraction volume content of bed-load of all size ranges as it was observed in two experimental runs. The temporal variation is described by the ratio of measured fractional volume content of ith grain class at different time intervals to the corresponding fractional content at the beginning of each experiment.
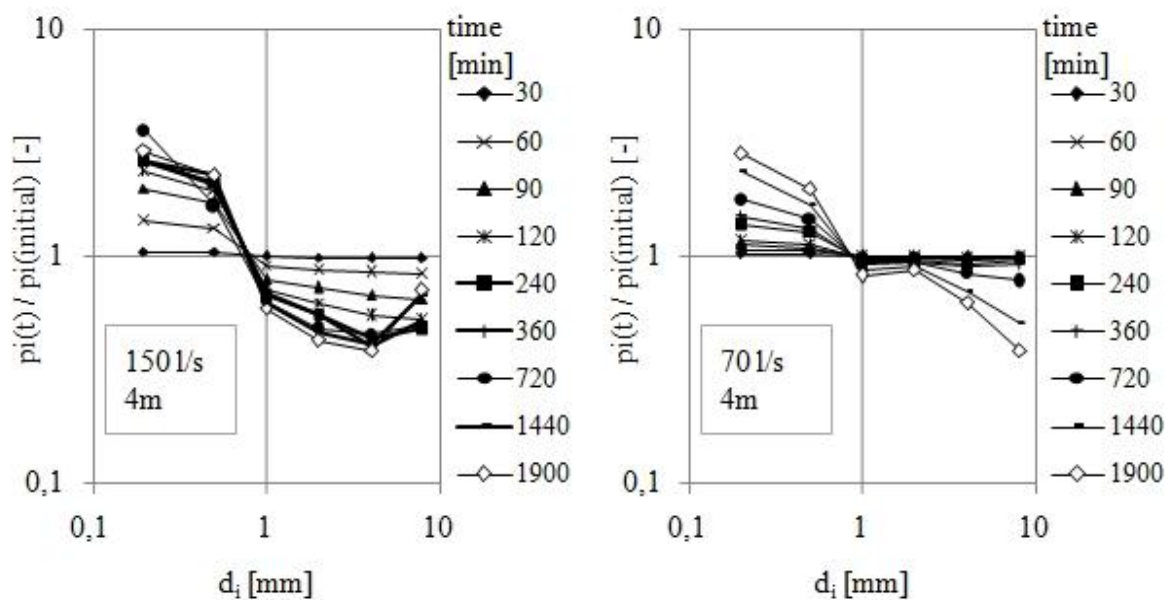
Fig. 6.11 Temporal variation of fraction content of ith grain class as observed in experiments conducted with movable bed of 4 m length and 70 and 150 l/s respectively

In all the experiments the fractional content by volume of grain classes with diameter 0,2 mm and 0,5 mm respectively increased with time. The grain class 0,2 mm showed a larger increase of the fractional content compared to grain class 0,5 mm. At the same time, the percentages of grain classes with diameter 1, 2, 4 and 8 mm diminished with time. The observed reduction of fractional content of these grain classes seems to become size independent as flow intensity increases.

The magnitude of changes in the composition of transported material increased with increasing flow strength, which is reflected in the larger decrease of bed-load d_{50} with increasing shear stress. This behavior is better illustrated in Fig. 6.12, where the

temporal variation of each grain class is plotted separately for different imposed shear stresses. In this figure it is clear that the fractional content of all grain classes is reduced over time except for grain classes with diameter 0,2 and 0,5 the fractional content of which is increased. The reduction or increase of fraction content becomes larger as the imposed flow strength is increased.
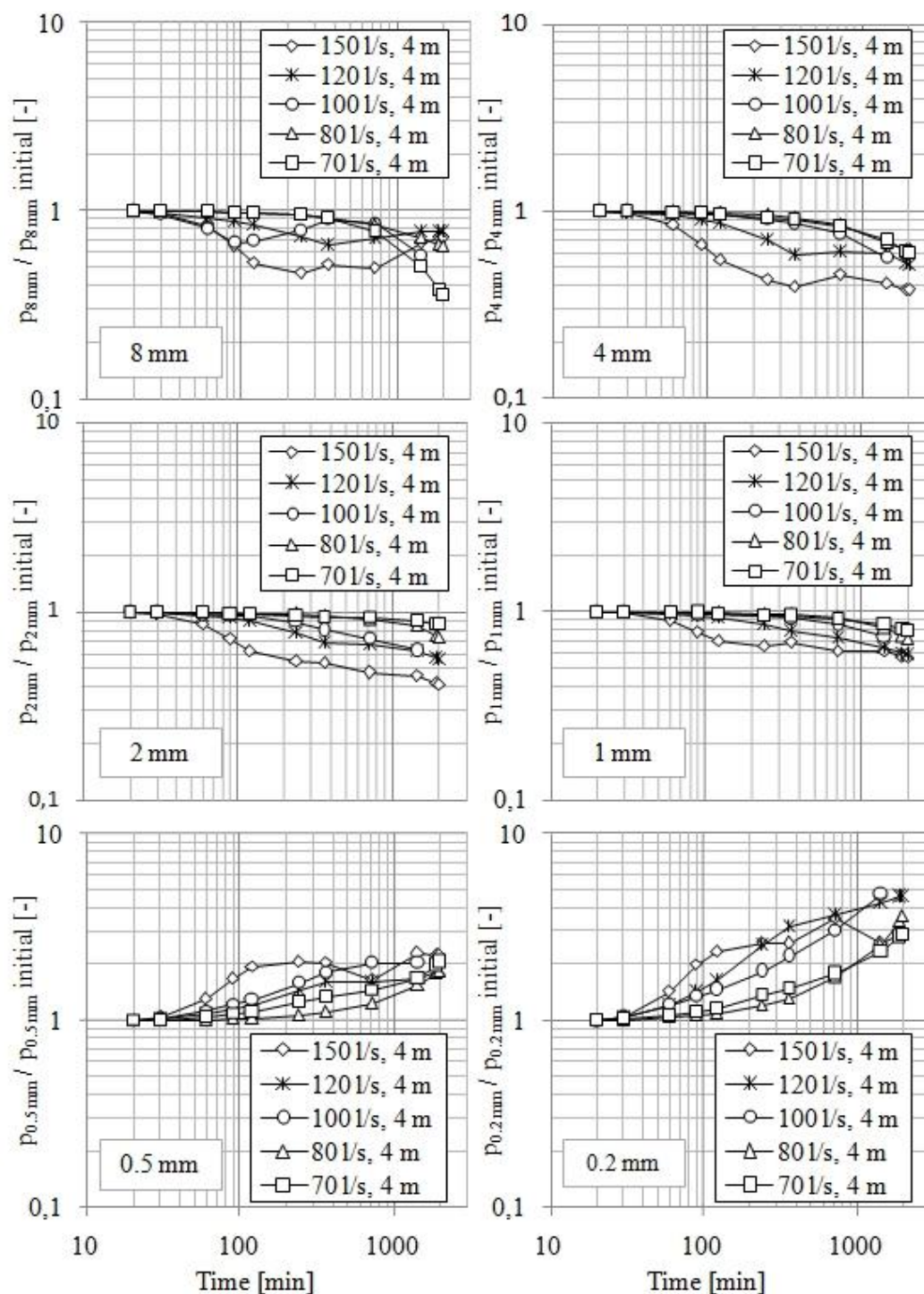

Fig.6.12 Temporal variation of fractional content in bed-load of all grain classes for different shear stresses as observed in experimental runs with working length of 4m

6.5   Fractional transport rates

The fractional bed-load transport rates were calculated as the product of total transport rate with fractional volume content of each grain class. The knowledge of transported material's grain size distribution together with continuous measurement of weight of extracted material at different time intervals as well as at different locations along the flume allowed for the determination of temporal and spatial variation of bed-load discharge of each individual grain class.

6.5.1   Temporal variation of fractional transport rates

Fig. 6.13 shows the temporal variation of fractional transport rates measured during the experiment conducted with 100 l/s and flume length of 8 m.
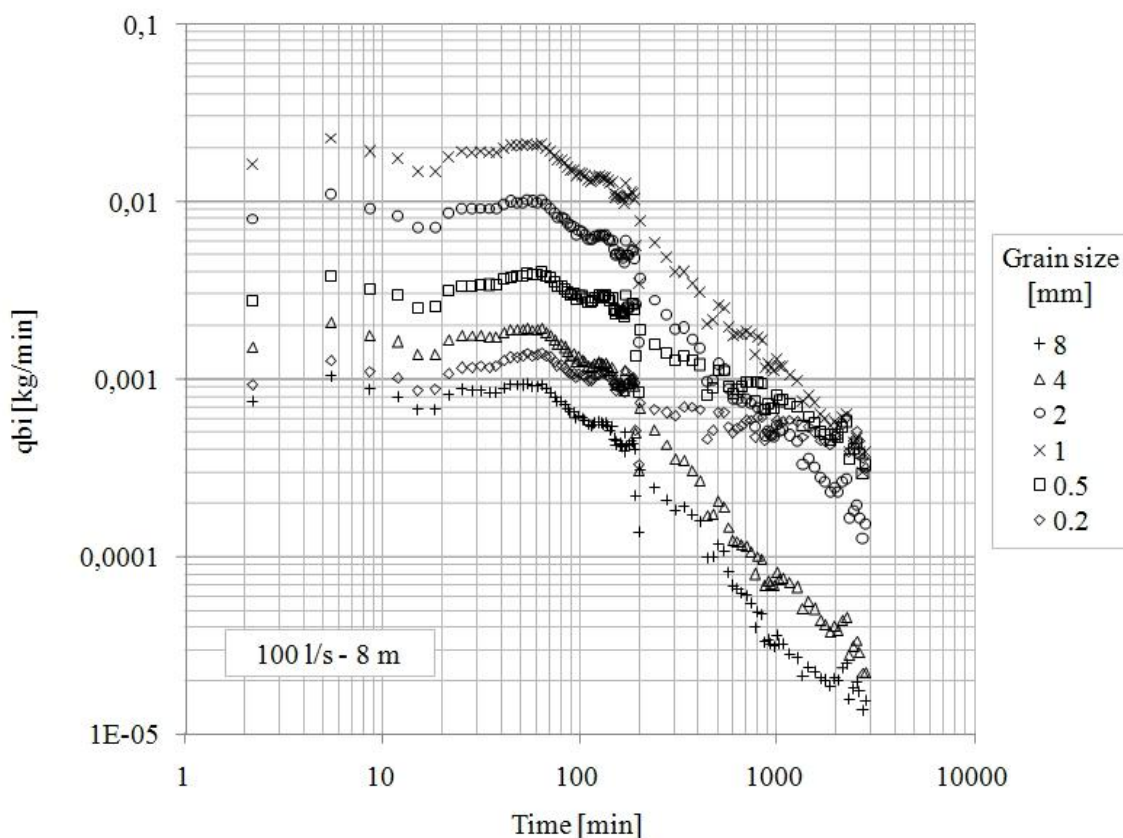

Fig. 6.13 Temporal variation of fractional transport rates (Experimental run 100 l/s –
          8 m)

As with total bed-load transport rate, the fractional transport rates were constant at the beginning of each experiment. In all the experiments the transport rate of grains with diameter between 1and 2 mm was the highest, while the grains with size between 8

and 16 mm always showed the lowest transport rates, although the difference with the transport rates of other finer grain classes was relative small. This result was surprising as the finer grains were expected to show the highest transport rate due to their intrinsic larger mobility. After this initial phase the transport rates diminished with time. In all the experiments a certain pattern recurs. The grains belonging to sand size range were at the end transported with the same transport rate and the grains belonging to the gravel size range continued to have a size depending behavior, meaning that the coarser the grains, the lower the bed-load discharge at which they were transported. The transport rates of the grains belonging to sand size range were always higher than the corresponding transport rates of the gravel grains. This behavior is illustrated in fig. 6.13.

The fractional transport rates followed the two phase pattern that characterized the total transport rate regarding their temporal variation. In the first phase the transport rates were constant, while in the second they declined as time proceeded. The duration of the initial phase was the same with the one that was determined for total transport rate and showed no variation with grain class size. Thus, all fractional transport rates started to decline simultaneously as long as the same shear stress was imposed. Furthermore, the duration of the first phase was shorter with increasing flow strength and distance from the flume inlet. Taking into account, first, Tait's et al. (1992) observation that the duration depended on the composition of the parent bed material, whereas a coarser parent bed material was characterized by shorter durations of initial constant transport rates; and, second, the fact that bed surface armored much faster with increasing flow strength, one is led to the conclusion that the transport rates start to decline when the bed surface attains a certain composition.

The reduction of fractional transport rates during the second phase of the armoring process were adequately described by a power relation as shown by Proffitt (1980). The exponent of the power function is a measure of the reduction rate. In fig. 6.14 the exponents of the power functions which were fitted to the measurements of fractional transport rates against grain class size are plotted. The sand grains, that is, those that were smaller than 2 mm showed a size depending behavior. The value of the exponent of the relation fitted to the transport measurements decreased consistently as grain size increased. As a consequence, the coarser the sand grain, the larger the reduction of its transport rate with time. On the contrary, the grains belonging in the gravel size range showed no size depending behavior. The exponents of the fitted power functions did not vary systematically with grain size. Hence, it is concluded that the fractional transport rates of gravel size ranges were reduced at the same rate with time regardless of their grain size. This conclusion is also supported by optical inspection of log-log plots of fractional transport rates against time.
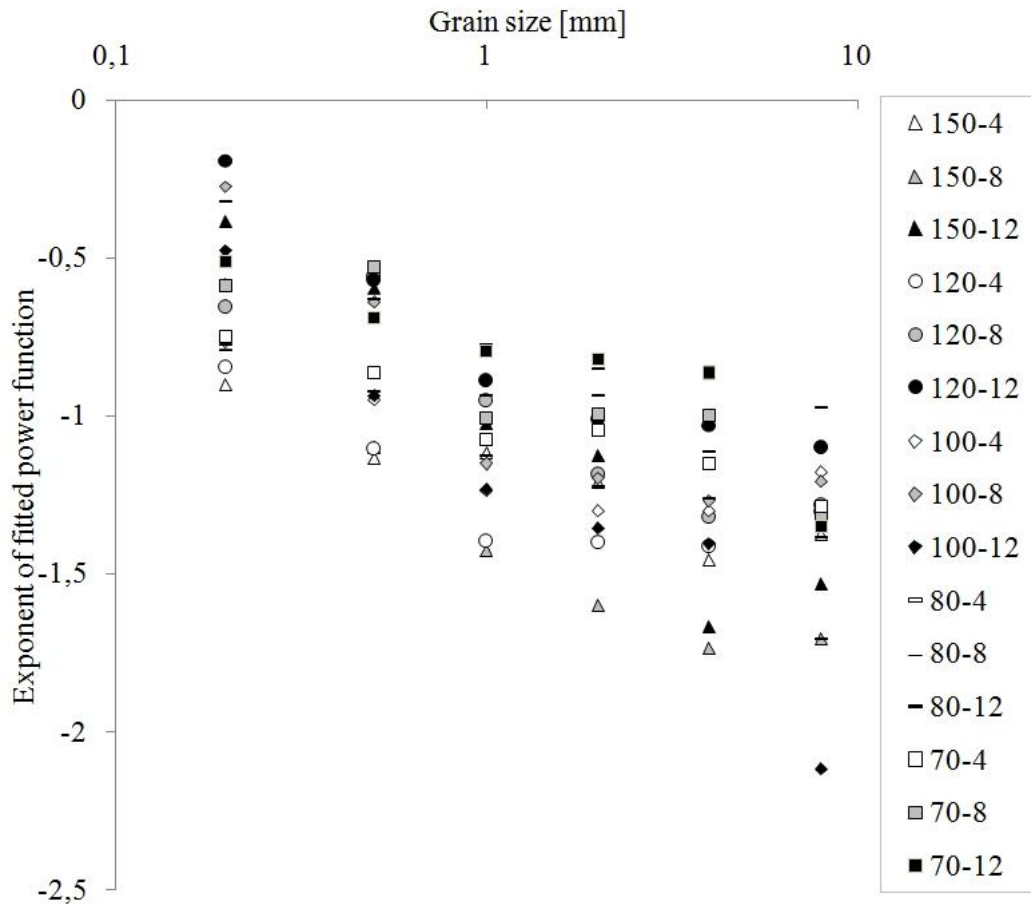
Fig. 6.14 Exponents of fitted power functions to fractional transport measurements for all experimental runs

No correlation was apparent between fractional transport rate reduction rate and flow strength or distance from the flume inlet.

6.5.2 Spatial variation of fractional transport rates

The spatial variation of fractional transport rates was found by applying the same analysis method as in the case of total transport rate. Fractional transport rates that were measured at the same time interval were plotted against distance and power relations were fitted onto the experimental measurements. An example is shown in fig. 6.15 based on the experimental runs performed with 150 l/s.
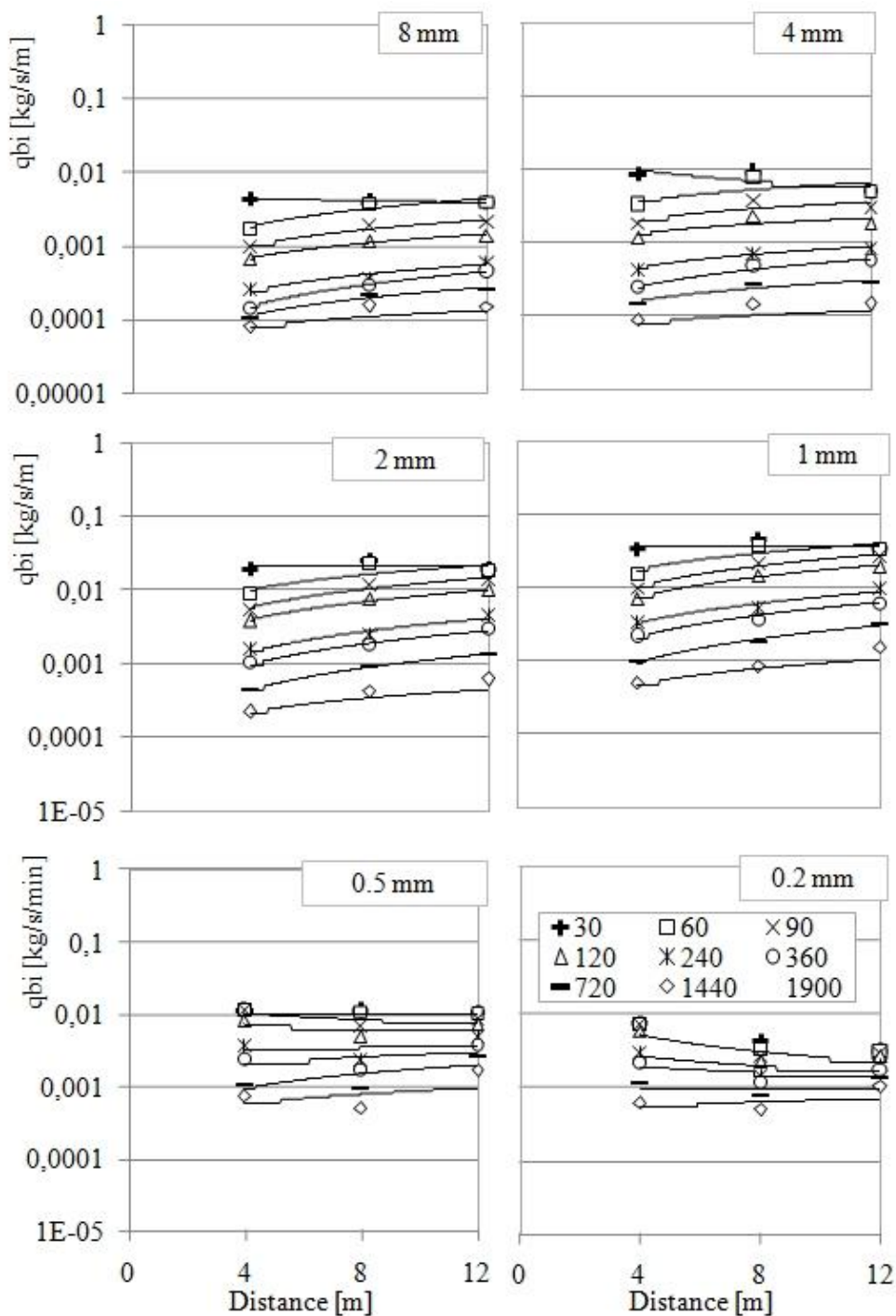
Fig. 6.15 Spatial distribution of fractional transport rates as observed in experimental runs conducted with 150 l/s

The fitted equations had the form

$$q_{bi} = a_i \cdot x^{n_i}$$ Eq. (6.3)

where: x is distance from the flume inlet

a_i and n_i are constants for each run and grain class

The exponents n_i of the functions that were fitted to the experimental measurements reflect the variation of fractional transport rates with distance. When n_i equals 0 then the fractional transport rate attains the same value in all measuring stations. When n_i becomes equal to 1 then q_{bi} increases linearly with distance. The determined n_i values always increased as time elapsed. At the beginning of each experiment the exponents took values near zero, that is, the fractional transport rates were almost the same along the flume. As time progressed, their value increased as the distance from the flume inlet became greater. This behavior was verified by optical observations performed during the experiments.

In fig 6.16 the temporal variation of determined exponents n_i in experiments that were conducted with 70 and 150 l/s respectively is shown. The different symbols refer to different grain classes. The increase of n_i value with time is obvious in all cases. Grain classes with diameter 0,2 and 0,5 mm were characterized by smaller values compared to the other grain classes, i.e. the fractional transport rates of these fractions did not vary significantly with distance. In addition, the slight observed increase of their value occurred more slowly in comparison to the observed increase of coarser grain sizes.
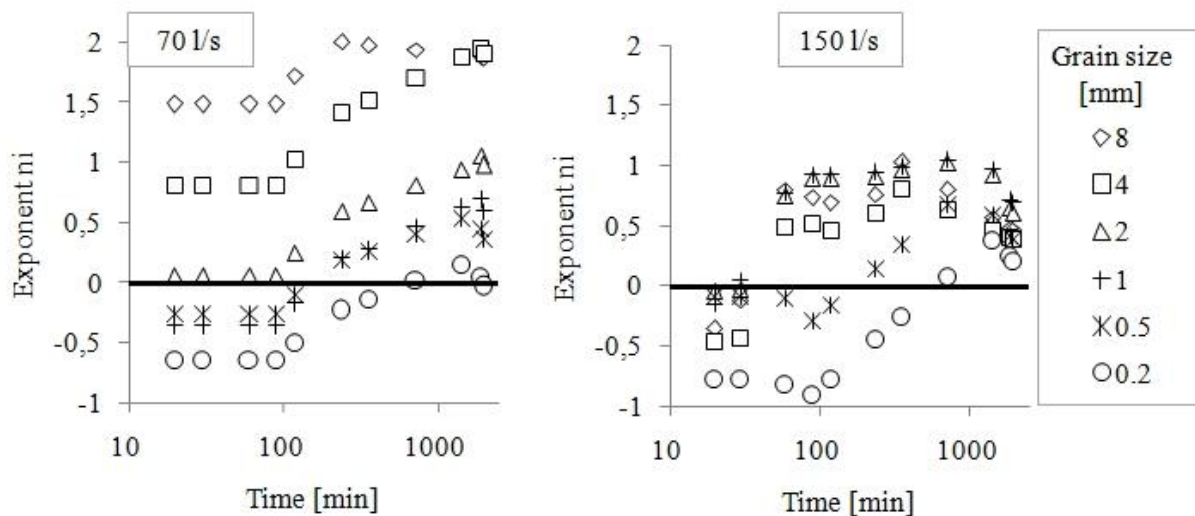
Fig. 6.16 Temporal variation of determined exponents n_i in experiments that were conducted with 70 and 150 l/s respectively.

The coarse grain classes were characterized by the same pattern of increase with time of n_i value. However, the determined ni values were always larger than the corresponding of 0,2 and 0,5 mm, meaning that the fractional transport rates increased with distance. The differences in the spatial distribution of fractional transport rates among different grain classes were more profound for small shear stresses. This is illustrated in fig 6.16 where is shown that the determined n_i values vary within a wider range in the case of experiments performed with 70 l/s (n_i values vary from -0,7 to 2) than in the case of experiments performed with 150 l/s (n_i values vary from -1 to 1).

6.5.3 Variation of fractional transport rates with flow strength

As expected, fractional transport rates of all grain classes increased as the imposed flow strength became larger. Fig. 6.17 shows the variation of q_{bi} with flow discharge at different time intervals for all fractions. The plotted measurements were obtained during experiments which were performed with working length of 4 m. For clearer illustration the measured fractional transport rates have been normalized with measured fractional transport rates that correspond to the smallest imposed water discharge. For example, a value of 10 means that the fractional transport rate was 10 times larger than the corresponding q_{bi} that was measured in the experiment performed with discharge of 70 l/s at the given time point.
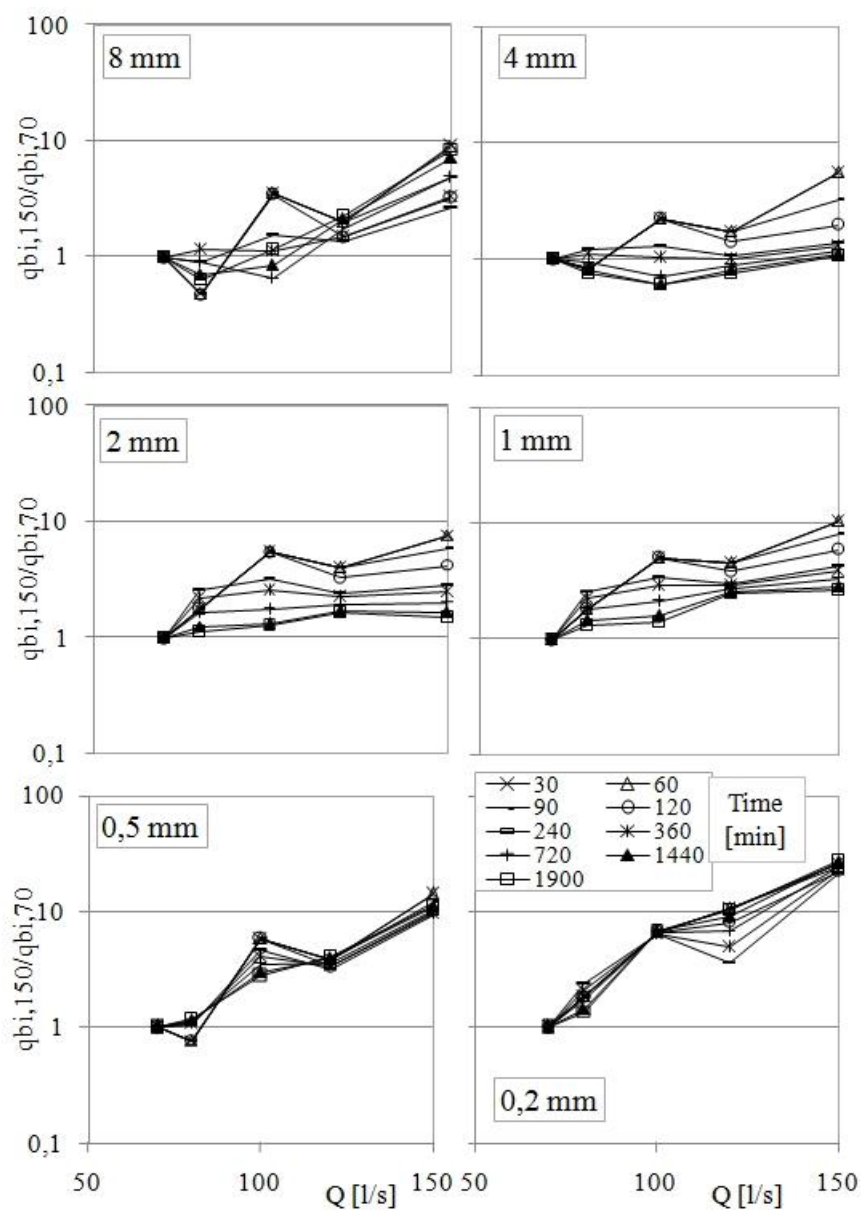

Fig. 6.17 Variation of fractional transport rates q_{bi} with flow strength, as observed in experiments with flume length of 8 m

The increase of q_{bi} with flow strength is clearly illustrated in fig. 6.17. It is also noteworthy that the coarse grain fractions showed a time depending variation of q_{bi} with flow strength. At the beginning of each experiment the curve that connects the measurements appears to possess a steep slope, while as time advances the curve tends to become horizontal, that is, the observed difference among the fractional transport rates for different shear stress is reduced. On the contrary, the variation of measured fractional transport rates with flow strength remained constant during the whole duration of the experiments for the two finest grain classes with diameter of 0,5 and 0,2 mm respectively. This time independent behavior is graphically illustrated by the fact that the curves that connect the experimental measurements lie close to each other in the last two diagrams of fig. 6.15.

6.6   Composition of bed surface

The processing of plan view photographs of bed surface gave as result the changes that occurred to bed surface grain size distribution during the experiments. In Fig.6.18 the determined d_{50} of bed surface in three different positions is plotted. Solid lines connect the measurements that were taken 60 minutes after the beginning of the experimental runs and dashed lines connect the d_{50} values at the end of the experiments, after 2000 minutes.
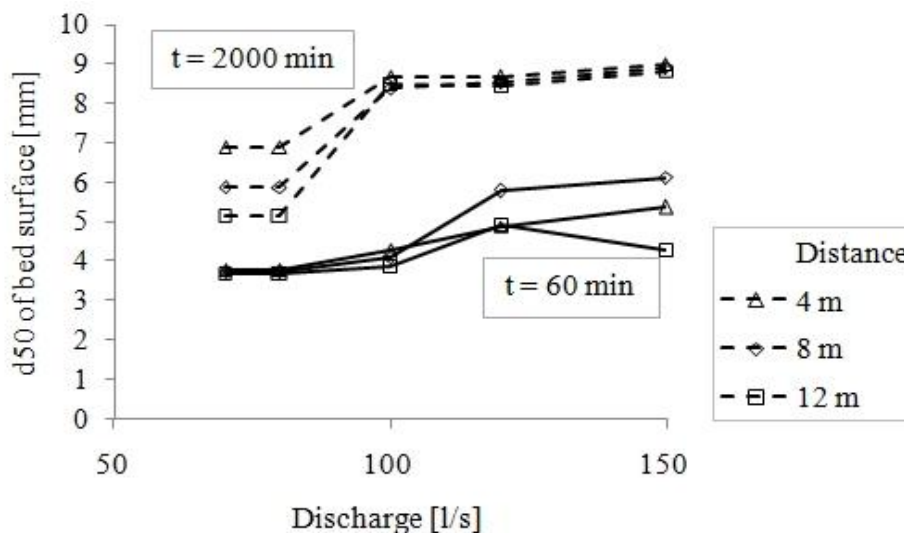
Fig. 6.18 Determined median grain size of bed surface at the beginning and end of experiments, at three different positions along the flume

It is clear that bed surface coarsened with increasing flow strength, a result that is in agreement with findings of previous studies. For higher water discharges the surface layer at the end of the experiments had attained the same degree of coarsening along

the investigation area. Conversely, for lower water discharges after 2000 minutes the bed surface is significantly finer as we move downstream the investigation area. This shows that the process of bed armoring after 2000 minutes was still in progress.

The spatial variation of d_{50} of bed surface for three different water discharges is shown in Fig. 6.19. It was clear from the photographs that the bed surface coarsening began almost simultaneously along the investigation area and took place faster closer to the flume inlet. The main changes in the bed surface composition occurred within the first hours of each experiment and after this initial phase the changes were minor. The duration of the first phase varied mostly with flow strength and distance from the upstream end of the flume. The development of the coarse surface layer was faster with increasing flow strength.
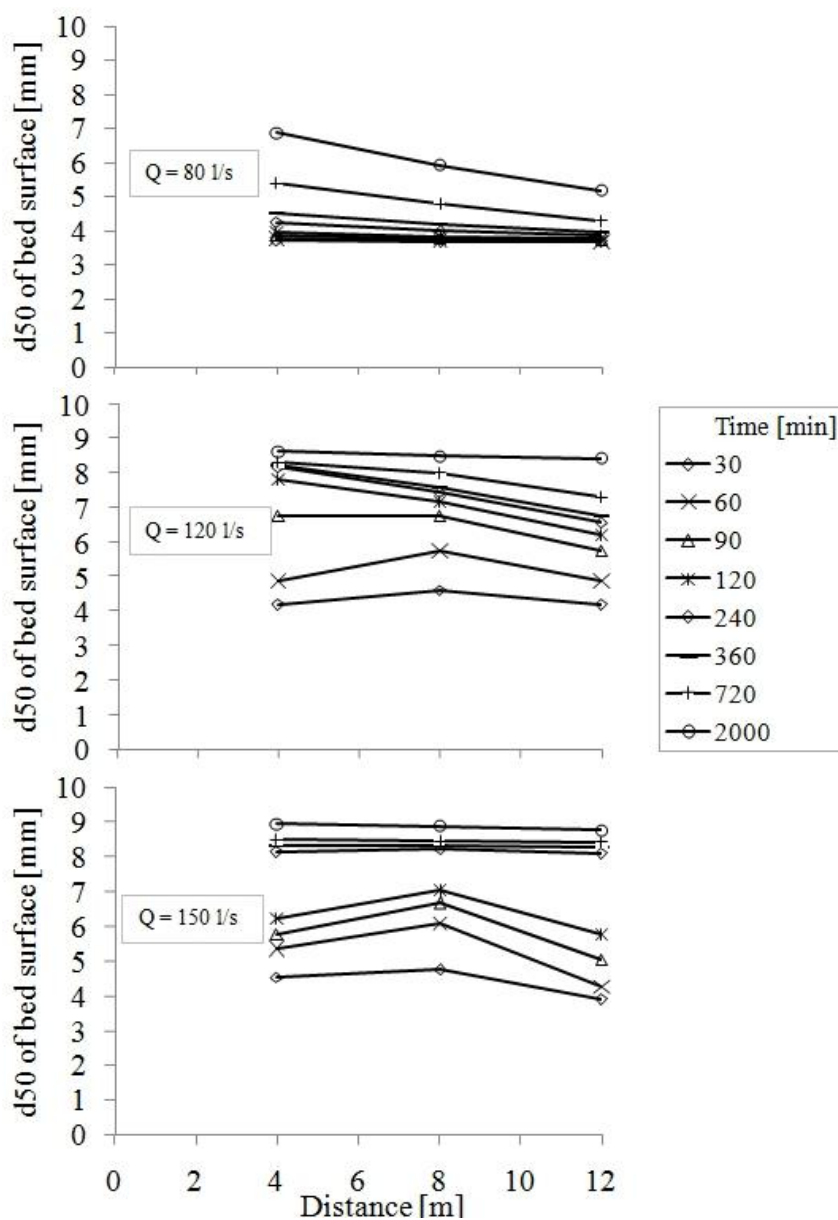
Fig. 6.19 Spatial variation of d_{50s} in experiments performed with 80, 120 and 150 l/s

The bed surface coarsened due to an increase of the fractional content of coarse grain classes and a reduction of the fine fractions percentage. Fig. 6.20 displays the variation of fractional percentages with time as determined at location 8m downstream from the flume inlet and when the flow discharge was set to 100 l/s. For clarity the determined fractional percentages are normalized by dividing with the corresponding initial fractional content.
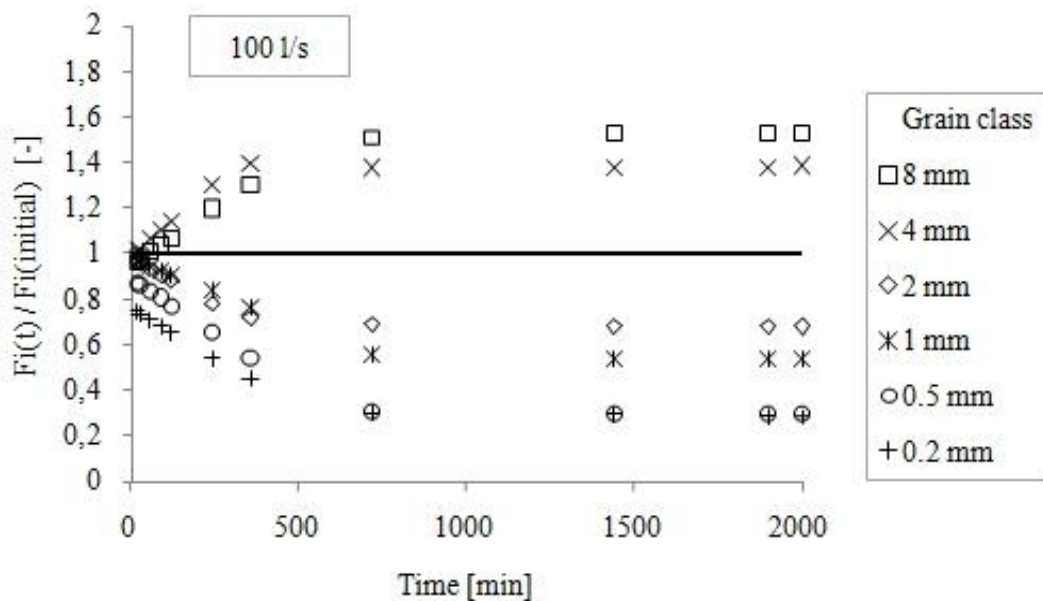
Fig. 6.20 Temporal variation of fractional content of ith grain class as observed in experiment with 100 l/s at distance 8m from flume inlet

The presence in the surface layer of grains with diameter larger than 4 mm increased as time elapsed, apporaching asymptotically a maximum value of fractional content. On the contrary, the percentage of grains with diameter smaller than 4 declined. In the first case, the observed increase was larger as grain size increased, whereas in the second the finer grains showed a larger depletion with the progression of time. This pattern recurred in all of the experiments.

The comparison of fig. 6.10 and 6.19 shows that under the given sedimentological boundary conditions of zero sediment feed the coarsening of bed surface is closely associated with a reduction of the median grain size of the transported material. This observation is in good agreement with experimental results of previous studies, e.g. studies of Lamberti and Paris (1991), Pender (2002) and Gessler (1961). The transported materials median grain size is rapidly reduced in the early stages of each experimental run when the coarsening of bed surface takes place too. When the bed surface achieves asymptotically the highest degree of coarsening under a given flow strength the transported material reaches the lowest median grain size. It could be said

that the fining of bedload results in deceleration of the armoring process and vice versa. If the flow is capable to entrain and hence transport further downstream grains with size corresponding e.g. to bed surface d_{10} then the d_{50} of bed surface will suffer only a small increase.

Of course an experimental study of sediment transport is always associated with considerable scatter within the experimental results. For example fig. 6.10 shows that in the experimental runs that were performed with a water discharge of 150 l/s the median grain size of transported material was reduced from 1,60 mm to 0,85 mm within the first 100 minutes when the bedload was directly measured 4 m downstream of the upper edge of the erodible bed. After this initial phase of intense fining, the transported material was characterized by a constant median grain size over time. Similarly, when the bedload was measured 12 m downstream of the upper boundary of the erodible bed, the initial phase of considerable fining of transported material lasted about 1000 minutes. At that time the median grain size of bedload discharge was reduced from 1,8 to 1,0 mm. The initial phase was again followed by a phase of transport of almost constant composition. Fig. 6.19 shows that for that given flow strength of 150 l/s after 4 hours of experimental duration the grain size distribution of bed surface was almost the same along the sediment bed. Thus the bedload should have reached the lowest d_{50} value of about 0,9 mm sooner, i.e. by 240 minutes and not after 1000 minutes as measured.

This error can be attributed to an error by the estimation of bed surface grain size distribution. At this point should be mentioned that the determination of the temporal variation of the bed surface grain size distribution is a difficult task which is associated with considerable uncertainties. These uncertainties which are the most common sources of the involved error in the estimation of bed surface composition are caused by shortcomings of the applied image analysis method, the difficulties in area sampling and the conversion of grain size distributions that were derived from area samples to corresponding grain size distributions of equivalent volumetric samples.

It is the author's opinion that such deviations between the measured experimental results even under the controlled laboratory conditions are justified in terms of an experimental study of such a complicated phenomenon as bedload transport of sediment mixtures is. Nonetheless, the general trend of bed surface coarsening and associated fining of transported material is not weakened by the observed deviations.

6.7 Dimensionless fractional transport rates

The results that have been so far presented allow for calculation of dimensionless fractional transport rates W^*_i, which express the mobility of a grain class. Mobility is comparable to the transport rate but at the same time is independent of the grain class proportion on bed surface. In case of uniform bed material, mobility can be considered to be equal to transport rate.

The dimensionless transport rate W^*_i is determined by:

$$W^*_i = \frac{(s-1)gq_{bi}}{F_i u^3_*}$$

Eq. (6.4)

where: s is the ratio of sediment to water density
g is gravity acceleration
q_{bi} is volumetric transport rate per unit width of size i
F_i is proportion of size i on bed surface
u_* is shear velocity

The main advantage of the above formulation for the calculation of dimensionless transport rate lies on the fact that by definition it does not contain grain size d_i. Thus, the investigation of grain size influence on fractional bed-load transport becomes easier.

6.7.1 Variation of dimensionless fractional transport rates with degree of bed surface coarsening and grain size

In Fig. 6.21 are plotted the values of dimensionless bed-load transport rate W^*_i for all grain sizes that were calculated from the measurements taken during the experimental run performed with water discharge of 100 l/s and flume length 4 m. Instead of a time scale, the different lines correspond to different degrees of bed armoring defined as the ratio of bed surface median grain size d_{50s} to substrate median grain size d_{50o}.

It is clear that W^*_i of all grain classes is reduced with time or armoring of bed surface. Additionally, the fractional distribution of W^*_i changes as bed surface becomes coarser. At the beginning of each experimental run the grain classes with diameter 1 mm and 2 mm are more mobile than the fine and coarse tails of the sediment mixture grain size distribution i.e. 0,2 mm, 0,5 mm and 4 mm and 8 mm respectively. As time progresses and consequent bed armors the distribution of W^*_i changes and grains

belonging to sand size range approach gradually a condition of almost equal mobility showing a size independent behavior, while the mobility of grains belonging to gravel size range becomes considerable smaller as grain size increases holding though always a size depending behavior. In fig. 6.21 the above described pattern is illustrated graphically by a rotational displacement of the distribution of W^*_i for sand grain sizes with a simultaneous lowering. Contrary the distribution of W^*_i in gravel size range is displaced almost parallel to itself toward lower values. Hence, the mobility reduction due to bed surface coarsening is not equivalent for all grain sizes.
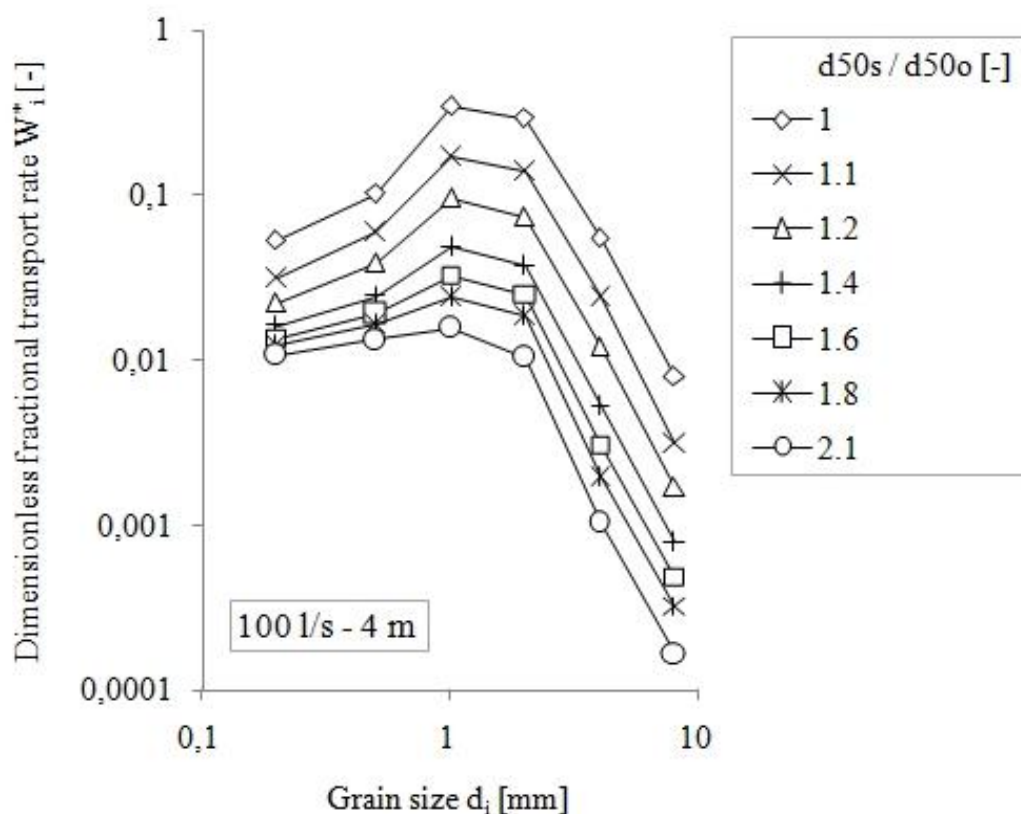
Fig. 6.21 Variation of dimensionless fractional transport rate W^*_i with degree of bed surface coarsening as observed in the experimental run performed with water discharge of 100 l/s and flume length of 4 m

Fig. 6.22 displays the ratio of fractional mobility that corresponds to a degree of armoring of 1,9, to the initially estimated fractional mobility corresponding to an unarmored bed, against grain size. The plotted results were calculated from measurements taken at the onset and near end of experiments performed with flume length of 12 m. Different types of symbols correspond to different imposed shear stresses. The value of the ratio is a measure of mobility variation with bed surface coarsening. For example, if the ratio value equals 1, then the mobility of a given grain class at the end of the experiment, when bed surface median grain size was 1,9 times

the parent bed material median grain size, was the same with the initial mobility of the grain class, when bed surface had the same composition as substrate. A value of 0,1 indicates that the fractional mobility was reduced and became 10 times smaller than the initial one.

Fig. 6.22 shows that mobility variation becomes larger with increasing grain size. Thus, the coarser a grain class, the larger the reduction of its mobility. However, the influence of grain size in observed reduction of mobility is more significant within the sand size range, where the mobility reduction was considerably smaller, i.e. closer to value 1, for fine sand grains (0,2 mm) than coarse sand grains (1 mm). Conversely, the effect of grain size in mobility reduction was smaller within the gravel size range, although a small increase in mobility reduction with increasing grain size was apparent. Hence, the value of the ratio that expresses the mobility variation of grains with diameter 8 mm was only slightly smaller than the ratio value related to grains of 4 mm.
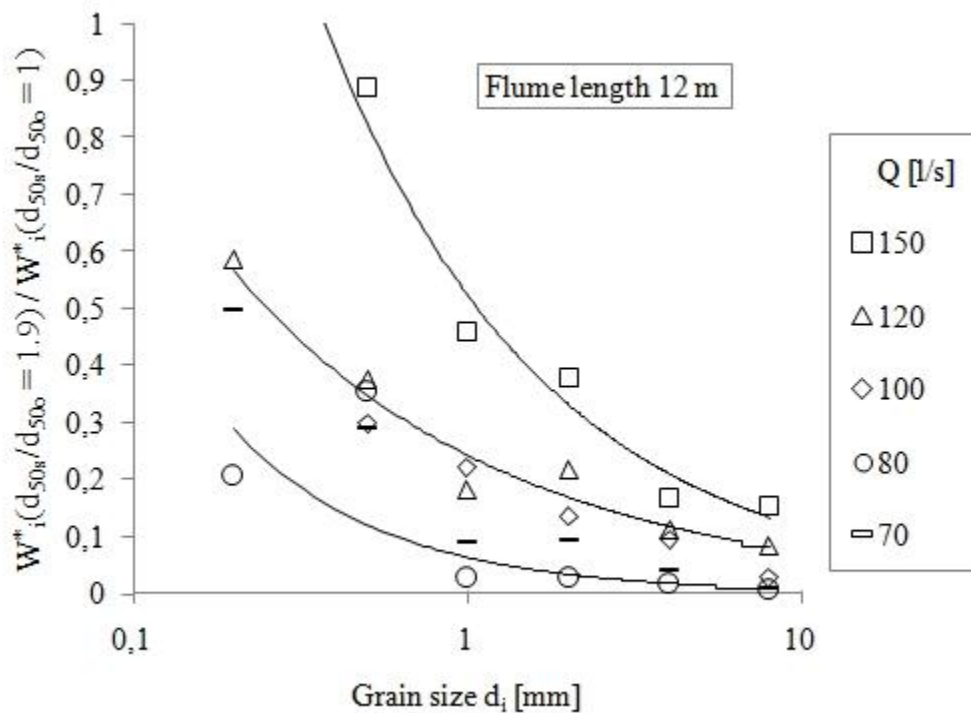
Fig. 6.22 Fractional mobility variation, as observed in experimental runs performed with movable bed length of 12 m

Fig. 6.22 also shows that the observed reduction of fractional mobility is affected by the exerted flow strength. Increase of the imposed shear stress resulted to a smaller reduction of grain mobility for all grain classes as bed surface coarsened. As a consequence, the symbols in fig. 6.22 are located higher as flow discharge becomes larger. Furthermore, increased flow strength results in a more size depending behavior regarding the reduction of grain mobility. This is revealed by the fact that the curves

that fit better to the data tend to become steeper as flow discharge increases and are not simply displaced in a parallel fashion at higher values. The more flow strength increases the more size dependent becomes the fractional mobility reduction explains the larger variation of transported material's median grain size with progressive bed surface coarsening that was observed at higher shear stresses and is shown in fig. 6.10.

An additional observation is that at early stages when bed surface is not considerably coarser than substrate material the difference in mobility between sand and gravel grains is small. For instance, in the example presented in fig. 6.21, when $d_{50s} / d_{50o} = 1$, the calculated W^*_i value of grains with diameter 0,2 mm was about 0,07 and the corresponding W^*_i value of grains with diameter 8 mm was about 0,01, i.e. 7 times smaller. The overall mobility difference between sand and gravel grains was even smaller as grains with d_i equal to 0,5 mm and 1 mm attained the same mobility with grains with d_i equal to 4 mm and 2 mm respectively. Nonetheless, as bed surface becomes coarser, the mobility differences between sand and gravel grains become gradually larger. E.g. when $d_{50s} / d_{50o} = 2,1$, the W^*_i value of grains with d_i equal to 8 mm is almost 100 times smaller than the W^*_i value of sand grains.

In fig. 6.23 the estimated fractional mobility is plotted after being normalized by the mobility of grains with diameter of 8 mm. The plotted normalized fractional mobility expresses how many times the mobility of ith grain class is larger relative to the mobility of grains with diameter of 8 mm. The solid black symbols represent the normalized mobility at the onset of each experiment performed with flume length of 12 m. The empty symbols represent normalized mobility when bed surface was 1,9 times coarser than parent bed material, a condition that was achieved almost at the end of every experimental run. Different geometrical forms of symbols are used in order to represent the variation of flow strength.

Fig. 6.23 shows that the relation between the estimated mobility of separate fractions varied dynamically with progressive bed surface coarsening. The differences in normalized mobility among separate grain sizes were less profound when bed surface was unarmored as when the bed had achieved a higher degree of armoring. The bell form of fractional distribution of normalized mobility reveals that the difference in mobility between sand grains and gravel grains is small, although size depending phenomena appear to take place only within the sand size range as well as only within the gravel size range. Thus:

$$W^*_{0,2mm} < W^*_{0,5mm} < W^*_{1mm} \approx W^*_{2mm} > W^*_{4mm} >> W^*_{8mm}$$

$$W^*_{0,2mm} \approx W^*_{8mm} \, , \, W^*_{0,5mm} \approx W^*_{4mm} \, , \, W^*_{1mm} \approx W^*_{2mm}$$

The mobility of fine sand grains is comparable to the mobility of coarse gravel grains

and the mobility of coarse sand grains approaches the mobility of fine gravel grains. Thus, a state of equal mobility is achieved despite the individual differences among separate grain sizes. As time progresses, the fractional distribution of normalized mobility is transformed. The observed differences in mobility among fine grain classes were minimized while the differences in mobility between fine and coarse grain classes became larger, i.e

$$W^*_{0,2mm} \approx W^*_{0,5mm} \approx W^*_{1mm} \approx W^*_{2mm} > W^*_{4mm} >> W^*_{8mm}$$
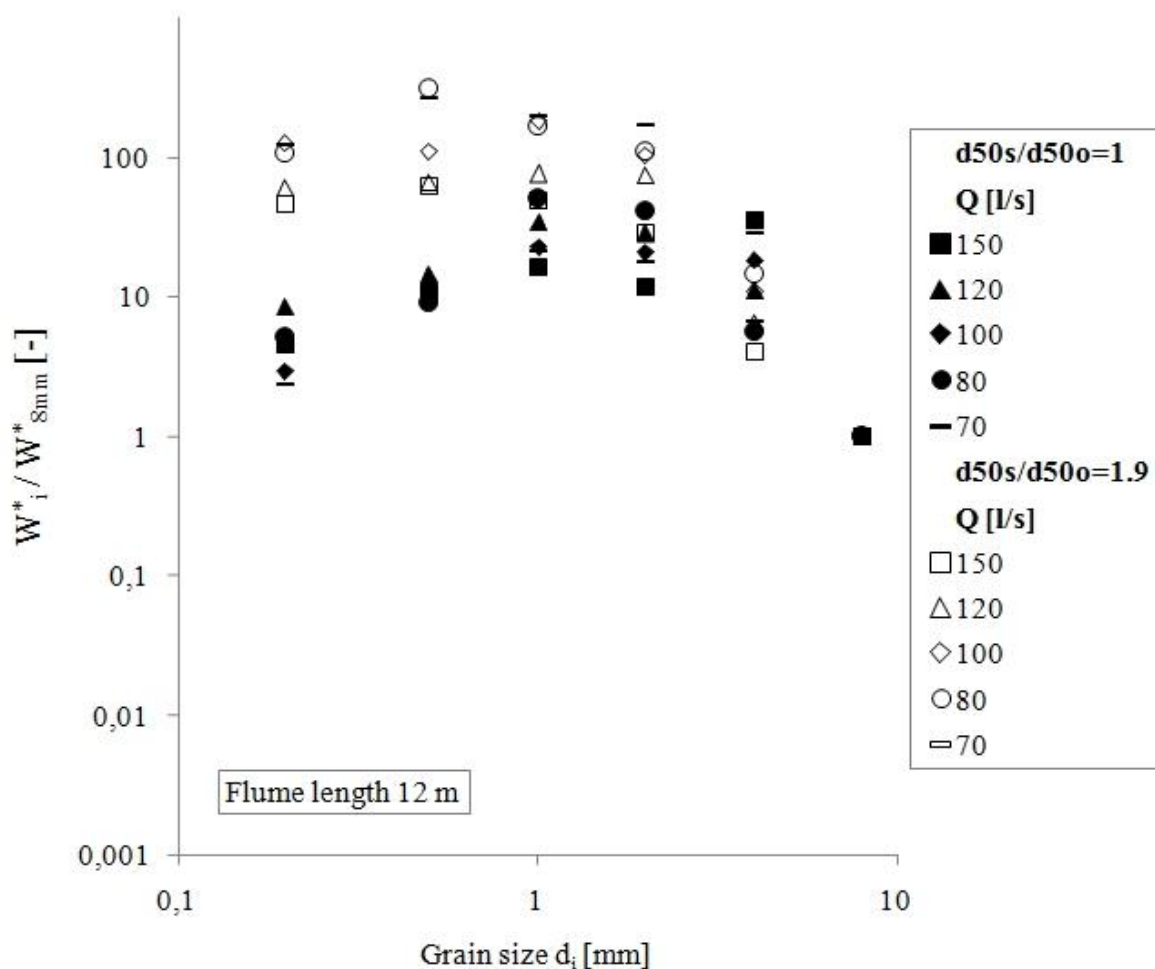
Fig. 6.23 Variation of proportionality of fractional mobility among separate grain classes with bed surface coarsening

The above described pattern of mobility variation with degree of bed surface coarsening and grain size was reproduced in every experimental run

6.7.2 Variation of dimensionless fractional transport rates with flow strength

In order to investigate the influence of exerted shear stress on observed dimensionless fractional transport rate, the latter was plotted on log-log diagram against dimensionless fractional shields stress and power functions were fitted on the resultant groups of data. Fig. 6.24 shows two plots of W^*_i against τ^*_i. The upper corresponds to degree of armoring 1, i.e. unarmored bed, and the lower to degree of armoring 2. In the legend of the graphs the equations of the fitted functions are also presented.
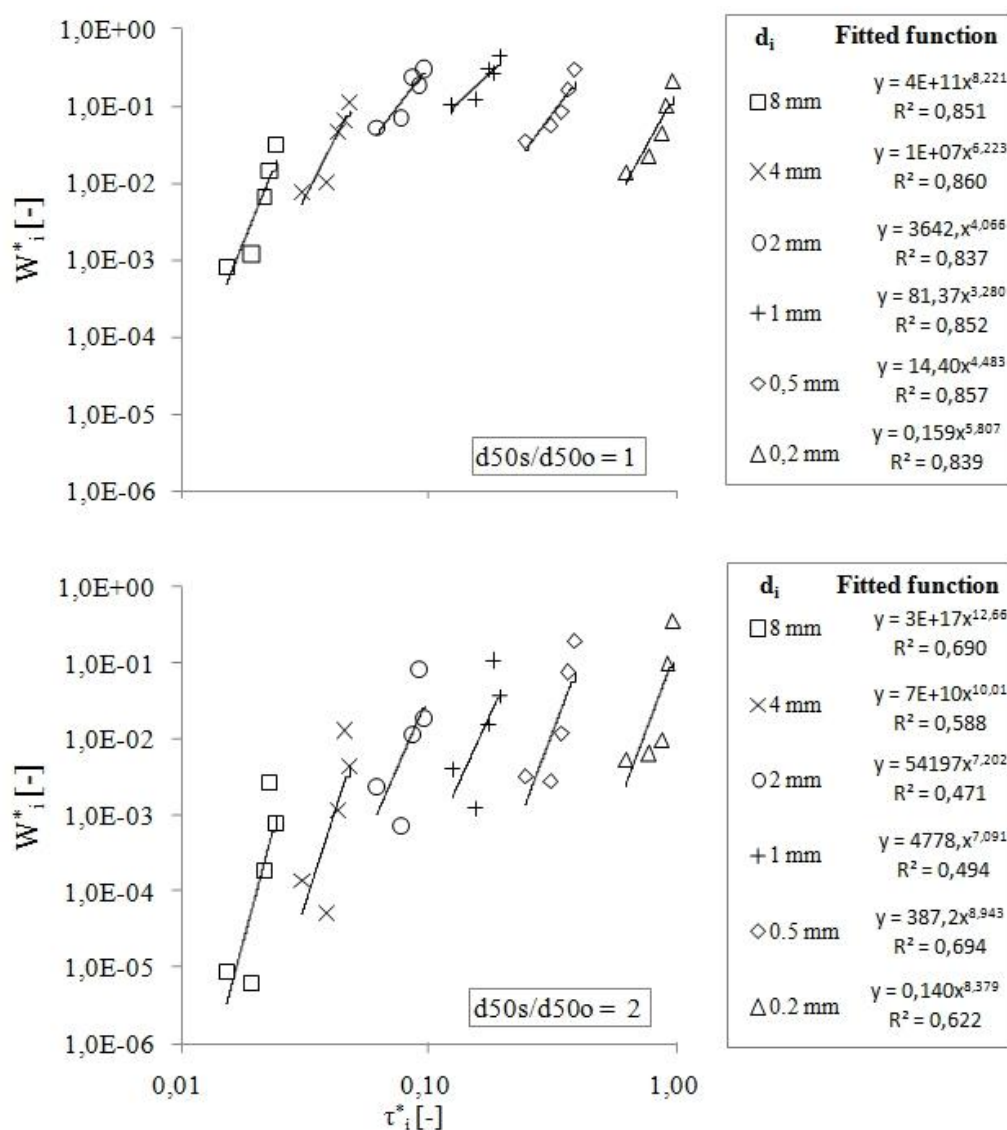
Fig. 6.24 Plot of fractional dimensionless transport rate W^*_i against fractional dimensionless shear stress τ^*_i, for two different conditions of bed armoring

The mobility of all grain classes increased with increasing shear stress. Optical inspection of the two graphs shows that the variation of W^*_i with flow strength became larger as bed surface coarsened. Moreover, the variation of fractional mobility with

flow strength was affected by grain size. Thus, the mobility of coarser grain classes varied within a range of three magnitudes of order while the mobility of fine grain classes varied within a range of two magnitudes of order, for the same shear stress increase.

These observations regarding the relation between flow strength and dimensionless fractional transport rate are illustrated clearly in fig. 6.25. The value of exponent m_i of the power function that fitted best the experimental results against relative grain size d_i/d_{50s} is plotted. The different geometrical symbols represent different phases of bed surface armoring. The groups of symbols that are easily identified on the diagram correspond to the same absolute grain size d_i. Due to increase of bed surface median grain size d_{50s} the separate groups cover a range of d_i/d_{50s} values. For example the m_i values that were determined for grain size 8 mm cover the range from $d_i/d_{50s} = 2$ (approximately) for $d_{50s}/d_{50o} = 1$ till $d_i/d_{50s} = 1$ (approximately) for $d_{50s}/d_{50o} = 2$.
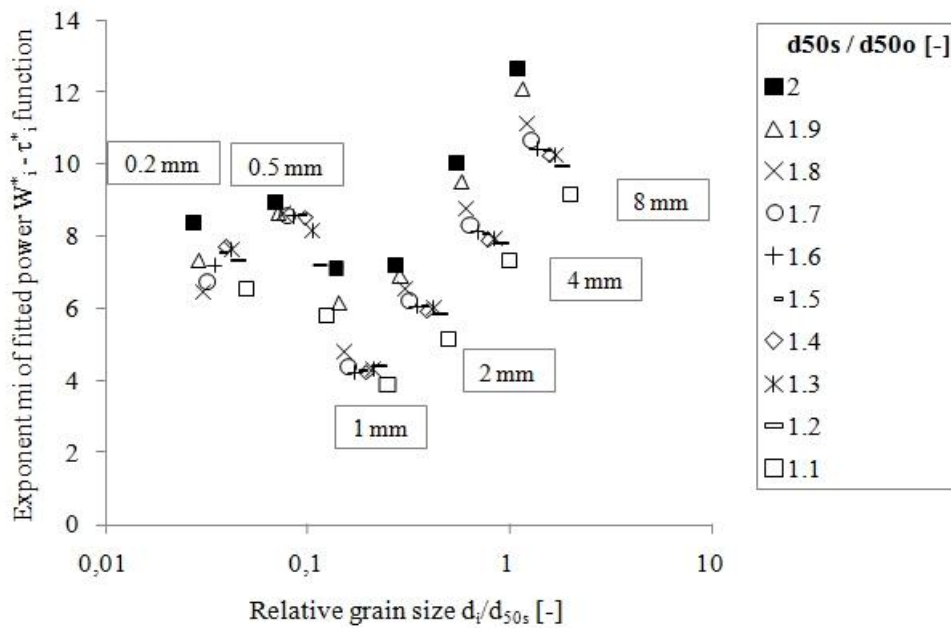
Fig. 6.25 Exponent m_i of power functions fitted on W^*_i vs τ^*_i plots for different grain sizes and phases of bed surface armoring

The value of exponent m_i is a direct measure of W^*_i variability with flow strength. Large values mean that a steep function is required for the description of W^*_i variation with τ^*_i or, in other words, that the observed increase of W^*_i due to increase of τ^*_i is large.

Fig. 6.25 shows that the determined m_i values increased with progressive armoring of bed surface for all grain classes, i.e. the fractional mobility increased more with increasing flow strength as bed surface became coarser. The grains with diameter 0,2

and 0,5 mm where characterized by a considerably smaller m_i increase with progressive coarsening, i.e. their m_i value varied from about 6 for $d_{50s}/d_{50o} = 1$ to 8 for $d_{50s}/d_{50o}=2$. On the contrary, the other grain classes showed a larger m_i variation with progressive armoring, e.g. the determined m_i values for grains with diameter of 8 mm varied between 8 for $d_{50s}/d_{50o} = 1$ and 13 for $d_{50s}/d_{50o} = 2$. The determined m_i values for grains with diameter larger than 1 mm showed a size dependent behavior which was characterized by a consistent increase of m_i value with grain size. This behavior was observed at every stage of bed surface armoring. At the same time, the two finest grain classes with diameter 0,2 and 0,5 mm respectively showed a size independent behavior, as far as the variation of m_i value with grain size is concerned. The determined m_i values for these two grain classes were almost identical, regardless of the degree of armoring. Furthermore, the determined mi exponents for 0,2 and 0,5 mm grain classes were considerably larger than the corresponding values of grains with diameter 1 mm, declining, thus, from the overall size dependent trend that characterized the rest of the grain classes. However, the observed difference in mi between the sand grains became smaller as bed surface coarsened. For example, when $d_{50s}/d_{50o} = 1$ then $m_{0,2 \text{ mm}} \approx m_{0,5 \text{ mm}} \approx 6,0$ and $m_{1 \text{ mm}} \approx 3,5$. But when $d_{50s}/d_{50o} = 2$ then $m_{0,2 \text{ mm}} \approx m_{0,5 \text{ mm}} \approx 8,5$ and $m_{1 \text{ mm}} \approx 7,0$. As a consequence, the behavior of fine sand grains approached that of coarse sand grains as bed surface coarsened.

6.8   Discussion on experimental results

The results that have been presented so far demonstrate clearly the high unsteadiness both in time and space that characterizes non-equilibrium bed-load transport during the formation of a coarse surface layer. In order to support the following discussion the main findings are herein summarized.

- A parallel degradation took place and thus the imposed shear stress remained constant during the whole duration of each experimental run, as bed and water surface slope did not vary and flow depth was adjusted in order to follow the bed level alteration.
- The bed surface coarsened as time elapsed approaching asymptotically a maximum degree of armoring which varied with flow strength. As the exerted shear increased the process of armoring occurred faster. The median grain size of armor layer after 2000 minutes that was the duration of the experiments became coarser with increasing flow strength. Bed surface coarsening started almost simultaneously along the flume. However, coarsening occurred faster the closer to flume inlet. Therefore, at the same time interval bed surface was observed to be finer with

increasing distance from upstream boundary. As time progressed the spatial variation of bed surface d_{50s} became smaller. At the end of the experiments after 2000 minutes the determined grain size distribution of bed surface was almost the same along the flume.

- Despite the constant exerted flow strength, bed-load discharge became smaller as bed surface coarsened, showing clearly thus the effect of surface layer grain size distribution on bed-load transport.

- The transport rate of all grain classes was reduced. However, the grains belonging to sand size range were significantly less affected by bed surface coarsening compared to coarse grains belonging to gravel size range.

- The size depending behavior of fractional transport rate reduction was reflected on the grain size distribution of transported material. As time elapsed and bed surface coarsened, the fractional content of fine sized grains became in all experimental runs gradually larger. The change in composition of transported material became more profound with increasing exerted flow strength.

- Increasing the imposed flow strength resulted in larger transport rates. Nevertheless, the variation of fractional bed-load transport rate with flow strength appeared to be dependent on degree of bed surface armoring. As bed surface coarsened bed-load discharge showed smaller variation with flow strength. This observation is valid mainly for coarse grains. The relation of transport rate with flow strength for sand grain classes showed a considerable smaller variation with degree of armoring.

- The strong dependence of fractional transport rates on grain size distribution led to the observation of an almost linear bed-load spatial lag. Due to the faster coarsening of bed surface in the upstream direction, the fractional transport rates, and the associated reduction of bed-load, the measured fractional transport rates increased in the downstream direction. Again the observed spatial lag was size dependent, as fines show a considerable smaller variation with distance, contrary to coarse grains.

6.8.1 Compatibility of measured local transport rates that were used for the determination of spatial variation of bedload discharge.

One of the objectives of the present work is to describe as accurate and detailed as possible the transient changes that occur during the formation of a finally static armor layer. The temporal variation of transport rate was determined by means of unambiguous continuous measurement of the cumulative submerged weight of the entrained grains that were trapped in the bedload collector at the downstream end of the movable bed. The determination of the spatial variation of the bedload discharge

during ongoing experiments was more complicated because it required simultaneous measurement of the fractional transport rates at different locations along the flume. The applied methodology is illustrated schematically in fig. 6.26. Ideally, the measurements for this purpose should be conducted by bedload traps, installed at different locations along the flume, which would be able to measure the fractional transport rates instantly without interrupting at the same time the transport of the grains further downstream.
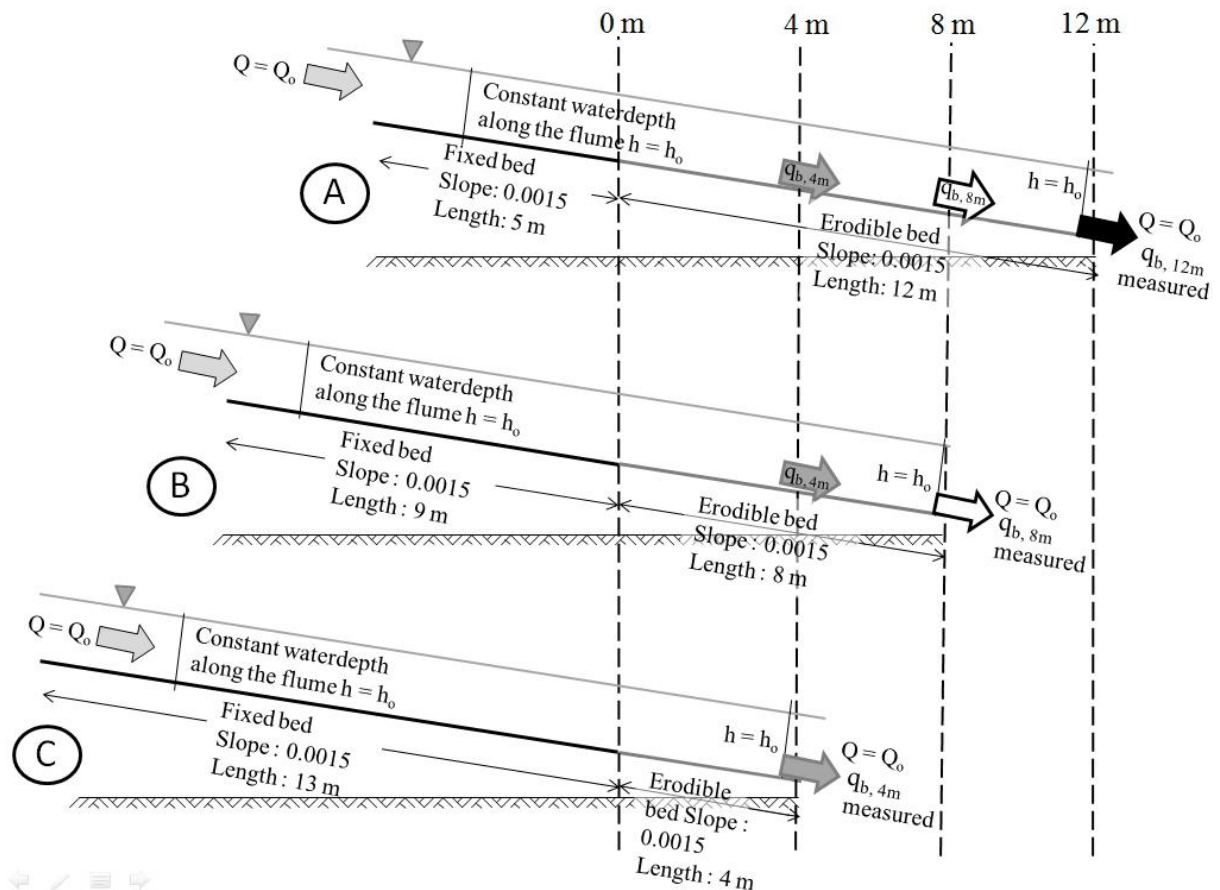
Fig. 6.26 Applied methodology for determination of spatial distribution of bedload discharge

For example, in order to determine the local transport rate at three different locations at distance 4, 8 and 12 m from the upstream boundary of the erodible bed, three different bedload traps should be installed at the corresponding locations. These bedload traps should capture the transported material, determine its weight or volume and grain size distribution and supply the captured material to the subsequent flume reach as sediment feed instantly. Unfortunately a transport rate measuring device with the above mentioned specifications has not been developed yet.

Therefore, the bedload discharge at three different locations for a given water discharge was estimated by measuring the cumulative submerged weight of the

transported material during three individual experiments that were performed with different lengths of the erodible bed and identical hydraulic conditions. The length of the erodible bed was reduced by expanding the fixed bed that was installed for the full development of a turbulent boundary layer before the flow inserts the area of the sediment bed. Hence, for each tested water discharge three experiments were performed with lengths of movable bed 4, 8 and 12 m. The length of the fixed bed was 13, 9 and 5 m respectively. The same method has been applied also in the past by Bell & Sutherland (1983), Phillips & Sutherland (1989) for the investigation of non-equilibrium bedload transport of uniform bed material in the scour hole which is developed due to constrained sediment feed and Mosconi (1988) in the case of graded bed material under constrained sediment boundary conditions.

The transport rate that is determined by measurement of the cumulative submerged weight of the trapped material in a bedload collector installed at the downstream edge of a movable bed with length of 4 m is equal with the transport rate at the cross-section located 4 m downstream of the upper edge of a movable bed of length, e.g. 12 m, when exactly the same hydraulic conditions and thus exerted average bed shear stress prevail throughout the two experiments with different lengths of erodible bed. The results that are presented below support the thesis that the exerted average bed shear stress was the same throughout all experiments that were performed with the same flow discharge, regardless of the length of the movable bed. In order to support this thesis, herein are presented data regarding the measured evolution of bed degradation at the same measuring station during experiments with different lengths of movable bed. These results are compared with the measured water level in order to show that the water depth was kept constant throughout the experiments. It is shown that the water depth was the same from run to run, regardless of the length of the erodible bed as long as the same discharge was applied as upstream hydraulic boundary condition. Finally, a comparison is made between data, which were obtained during different experiments, regarding the bed surface composition at the same location when the same water discharge was applied.

Figure 6.27 shows the temporal variation of the measured values of bed elevation in m above zero level, 4 m downstream of the upper edge of the movable bed. The different colors, grey, black and white, correspond to three different discharges 70, 100 and 150 l/s. These three discharges were chosen because they keep the figure clear, and represent the complete range of tested shear stresses. The points belonging to the same color, i.e. water discharge group are subdivided to smaller measurement series that are differentiated in their annotation by their geometrical shape. The different geometrical shapes of the marks correspond to measurements taken at the same location during experiments that were performed with different lengths of movable bed. The circles

represent the elevation of bed surface at the cross-section located 4 m downstream of the upper boundary of the erodible bed when the length of the movable bed was 4 m, i.e. exactly before the bedload trap. The rhombuses indicate the bed elevation measurements that were at the cross-section 4 m during experiments performed with a length of movable bed of 8 m, i.e. in the middle of the movable bed. The rectangles show the measured values at the point 4 m when the length of the bed was 12 m.
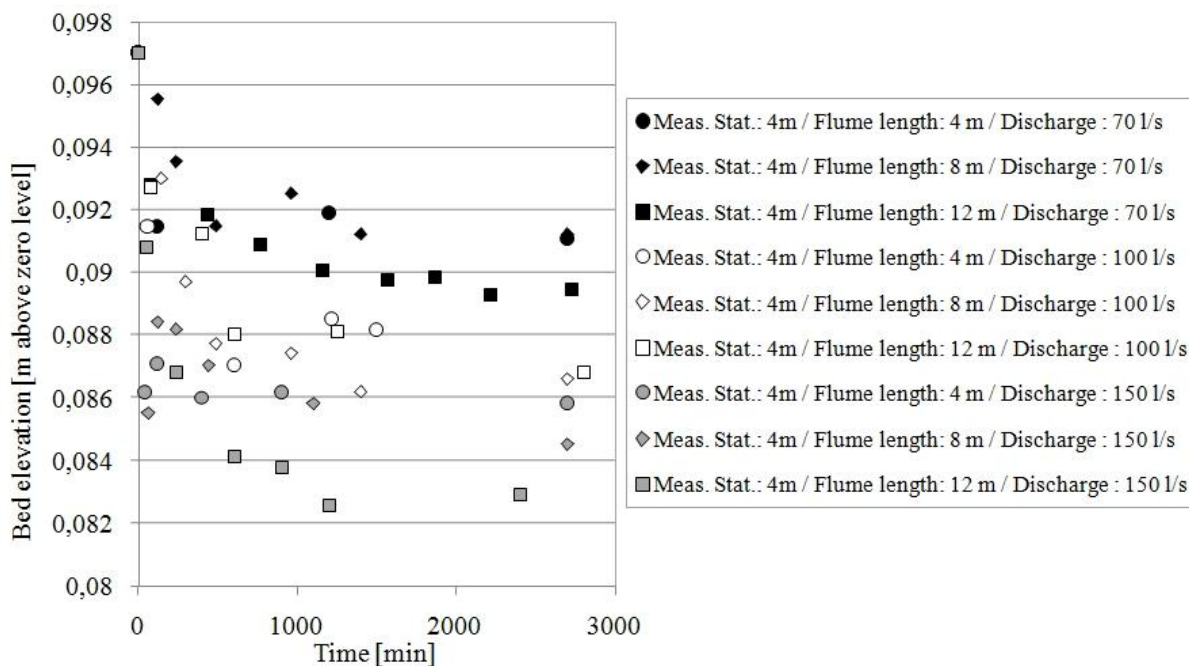
Fig. 6.27 Temporal development of bed elevation 4 m downstream of the upper edge of movable bed

Similar measurements of bed elevation are shown in figure 6.28. Only this time, the plotted elevations regard the cross-section located 8 m downstream of the erodible bed upper edge. Therefore, each individual color group is divided into two subgroups instead of three, as in the previous figure. When the bedload trap was located 4 m downstream of the upper boundary of the erodible bed is logically concluded that the bed was not long enough in order to measure the bed elevation at distance 8m from the inlet to movable bed.

Figures 6.27 and 6.28 show that the observed bed degradation at a given cross-section during three different experiments, that were performed with the same flow discharge and different lengths of erodible bed, was practically the same. Of course some scatter within the points belonging to the same color group is evident in the above figures. The observed deviations from a hypothetical middle line for each individual water discharge are within a range of 0,5 to 1 mm, which corresponds to the measurement accuracy of the point gauge, that was used for the determination of the bed level. Hence it can be concluded that the length of the erodible and consequently the length of the fixed bed did not affect the observed bed degradation. Thus is further supported

the assumption of hydraulic similarity from run to run, regardless of the movable bed length as long as the water discharge was the same.
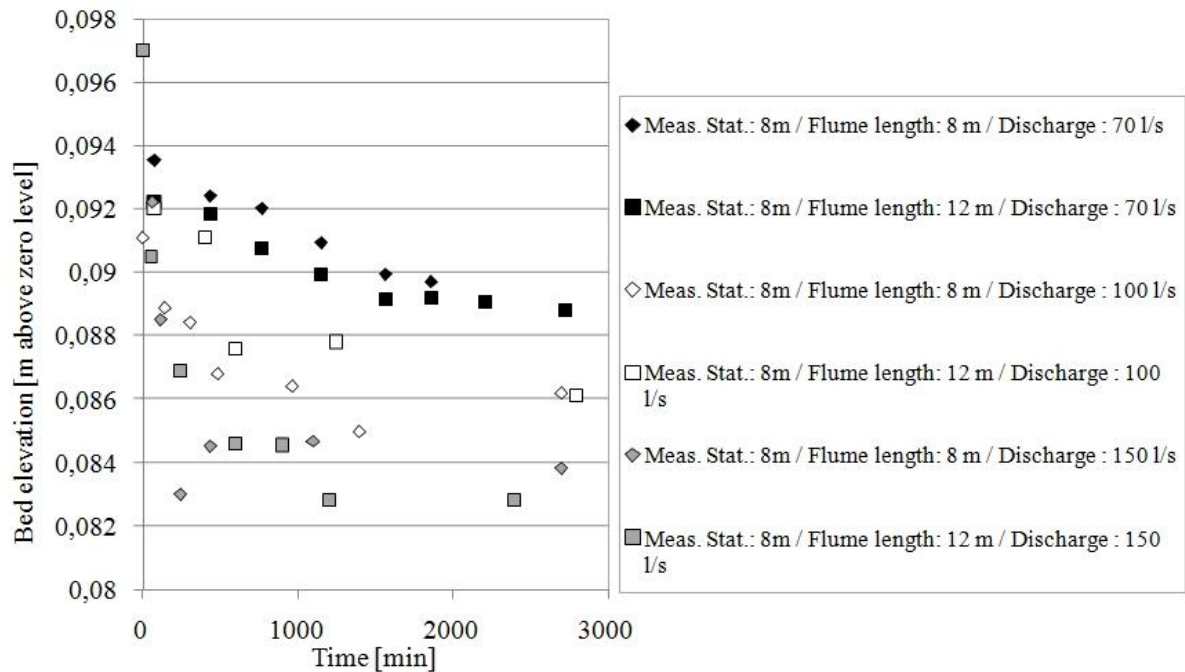
Fig. 6.28 Temporal development of bed elevation 8 m downstream of the upper edge of movable bed

Figure 6.29 shows the variation with time of the water level during three experiments that were performed with a water discharge of 150 l/s. The grey line represents the continuous measurements of water level conducted by the electronic device that was permanently located 1 m upstream of the bedload trap. The solid black circles indicate the water level measurements that were taken with use of the point gauge at the last cross-section before the bedload trap, i.e. the cross-section 4, 8 and 12 m respectively. In the same figure are also shown with grey rhombuses the measured bed elevation of the last cross-section before the bedload trap. The measured water levels with use of point gauge are 1-2 mm lower than the continuous measurements because the measurements were conducted at two different cross-sections within a distance of 1 m.

Figure 6.29 shows that the water depth was kept constant throughout the experiments by adjusting the water level to the bed surface elevation according to the measured bed degradation. This was accomplished by regulating the vertical position of the downstream hydraulic boundary condition. The deviations of the measured water depths from run to run were 1-3 mm, as long as these runs were performed with the same water discharge and therefore could not influence the exerted shear stress.
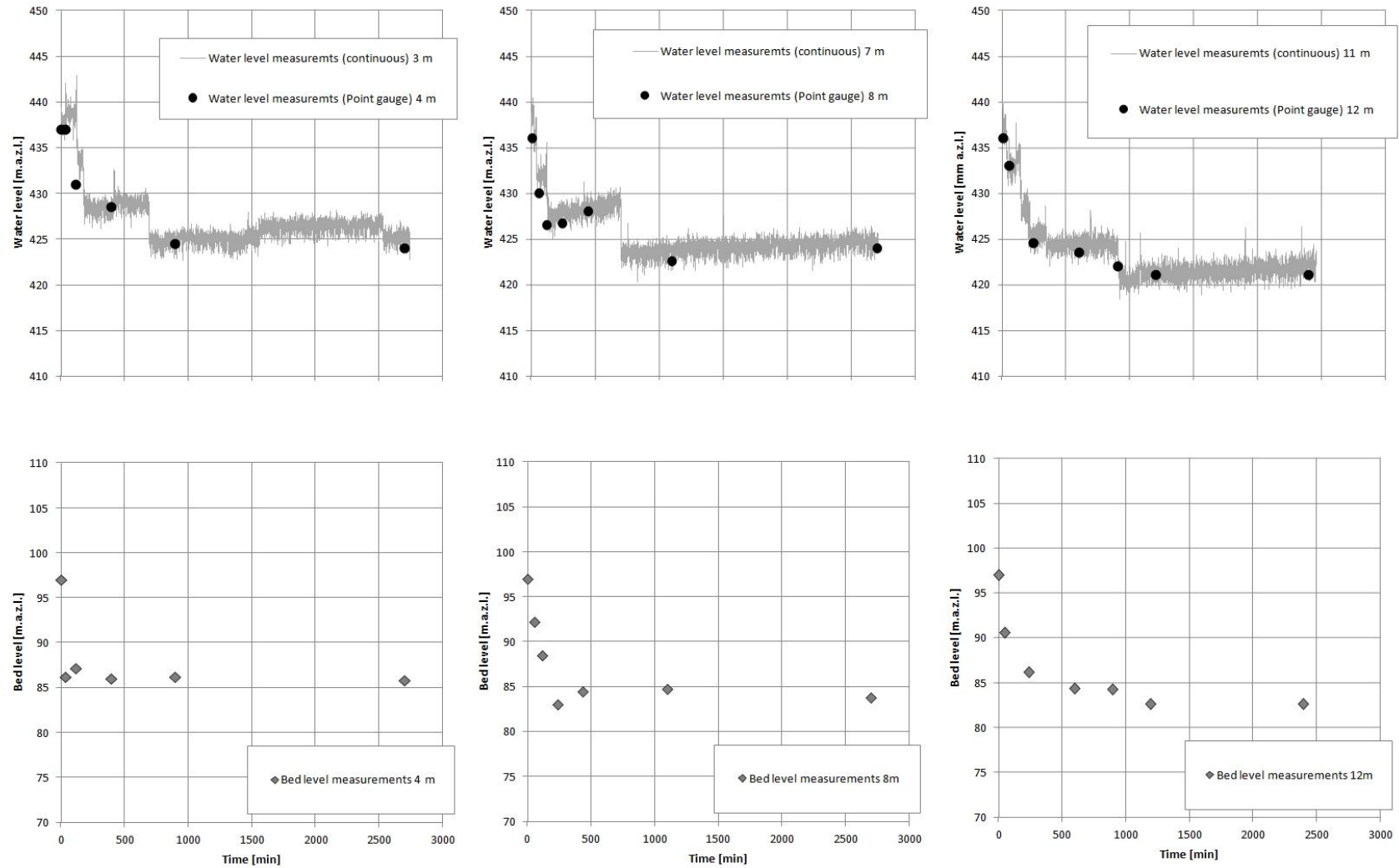
Fig. 6.29 Temporal development of water level and bed elevation at the downstream boundary of the movable bed during experiments performed with 150 l/s

Finally, figure 6.30 shows the measured values of the bed surface d_{50} at the end of the experiments with discharge 70, 100 and 150 l/s. Again the symbols with different colors represent measurements taken during experiments that were performed with different water discharge. The three different geometrical shapes correspond to results obtained during experiments that were performed with different lengths of movable bed. The bed surface grain size distribution at the cross-section located 4 m downstream of the upper edge of the erodible bed could be measured during three individual experiments. Hence in the following figures at the horizontal axis value 4 m are plotted three different values of bed surface d_{50}. Similarly, the bed surface composition at the cross-section 12 m could be determined during only one experiment for each individual water discharge. Hence the d_{50} of bed surface is represented by only one value in figure 4.

The results that are shown in figure 6.30 reveal that the determined values of bed surface d_{50} at the same location (e.g. 4 m) during three different experiments which were performed with the same discharge and different length of movable bed are comparable. Of course there is a considerable scatter. This scatter is to be attributed to the uncertainties and inaccuracies that are involved in the applied determination procedure of bed surface grain size distribution. The determination of the grain size distribution of bed surface is a demanding task associated with large uncertainties. These uncertainties are introduced by errors in the recognition of the grain edges due to complex lithographic textures and shade effects, the transformation of segmented random particle shapes to equivalent ellipses for the measurement of the grain axes and the necessary application of area-by-weight to equivalent volume-by-weight conversion procedures. Despite these uncertainties, the applied method for determination of bed surface gradation, which was based on processing of plan view photos of the bed surface during ongoing experiments, remained the best available option for the acquaintance of this essential data because allowed a non-intrusive determination without interrupting the continuity of the experiments. Finally the good agreement between the grain size distributions that were obtained after areal sampling with use of wax as adhesive and image analysis of plan view photos supported the reliability of the applied methodology.

The observed deviations do not reveal any systematic pattern of change of bed surface composition at a given location with the length of the movable bed. Consequently, it can be assumed that the variation of the movable bed length and subsequent of the fixed bed length was not a controlling factor of the bed surface grain size distribution development.
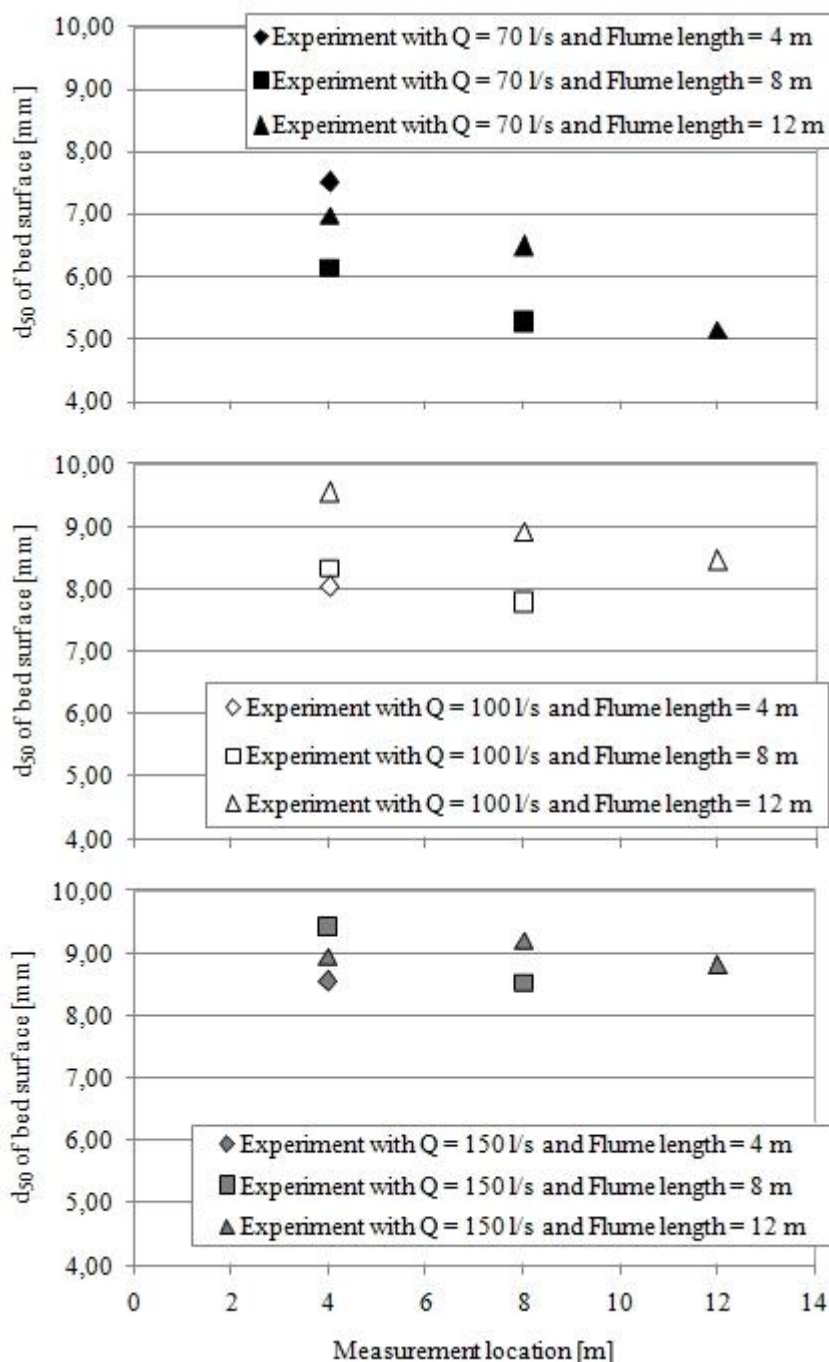
Fig. 6.30 Comparison of estimated d50 of bed surface at the end of experiments that were performed with the same water discharge and different flume lengths

The combination of the herein presented experimental measurements, the observation of parallel bed degradation along the flume, which is illustrated in Fig. 6.1 and Fig. 6.2 and the prevalence of normal flow conditions throughout all experimental runs show that the exerted average bed shear stress was the same in all runs that were performed with the same water discharge and different sediment bed lengths. Hence, it can be stated with certainty that the length of the fixed bed did not affect the mass of shear throughout the conducted experiments and subsequently the bedload transport processes. Thus the determined local transport rates are compatible and describe

accurately the spatial variation of the bedload discharge during the under investigation phenomenon of transformation of a matrix supported to a framework supported bed under constrained sedimentological boundary conditions.

A note on the employed method for the determination of the spatial variation of bedload.

The spatial variation of bedload discharge could be obtained alternatively via measurements of bed level and the sediment continuity equation, i.e. the Exner equation, when the latter is written on finite difference form. The bed profile measurements in different time periods allow for the calculation of the change in volume, over a specific reach length and given time interval. This change in bed volume can be converted into an equivalent mass transport rate. Considering that the bed volume change varies with distance from the flume inlet, the spatial variation of the mass transport rate can be obtained.

This method was applied by Bell & Sutherland (1983) and Phillips & Sutherland (1989) in combination with local transport rate measurements similar with those performed in the present study. This method was not employed in the present study because it is associated with large uncertainties. Furthermore the objectives of the work did not require an as detailed as possible knowledge of the variation pattern of transport rate as long as they did not focus on the transport processes in the area of the strong non-equilibrium (area of scour hole development).

- The measurements of bed elevation were taken within an area lying on the flume centerline. Hence, the estimation of average cross-section bed elevation would require a correction for sidewall effects. This would introduce an additional uncertainty in the calculation of the transport rates.
- The experiments were performed under conditions of low shields stresses. This was necessary in order to assure the creation of a finally static armor layer. A consequence of the low exerted shear was that the observed degradation was very small. Therefore after the initial phase of each experiment the observed bed level changes were small and within the measuring accuracy of the point gauge. Thus, the estimation of mass transport rate by means of mass continuity equation would be inevitably associated with large uncertainties.
- Fig. 6.1 shows that the bed level measurements revealed that the bed geometry was not perfectly plain rather was characterized by small elevation fluctuations of ± 2 mm around an average line. Considering that the measurements were taken at cross-sections that were 0,5 m away from each other a lot of information regarding the change in volume would be neglected, something that could eventually affect the quality of the estimated transport rates.

- The conversion of volume change into mass transport rates would require the as accurate as possible knowledge of bed porosity something that is difficult to be estimated, especially as far as the surface layer is concerned that suffers from an alteration of its grain size distribution.

The estimation of the fractional mass transport rates requires the knowledge of the volume-by-weight bed surface gradation. The uncertainties that are unavoidably interfered with the determination of this parameter would affect subsequently the estimated fractional transport rates.

6.8.2 On necessity of surface-based transport models for simulation of processes driven by dis-equilibrium

In 6.2.2 and 6.4.2 the fact that the bed-load transport rate increased in the downstream direction was demonstrated. The spatial variation of bed-load discharge was quantified by fitting power relations on sets of measurements of transport rate taken at the same time interval but at different locations along the flume. The exponent of the fitted power function is a measure of bed-load discharge increase with distance. It is considered that steady flow conditions prevailed throughout the experimental runs and therefore the spatial variation of bed-load discharge cannot be attributed to a locally differing hydraulic regime. The assumption of steady and uniform exerted shear along the movable bed is supported by the following observations. The bed slope remained constant throughout each experiment. Only a very small scour hole developed in the neighborhood of the upstream boundary of movable bed, which remained restricted to a length of about 1 m. Thus, its effect was confined in a very small area and did not affect the experimental measurements, which were conducted further downstream. Finally, no bed-forms developed, which could cause a non-uniform spatial distribution of shear stress. Subsequently, it is concluded that bed-load varies spatially due to transient changes of bed surface grain size distribution.

The influence of bed surface composition on observed spatial lag of bed-load transport rate is further investigated herein. The method, described in 6.2.2 and 6.4.2, was applied for the analysis of spatial variation of calculated dimensionless fractional transport rates. The use of dimensionless transport rates is necessary, because in this way the effect of fractional content on observed transport rates is neutralized. On the left hand side of fig. 6.31 the exponents of power functions that were fitted on sets of W^*_i values are plotted. The W^*_i values were calculated from experimental measurements of fractional transport rates q_{bi} and proportion of ith grain class on bed

surface F_i taken at the same time interval but at three different locations across the flume. On the right hand side of fig. 6.31 the exponents of power functions that were fitted on data sets of W^*_i are plotted. These were calculated from experimental measurements taken at different time intervals for each of the three measuring stations. The criterion for grouping three measurements into one data set was that they corresponded to the same degree of bed surface coarsening d_{50s} / d_{50o}. In fig. 6.31 the results of the above analysis are presented, based on measurements taken during the experiments performed with water discharge of 70 and 120 l/s respectively.
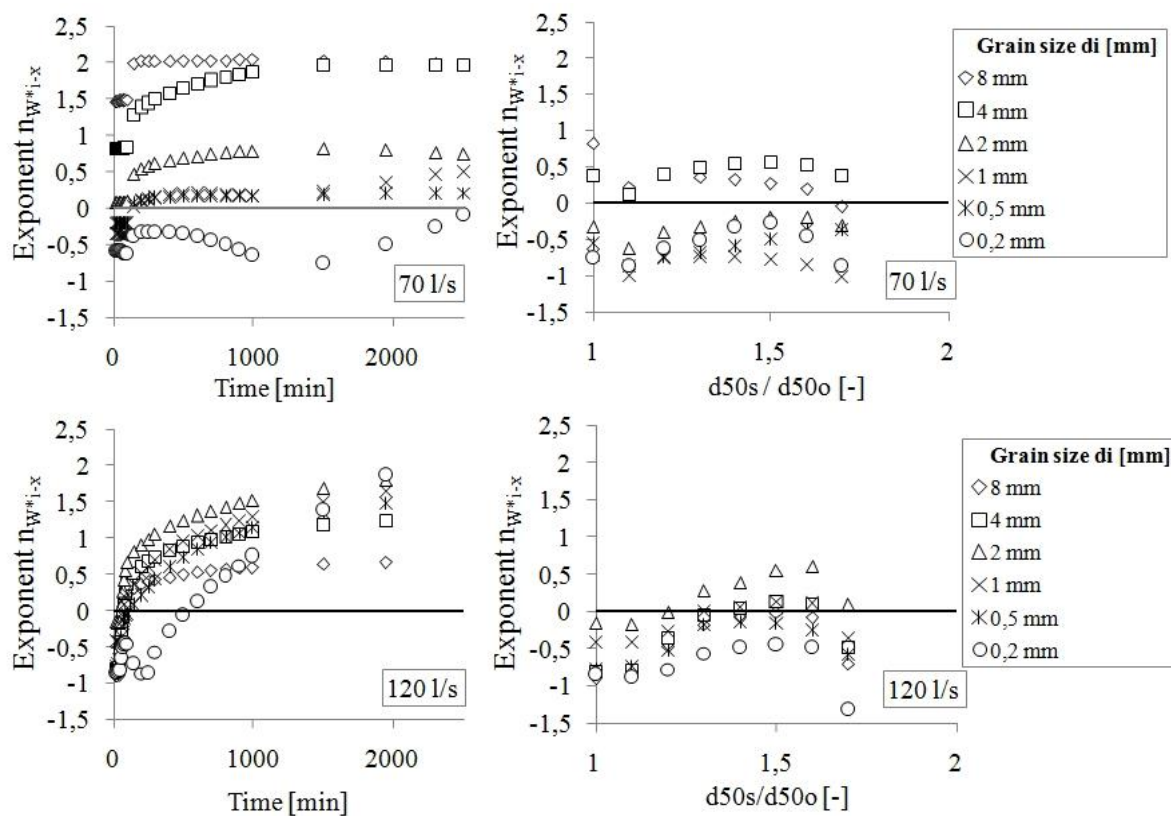
Fig. 6.31 Comparison of observed spatial variation of fractional transport rates when the latter is referred to time and to degree of armoring

Comparison of fig. 6.16 and fig. 6.31 reveals that the variation with distance of dimensionless fractional transport rates W^*_i is slightly smaller than the spatial variation of measured fractional transport rates q_{bi}. This difference between W^*_i and q_{bi} can be attributed to the fact that dimensionless transport rates are proportional to transport rate when the latter is divided by the proportion of ith size range in bed surface. However, the increase with distance, as expressed by the value of exponent remains still large, even though the effect of grain availability is removed. In other words, grain mobility does not remain the same as distance from upstream boundary increases; rather it becomes larger, except for the first minutes. It is concluded, then, that the observed spatial lag is caused by the reduction of bed-load transport that occurs when

bed surface coarsens. In 6.5 it was shown that coarsening takes place faster the nearer to upstream boundary of movable bed. Thus, at the same time interval bed surface is finer as we move downstream and subsequently grain mobility is also increased, creating the observed spatial lag.

The aforementioned mechanism for the explanation of the observed spatial lag is supported by the results of the analysis on spatial variation of grain mobility that are illustrated on the right hand side of fig. 6.31. When the exponent is referred to measurements corresponding to the same degree of armoring d_{50s} / d_{50o}, its value is considerably reduced. There is still scatter but the values fluctuate near zero, meaning that the fractional mobility is the same regardless of distance from flume inlet as long as bed surface has the same grain size distribution at the measuring points. A reason for the observed scatter might be possible error in the estimation of bed surface composition.

The most important implication of the above observation regards the necessity to apply a surface-based transport model in order to simulate a process of selective sorting driven by disequilibrium. A substrate-based transport function will predict bed-load transport rate of each grain class based on the availability in parent bed material of each size range separately. Moreover, the grain size distribution of parent bed material will define the relative grain size d_i / d_{50o}, which is the parameter that will determine the extent of hiding-exposure effects by means of hiding function formulation and consequently the grain mobility of each grain class separately. Considering that substrate material does not change over time, the fractional distribution of grain mobility will remain the same regardless of bed surface composition transient changes. Hence, the substrate-based model is not suited to reproduce the observed reduction of bed-load discharge with surface coarsening and consequently the observed spatial lag of transport rate. Therefore, the substrate-based model might describe adequately the initial or final state but it cannot be employed efficiently to reproduce the intermediate stages of the non-equilibrium procedure.

On the contrary, a surface based transport model not only relates fractional bed-load transport rate to the availability of each individual grain class on bed surface but it also adjusts fractional mobility according to a characteristic grain size of bed surface, e.g. median diameter d_{50s}, by means of a proper formulated hiding function that takes into account the relative grain size d_i / d_{50s}. Thus, the predicted grain mobility and subsequent fractional transport rate follow the transient changes that take place on bed surface and specifically the reduction of fractional mobility with bed surface coarsening.

The correlation of grain mobility to bed surface grain size distribution, by means of a surface-based transport model is supported by the theoretical consideration that the source of bed-load transport is the surface layer. This layer, with thickness of about the diameter of the largest grain contained in bed material, contains the grains that are directly subjected to the exerted shear and are subsequently available for entrainment into motion. Therefore, the proper computation of non-equilibrium transport processes requires that the bed-load predictor takes into account the current availability of each grain class in bed surface and estimates its mobility considering the grain size distribution of surface layer and not that of substrate.

6.8.3 Comparison of results of present study with results of previously published related investigations

The experimental results of the present study reveal trends that have also been observed in related studies that were published in the past. The easily identifiable patterns that dominate non-equilibrium bed-load transport during formation of a static armor layer are:

- Parallel bed degradation.
- Increase of transport rate with distance from upstream boundary.
- Reduction of transport rate with time.
- Reduction with time of median grain size of transported material due to increase of fractional content of fine grain classes.

As far as the bed deformation is concerned, the parallel degradation that appears in all experiments of the present study was also observed and reported in previous investigations regarding static armoring, e.g. Harrison (1950), Gessler (1961) and Pender (2001) who performed experiments with the same configuration.

Mosconi (1988) also investigated the spatial variation of fractional transport rates during the formation of an armor layer and found that fractional rates increased slightly in the downstream direction. A characteristic plot of his experimental results is shown in 3.6.2 (fig. 3.4). The increase of q_{bi} with distance was of the same magnitude of order with that reported in the present study. Thus, the experimental results of Mosconi are in agreement with the results of the present study.

The temporal variation of bed-load discharge, which was characterized by two distinct phases, is met also in previous relevant studies, which are reported in 3.6.1.

Accordingly, the progressive change of grain mobility with bed surface coarsening which is revealed by the observed reduction in median grain size of transported material has been reported by other researchers as well. For example, Gessler (1965) published a diagram that showed the grain size distribution of transported material which was determined by samples taken at different time intervals. The material that was eroded during his experiments became gradually finer due to an increase of the fractional content of the finer grain classes. In paragraph 3.6.3 are reported also other studies that exhibited the same variation pattern regarding the composition of transported material.

Gessler (1965) and Mao & Frohstick (2010) reported that the armor layer that was created at the end of their experiments became coarser when the exerted flow strength increased. Thus, the present study verified the findings of the previous researchers.

The observation of fining of transported material with increasing flow strength seems counterintuitive to Wilcock's observation that transported material coarsened when the exerted shear force increased (see section 2.4.2.2). Wilcock et al. (2001) applied a recirculating sediment feed configuration and, hence, the bed responded in a different manner to the increase of flow strength. The flow strength increase resulted in an increase of bed-load transport rate while the grain size distribution of bed surface remained almost the same from run to run, being at the same time coarser than that of parent bed material. Conversely, in the case of experiments that were performed under zero sediment feed conditions, the increase of flow strength had also as a result an increase in observed transport rate, but the bed surface became coarser from run to run. In fig. 6.9 it is shown that the difference in total bed-load transport rate among experiments performed with different shear stress was larger when the bed surface was unarmored and decreased with progressive coarsening of armor layer.

6.8.4 Variation of fractional mobility and its implication in reference shear stress

The spatial and temporal variation of W^*_i during experiments can provide hints on the required behavior of bed-load transport predictor that will allow for an accurate simulation of non-equilibrium bed-load transport taking place during formation of static armor layer.

The dimensionless fractional transport rate is a function of excess shear stress. Excess shear stress expresses the difference between exerted shear and the required shear for

entrainment of grain of a given relative size. The latter is defined as critical or reference shear stress. This marginal shear stress at threshold or reference value of transport is given by a hiding function. The hiding function provides an estimate of critical or reference shear stress of grains with size d_i depending on the relative grain size d_i / d_m, where d_m is a characteristic grain size either of substrate or bed surface. It was found that a power function is able to describe adequately the relation between W_i^* and excess shear stress. The exponent of the power function is reduced with increasing flow strength, rendering, thus, grain mobility independent of grain size when the exerted shear stress is high. When reference shear stress is used as the normalization term of exerted shear stress the $W_i^* - \tau$ relation takes the following form

$$W_i^* = W_r^* \left(\frac{\tau}{\tau_{ri}} \right)^m$$
Eq. (6.5)

where: W_i^* is dimensionless transport rate of ith grain class

W_r^* is reference value of dimensionless transport rate

τ is exerted shear stress

τ_{ri} is fractional reference shear stress of ith grain class

m   exponent that adjusts variation of mobility with increase in shear stress

Herein, an effort is made to draw some conclusions regarding the behavior of reference shear stress of each separate grain class as bed surface coarsens, based on the experimental results that were obtained in the present study. The grain mobility adjustment that was observed during ongoing experiments is caused by changes in excess shear stress. The invariance of exerted shear stress due to the parallel bed degradation signifies that any change in fractional excess shear stress is caused by the adjustment of fractional reference shear stress to the gradually coarsening bed surface. Thus, the observed changes in fractional dimensionless transport rate W_i^* can be linked directly to adjustments of reference shear stress.

The transient changes of grain mobility are thoroughly described in 6.7 and are summarized below:

- Mobility of all grain classes was reduced with progressive coarsening of bed surface. (Fig. 6.21)
- Within the sand size range the mobility reduction was larger with increasing grain size. Within the gravel size range the mobility reduction with progressive bed surface coarsening showed significantly smaller dependence on grain size; however, it was always larger than the corresponding mobility reduction of sand grains. (Fig. 6.22)

- The difference in mobility between sand and gravel grains was small in the early stages of each experiment when bed surface was unarmored and increased as the armor layer became gradually coarser. The relation between mobility of gravel grains of different size did not change with the development of armor layer. On the contrary, the mobility of sand grains was initially inversely proportional to grain size (smaller grains, larger mobility) and as bed surface coarsened the mobility of sand grains of different sizes tended to become equal. (Fig. 6.23)

- The mobility – Shields stress relation or, in other words, the increase of grain mobility with increasing flow strength showed a dependency on grain size and degree of armoring. Grains with diameter smaller than 1 mm showed almost the same response to increases in shear stress ($m_{0,2mm} \approx m_{0,5mm}$ in fig. 6.25). On the other hand, the mobility of grains with diameter larger than 1 mm showed consistently a more sensitive response to increasing shear stress as grain size increased (The mobility of 8 mm grains increased more than the mobility of 1 mm grains due to the same increase in shear stress for both fractions $m_{8mm} > m_{1mm}$ in Fig. 6.25). The fractional mobility response to increases in shear stress became more sensitive as bed surface coarsened. (The mobility increase of grains 8 mm when $d_{50s}/d_{50o} = 2$ was larger than the mobility increase of the same grain class when $d_{50s}/d_{50o} = 1$, due to the same increase of shear stress in both states of armor layer development). Again, the grains with diameter smaller than 1 mm showed a much smaller dependence on degree of armoring.

Based on the above observations, the following assumptions regarding the adjustment of fractional reference shear stress to a progressive coarsening bed surface can be drawn. The reference shear stress of all grain classes increases with progressive bed surface coarsening. The increase is not equal for all grain fractions. The reference shear stress increase of fine sand grains is small and becomes larger as the diameter of sand grains becomes larger. The reference shear stress increase of gravel grains is larger than that of sand grains. However, within the gravel size range the increase in reference shear stress is almost equivalent, regardless of grain size. Initially, when bed surface is not armored, the reference shear stress of fine sand grains is smaller than the reference shear stress of coarse sand grains. This relation is modified with progressive armoring and fractional reference shear stresses of sand grain classes tend to equalize. As far as gravel size range is concerned, the fractional reference shear stress of separate gravel grain classes is proportional to grain size. Thus, τ_{ri} of coarse gravel grains is higher than τ_{ri} of fine gravel grains. The $\tau_{ri} - d_i$ proportionality for gravel grains remains almost invariant during the process of formation of coarse surface layer. When bed surface is unarmored, the reference shear stress of grains 8 mm is higher than the reference shear stress of grains 0,2 mm but the difference is relatively

small and becomes larger as coarsening progresses. The variation of fractional reference shear stress with grain size and degree of armoring has been extracted from observations on variation of grain mobility with progressing armoring and is schematically illustrated in fig. 6.32.
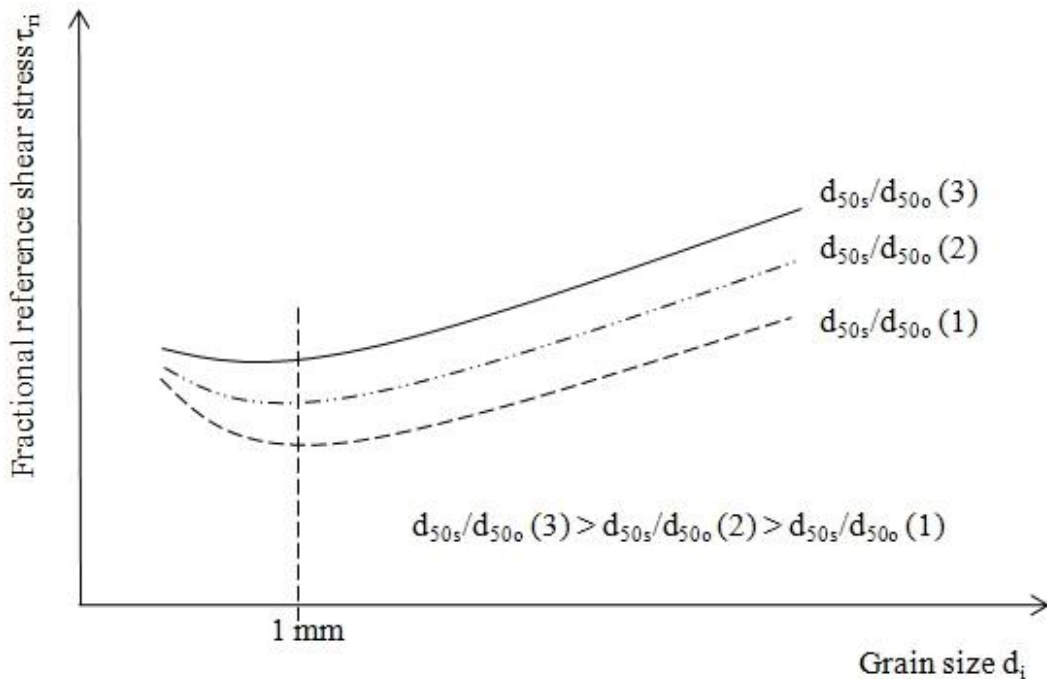

Fig. 6.32 Schematic illustration of assumed variation of fractional reference shear stress with grain size and degree of armoring, that has been based on observation of grain mobility variation

In this figure the three different curves correspond to different conditions of bed surface armoring. The curve $d_{50s}/d_{50o}(3)$, shows the variation of fractional reference shear stress with grain size when the bed surface has attained a coarser condition than the one that corresponds to curve $d_{50s}/d_{50o}(2)$. Fig. 6.32 shows that the fractional reference shear stress will increase with progressive coarsening but not equivalently for all grain classes

The above described scenario on adjustment of fractional reference shear stress to progressive bed surface coarsening is further supported by the observations on variation of fractional mobility with increasing flow strength. The value of exponent m, the variation of which is shown in Fig. 6.25, expresses a measure of the mobility variation with increasing flow strength. Small values of exponent m correspond to high flow events, whereas large values of exponent m correspond to low flow events. Thus, grain mobility tends to become invariant to excess shear stress increases at high flow events and diverse at low flow events, small variations of excess shear stress cause large changes in grain mobility. Based on two assumptions, it can be concluded

that a low value of exponent m is related to a low fractional reference shear stress and vice versa. The relation between exponent m and excess shear stress is schematically illustrated in fig. 6.33
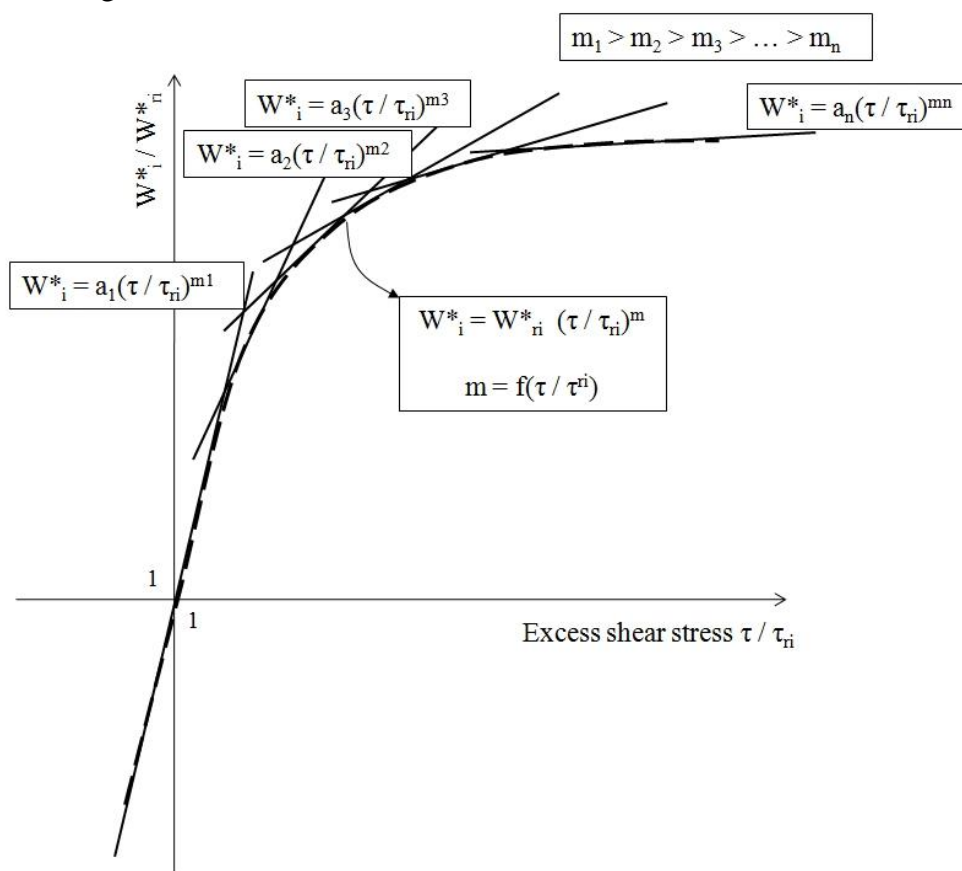

Fig. 6.33 Variation of exponent m with excess shear stress

The first assumption is that of similarity collapse of fractional transport functions or, in other words, that a unique function can express adequately the relation between fractional dimensionless transport rate and fractional excess shear stress. This notion is widely accepted and has been used by many researchers for the development of fractional bed-load transport predictors. The second assumption is that the same shear stress is exerted to all grains exposed on bed surface, regardless of their size and that shear stress remains invariant throughout the process of bed surface coarsening. The latter is supported by the measurements of bed surface elevation and water level that were conducted during the experiments of the present study. Hence, the claim that a reduction of exponent m is related to an increase of excess shear stress and, subsequently, to a reduction of reference shear stress, as long as the exerted shear stress does not change, is in accordance with these assumptions.

Based on the above considerations and the variation of exponent m with grain size and degree of armoring that is depicted in fig. 6.25, it is verified that the fractional reference shear stress is increased with increasing grain size with the exception of the

two finest grain classes with diameter 0,2 and 0,5 mm. Furthermore, the progressive coarsening of bed surface causes an equivalent increase to reference shear stress of grain larger than 1 mm, which is stronger than the increase in reference shear stress of grains 0,2 and 0,5 mm respectively. Finally, the observed differences in reference shear stress within sand size range tend to become eliminated as bed surface coarsens.

6.8.5 A possible mechanism that explains the observed variation of fractional transport rates with progressive coarsening

The main conclusion that can be drawn from the analysis of the experimental results so far is that all grain classes became less mobile with progressive bed armoring. However, the extent of mobility reduction was not the same for all grain classes. The mobility reduction of sand material was size dependent and smaller than the mobility reduction of gravel particles which was almost size independent. The mobility reduction is associated with an increase of fractional reference shear stress, especially in the case of the experiments performed in the present study, during which the exerted flow strength remained invariant. The reference shear stress of grains belonging to a given grain class depends on various parameters. Among these are:

- The absolute weight or size d_i of the particle.
- The relative size defined as d_i/d_{50s} that determines the hiding sheltering effect.
- In addition, according to Southard the rollability effect plays an important role, whereby coarse particles can roll easily over a fine grained bed, whereas fine particles roll with difficulty over a bed of larger particles.

The effect of the aforementioned parameters might be countervailing, that is, the effect of relative size tends to neutralize the effect of absolute size, rendering, thus, the estimation of grain stability complicated.

The fractional transport rate and, consequently, grain mobility under a given flow strength is defined by the product of displacement length of the grain and displacement frequency. Wilcock (1997) suggested that fractional transport rate depends also on spatial entrainment frequency in order to account for partial transport, yet this term is herein ignored for reasons of simplicity. A reduction either of displacement length or displacement frequency results in bed-load discharge reduction. Considering that reference shear stress is actually the shear stress that produces a predefined reference dimensionless transport rate it appears that when the exerted flow strength remains invariant, any change in displacement length or displacement frequency of particles of a given grain size will affect directly the reference shear stress of the given grain class.

Herein a justification of the observed pattern of mobility variation and, consequently, fractional reference shear stress adjustment is attempted by describing the physical processes of hiding that take place during the formation of a coarse surface layer. The described mechanism is based on optical observations of bed-load transport that were made at different stages of ongoing experiments of the present study, as well as on theoretical considerations that could be verified with experiments with tracers.

Optical observation of bed-load transport at different stages of armor layer formation showed that both the displacement frequency as well as the displacement length of coarse grains became smaller as bed surface coarsened. The roughness of bed surface increased with progressive armoring of bed surface and, thus, the coarse grains met more obstacles when they were in motion that made their transportation more difficult; hence, their displacement length was reduced. Furthermore, the locations that provided a better shelter against the exerted shear force increased as bed surface was organized to a more stable and shear resistant structure. Accordingly, the time intervals between two successive displacements of the same grain increased as bed surface became coarser. This was confirmed by the fact that movement of coarse grains became more and more sporadic as time progressed.

As far as sand grains are concerned, optical observations verified that both displacement step length and frequency were reduced as bed surface became coarser but were always larger than that of gravel grains. At the late stages of the experiments the entrainment and downstream transportation of fine sand grains could be easily identified contrary to the motion of gravel grains that occurred rarely. At that time the transport of sand grains was caused by the slightest displacement of coarse particles that revealed the substrate material or by the impact of an already moving large particle on an area where fine grains had settled down. When the sand grains were in motion they were transported downstream until they were trapped in the interstice in-between of coarser particles or in a position that offered increased protection from flow attack, usually in the wake of coarse particles, where other fine grains were concentrated as well.

During the first minutes of each experiment, almost all grains exposed on bed surface were regularly entrained and the displacement step length was considerably larger than in the later experimental stages. The sand grains could almost traverse the entire length of movable bed by rolling without finding an obstacle that could make them settle down. Similarly, the gravel grains were regularly re-entrained although their transport was characterized by considerably smaller displacement length. Furthermore, the gravel grains were initially entrained as soon as their exposure to exerted forces by the flow became sufficiently large. The exposure of coarse grains was gradually increased

in the early stages due to removal of fine grains lying on the area in front of the coarse particle, creating, thus, a small scour hole that rendered the gravel grain more unstable.

The above observations show that the hiding-shelter effects as well as the ease with which a grain could be transported downstream, evolved in a different way for separate grain classes as bed surface coarsened and changed from a matrix supported to a framework supported bed. Based on these observations, the following scenario regarding the evolution of hiding effects among various grain sizes with progressive armoring of bed surface can be formulated.

Initially when the sand content is high (larger than 30 %) the gravel grains actually float between the sand grains. Thus, their mobility is affected by the transport rate of sand grains because it determines their exposure to exerted shear force by the flow. Nonetheless, grain size plays an important role. All gravel grains will be exposed easily and at the same rate because this procedure depends on removal of sand grains that surround them. However, the fine gravel grains will be transported more easily than the coarser gravel grains for the following two reasons. Firstly, their mass is smaller than that of coarse gravel grains due to their smaller absolute size and, hence, they require a smaller turbulence peak that occurs more often in order to be entrained. On the other hand even a small exposure increases considerably the possibility that they will be entrained when the same exposure might not be sufficient for a coarse gravel grain. For example, assume that two grains with diameter 4 and 8 mm respectively are buried into the sand and the upper point of their periphery is scarcely/barely on bed surface (in other words, the center of the two gravel grains are 2 and 4 mm respectively lower than the bed surface). When the sand material that surrounds them is removed in a depth of 2 mm then the created exposure of 2mm will provide a larger possibility for the small gravel grain to be entrained than for the coarse gravel grain. After the initial entrainment, the two gravel grains will be easily transported further downstream without obstacles on their way. However, even now the absolute size will affect the displacement length, which is inversely proportional to grain weight. This explains the inverse proportionality of mobility with grain size within gravel size range in the early stages of each experiment, when sand content on bed surface was high.

At the early stages of each experiment it was observed that within the sand size range the fractional mobility increased with grain size, which, at first sight appears to be paradoxical. It would be expected that the fine sand grains would be intrinsically more mobile than the coarse sand grains, due to their smaller mass. The observed behavior can be explained in terms of an excessive hiding of fine sand grains. The fine sand grains will be instantly entrained as soon as they are exposed to the flow. This means

that they are protected by all other grain fractions and only when the grains above them are removed, will they be entrained. On the other hand, the coarse sand grains tend to behave like the fine gravel particles. They are almost all the time partly exposed to the flow and also light enough to be easily entrained. Thus their entrainment possibility is very large. Fig. 6.34 provides graphically an example of the hiding conditions that prevail when the bed surface is unarmored and matrix supported. The active layer is defined as a layer with finite depth that is discriminated by substrate by the fact that the grains contained in there are likely to be entrained, while the grains that belong to substrate are not. Assume that the active layer depth for sand grains is 8 mm, or, in other words, that the sand grains located in the surface zone with depth of 8 mm are likely to be entrained into motion while those lying deeper are not. The possibility that a single grain with diameter 0,2 mm will be entrained is reduced depending on its depth within the active layer. Thus, the overall possibility for entrainment of particles of this grain size is reduced due to the effect of burial depth within the active layer. Conversely, the effect of burial depth becomes smaller as the sand grain size increases, while counteracting is the fact that coarse sand grains will be considerably more exposed to the flow. This explains the observed smaller mobility of fine sand grains when compared to the mobility of coarse sand grains while the sand content of bed surface was high.
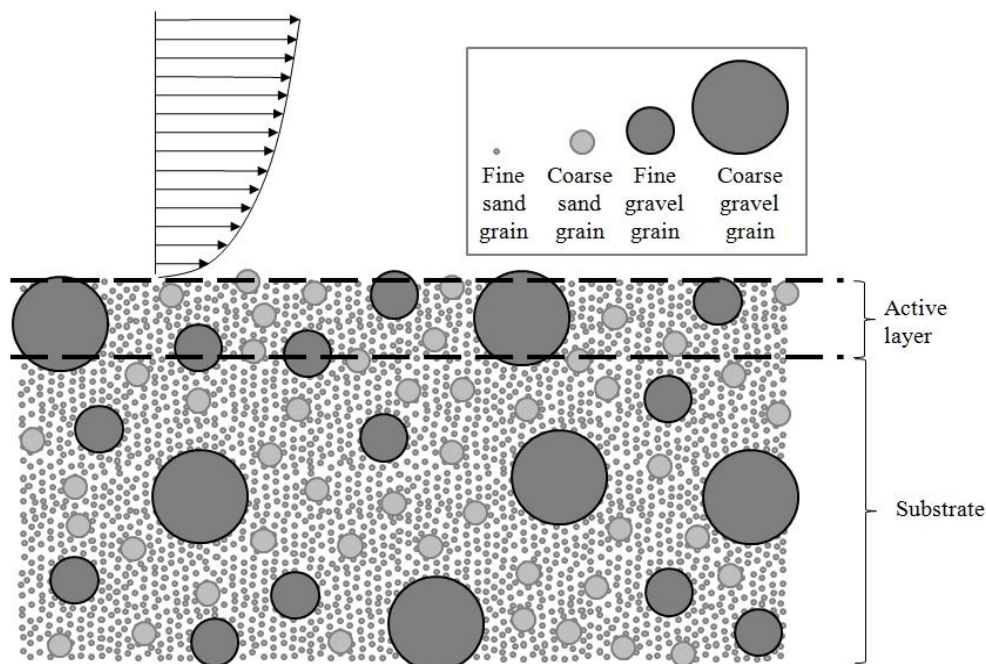
**Fig. 6.34** Schematical illustration of hiding in active layer when the bed surface is unarmored and matrix supported (sand content in active layer > 30%)

With progressive armoring the bed surface is transformed from matrix supported to framework supported. A schematical example of hiding-exposure effects that influence displacement length and frequency when the bed surface is armored and framework

supported is given in fig. 6.35. As far as gravel grains are concerned, their mobility is considerably reduced for two reasons. On the one hand, the displacement length that they traverse becomes smaller due to increased roughness of bed surface that imposes more obstacles into their way. On the other hand, the creation of a gradually large number of positions that provide increased stability along the flume results in a reduction of their displacement frequency. However, the absolute size effects obviously still affect the fractional mobility, rendering thus fine gravel grains more mobile than coarse gravel grains. In addition, the sporadic movement of a coarse gravel grain can push a fine gravel grain to a more unstable position that will increase the possibility of entrainment of the latter. On the contrary, the sporadic movement of fine gravel grains cannot affect significantly the mobility of coarse gravel grains through the impact they cause when they touch bed surface during their motion. Imagine the impact of the collision of a moving grain with diameter of 8 mm with a standing grain of diameter of 2 mm on the latter and vice versa.
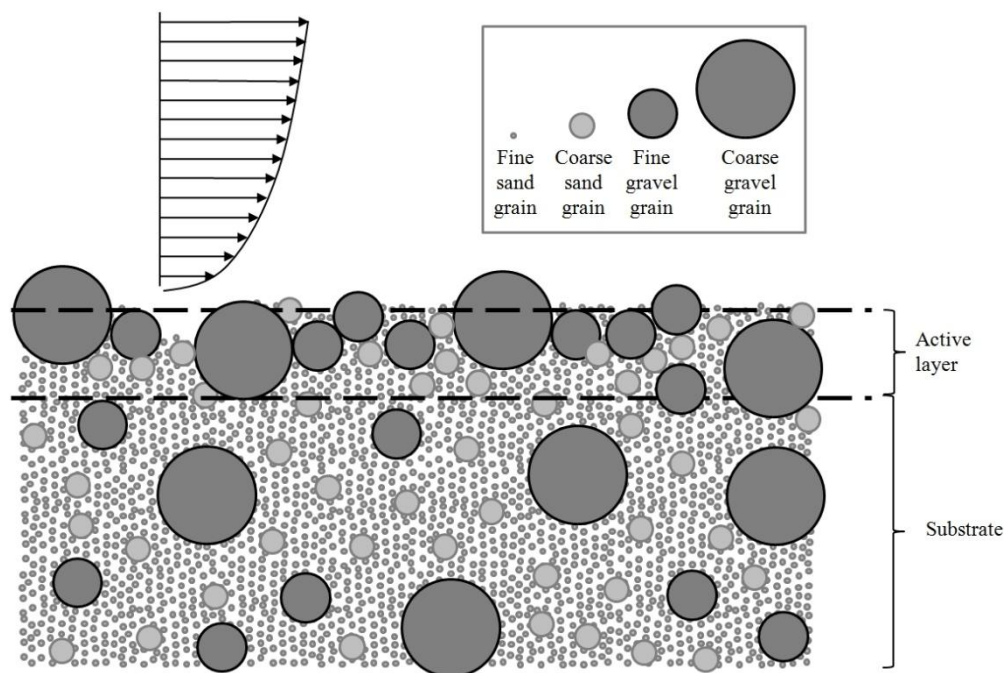
Fig. 6.35 Schematical illustration of hiding in active layer when the bed surface is armored and framework supported

The mobility of sand grains is also reduced with bed surface armoring but in a different way than the mobility of gravel grains. The mobility reduction of fine sand grains is considerably smaller than that of the rest of the grain classes because they are always protected by the remainder fractions. This means that what changes with progressive coarsening is the grain size distribution of their protection, which is not essential. Furthermore, due to their small weight, they are usually transported in the mode of saltation and, thus, their displacement length is less affected by the increased

roughness of bed surface than that of the other grain classes that are rolling. Nonetheless, the overall reduction of mobility of coarser grains causes the observed reduction in mobility of fine sand grains. The mobility of coarse sand grains is also reduced and tends to become the same or slightly smaller than that of fine sand grains. The majority of the available for transport coarse sand grains (i.e. the coarse sand grains contained in active layer) are now located underneath coarser grains. This happens, either because when they are transported they usually settle down in the interstices between the already still coarse grains or because, due to progressive erosion, the coarse grains are slowly exposed and sand grains near them that previously belonged to substrate are now contained in active layer. Due to this vertical segregation, the mobility of coarse sand grains tends to become equal with the mobility of fine sand grains because their displacement frequency depends mainly on the shelter that the above coarser grains provide.

The above mechanism that governs the grain hiding-exposure phenomena occurring in active layer can explain the two-phase temporal variation of bed-load transport rate. As long as the bed surface is matrix supported, i.e. sand content is larger than about 30 %, the sand bed material is extracted with a steady transport rate, that is determined by the exerted flow strength, because the fractional content of coarse grains in active layer is not large enough to provide efficient protection. The removal of sand material leads to a gradual exposure of coarser grains that are located at different depths within the active layer. Due to the constant transport rate of sand material the exposure of coarse grains occurs with a steady pace keeping, thus, the transport rate of coarse grains also constant. For example, during the first 5 minutes the upper 5 mm of bed surface will be eroded and the grains with diameter 8 mm that are located within this zone will be removed. Similarly, within the next 5 minutes the same procedure will be repeated and the same number of coarse grains lying now deeper will be removed, keeping thus a constant transport rate. In the above example the numbers were chosen randomly.

However, the fine sand grains are intrinsically more mobile and therefore their initial bed-load transport is higher. Thus, they are removed faster from active layer which has as a consequence the reduction of their fractional content on bed surface. As soon as the bed surface begins to transform to framework supported, that is, the sand content in bed active layer becomes smaller than a threshold value, the transport rate of sand material starts to decline gradually because the coarse grains now offer a better shelter due to their progressively increasing fractional content on bed surface. The transport rate of gravel grains is also influenced by the transformation of bed surface from matrix supported to framework supported due to progressively increased bed roughness and more stable structure. Hence, the transport rate of gravel fractions starts to decline as well when the threshold value of sand content is trespassed

6.9   Chapter summary

- The experimentally determined transient changes in bed-load transport rate and composition as well as in bed surface composition, that take place during an event of bed-load transport driven by disequilibrium due to zero sediment feed, are described in detail in the present chapter. An extensive summary of the experimental results is given in section 6.8.

- The experimental results are in good agreement with results of previously published related studies on transport of non-uniform sediments under the given sedimentological and hydraulic boundary conditions.

- It was shown that only a surface based bed-load predictor is able to reproduce adequately the observed phenomena.

- The analysis of the observed grain mobility variation provided hints on the pattern that characterizes the variation of fractional reference shear stress with progressive coarsening of bed surface. A summary of the observed transient changes in fractional mobility is provided in section 6.8.3

- Based on optical observations of bed-load transport and theoretical considerations, a mechanism is proposed that explains the variation of fractional reference shear stress with bed surface coarsening in terms of evolving hiding-exposure effects.

- The main implication of the present chapter is that a bed-load predictor in order to capture the observed transient changes during the transformation of a matrix supported to a framework supported bed surface should incorporate a hiding function which will be able to reproduce the observed variation pattern of fractional reference shear stress. This hiding function should take into account as additional term the degree of bed surface coarsening.

7. Development of a surface based disequilibrium transport model

7.1 Introduction

The presentation of the experimental results and the discussion that followed clearly reveals that during the process of static armoring the composition and the transport rate of bed-load as well as the grain size distribution of bed surface varies over time and space. It was demonstrated that a strong interrelationship among these three parameters exists and they should be accounted from a transport model in order to simulate the evolution of the phenomenon of static armoring correctly. The transport rate and the composition of the bed-load depends and at the same time defines the grain size distribution of the bed surface. As expected, the progressive coarsening of the surface layer resulted in a decline of the observed fractional transport rates. However, the grains belonging to the gravel size range had an almost equal reduction of their transport rates, regardless of the grain size, while the grains belonging to the sand size range showed a size depending behavior. The transport rate of the finer grains was less influenced by the development of the armor layer, showing invariance over time and subsequently over progressive stages of bed surface coarsening, while the transport rate of the coarser sand grains showed a significantly larger reduction.

The data set of coupled measurements of the fractional transport rates and the bed surface composition that was presented in the previous chapter will be used herein for the development of a functional relationship that will be suited for a proper reproduction of the disequilibrium processes that was observed during the formation of a static armor layer. The method that will be used is based on a similarity analysis of the measured dimensionless fractional transport rates W^*_i. This method, which was introduced by Ashida and Michue (1971) and was applied for the development of bed-load transport functions by Parker et al. (1982) and Wilcock & Crowe (2003), describes the bed-load transport under equilibrium conditions. Within this method the dimensionless fractional transport rates W^*_i are plotted versus dimensionless shear stress τ^*_i and is investigated whether the resulting bed-load curves can be collapsed into a single curve that will sufficiently describe the measured data.

The model will be developed from bed-load measurements scaled by fractional content of surface bed material and therefore will belong to the category of surface based transport models. The already existing surface transport models were based on observations of transport rates for different flow intensities, which were obtained when an equilibrium condition was established at the end of the experiments either with sediment recirculation or sediment feed. The state of equilibrium was considered to have been reached when the input and output sediment transport rate were equal. In the state of equilibrium the bed surface was usually remarkably coarser than the parent

bed material. The equilibrium bed-load measurements were related to the bed surface composition and were further correlated to the imposed flow strength.

The transport model will consist of a relationship which will allow the calculation of the dimensionless surface as a function of excess shear stress and a hiding function for the calculation of the reference shear stress as a function of the relative grain size d_i/d_{ms}.

7.2 Estimation of reference shear stress τ_{ri}

The reference shear stress is defined as the shear stress τ at which the dimensionless fractional transport rate W^*_i becomes equal to a reference value W^*_r which corresponds to a small but measurable transport rate. Reference shear stress τ_{ri} is a surrogate of critical shear stress τ_{ci}. The difference is that the critical shear stress represents the threshold value of τ at which a grain will be entrained into motion. Below this value the grain should be at rest. Considering the turbulent nature of the flow, meaning that τ fluctuates with time, the definition of the critical shear stress becomes abstract because the length of time that the bed surface should be observed in order to certify whether grains are moving or not is not defined. Shields (1936) and Gessler (1971), among others, mentioned that incipient motion is a statistical problem which depends on the probability function of the turbulent shear stress as well as on the bed material geometry, the packing and sorting. That makes the determination of critical shear stress a difficult task, associated with large uncertainty which is revealed in the large scatter observed in relevant studies e.g. Buffington & Montgomery (1997).

By its definition the reference shear stress should be close to but slightly larger than the critical shear stress. The value of the reference shear stress is determined by fitting an appropriate functional relationship to plots of the fractional dimensionless transport rate W^*_i against the corresponding fractional Shields stress τ^*_i for each grain class. Afterwards, the fitted function is solved in order to determine the value of τ^*_i that corresponds to the reference value W^*_r. The main advantage of this method is that it is not always necessary to extrapolate the fitted function in order to determine the value of τ^*_{ri} that corresponds to W^*_{ri}. This eliminates in a large extent the errors that are associated with the estimation of the critical shear stress due to the extrapolation of measured data to zero.

7.2.1 Procedure for determination of reference shear stress

The comparison of the fractional transport rates q_{bi}, that were measured at the same time point after experimentation began but at different locations along the flume,

revealed the existence of a spatial lag, except for the early stages of each experiment. The measured transport rates showed a consistent increase with distance from flume inlet that was almost linear. The conversion of transport rates to their corresponding dimensionless values slightly reduced the observed spatial lag but did not eliminate it, although the effect of fractional content was neutralized. However, when the comparison between bed-load measurements was carried out, which were taken at different locations along the flume but corresponded to time points at which the bed surface at the measuring stations was characterized by the same degree of armoring, the spatial variation of measured transport rates was considerably smaller and tended to be eliminated. Therefore, the estimation of the fractional reference shear stress τ_{ri} was based on data sets that contained pairs of dimensionless transport rates and related dimensionless Shields stresses τ^*_i that corresponded to the same degree of armoring d_{50s}/d_{50o}.

The procedure that was followed in order to group the estimated dimensionless transport rates is illustrated in fig. 7.1. The determined degree of the bed surface coarsening in a given location, i.e. either 4, 8 or 10 m downstream from the flume inlet, was plotted against experimental time for all discharges that were tested, i.e. 70, 80, 100, 120 and 150 l/s. In fig. 7.1 only three curves are plotted - instead of five - and they represent the temporal variation of the degree of armoring for the sake of clarity. This plot allowed the determination of the time point that the bed surface achieved a given degree of armoring (in fig, 7.1 is denoted as $d_{50s}/d_{50o}(a)$), which in fig. 7.1 is denoted as e.g. $t_{d50s/d50o(a), 150 \; l/s, 4m}$ in each separate experiment that was performed under different imposed flow strength. Subsequently, the estimated dimensionless transport rate was plotted against experimental time for all tested water discharges. From the plot of W^*_i against time, the fractional dimensionless transport rate that corresponded to the given degree of armoring was easily determined for all imposed water discharges. In fig. 7.1 the seeked dimensionless transport rate is denoted as, e.g. $W^*_{id50s/d50o(a), 150 \; l/s, 4m}$ (interpreted as dimensionless transport rate of ith grain class, when the degree of armoring is "a", the flow discharge 150 l/s and it has been estimated from q_{bi} and F_i (fractional content of ith grain class in bed surface) measurements taken 4 m downstream from the flume inlet). This procedure was repeated 10 times for 10 different values of degree of coarsening (i.e. 1, 1,1, 1,2,….,2) for all grain classes (i.e. 0,2, 0,5, 1, 2, 4 and 8 mm) and for measurements taken at three different locations (4, 8 and 10 m downstream from flume inlet).
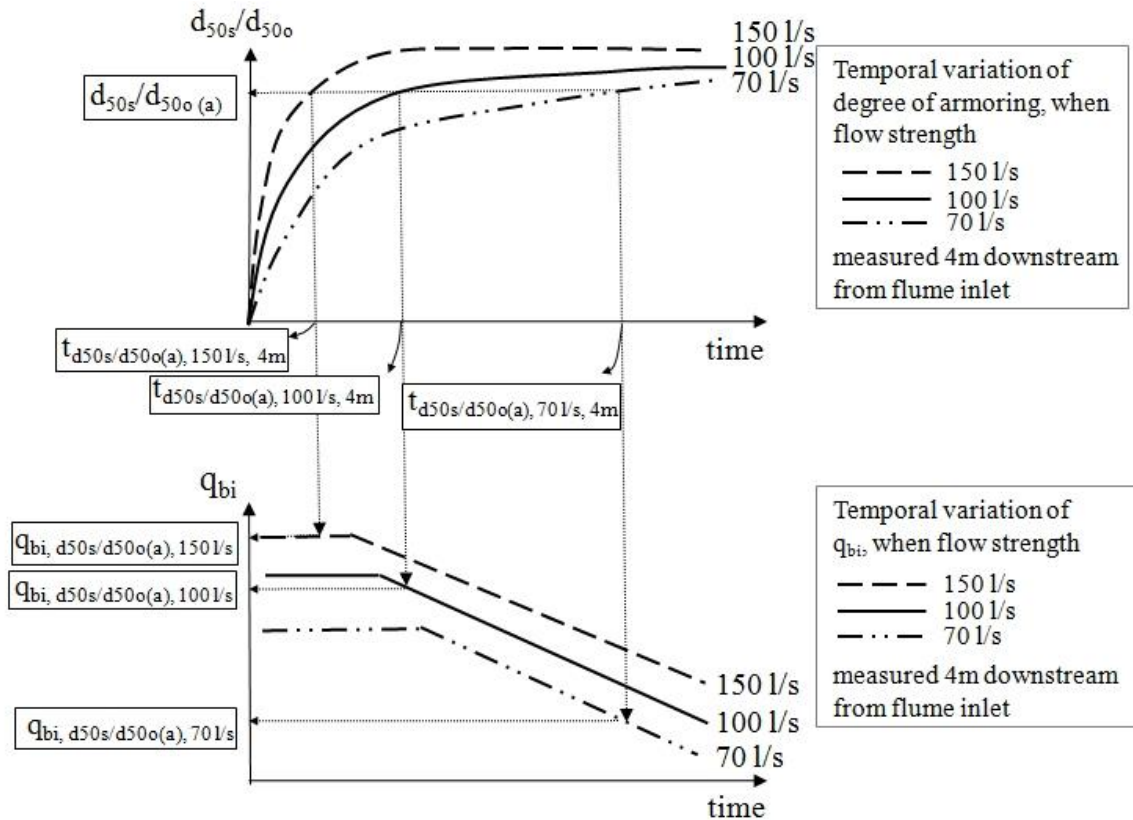
Fig. 7.1 Procedure for determination of W^*_i that correspond to a given degree of bed armoring

The reference shear stress of each separate grain class for a given degree of coarsening was determined from plots that showed the variation of W^*_i with τ^*_i. A large number of $W^*_i - \tau^*_i$ plots were made with values of measured dimensionless fractional transport rates at different shear stresses and each of them corresponded to a certain value of bed surface coarsening, which ranged from $d_{50s}/d_{50o} = 1$, i.e. unarmored bed surface, identical with the subsurface, to $d_{50s}/d_{50o} = 2$. Thus, the reference shear stress of each separate grain class at different conditions of the bed surface coarsening was estimated.

The reference shear stress was determined either by interpolation or by eye with respect to the general trend of variation of W^*_i with τ^*_i. In most of the cases the observed values of W^*_i were both larger and smaller than the reference value of $W^*_r = 0,002$. Therefore, the reference shear stress could be easily determined with interpolation. In some cases, the determined values of W^*_i were larger than the reference value of 0,002 and therefore it was necessary to perform extrapolation. In that case τ_{ri} was determined with the aid of a relation which was similar to the final transport curve and also similar to the functional relationship of Wilcock & Crowe (2003). A regression analysis for fitting e.g. a power equation to the observed data was avoided due to the strong nonlinear character of the data and the presence of outliers which strongly influenced the regression analysis results and led to erroneous values of

reference shear stress. Fig. 7.2 shows the plots of W^*_i against τ^*_i for $d_{50s}/d_{50o} = 1$ and $d_{50s}/d_{50o} = 2$.
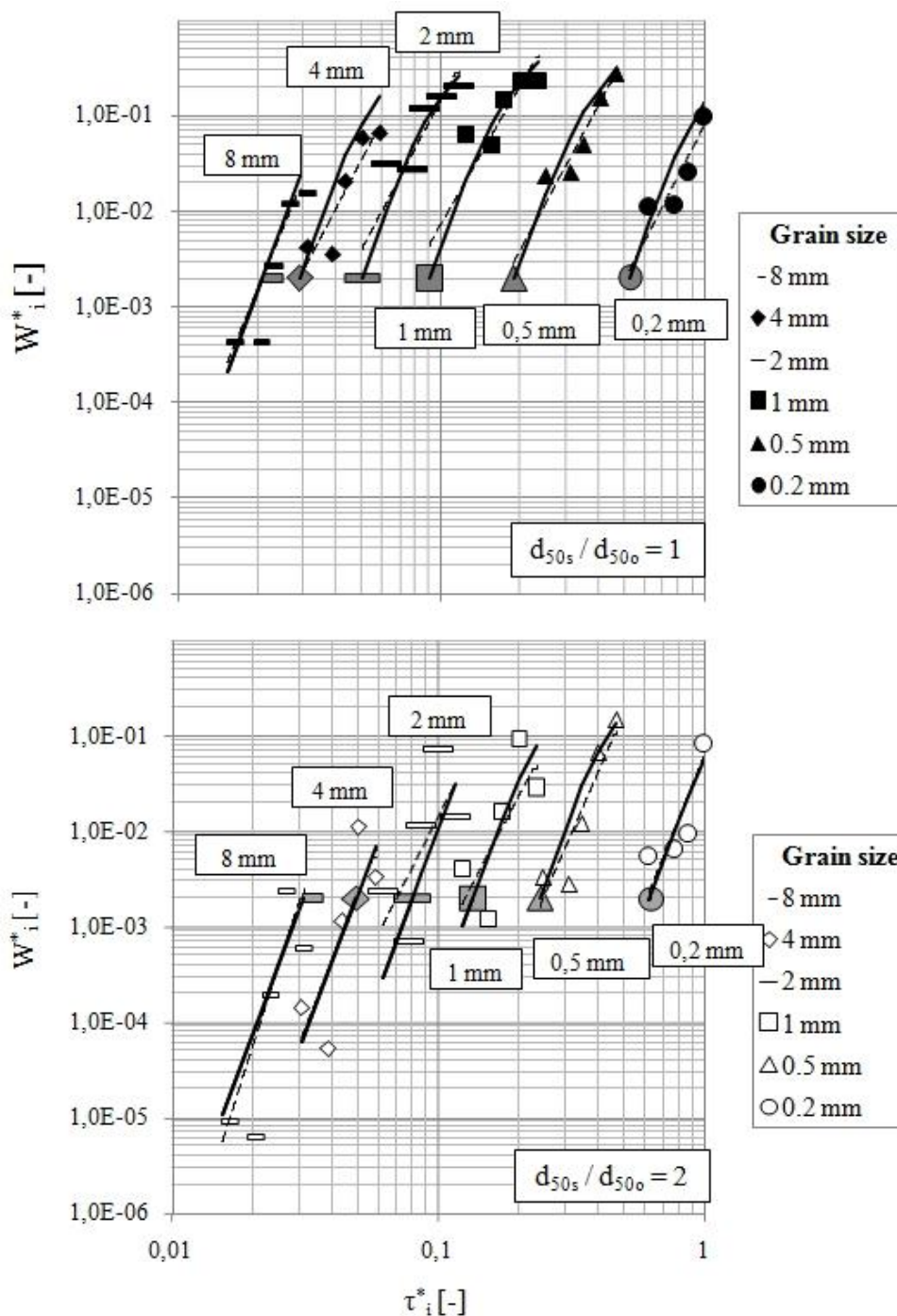
**Fig. 7.2** $W^*_i - \tau^*_i$ plots for two different conditions of bed armoring and determined fractional dimensionless reference shear stress τ^*_{ri}

The different geometrical shapes of the symbols correspond to different grain sizes while the black symbols represent the estimated values of W^*_i when the bed is unarmored. The empty symbols represent the determined W^*_i when the bed has a median grain size which is two times coarser than that of parent bed material. The large symbols with grey filling represent the determined values of reference shear

stress for each grain class and degree of bed surface coarsening. The straight lines are the transport curve of Wilcock & Crowe (2003) while the dashed lines are fitted power trendlines.

When the set of determined values of W^*_i was below the threshold of 0,1 it was considered that the general trend of the data was better described by a simple power function and therefore the reference shear stress was found by extrapolating the fitted power regression curve (e.g. d_i = 2, 1, 0,5 mm for d_{50s}/d_{50o} = 1). On the other hand, when the data set was above the threshold value of 0,1 - in order to take into account the nonlinearity of the transport curve - the reference shear stress was found by fitting the transport curve of Wilcock and extrapolating to the reference W^*_i value (e.g. d_i = 2, 1, 0,5 mm for d_{50s}/d_{50o} = 1).
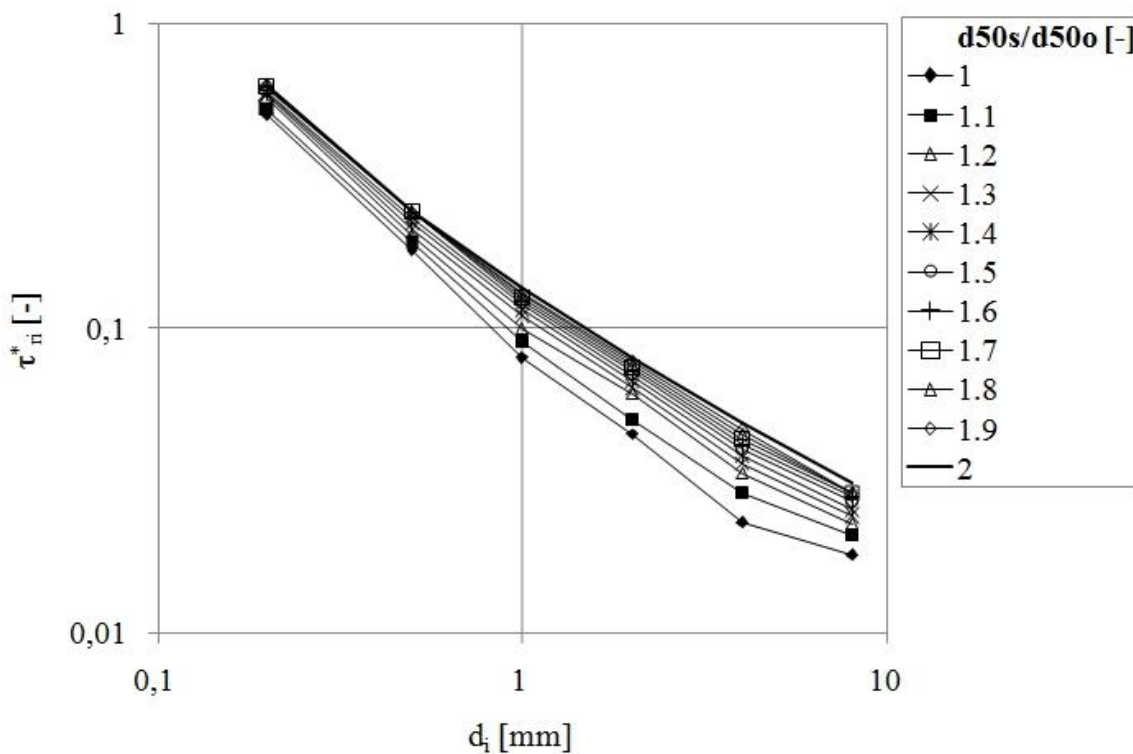

Fig. 7.3 Plot of determined values of dimensionless reference shear stress τ^*_{ri} against absolute grain size d_i at different stages of armor development.

7.2.2 Variation of determined reference shear stress τ_{ri} with grain size and degree of armoring

The employment of the above described methodology allowed the determination of the dimensionless reference shear stress of each grain class τ^*_{ri} at different stages of bed surface coarsening. The fractional reference shear stress τ^*_{ri} was then easily calculated by the following relation

$$\tau_{ri} = \tau_{ri}^{*}(s-1)\rho g d_i \qquad\qquad \text{Eq. (7.1)}$$

where: τ_{ri} is reference shear stress of ith grain class

              τ_{ri}^{*} is dimensionless reference shear stress of ith grain class

              s   is the submerged specific gravity of sediment

              ρ is water density

              g   is gravitational acceleration

              d_i is size of ith grain class

In fig. 7.4 the calculated values of reference shear stress of each grain class τ_{ri} against are plotted grain size d_i. In addition, in the same figure the reference shear stress of median grain size of bed surface d_{50s} is shown. The latter was found with linear interpolation between the already determined values of its neighboring grain sizes
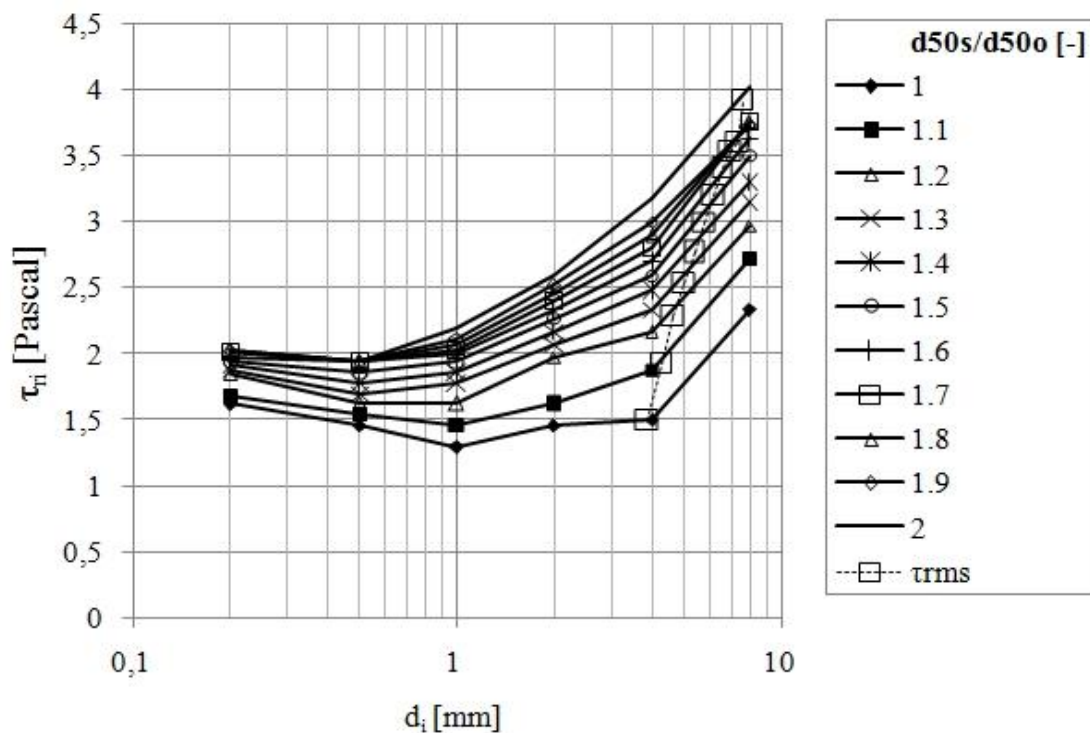

Fig. 7.4   Reference shear stress of ith grain class at different stages of armor development

The results regarding the variation of reference shear stress with grain size and the degree of armoring are in perfect agreement with the pattern that was based on the analysis of experimental measurements which was presented in the previous chapter. Fig. 7.4 shows that the gravel grains are less mobile than the sand grains in all stages of armoring process. This is revealed by the higher shear stress that the gravel grains require in order to be transported with the reference value of dimensionless transport rate. The reference shear stress increases as bed surface becomes coarser. However, the reference shear stress of sand grains showed a considerably smaller variation with

progressive bed surface coarsening, than that of gravel grains. For example, the reference shear stress of the grains with diameter between 0,2 and 0,5 mm increased from 1,6 to 2,0 Pascal, an increase of 20%, while the reference shear stress of the grains with diameter between 8 and 16 mm increased from 2,3 to 4,0 Pascal, an increase of about 40%. This explains why the transport rate of coarse grain classes showed a stronger reduction than that of fine grain classes. Subsequently, this behavior leads to an increase of the difference among the mobility of fine and coarse grain sizes as bed surface becomes coarser and therefore it is held responsible for the observed fining of transported material.

The distribution of reference shear stress with grain size shows considerable differences between the sand and gravel size range respectively. The distribution of the reference shear stress within the sand size range becomes gradually horizontal as bed surface becomes coarser. That means that the particles with diameter smaller than 2 mm tend to be entrained into motion at the same shear stress, thus approaching a behavior of grain size independence, when the bed surface obtains a coarser and better organized structure. The grain size independent entrainment into motion is a key element of the condition of equal mobility, which was observed in the final stage of the experiments. When the bed surface is not yet armored something that is theoretically paradox is observed. The fine sand grains with diameter between 0,2 and 0,5 mm have a higher reference shear stress than the larger and subsequently heavier sand grains with diameter between 0,5 and 2 mm. This paradox could be attributed to the hiding effects that take place on bed surface. The very fine sand grains are sheltered or hidden and therefore protected from the attacking fluid force by all other grain classes. On the contrary, these fine particles cannot contribute to the protection of larger sand grains which are more exposed to the flow. At the early stages, when the bed surface was still unarmored it could be classified as matrix supported, meaning that the sand percentage was relative large. The transformation of bed surface from matrix supported to framework supported results in the equalization of the sheltering effects on sand particles of different grain size. This is due to the increasing fractional content of large gravel grains, which offered the same protection to the sand grains regardless of their grain size.

7.2.3 Variation of dimensionless reference shear stress of median grain size of bed surface τ^*_{r50s}

In Fig. 7.5 the determined dimensionless reference shear stress of median grain size of bed surface τ^*_{r50s} for different values of degree of armoring is plotted. τ^*_{r50s} was initially 0,023 and gradually increased till the value of 0,032, which was achieved when the median grain size of bed surface d_{50s} was 1,4 times coarser than that of

parent bed material, i.e. $d_{50s}/d_{50o} = 1{,}4$. Further coarsening of bed surface did not affect the determined value of τ^*_{r50s}, which remained constant at the value of 0,032. Wilcock & Crowe (2003) found that the value of τ^*_{r50s} increases when the sand content in bed surface becomes smaller. This observation is in good agreement with the trend of increase of τ^*_{r50s} with bed surface coarsening, because bed armoring is actually caused by the reduction of fractional content of sand material in bed surface
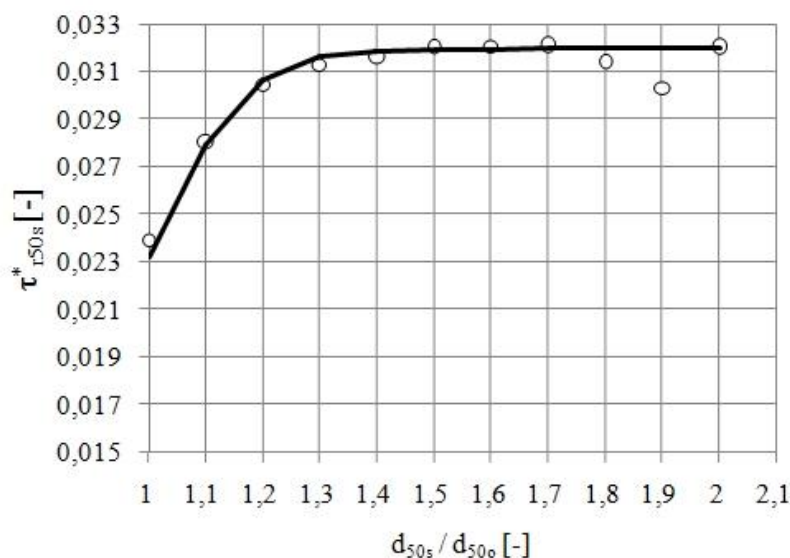

Fig. 7.5 Variation of dimensionless reference shear stress of median grain size of bed surface with degree of armoring

The following function was fitted on the determined values of τ^*_{r50s} in order to describe the increase with degree of armoring:

$$\tau^*_{r50s} = 0{,}018 + \frac{0{,}014}{1 + exp\left(14{,}5 - 14\dfrac{d_{50s}}{d_{50o}}\right)} \qquad \text{Eq. (7.2)}$$

7.3   Development of a new dynamic hiding function

The main conclusion of the analysis of experimental results as well as of the analysis that was presented in the previous paragraph is that the reference shear stress of sand grains varies with progressive bed surface coarsening in a different way than the reference shear stress of particles that belong to the gravel size range. A new hiding function was developed in order to incorporate a transport model into the observations regarding the variation of reference shear stress during the process of armor layer development. The objective was to fit a predictive relation, which could lead to consistent collapse of the observed data into a single curve.

7.3.1 Variation of normalized reference shear stress τ_{ri}/τ_{r50s} with relative grain size d_i/d_{50s}

This was accomplished by scaling the determined fractional reference shear stress values by reference shear stress of d_{50} of bed surface and plotted as function of grain class diameter d_i scaled by d_{50} of bed surface. As mentioned before and shown in Fig. 7.5 τ_{r50s} increases as bed surface becomes coarser and therefore the curves will tend to collapse into one single curve after this axis transformation. The normalizing of d_i with d_{50s} will lead in an offset to the left of the curves that belong to larger degree of bed surface coarsening due to the reduction of the value of ratio d_i/d_{50s}.

The determined fractional reference shear stress values after the above described transformations are plotted in Fig. 7.6. The hiding function of Wilcock & Crowe is also plotted in the same figure, as well as the lines of equal mobility and grain size independence. Finally, the range of d_i/d_{50s} value that corresponds to each absolute grain size d_i is also shown on the same figure (for example the relative grain size d_i/d_{50s} of particles with diameter 8 mm is almost 2 when $d_{50s}/d_{50o} = 1$ and d_i/d_{50s} is almost 1 when $d_{50s}/d_{50o} = 2$).
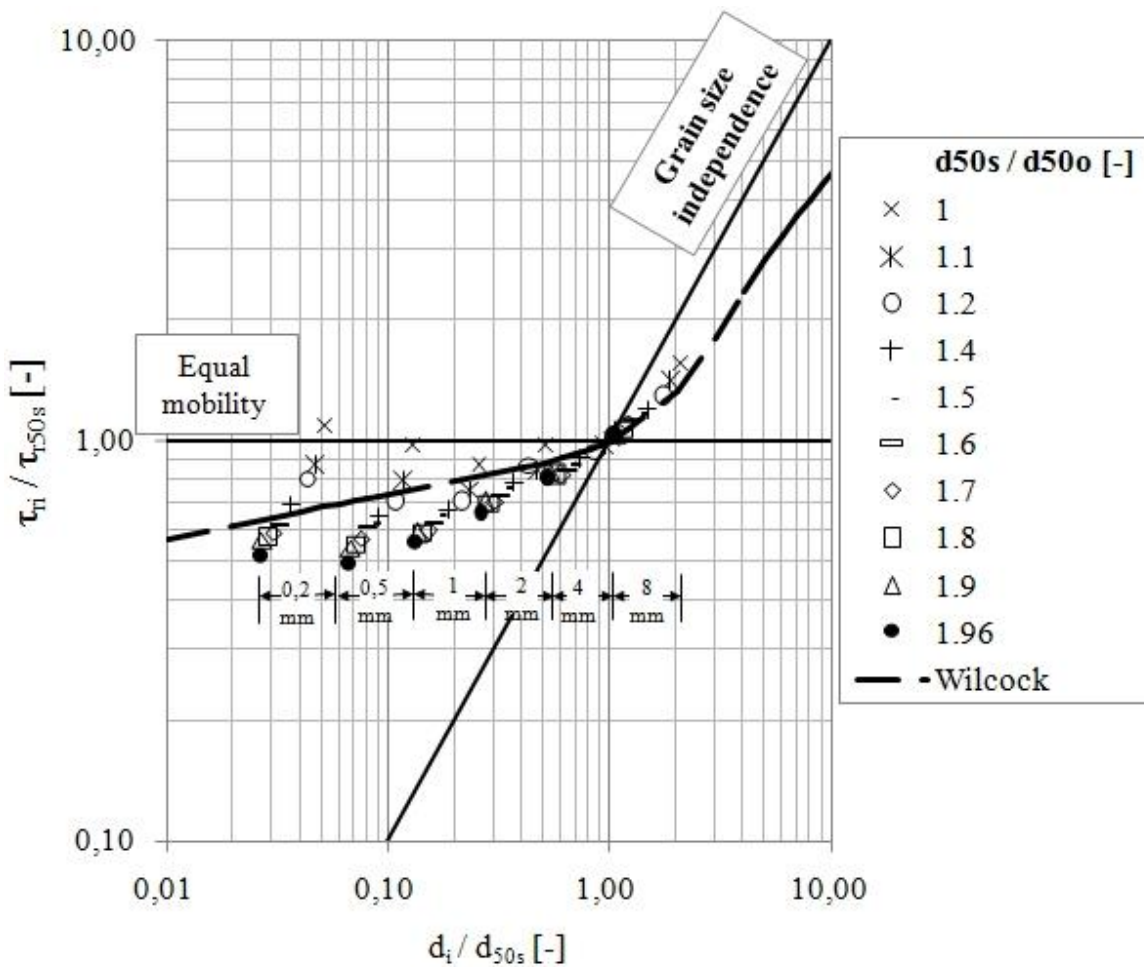

Fig. 7.6 Normalized fractional reference shear stress τ_{ri}/τ_{r50s} against relative grain size d_i/d_{50s}

The determined values of normalized reference shear stresses of grains τ_{ri}/τ_{r50s} with size larger than 4 mm collapsed on a unique curve, which in turn is in very good agreement with the hiding function of Wilcock & Crowe. Thus, the Wilcock & Crowe hiding function is able to predict the reference shear stress of these grain classes. The value of the ratio τ_{ri}/τ_{r50s} for these particles showed a larger variation with d_i/d_{50s} with increasing d_i. The observed two-part trend regarding the variation of ratio τ_{ri}/τ_{r50s} with d_i/d_{50s} size is consistent with the finding that a simple power low is not sufficient to describe the variation of reference shear stress with relative grain size, which derived from the experimental data of Proffitt & Sutherland (1983) and Wilcock & Crowe (2003). Therefore the hiding function of Wilcock & Crowe is separated into two limbs that have different slopes. The slope of the limb for values of relative grain size d_i/d_{50s} larger than one is steeper than the slope of the second limb for values of d_i/d_{50s} smaller than one, which is considerably milder.

On the contrary, the determined normalized reference shear stress of particles smaller than 4 mm showed a different behavior. The value of the ratio τ_{ri}/τ_{r50s} showed a larger decrease with relative grain size d_i/d_{50s} as the absolute grain size d_i became smaller. As a result the curve that connects the normalized t_{ri} values that were determined for the same degree of armoring but different absolute grain sizes (within the size range 0,2 mm – 2 mm) have a varying slope which tend to increase as the degree of armoring becomes larger. Thus a unique relation that takes into account only the relative grain size d_i/d_{50s} cannot predict the reference shear stress of sand grains.

7.3.2 Discussion on the behavior of hiding functions that are defined by a single predictive relation

An important remark on the variation of normalized reference shear stress with relative grain size d_i/d_{50s} is that when $d_i/d_{50s} < 1$, two values of τ_{ri}/τ_{r50s} correspond to each d_i/d_{50s} value. For example, when $d_i/d_{50s} \approx 0,15$ the normalized reference shear stress τ_{ri}/τ_{r50s} is equal to 0,9 when associated with particle size $d_i = 0,5$ and degree of armoring $d_{50s}/d_{50o} = 1$ and equal to 0,55 when associated with $d_i = 1$ mm and $d_{50s}/d_{50o} = 2$. The difference between the two τ_{ri}/τ_{r50s} values corresponding to the same d_i/d_{50s} tends to become smaller as the relative grain size is reduced and approaches unity. For relative grain size larger than 1 the determined normalized reference shear stresses collapse into a unique curve regardless of the absolute grain size. Thus a unique value of τ_{ri}/τ_{r50s} corresponds to each d_i/d_{50s} value. For example, τ_{ri}/τ_{r50s} is equal to 1, when associated with $d_i = 4$ mm and $d_{50s}/d_{50o} = 1$ (relative grain size $d_i/d_{50s} = 4 / d_{50o}$) as well as when associated with $d_i = 8$ mm and $d_{50s}/d_{50o} = 2$ (relative grain size $d_i/d_{50s} = 8 / 2d_{50o} = 4 / d_{50o}$).

The main implication of the above remark is that a single defined τ_{ri}/τ_{r50s} - d_i/d_{50s} function cannot describe the observed variation of reference shear stress and only a family of power functions with varying exponents is suited for this purpose. In order to justify the previous conclusion, the following thought experiment is described.

We assume that the parent bed material contains grains with diameter $d_1 = 0,5$ mm, $d_2 = 1$ mm, $d_3 = 2$ mm, $d_4 = 4$ mm, $d_5 = 8$ mm and so on. When the degree of armoring $d_{50s}/d_{50o} = 1$, the bed surface is unarmored and $d_{50s} = d_{50o}$, but when $d_{50s}/d_{50o} = 2$, then $d_{50s} = 2\ d_{50o}$. The reference shear stress of d_{50s} when $d_{50s}/d_{50o} = 1$, denoted as $\tau_{r50s,d50s/d50o=1}$ is proportional with the product $\tau^*_{r50s,d50s/d50o=1}$ x d_{50o}. For reasons of simplicity the proportionality is ignored and it is assumed that $\tau_{r50s,d50s/d50o=1} = \tau^*_{r50s,d50s/d50o=1}$ x d_{50o}. Accordingly when $d_{50s}/d_{50o} = 2$ is assumed that $\tau_{r50s,d50s/d50o=2} = \tau^*_{r50s,d50s/d50o=2}$ x $2d_{50o}$. In the previous paragraph it was explained that a single defined τ_{ri}/τ_{r50s} - d_i/d_{50s} function means that to each d_i/d_{50s} value corresponds only one τ_{ri}/τ_{r50s} value. Finally, we assume that if the relative grain size takes a constant value i.e. $d_i/d_{50s} = 1/d_{50o}$ the normalized reference shear stress τ_{ri}/τ_{r50s} is equal to a constant value a. However $d_i/d_{50s} = 1/d_{50o}$ when $d_i = 1$ mm and $d_{50s}/d_{50o} = 1$, as well as when $d_i = 2$ mm and $d_{50s}/d_{50o} = 2$.

Subsequently

$$\frac{\tau_{r,1\ mm,\frac{d50s}{d50o}=1}}{\tau_{r,50s,\frac{d50s}{d50o}=1}} = \frac{\tau_{r,2\ mm,\frac{d50s}{d50o}=2}}{\tau_{r,50s,\frac{d50s}{d50o}=2}} = a$$

$$\frac{\tau_{r,1\ mm,\frac{d50s}{d50o}=1}}{\tau^*_{r,50s,\frac{d50s}{d50o}=1}\ d_{50o}} = \frac{\tau_{r,2\ mm,\frac{d50s}{d50o}=2}}{\tau^*_{r,50s,\frac{d50s}{d50o}=2}\ 2d_{50o}}$$

Assuming that $\tau^*_{r50s,d50s/d50o=1} = \tau^*_{r50s,d50s/d50o=2}$

$$\tau_{r,1\ mm,\frac{d50s}{d50o}=1} = \frac{\tau_{r,2\ mm,\frac{d50s}{d50o}=2}}{2}$$

$$\tau^*_{r,1\ mm,\frac{d50s}{d50o}=1}\ 1 = \frac{\tau^*_{r,2\ mm,\frac{d50s}{d50o}=2}\ 2}{2} \quad or \quad \tau^*_{r,1\ mm,\frac{d50s}{d50o}=1} = \tau^*_{r,2\ mm,\frac{d50s}{d50o}=2}$$

In the above relations $\tau_{r,\ 1\ mm,d50s/d50o=1}$ is the reference shear stress of particles with diameter 1 mm, when $d_{50s}/d_{50o} = 1$ and $\tau^*_{r,\ 1\ mm,d50s/d50o=1}$ is the corresponding dimensionless reference shear stress.

The relation

$$\tau^*_{r,1\,mm,\frac{d50s}{d50o}=1} = \tau^*_{r,2\,mm,\frac{d50s}{d50o}=2}$$

can be generalized if recast as

$$\tau^*_{r,\,di\,mm,\frac{d50s}{d50o}=1} = \tau^*_{r,(b\,di)mm,\frac{d50s}{d50o}=b}, \quad with\ b \geq 1 \qquad\qquad \text{Eq. (7.3)}$$

Considering that the published hiding functions are actually power functions, where τ_{ri} and d_i are the dependent and independent variables respectively, and that the predicted fractional reference shear stresses vary between the boundaries of equal mobility and grain size independence, eq. 7.3 has one important implication. This is that eq. 7.3 forces a parallel displacement to the right of the t_{ri} distribution with grain size when the latter is plotted on a log-log diagram. This is illustrated schematically in fig. 7.7.
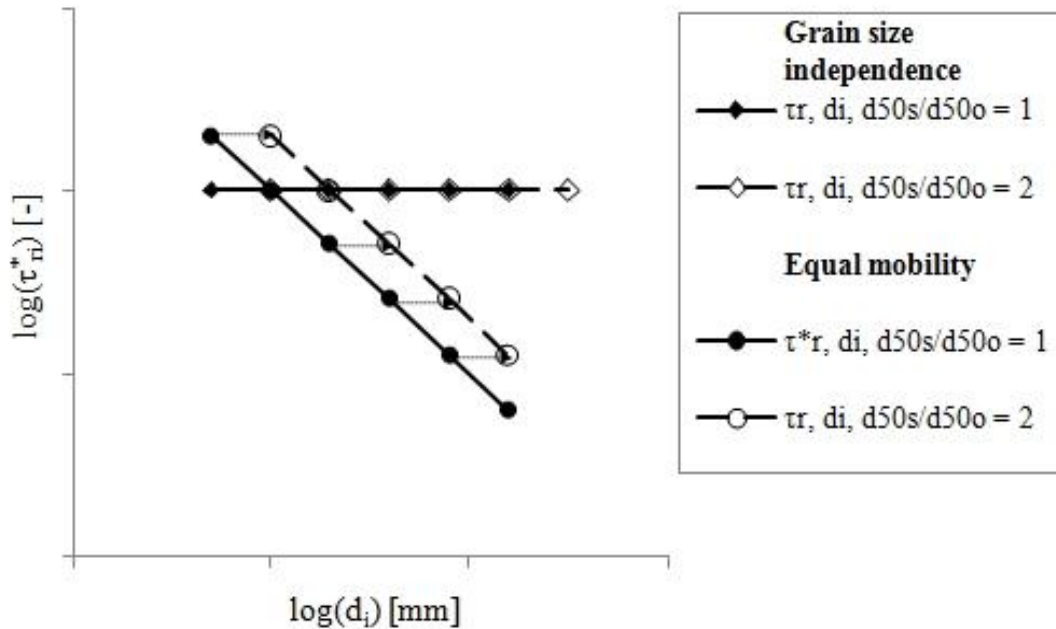

Fig. 7.7   Graphical solution of eq. 7.3 and equivalent eq. 7.4

Even if the assumption that $\tau^*_{r50s,d50s/d50o=1} = \tau^*_{r50s,d50s/d50o=2}$ does not hold, the parallel displacement will still take place but the offset will change depending on the value of ratio $\tau^*_{r50s,d50s/d50o=1}/\tau^*_{r50s,d50s/d50o=b}$. When the hiding function is defined as power function, then with progressive coarsening, i.e. increase of d_{50s}/d_{50o}, the predicted reference shear stresses of all grain classes will be increased to the same extent, i.e.

$$\tau^*_{r,\,di\,mm,\frac{d50s}{d50o}=1} = c_1\,\tau^*_{r,di\,mm,\frac{d50s}{d50o}=b}, \quad with\ b \geq 1 \qquad\qquad \text{Eq. (7.4)}$$

Where c_1 is function of b (degree of coarsening) and the ratio $\tau^*_{r50s,d50s/d50o=1}/\tau^*_{r50s,d50s/d50o=b}$.

We draw the same conclusion if we consider that the hiding functions are the final product of the collapse of different $\tau_{ri} - d_i$ distributions. When these distributions are parallel then the suitable normalization leads to a perfect collapse of the individual $t_{ri} - d_i$ distributions on a unique curve.

However, fig. 7.6 shows that when $d_i/d_{50s} < 1$, two values of τ_{ri}/τ_{r50s} correspond to each d_i/d_{50s} value (assume that the first value is a_1 when $d_i = 1$ mm and $d_{50s}/d_{50o} = 1$ and the second is a_2 when $d_i = 2$ mm and $d_{50s}/d_{50o} = 2$, with $a_1 > a_2$).

Subsequently

$$\frac{\tau_{r,1\,mm,\frac{d50s}{d50o}=1}}{\tau_{r,50s,\frac{d50s}{d50o}=1}} = a_1 > \frac{\tau_{r,2\,mm,\frac{d50s}{d50o}=2}}{\tau_{r,50s,\frac{d50s}{d50o}=2}} = a_2$$

Performing the same analysis as above leads to the general relation

$$\tau^*_{r,\,di\,mm,\frac{d50s}{d50o}=1} = \frac{a_1}{a_2}\,\tau^*_{r,(b\,di)mm,\frac{d50s}{d50o}=b}, \quad with\ b \geq 1\ and\ \frac{a_1}{a_2} \geq 1 \qquad \text{Eq. (7.5)}$$

In addition, fig. 7.6 shows that the value of the ratio of the two values that correspond to the same d_i/d_s, i.e. a_1/a_2 tends to decline with increasing d_i/d_s and it approaches unity when $d_i/d_s >= 1$.

The graphical solution of eq. 7.4 is shown in fig. 7.8
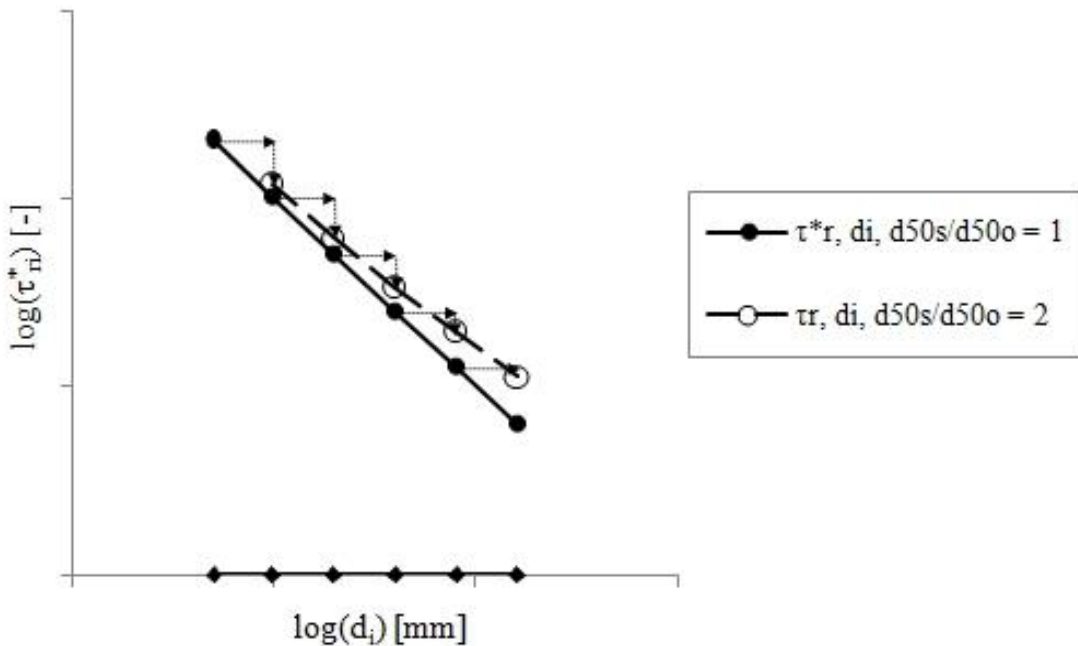
Fig. 7.8   Graphical solution of eq. 7.5 and equivalent eq. 7.6

According to fig. 7.8 the increase of dimensionless reference shear stress τ^{*}_{ri} due to progressive coarsening is proportional to grain size d_i, i.e. the coarser the grain, the larger the increase of its dimensionless reference shear stress with coarsening of bed surface. Thus, eq. 7.5 is equivalent to the following relation

$$\tau^{*}_{r,\ di\ mm,\frac{d50s}{d50o}=1} = c_2\,\tau^{*}_{r,di\ mm,\frac{d50s}{d50o}=b}, \quad with\ b \geq 1 \qquad\qquad \text{Eq. (7.6)}$$

Where c_2 is function of b (degree of coarsening), the ratio $\tau^{*}_{r50s,d50s/d50o=1}/\tau^{*}_{r50s,d50s/d50o=b}$ and the ratio a_1/a_2 which in turn depends on absolute grain size d_i.

The behavior described by eq. 7.5 or 7.6 is in agreement with the observed variation of τ^{*}_{ri} during the experiments of the present study, which is shown in fig. 7.8.

In order to finish the present discussion should be investigated, whether the parallel displacement of τ_{ri}-d_i relation, which is imposed by a hiding function with constant exponent, would allow for a reproduction of the experimental results. Therefore, the effect of eq. 7.4 on variation of fractional mobility W^{*}_{i} when bed surface becomes coarser will be investigated.

When τ remains constant as in the experiments of the present study, eq. 7.4 is equivalent with

$$\frac{\tau}{\tau_{r,\ di\ mm,\frac{d50s}{d50o}=1}} = \frac{1}{c_1}\frac{\tau}{\tau_{r,\ di\ mm,\frac{d50s}{d50o}=b}}, \quad with\ b \geq 1 \qquad\qquad \text{Eq. (7.7)}$$

That means that the excess shear stress of all grain classes will be reduced to the same extent with progressive bed surface coarsening.

In fig. 7.9 a hypothetical $W^{*}_{i} - \tau/\tau_{ri}$ relation is plotted and the mobility of each grain class when $d_{50s}/d_{50o} = 1$ is shown with black symbols. It is assumed that the same $W^{*}_{i} - \tau/\tau_{ri}$ relation describes the variation of W^{*}_{i} with τ/τ_{ri} adequately for all grain classes, i.e. the assumption of perfect similarity collapse is made. The individual fractional W^{*}_{i} values have been positioned on the graph with criterion to keep the same variation pattern of W^{*}_{i} with d_i as the one observed at the beginning of all experiments, which is described in 6.7.1. Therefore, the mobility of grains with size $d_i = 1$ mm and 2 mm are the highest, the mobility of grains 0,5 mm and 4 mm are lower than those of 1 and 2 mm and the mobility of grains with diameter 0,2 and 8 mm are even lower. The empty symbols represent the fractional mobility when $d_{50s}/d_{50o} = 2$ and when the same excess shear stress reduction has been imposed to all grain classes. Finally, different geometrical shapes correspond to each grain class separately.
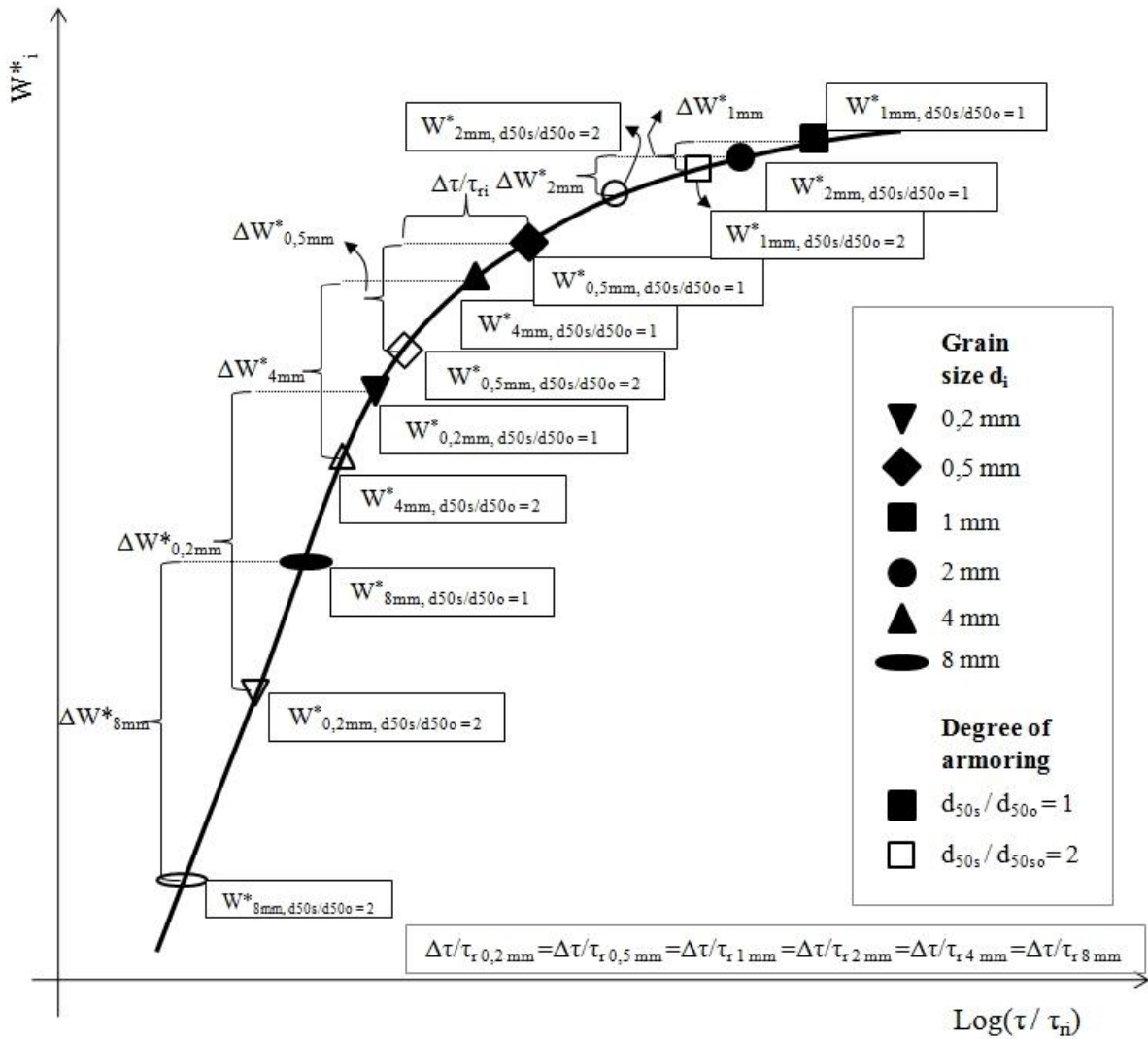
Fig. 7.9 Fractional mobility reduction when the excess shear stress of all grain classes is equally reduced due bed surface coarsening

Fig. 7.9 shows that the lower the initial fractional mobility is the larger the reduction of the fractional mobility will be. Consequently, the dimensionless transport rate W_i^* of particles with diameter 8 and 0,2 mm will be more reduced when compared to W_i^* of particles with size 4 and 0,5 mm, which in turn will suffer a larger mobility reduction than the grains with size 2 and 1 mm. Nonetheless, the pattern of fractional mobility reduction, which is shown in fig. 7.9, does not agree with the one that was observed during the experiments of the present study (shown in fig.6.21 and fig. 6.22). The experimental measurements showed that the particles with diameter 1 and 2 mm suffered the largest mobility reduction, which was larger than that of grains with size 4 and 8 mm. The mobility of grains with size 0,2 mm showed the largest invariance with progressive coarsening, while the mobility reduction of particles with size 0,5 mm grains was between that of grains with size 0,2 and 1 mm respectively.

Thus a hiding function which is defined as power function with constant exponent will considerably overestimate the mobility reduction of particles with diameter 0,2 and 0,5

mm. On the other hand, it will underestimate the mobility reduction of grains with size 1 and 2 mm when bed surface becomes coarser, assuming that it will predict the mobility reduction of the coarse particles correctly .

In addition, progressive coarsening is associated with increased fractional content F_i in bed surface of grains with size 8 and 4 mm, which partly neutralizes the effect of mobility reduction on observed transport rate (q_{bi} is proportional to W^*_i and F_i), while the opposite happens for grains with diameter 0,2 and 0,5 mm. Considering that the observed d_{50} of transported material was near 2 mm at the beginning of each experiment (i.e. at the boundary of the sand size range) the pattern of mobility reduction (shown in Fig. 7.9) will result in a coarsening of transported material with progressive armoring, because of the wrong estimation of mobility reduction for the grains with size 0,2 mm till 2 mm.

The conclusion that can be drawn from the above discussion is that the data that correspond to gravel size range collapse in a consistent way into one single curve regardless of the degree of bed surface armoring. On the other hand, the determined values of normalized reference shear stress for grains with relative grain size smaller than 1 cannot be collapsed into one unique predictive relation but they belong to a family of power equations, the exponent of which can be expressed as a function of the degree of bed surface coarsening. The prediction of reference shear stress of particles with relative grain size $d_i/d_{50s} < 1$ by a hiding function, which is defined as a power function with constant exponent, will lead to overestimation of the mobility reduction of the fine grains and underestimation of the mobility reduction of coarser grains (with relative grain size always smaller than 1). Thus, such a hiding function might successfully predict the initial or final condition but it is not suited to follow the transient changes that take place with progressive bed surface armoring.

7.3.3 Mathematical expression for prediction of fractional reference shear stress for the sediment employed in the present study

In order to describe the observed variation of normalized reference shear stress τ_{ri}/τ_{r50s} with relative grain size mathematically, exponential functions were fitted to the data of each grain class separately. The general form of the fitted functions was:

$$\frac{\tau_{ri}}{\tau_{r50s}} = a_i \, e^{b_i \frac{d_i}{d_{50s}}} \qquad \text{Eq. (7.8)}$$

where: τ_{ri} is reference shear stress of ith grain class

τ_{r50s} is reference shear stress of median grain size of bed surface

a_i, b_i are multipliers of the fitted functions

d_i/d_{50s} is relative grain size of ith grain class associated with d_{50s}

Under the employed experimental configuration it was possible to measure the fractional transport rates of grains with maximum diameter that ranged between 8 and 16 mm. In order to expand the applicability of the herein developed hiding function, exponential functions should describe the variation of τ_{ri}/τ_{r50s} with d_i/d_{50s} for grain classes larger than 8 mm as well, despite the lack of experimental measurements. Based on the observation, that the values of reference shear stress of grains larger than 4 mm, which were determined from the experimental results of the present study, are in good agreement with the predictions of the Wilcock and Crowe hiding function, the parameters of the fitted exponential functions for grains larger than 16 mm were chosen. The criterion was the reproduction of the reference shear stress values that the hiding function of Wilcock & Crowe would give.

.

	d_i	Fitted function
△	0.2 mm	$\tau i/\tau s50 = 0.2 \exp(30\ di/d50s)$
×	0.5 mm	$\tau i/\tau s50 = 0.28 \exp(8.5\ di/d50s)$
◇	1 mm	$\tau i/\tau s50 = 0.38 \exp(2.93\ di/d50s)$
+	2 mm	$\tau i/\tau s50 = 0.47 \exp(1.27\ di/d50s)$
○	4 mm	$\tau i/\tau s50 = 0.64 \exp(0.42\ di/d50s)$
□	8 mm	$\tau i/\tau s50 = 0.82 \exp(0.25\ di/d50s)$
✳	16 mm	$\tau i/\tau s50 = 1.1 \exp(0.16\ di/d50s)$
▫	32 mm	$\tau i/\tau s50 = 1.6 \exp(0.1\ di/d50s)$

— — Wilcock
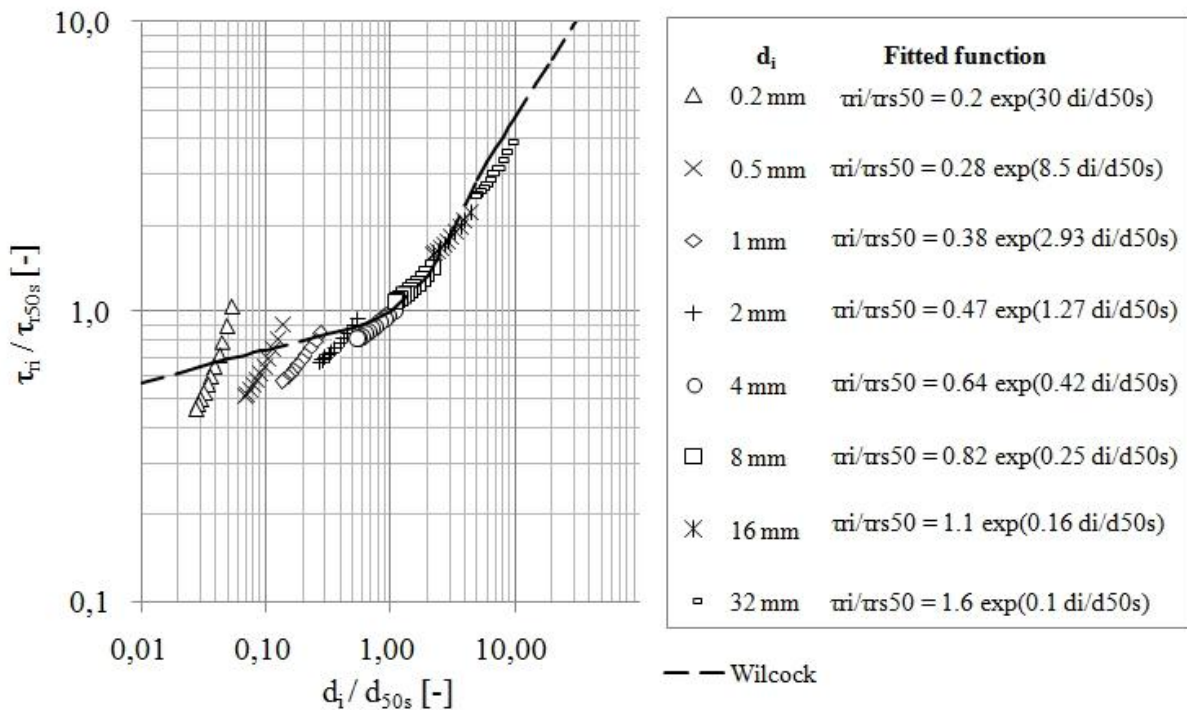
Fig. 7.10 Predicted values of normalized fractional reference shear stress τ_{ri}/τ_{r50s} against relative grain size d_i/d_{50s}

The parameters a and b of the fitted exponential functions for grain sizes from 0,2 mm till 64 mm are shown in table 7.1

The parameter a_i controls the vertical position of each separate curve on the d_i/d_{50s} - τ_{ri}/τ_{r50s} diagram, while the parameter b_i determines the slope of each curve. Each separate curve expresses the variation of normalized reference shear stress of a given grain class with relative grain size. Thus, both these parameters determine the relation between fractional reference shear stress τ_{ri} and reference shear stress of median grain size of bed surface τ_{r50s}.

Table 7.1 Parameters of fitted exponential functions that describe variation of τ_{ri}/τ_{r50s} with d_i/d_{50s}

Absolute grain size [mm]	Relative grain size (related to d_{50o}) [-]	Parameter a_i of exponential function [-]	Parameter b_i of exponential function [-]
0,2	0,05	0,2	30
0,5	0,14	0,28	8,5
1	0,27	0,38	2,93
2	0,55	0,47	1,27
4	1,10	0,64	0,42
8	2,19	0,82	0,25
16	4,38	1,1	0,16
32	8,77	1,6	0,1

In fig. 7.11 the a_i and b_i values that provided the best fit to experimental data against relative grain size (associated with median grain size of parent bed material) d_i/d_{50o} are plotted. The determined a_i and b_i values show a consistent trend when the relative grain size d_i/d_{50o} increases. The parameter a_i increased and the parameter b_i was reduced with increasing d_i/d_{50o}. In the same figure the fitted functions that described best the variation of a_i and b_i with relative grain size d_i/d_{50o} are also shown. The solid black lines represent the fitted functions for $d_i/d_{50o} < 1$ and the dashed black lines represent the fitted functions for $d_i/d_{50o} \geq 1$. Considering that both values together determine the variation of τ_{ri}/τ_{r50s} with d_i/d_{50s} it is difficult to seek physical explanation for the variation a_i and b_i with d_i/d_{50o} separately. Nonetheless, the variation of the two parameters together results in the behavior that was observed in the experiments as far as the variation of reference shear stress is concerned. Using d_i/d_{50o} was necessary in order to assure the non-dimensionality in both sides of the equation that describes the variation of a_i and b_i with absolute grain size d_i.
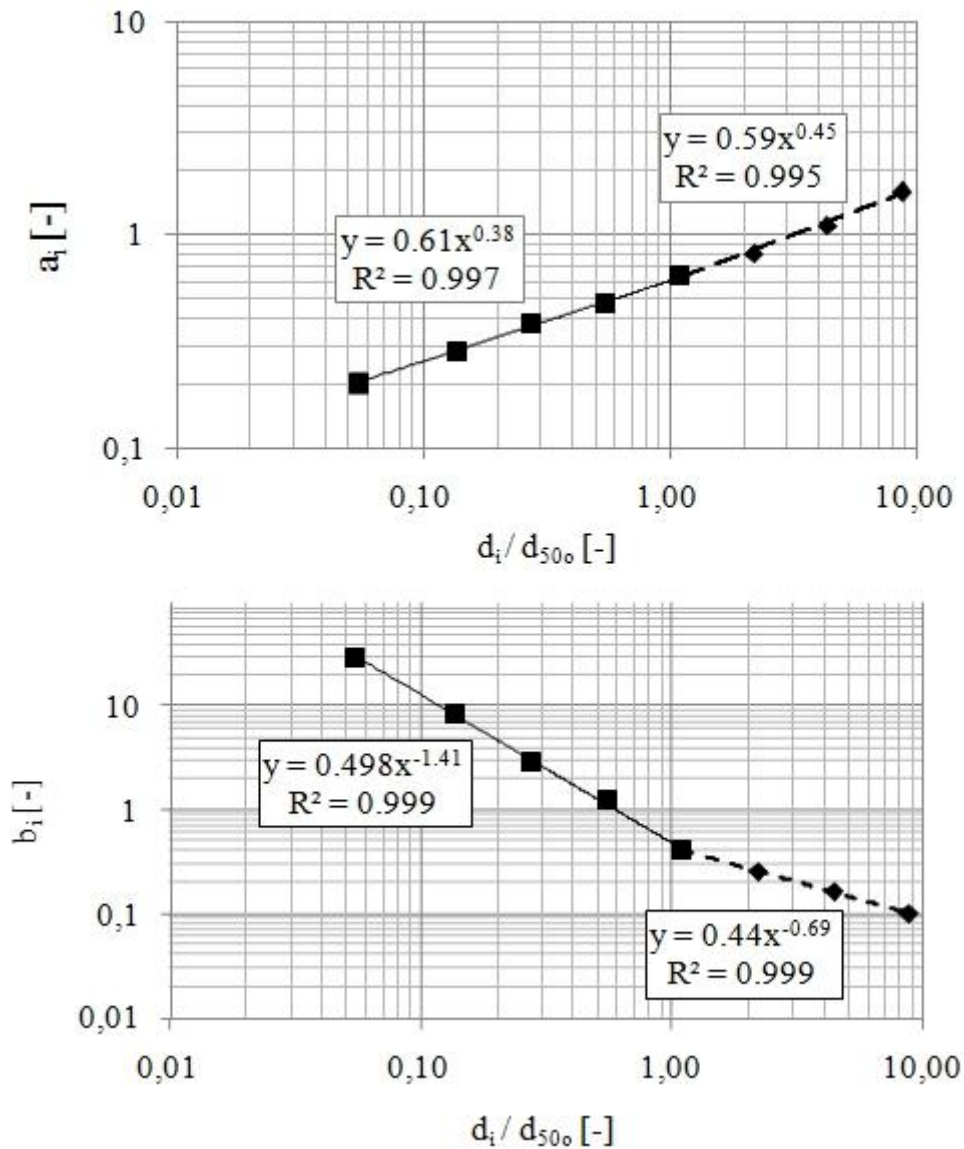
Fig. 7.11 Variation of a_i and b_i with d_i/d_{50o} for the parent bed material employed in the present study

The functions that describe the variation of a_i and b_i with d_i/d_{50o} (relative grain size associated with d_{50o}) are

$$
a_i = \begin{cases} 0{,}61 \left(\dfrac{d_i}{d_{50o}}\right)^{0{,}38} & , \dfrac{d_i}{d_{50o}} \leq 1 \\[2ex] 0{,}59 \left(\dfrac{d_i}{d_{50o}}\right)^{0{,}45} & , \dfrac{d_i}{d_{50o}} > 1 \end{cases}
\qquad \text{Eq. (7.9)}
$$

$$
b_i = \begin{cases} 0{,}50 \left(\dfrac{d_i}{d_{50o}}\right)^{-1{,}41} & , \dfrac{d_i}{d_{50o}} \leq 1 \\[2ex] 0{,}44 \left(\dfrac{d_i}{d_{50o}}\right)^{-,069} & , \dfrac{d_i}{d_{50o}} > 1 \end{cases}
\qquad \text{Eq. (7.10)}
$$

All in all, the hiding function defined by eq. 7.2, 7.3, 7.8, 7.9 & 7.10 was based solely on data which were performed with a certain sediment mixture. The relations 7.3, 7.8, 7.9 and 7.10 can accurately reproduce the normalized reference shear stresses τ_{ri}/τ_{r50s} that were determined from the measurements of fractional transport rates and bed surface composition, which were taken during the experimental part of the present study. The reference shear stress τ_{ri} of a given grain class is calculated by multiplying the predicted τ_{ri}/τ_{r50s} with the reference shear stress of bed surface median grain size τ_{r50s}, which is given by eq. 7.3. The main innovation of the hiding function is the ability to adjust the reference shear stress and subsequently the mobility of fine particles (particles with relative grain size $d_i/d_{50s} < 1$) when the condition of bed surface is relative to parent bed material, i.e. the degree of armoring changes. This is realized by adjusting the slope of the limb of the hiding function that is responsible for the fine grains. On the other hand, it is assumed that the reference shear stress of coarse particles (the particles with relative grain size $d_i/d_{50s} > 1$) will change during progressive coarsening of the bed surface because they follow a certain pattern that is described by a unique curve. Thus, the slope of the limb of the hiding function for large relative grain sizes remains constant regardless of the degree of armoring.

7.3.4   Generalization of the mathematical expression for other sediment mixtures

The equations 7.8, 7.9 and 7.10 that define the hiding function have been developed from experiments that were performed with a single type of sediment. The employed parent bed material had a high sand content of 37% and median grain size d_{50o} 3,65 mm (its sediment mixture is thoroughly described in 3.2.3). The question that is raised is whether the proposed equations can reproduce (as for the herein employed sediment) the variation of fractional reference shear stress τ^{*}_{ri} with the same accuracy when the surface of a bed that contains a different sediment mixture will become coarser.

7.3.4.1 Discussion on the behavior of hiding functions when the characteristic grain size of parent bed material changes

The proposed hiding function embodies the median grain size of parent bed material d_{50o} as independent variable. Thus, the behavior of the function will change when applied to different bed materials. Fig. 7.12 shows the normalized reference shear stress that was predicted for three sediment mixtures with different d_{50o} from the

hiding function that is defined from equations 7.8, 7.9 and 7.10. In the middle the predicted τ_{ri}-τ_{r50s} values for a sediment mixture with d_{50o} equal with 4 mm are illustrated. On the left hand side the predicted τ_{ri}/τ_{r50s} values for a sediment mixture with d_{50o} equal with 2 mm are shown. Finally, on the right side the plotted τ_{ri}/τ_{r50s} values were calculated assuming that the d_{50o} of parent bed material is 8 mm. In addition, the hiding function of Wilcock & Crowe is shown on all plots
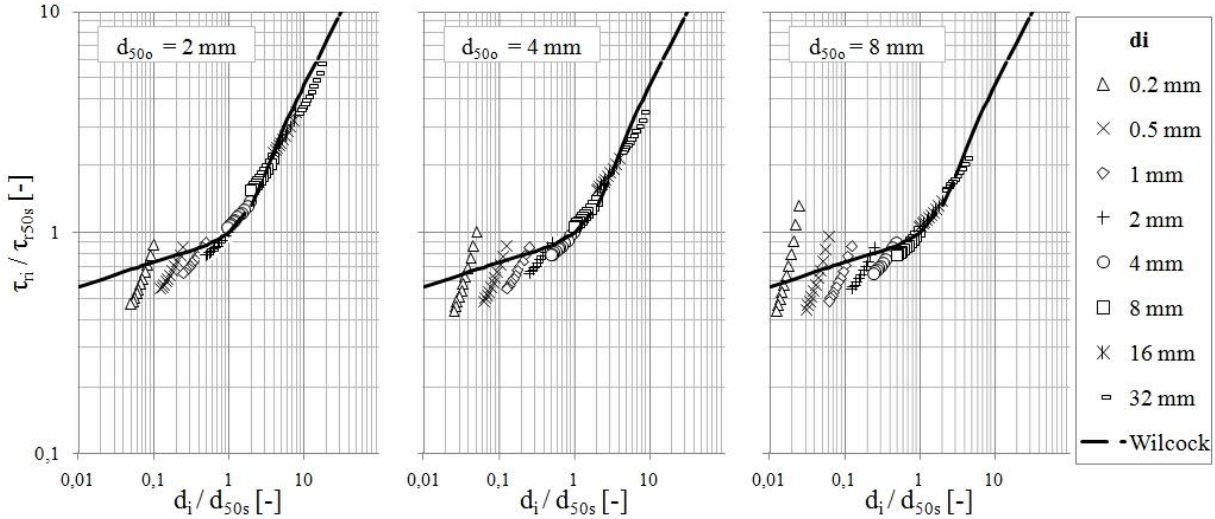
Fig. 7.12 Predicted τ_{ri}-τ_{r50s} values by eq. 7.8, 7.9 and 7.10 for three different sediment mixtures

The first impression is that when d_{50o} becomes larger, the calculated normalized reference shear stress τ_{ri}/τ_{r50s} is switched to the left. On the contrary, when the parent bed material is finer the plotted values are offset to the right. This happens because the increase of d_{50o} is associated with a proportional increase of bed surface d_{50s} for a given degree of armoring. For example, if the degree of armoring $d_{50s}/d_{50o} = 2$ then $d_{50s} = 4$ mm, when d_{50o} is 2 mm. Accordingly, $d_{50s} = 16$ mm, when $d_{50o} = 8$ mm, and the degree of armoring d_{50s}/d_{50o} remains equal to 2. The increase of d_{50s} results in the reduction of relative grain size d_i/d_{50s} and subsequently the offset of the plotted values to the left.

An additional observation is that the normalized reference shear stress of grains with diameter e.g. 2 mm, which belong in a sediment mixture with $d_{50o} = 4$ mm (thus $d_i/d_{50o} = 2/4 = 0,5$) will show exactly the same behavior as the grains with diameter 1 mm, which in turn belong in a sediment mixture with $d_{50o} = 2$ mm ($d_i/d_{50o} = 1/2 = 0,5$). Accordingly, the variation of normalized reference shear stress with d_i/d_{50s} of grains with diameter 2 mm that belong in a sediment mixture with $d_{50o} = 4$ mm (thus $d_i/d_{50o} = 4/8 = 0,5$) will show exactly the same behavior as the grains with diameter 4 mm, which in turn belong in a sediment mixture with $d_{50o} = 8$ mm ($d_i/d_{50o} = 4/8 = 0,5$). Therefore, the normalized reference shear stress of two grains (that belong to different mixtures) with different absolute grain size d_i but the same relative grain size d_i/d_{50o}

will be reduced to the same extent when the surface of both beds coarsens to the same degree (as long as the initial d_i/d_{50s} for both grains is smaller than one). Of course, this observation is valid for any hiding function, which is expressed by a power function with d_i/d_{50s} as independent variable and τ_{ri}/τ_{r50s} as dependent variable and not only the one that is developed so far.

An important aspect of the previous remark on the behavior of power hiding functions when the median grain size of parent bed material changes is given with the following thought experiment. We assume that a grain with $d_i = 1$ mm belongs in a sediment mixture with high sand content and therefore a d_{50o} of 4 mm (i.e. $d_i/d_{50o} = 0,25$ and $d_i/d_{50s\_initial} = 0,25$) and a second grain with $d_i = 10$ mm belongs in a sediment mixture with low sand content and $d_{50o} = 40$ mm (i.e. $d_i/d_{50o} = 0,25$ $d_i/d_{50s\_initial} = 0,25$). By applying on both initially unarmored beds a suitable shear force we induce the creation of an armor layer that in both cases is two times coarser than the initial bed surface (i.e. $d_{50s}/d_{50o} = 2$ or any other degree of armoring). Thus, the median grain size of bed surface d_{50s} is now 8 mm with considerably lower sand content for the first sediment mixture and 80 mm for the second. The classical hiding functions as well as the one defined by eq. 7.8, 7.9 and 7.10 will predict that the coarsening of bed surface will cause an equivalent reduction of normalized reference shear stress in both cases. However, the environment of the small grain with $d_i = 1$ mm changed dramatically with progressive bed surface coarsening, as the initially matrix supported bed has been converted into a framework supported bed. On the contrary, we can assume that the change in the environment of the coarse grain with diameter 30 mm was not so severe because the bed surface remained framework supported during the whole process.

Nonetheless, the lack of experimental data focusing on the description of the effect of progressive coarsening on the pattern that governs the increase of fractional reference shear stress for different types of sediment mixtures renders the prediction of that pattern difficult and speculative.

However, previous experimental studies provide some hints on that matter. Wilcock et al. (2001) performed experiments with different types of sand-gravel sediment mixtures. In order to prepare the employed sediment mixtures sand and gravel material was mixed. The individual sediment mixtures were differentiated by sand content. The grain size distribution of the two components i.e. sand and gravel material was the same for all sand-gravel sediment mixtures. The experiments were performed with recirculating sediment feed configuration. As soon as a state of equilibrium had been established the researchers measured the equilibrium fractional transport rates and the grain size distribution of bed surface.

Wilcock & Crowe (2003) developed a transport model that was based on the results of the previous investigation and was able to couple the measured transport rates with the corresponding bed surface gradation. The hiding function of the Wilcock & Crowe

transport model is shown in fig. 7.13. The values of normalized reference shear stress of each individual grain class that were used for the development of the hiding function are shown on the same figure.
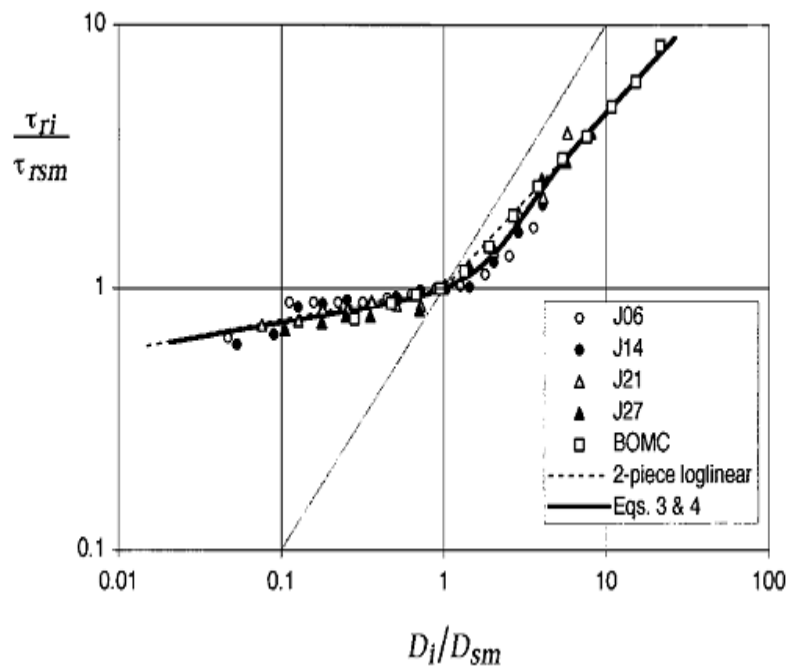

Fig. 7.13 Plot of hiding function incorporated in the transport model of Wilcock & Crowe and normalized reference shear stress that were used for the development of the function (Copied from Wilcock & Crowe (2003))

Wilcock and co-workers named the different sediment mixtures after the sand content. Thus J06 was a sand-gravel mixture with 6 % sand content, J14 had a sand content of 14 % and so on. BOMC was a sand-gravel mixture employed in even older studies (Wilcock & McArdell (1993)) and had a sand content of 34 % with slightly different gradation of the sandy counterpart when compared to the other mixtures.

The determined normalized reference shear stress for each grain class collapsed on a power function which was characterized by two limbs with different slopes. The breaking of the slope occurred when the relative grain size d_i/d_{50s} was equal to one. Although the fitted function captures the essential trend of τ_{ri}/τ_{r50s} - d_i/d_{50s} variation it seems that the function would fit better the experimental data, if the lower limb had a varying slope which would grow with increasing sand content in the parent bed material. For example, the determined τ_{ri}/τ_{r50s} values for the sediment J06 would be better predicted if the slope of the lower limb was close to zero, while the determined τ_{ri}/τ_{r50s} values for the sediment BOMC (sand content 34 %) or J27 would be better predicted if the slope of the lower limb was larger than the slope that corresponded to sediment J06.

The slope of the hiding function is still an unresolved problem in sediment transport of sand-gravel mixtures. Some investigations that focused on mixtures with small sand

content, e.g. Wilcock (1993) or Parker et al. (1982), showed that the reference shear stress does not vary considerably with grain size, i.e. the slope of the hiding function is close to zero. On the Contrary, investigations that focused on mixtures with high sand content, e.g. Wilcock (1993) or Asworth & Ferguson (1989), revealed a larger variation of reference shear stress with grain size and therefore a hiding function with large slope could reproduce better the measured τ_{ri} values. The above observations have actually been the subject of a large debate between the supporters of the concept of equal mobility, e.g. Parker et al. (1982), Andrews & Parker (1987) and others and the supporters of the concept of selective transport, e.g. Komar & Shih (1992), Wathen et al. (1995) and others.

It is the author's belief that a hiding function that predicts the fractional reference shear stress based solely either on the concept of equal mobility or a strictly defined degree of selectivity for all types of sand-gravel sediment mixtures regardless of their grain size distribution cannot have a wide applicability.

7.3.4.2 Modification of eq. 7.9 and 7.10 in order to fit the fractional reference shear stress that is determined in the investigations of Wilcock

The experiments of the present study were performed with a certain sediment mixture. From the data that were gathered during these experiments a hiding function (which is defined by eq. 7.2, 7.3, 7.8, 7.9 & 7.10) was developed. This hiding function is able to estimate the fractional reference shear stress for a given bed material when the bed surface composition changes. In order to test the quality of its predictions in the case of beds that are comprised of different sediment mixtures as well, the most direct method would be to compare the predictions of the function with fractional reference shear stress values that would be determined from data obtained during experiments with the same arrangement but different bed material. Unfortunately the lack of such data did not allow employment of this method. Therefore, the hiding function was tested against experimental data that were gathered during the investigation of Wilcock et al. (2001). This data set was convenient because it contained coupled measurements of fractional transport rates and corresponding bed surface composition when the equilibrium condition had been established for five different sand-gravel sediment-mixtures. The fractional reference shear stresses were estimated by the researchers and published in the following paper (Wilcock & Crowe (2003)). In addition, the grain size distribution of bed surface did not vary considerably from run to run but only from series to series (each series of experiments was performed with the same parent bed material and consisted of 8 – 10 experimental runs that were performed with different flow strength). Thus, the determined fractional reference shear stress for a given sediment mixture could be associated with a well defined degree of armoring.

Fig. 7.14 shows the normalized reference shear stress values that were determined from Wilcock and Crowe for the experimental results of Wilcock et al. (2001) as well as the hiding function that was developed by Wilcock & Crowe (2003). Furthermore, in the same figure the τ_{ri}/τ_{r50s} that were calculated by eq. 7.2, 7.3, 7.8, 7.9 & 7.10 (represented by grey lozenges) are plotted. Finally, in fig. 7.14 the τ_{ri}/τ_{r50s} values that were calculated after the modification of eq. 7.2, 7.3, 7.8, 7.9 and 7.10 (represented by white lozenges) are shown. The modification of these equations is described later in the same chapter. The individual diagrams in fig. 7.14 correspond to different sediment mixtures. It should be noted that in the experiments with BOMC the bed surface at the equilibrium was always finer than the parent bed material and thus the degree of coarsening was smaller than one. Therefore, by the application of equations 7.9 and 7.10, the d_{50o} was replaced by the median grain size of bed surface d_{50s}.
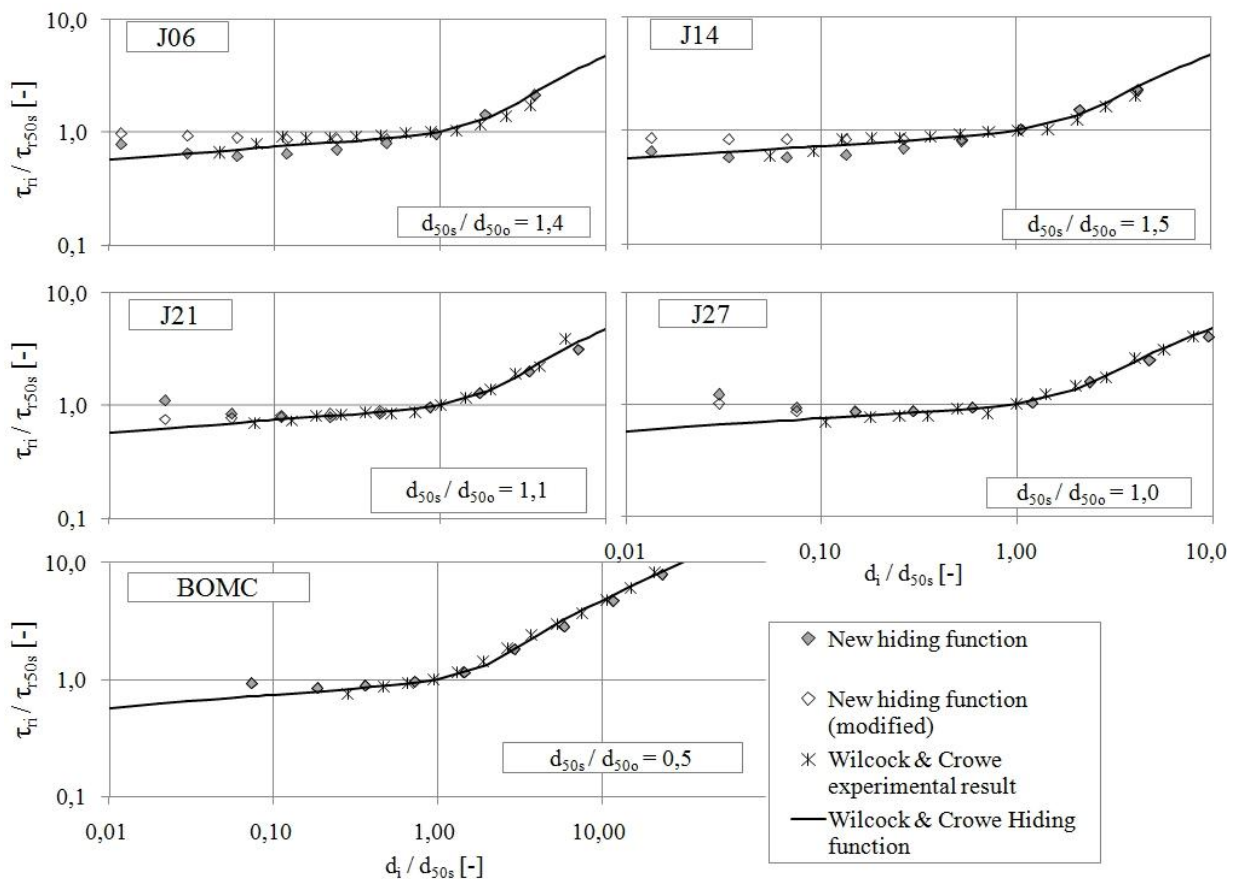
Fig. 7.14 Comparison between the predicted τ_{ri}/τ_{r50s} values of the new hiding function before and after the modification and the determined τ_{ri}/τ_{r50s} values in the investigations of Wilcock and co-workers for different sediment mixtures

Fig. 7.14 shows that the equations 7.3, 7.8, 7.9 and 7.10 predicted fractional normalized reference shear stress τ_{ri}/τ_{r50s} which was in good agreement with the τ_{ri}/τ_{r50s} values that were determined from experimental results when the sand content of the employed sediment mixture was high, i.e. for the sediments J21, J27 and BOMC. In addition, the estimated τ_{ri}/τ_{r50s} values were close to the predictions of the hiding

function of Wilcock & Crowe except for the two fine grain classes with diameter 0,2 and 0,5 mm respectively. For these grain fractions equations 7.3, 7.8, 7.9 and 7.10 predicted higher τ_{ri}/τ_{r50s} values than the hiding function of Wilcock & Crowe. However, the development of the hiding function of Wilcock & Crowe was based on reference shear stress values of grains with diameter larger than 1 mm, although the employed sediment mixtures contained significant amounts of finer sand grains. The exclusion of the determined τ_{ri} values for fine sand grains from the development process of the Wilcock & Crowe hiding function results in the prediction that τ_{ri} values for these grains is based on extrapolation of the observed behavior of coarser grain classes.

When the sand content of the employed bed material was small, i.e. sediments J06 and J14, the deviations between the predictions of the equations 7.3, 7.8, 7.9 and 7.10 and the experimentally determined τ_{ri}/τ_{r50s} values became larger. For relative grain sizes $d_i/d_{50s} < 1$ the predicted τ_{ri}/τ_{r50s} values were considerably finer than the determined ones in the experiments (except from the τ_{ri}/τ_{r50s} values of fine sand). In contrast, when $d_i/d_{50s} > 1$ the predicted τ_{ri}/τ_{r50s} values were higher than the determined ones in the experiments.

Based on the above theoretical considerations and comparison between predictions and experimentally determined normalized reference shear stress, the equations 7.9 and 7.10 which are the core of the proposed hiding function were modified. In conclusion, after summarizing what has been reported in the present section, it seems that the modification is considered to be necessary because previous studies have shown that bed material with increased sand content showed a size selective behavior contrary to coarser bed material which was closer to equal mobility. Furthermore, it sounds logical that the variation of fractional reference shear stress (especially that of the fine grains) with progressive armoring when the bed surface is transformed for matrix supported to framework supported will not be identical with the observed one when a framework supported bed surface becomes coarser but still remains framework supported. Finally, the observed scatter in the data of Wilcock and his co-workers shows a systematic change of the slope of the lower limb of the hiding function with varying sand content.

The hiding function that was developed from the experimental data of the present study was modified by changing equations 7.9 and 7.10. These equations control the variation of normalized reference shear stress with progressive coarsening for each individual grain class. These equations are power functions and thus their behavior is controlled by their multiplier and their exponent. The modification's objective was that the hiding function should predict a τ_{ri}/τ_{r50s} variation with d_i which would approach equal mobility when the sand content of parent bed material decreases. Additionally, the modified hiding function should predict a smaller variation of fractional normalized reference shear stress τ_{ri}/τ_{r50s} with progressive coarsening for coarser

parent bed material. The modification was performed as follows. The relative grain size d_i/d_{50o} as well as the relative grain size d_i/d_{50s} for each individual grain class was estimated based on the d_{50o} of the parent bed material that was employed in each series of experiments of Wilcock as well as the observed degree of coarsening during each series (which remained almost invariant from run to run). The normalized reference shear stress for each grain class and the given sediment mixture were calculated by changing the exponent and multiplier as well as the relative grain size d_i/d_{50o} value in eq. 7.9 and 7.10 and subsequently by applying the new a_i and b_i values in eq. 7.8. The predicted τ_{ri}/τ_{r50s} were compared to those that were determined in the studies of Wilcock. When the fit was adequately good (for the given degree of armoring that was observed in the experiments of Wilcock) and the variation of τ_{ri}/τ_{r50s} with degree of armoring satisfied the two criteria that were above mentioned (based on the grain size composition of parent bed material), the modification procedure was stopped for that given sediment mixture. The same procedure was applied for all sediment mixtures that were employed in the studies of Wilcock and co-workers.

Fig. 7.15 shows the modified equations that give the a_i and b_i parameters which allow for a better fitting of eq. 7.8 on the experimental results of Wilcock for each sediment mixture. In addition, the same figure shows the eq. 7.8 and 7.9 (denoted as PS from present study and represented by a black solid line) which allow the estimation of the a_i and b_i values for a bed material with sand content 37 %. There is no curve for the sediment mixture BOMC because it had a sand content of 34%, which is very close to the sand content of the sediment mixture that was employed in the present study. Therefore, it was assumed that the behavior of the two sediments can be described by the same equation.
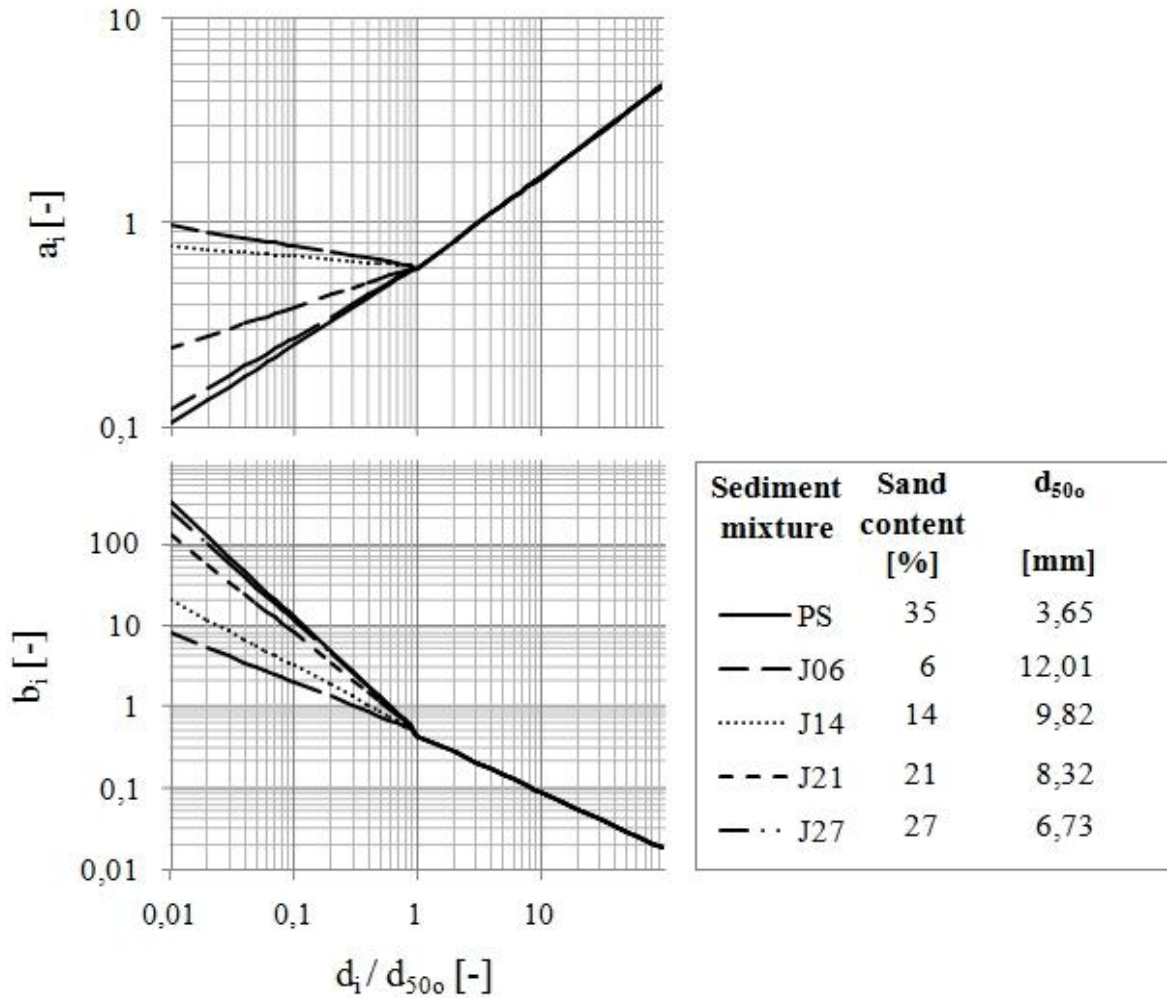
Fig. 7.15 Curves that allow for estimation of the a_i and b_i values providing the best fit of eq. 7.8 on experimental data of Wilcock and co-workers

The curves that are shown in fig. 7.15 are described by equations of the form

$$
a_i = \begin{cases} a_{1\,i} \left(\dfrac{d_i}{d_{50o}} \right)^{a_{2\,i}} & , \dfrac{d_i}{d_{50o}} \le 1 \\[3mm] a_{3\,i} \left(\dfrac{d_i}{d_{50o}} \right)^{a_{4\,i}} & , \dfrac{d_i}{d_{50o}} > 1 \end{cases}
\qquad \text{Eq. (7.11)}
$$

$$
b_i = \begin{cases} b_{1\,i} \left(\dfrac{d_i}{d_{50o}} \right)^{b_{2\,i}} & , \dfrac{d_i}{d_{50o}} \le 1 \\[3mm] b_{3\,i} \left(\dfrac{d_i}{d_{50o}} \right)^{b_{4\,i}} & , \dfrac{d_i}{d_{50o}} > 1 \end{cases}
\qquad \text{Eq. (7.12)}
$$

where: $a_{n\,i}$ and $b_{n\,i\ (n=1\text{-}4)}$ are parameters that regulate the variation of τ_{ri}/τ_{r50s} with d_i/d_s according to the value of relative grain size d_i/d_{50o}. Their value varies with sand content of parent bed material

The values of the parameters $a_{i\,1-4}$ and $b_{i\,1-4}$ that were determined with the procedure that was previously described are shown in table 7.2.

Table 7.2 Parameters $a_{i\,1-4}$ and $b_{i\,1-4}$ of fitted exponential functions that describe variation of τ_{ri}/τ_{r50s} with d_i/d_{50s} for sediment mixtures with different sand content

Sediment mixture	Sand content	$a_{i\,1}$	$a_{i\,2}$	$a_{i\,3}$	$a_{i\,4}$	$b_{i\,1}$	$b_{i\,2}$	$b_{i\,3}$	$b_{i\,4}$
	[%]	[-]	[-]	[-]	[-]	[-]	[-]	[-]	[-]
J06	6	0,61	-0,1	0,59	0,45	0,5	-1,40	0,44	-0,69
J14	14	0,61	-0,05	0,59	0,45	0,5	-0,60	0,44	-0,69
J21	21	0,61	0,20	0,59	0,45	0,5	-0,80	0,44	-0,69
J27	27	0,61	0,35	0,59	0,45	0,5	-1,20	0,44	-0,69
PS	34	0,61	0,39	0,59	0,45	0,5	-1,35	0,44	-0,69

The selected values of parameters $a_{i\,1,\,3\text{ and }4}$ as well as the value of parameters $b_{i\,1,\,3\text{ and }4}$ remained constant regardless of the sand content of the parent bed material. In contrast, parameter $a_{i\,2}$ grew with increasing sand content in parent bed material while parameter $b_{i\,2}$ decreased when the parent bed material became coarser. The variation of parameters $a_{i\,2}$ and $b_{i\,2}$ with sand content of parent bed material is shown in fig. 7.16 and could be adequately described by two sigmoid Gompertz curves which are also shown on fig. 7.16.
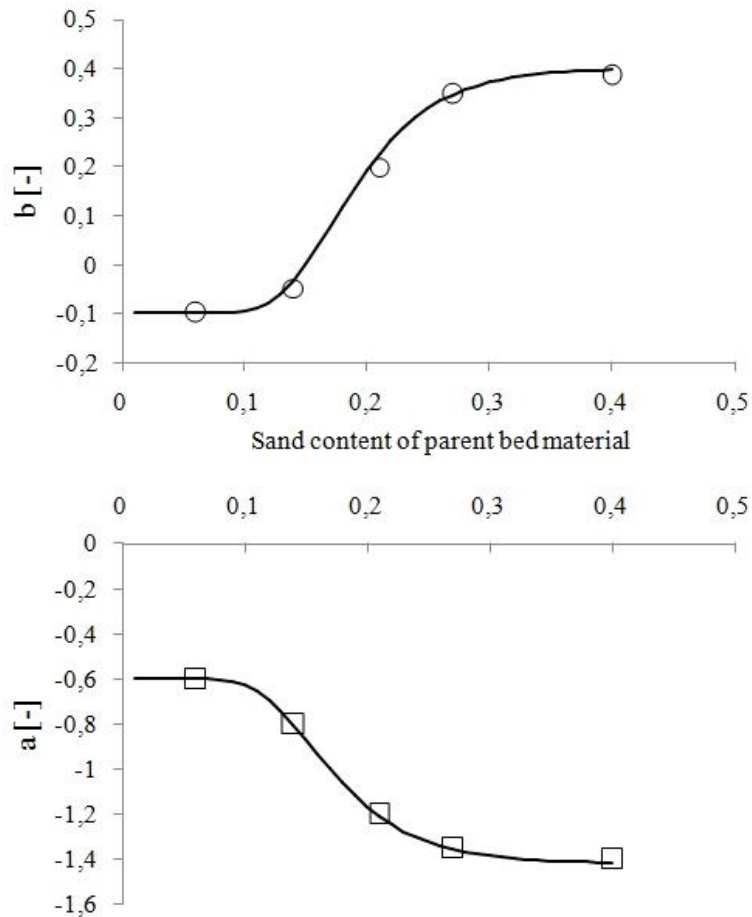
Fig. 7.16 Variation of parameters $a_{i\,2}$ and $b_{i\,2}$ with sand content of parent bed material

Thus, the parameter a_i and b_i can be calculated by equations 7.13 and 7.14 which are obtained after the above modifications.

$$a_i = \begin{cases} 0{,}61\left(\dfrac{d_i}{d_{50o}}\right)^{(-0{,}1+0{,}5\exp(-44\exp(-22\,f_{so}))} & ,\dfrac{d_i}{d_{50o}} \leq 1 \\[3mm] 0{,}59\left(\dfrac{d_i}{d_{50o}}\right)^{0{,}45} & ,\dfrac{d_i}{d_{50o}} > 1 \end{cases}$$
Eq. (7.13)

$$b_i = \begin{cases} 0{,}44\left(\dfrac{d_i}{d_{50o}}\right)^{(-0{,}6-0{,}82\exp(-30\exp(-22\,f_{so}))} & ,\dfrac{d_i}{d_{50o}} \leq 1 \\[3mm] 0{,}45\left(\dfrac{d_i}{d_{50o}}\right)^{0{,}68} & ,\dfrac{d_i}{d_{50o}} > 1 \end{cases}$$
Eq. (7.14)

where: f_{so} is the sand content of parent bed material

The complete hiding function is defined by equations 7.2, 7.3, 7.8, 7.13 and 7.14.

7.4 Similarity collapse of experimental data and $W^*_i - \tau/\tau_{ri}$ relation

The hiding function that was developed in the previous section allows the calculation of the reference shear stress of each individual grain class at different stages of bed surface armoring as well as for a wide range of different sand-gravel mixtures. In order to complete the development of a transport model, the hiding function should be incorporated in a bed-load predictor, i.e. a relation that will predict the mobility W^*_i and subsequently the bed-load discharge q_{bi} of each individual grain class as a function of fractional excess shear stress τ/τ_{ri}. This relation is found by fitting a mathematical expression on a plot that shows the variation of measured fractional mobility W*i with excess shear stress τ/τ_{ri}. This is done after an appropriate geometrical transformation of individual $W^*_i - \tau/\tau_{ri}$ curves into a single universal curve. The procedure of data reduction is called similarity collapse.

The following section presents the collapse of the experimental data that were obtained in the present study as well as those that were obtained in the investigations of Wilcock and his co-workers, - on a unique curve - when the herein developed hiding function is employed for the above mentioned geometrical transformation. Finally, a $W^*_i - \tau/\tau_{ri}$ is chosen that describes adequately the increase of W^*_i with increasing excess shear stress τ/τ_{ri}.

7.4.1 Data reduction or similarity collapse of individual $W^*_i - \tau/\tau_{ri}$ curves

Theoretically, each grain class should be characterized by a unique defined $W^*_i - \tau/\tau_{ri}$ relation. However, such a dependency of $W^*_i - \tau/\tau_{ri}$ and grain size d_i has not been found yet (although Diplas (1987) and Diplas & Shaheen (2005) have shown the existence of a systematic pattern in the data sets of Oak Creek and Proffitt). Therefore, the common approach is that all grain classes show the same variation of W^*_i with excess shear stress, i.e. the individual bed-load relations $W^*_i - \tau/\tau_{ri}$ are similar and a single curve is adequate for the prediction of W^*_i, regardless of grain size d_i as long as the data are reduced with a suitable similarity transformation. This approach is called concept of similarity collapse and was initially introduced by Ashida & Michiue (1971). It has been proved to be a useful tool in theoretical analysis and reduction of empirical data (Parker et al. (1982)).

Fig. 7.2 shows two plots of W^*_i against fractional dimensionless shear stress τ^*_i, that correspond to two different degrees of bed surface coarsening. The upper shows the determined plots of W^*_i when the bed surface is unarmored and therefore the plotted values are located higher than those shown in the lower diagram that corresponds to a degree of armoring equal to two. According to the concept of similarity collapse, the normalization of τ^*_i by the corresponding fractional dimensionless reference shear

stress τ^{*}_{ri} should result in the collapse of individual W^{*}_{i} - τ/τ_{ri} into one well defined curve. In other words, the determined values of W^{*}_{i} when plotted against the term φ_{i}, which is defined by equation 7.15 should be easily described by a single curve.

$$\varphi_i = \frac{\tau_i^*}{\tau_{ri}^*}$$

Eq. (7.15)

where: τ^{*}_{i} is dimensionless shear stress of ith grain class
         τ^{*}_{ri} is dimensionless reference shear stress of ith grain class

Eq. 7.15 is equivalent with

$$\varphi_i = \frac{\tau}{\tau_{ri}}$$

Eq. (7.16)

where: τ is exerted shear stress
         τ_{ri} is reference shear stress of ith grain class

Fig. 7.17 plots the W^{*}_{i} values that were calculated from the experimental measurements taken during the present study against the term φ_{i}, which expresses the exerted fractional excess shear stress when the herein developed hiding function is employed for the calculation of τ_{ri}. The three different geometrical symbols indicate the dimensionless transport rates that were calculated from measurements of cumulative submerged weight of transported material during experiments with different lengths of erodible bed. The collapse of the estimated W^{*}_{i} values on a well defined general trend, regardless of the length of the movable bed, supports further the thesis of hydraulic similarity among the experiments that were performed with the same discharge and different lengths of movable bed. If the exerted shear stress varied from run to run due to the length of the erodible bed and consequently of the fixed bed, a systematic pattern of grouping of the W^{*}_{i} values according to the length of the movable bed would be easily identified. The experiments were performed under low dimensionless shear stresses because the main purpose of the study was the development of a hiding function and hence transport rate measurements near the entrainment threshold were required. The transport processes in this area of exerted shear react very sensitive to changes in the exerted shear stress. Thus a considerable systematic increase or reduction of shear stress with length of fixed bed would be easily identified by a worse mixing of the experimental results on a general trend.
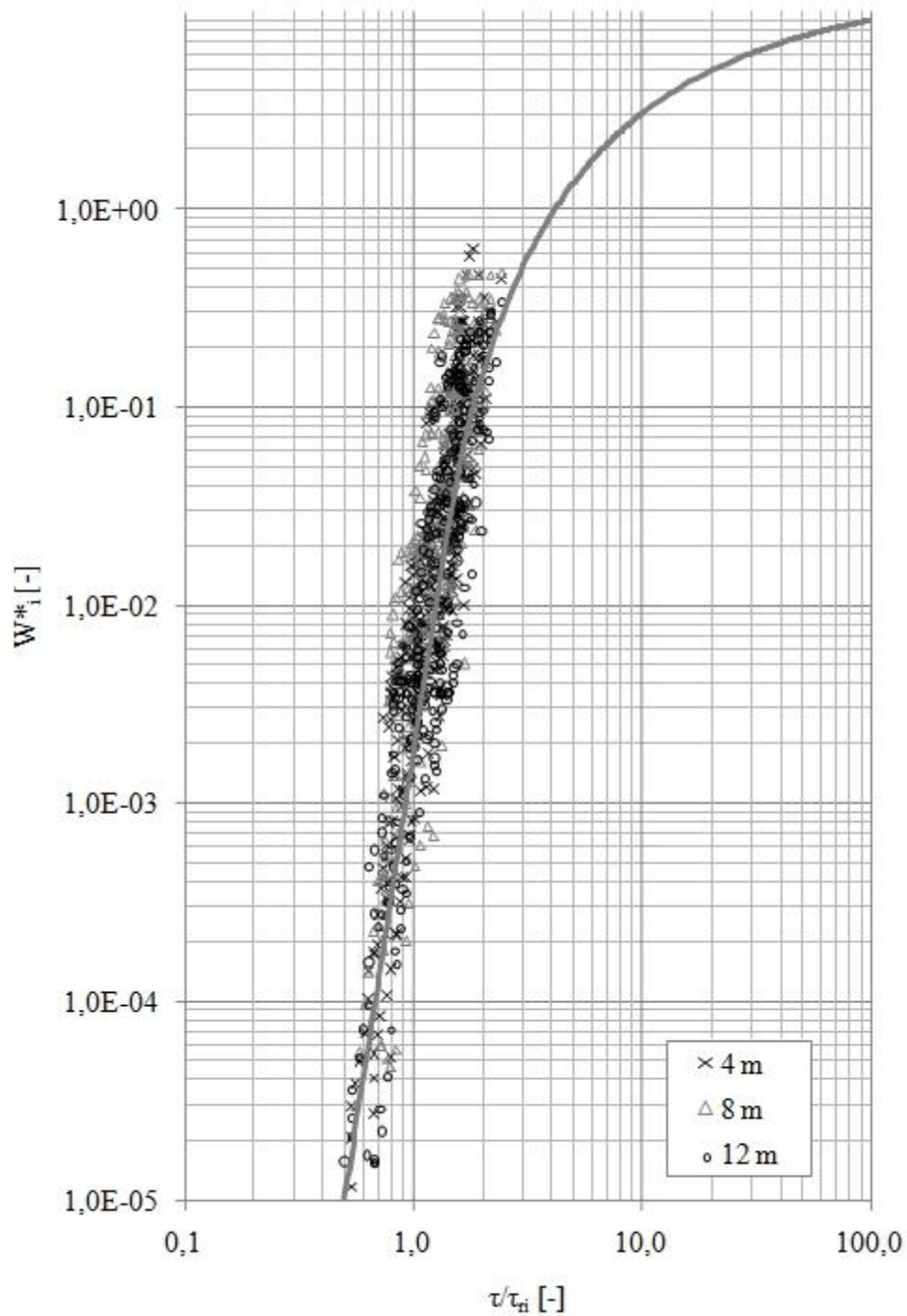
Fig. 7.17 W^{*}_{i} (determined in the present study) against τ/τ_{ri} when τ/τ_{ri} is estimated by the new hiding function

Accordingly, in fig. 7.18 the same procedure is repeated, this time for the W^{*}_{i} values that were determined from the experimental measurements in the investigations of Wilcock. The collapse of the experimentally obtained measurements is very well and a clear trend which can be described by a single similarity parameter is apparent.
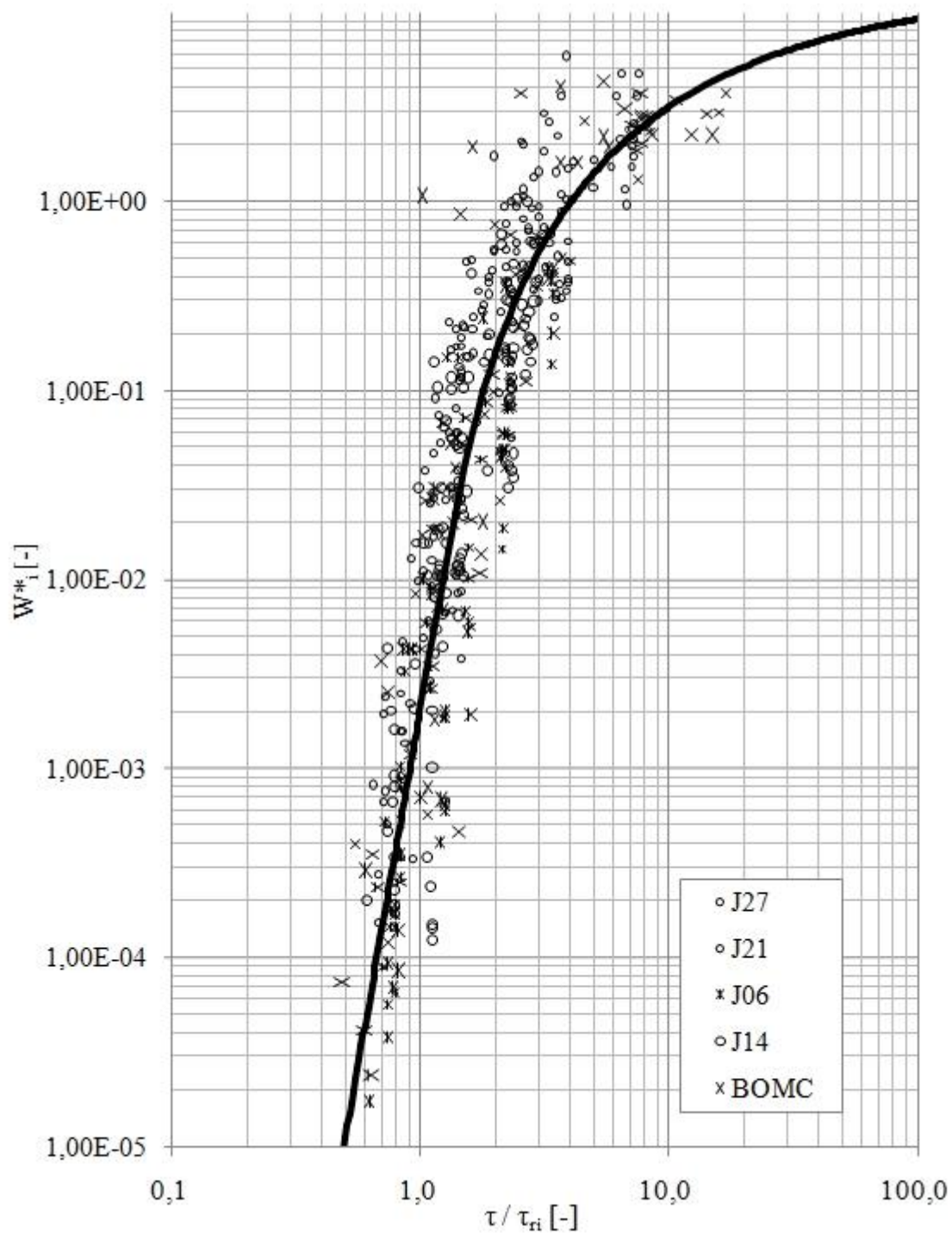
Fig. 7.18 W^*_i (determined in the investigations of Wilcock) against τ/τ_{ri} when τ_{ri} is calculated by the new hiding function

7.4.2 W^*_i - τ/τ_{ri} relation

In figures 7.17 and 7.18 the solid black line represents the transport relation that is incorporated in the transport model of Wilcock & Crowe (2003). This W^*_i - τ/τ_{ri} relation is given by

$$W_i^* = \begin{cases} 0,002\varphi_i^{7,5} & , \quad \varphi_i < 1,35 \\ 14\left(1 - \dfrac{0,894}{\varphi_i^{0,5}}\right)^{4,5} & , \quad \varphi_i \geq 1,35 \end{cases} \qquad \text{Eq. (7.17)}$$

Eq. 7.17 adequately describes the trend that characterizes the variation of determined W^*_i values with excess shear stress τ/τ_{ri}.

An additional reason for choosing this W^*_i - τ/τ_{ri} relation is that it preserves some of the form of the function that Parker (1990) used in his transport model. The objective of the present chapter was the development of a new hiding function. Thus, by using the same W^*_i - τ/τ_{ri} relation with the one that is incorporated in the transport model of Wilcock & Crowe (2003), any differences in the estimated transport rates can be attributed solely to the hiding function that each individual model employs

7.5 Comparison between predictions of the proposed transport model and experimental measurements during the present study

The transport model that was derived from the analysis of the experimental results of the present study is given by equations 7.2, 7.3, 7.8, 7.9, 7.13 and 7.14 which define the hiding function and allow the calculation of fractional reference shear stress. The excess shear stress is estimated as the ratio of exerted shear stress τ to reference shear stress τ_{ri} (eq. 7.16). The fractional mobility W^*_i is calculated from eq. 7.17. Finally, the bed-load discharge of each grain class q_{bi} is estimated by eq. 6.4. Consequently, the direct application of the model allows the prediction of fractional transport rate, providing that the imposed shear stress and the grain size distribution of bed surface as well as that of parent bed material are given.

In this section the predictive ability of the proposed model is tested against the measurements that were taken during the present study. It will be shown that the model was able to capture and reproduce all the transient changes that occurred during the progressive coarsening of bed surface, which finally leads to the formation of a static armor layer. The results that are herein presented regard the temporal and spatial

variation of total transport rate, fractional grain mobility and grain size distribution of transported material.

This comparison is required because the hiding function that is incorporated in the model was developed initially from the data of the present experimental study. Subsequently, however was modified in order to fit better the experimental data of Wilcock et al. (2001). This action was necessary because the experiments herein presented were performed with only one parent bed material. The comparison between model prediction and part of the measurements that were used for its derivation will demonstrate that it's predictive ability was not affected by the modification that followed the initial mathematical expression.

7.5.1 Comparison between predicted and measured total bedload discharge q_{bT}

The total transport rate that was predicted from the proposed transport model against the measured total transport rate is plotted in fig.7.19. For each experiment the total transport rate was calculated at 20 different time points and was compared with the corresponding measured value of total transport rate. Each circle represents a predicted/measured value of the total transport rate for a given time point, the imposed flow strength and the location. Thus, the total count of the plotted points is 20 x 5 x 3 = 300 predictions against measurements..
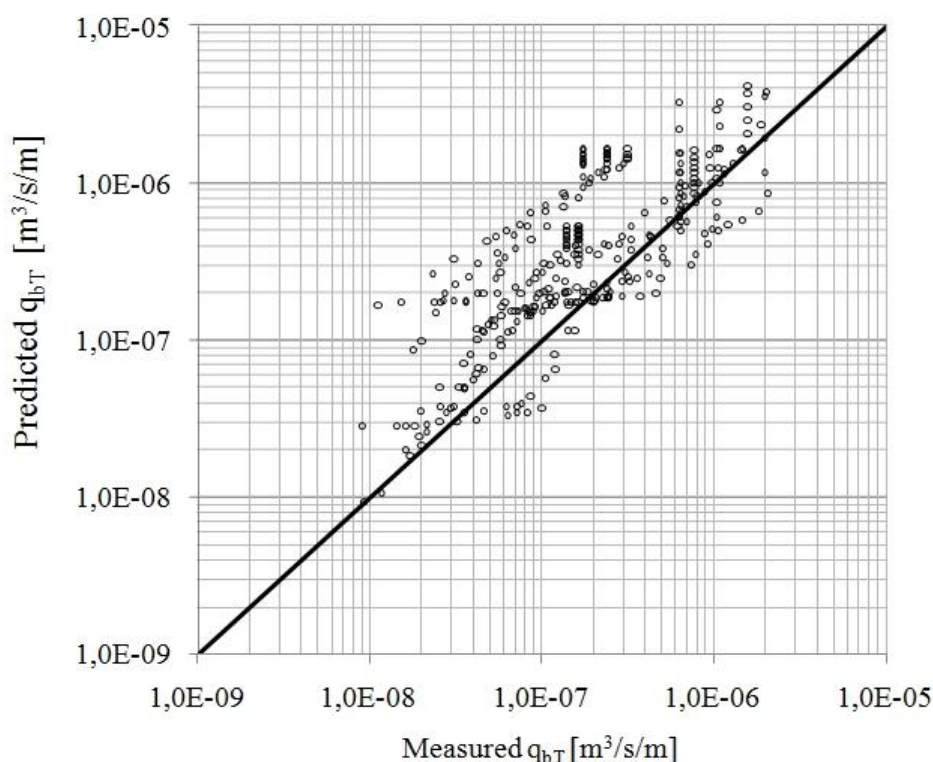
Fig. 7.19 Comparison between predicted by the proposed transport model and measured during the experiments total transport rate q_{bT}.

In the same figure the solid black line represents the line of perfect agreement between measurements and predictions.

The agreement between model predictions and experimental measurements is very harmonic except for the predictions for the experiments that were performed with flow discharge 70 l/s. In that case, the predicted total transport rates were slightly larger than the measured. This deviation causes the observed scatter in fig. 7.19 which can be attributed to erroneous estimation of shear stress or grain size distribution of bed surface. Nonetheless, it does not affect the overall trend, which shows that the proposed model was able to accurately predict the total transport rate that was observed during the experimental runs, at different time intervals from the experiment initiation and the locations along the flume.

Fig. 7.20 shows the temporal variation of total transport as predicted during experiments with three different water discharges (70, 100 and 150 l/s) at three different measuring stations downstream of the flume inlet (4, 8 and 12 m respectively). The proposed model was able to reproduce the observed temporal variation of the total transport rate with two distinct phases. In the early stages the predicted bed-load discharge showed invariance with time and when this phase was over the transport rate started to consistently, decline with time. The first phase is characterized by a shorter duration when the imposed flow strength is increased, something that is in accordance with the experimental observation. Furthermore, the reduction of the transport rate in the second phase does not show any considerable dependence on the imposed flow strength.

However, the pattern of transport rate reduction was disturbed when the measured bed surface grain size distribution stopped to coarsen in the late experimental stages. This shows that either a small variation in the grain size distribution of bed surface - which is very difficult to be documented with the current know how - or the reorientation of large particles and packing in more stable structures with progressing time (see Haynes and Pender (2006)) affects the bed stability significantly and thus the observed transport rate. It can be assumed that a reduction of the fine sand content in bed surface when the latter is already coarse enough will cause a very small increase of the median grain size of the bed surface but at the same time might considerably affect the stability of the large particles. The stability of large particles when the bed surface is armored depends on the dimensions of the interstices between grains. A reduction of the fines content might significantly affect the dimensions of these interstices among large particles and thus the stability and consequently the transport rate of coarse grain fractions.
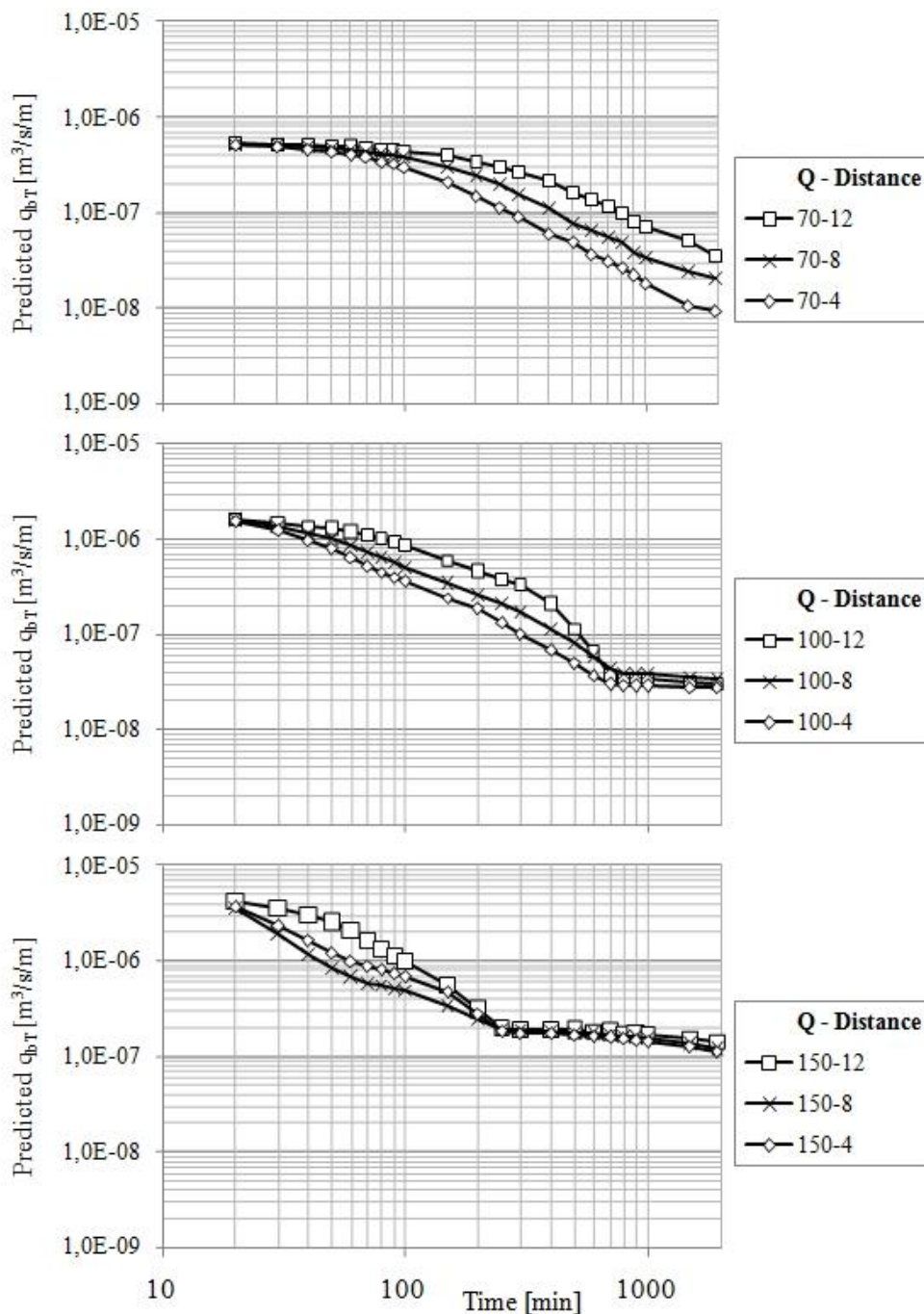
Fig. 7.20 Predicted spatial variation of total transport rate for three different water discharges.

Finally, the model was able to reproduce the observed spatial variation of transport rate. The predicted transport rates at the same time interval after experiment beginning showed a consistent increase with distance from the flume inlet. The difference among predicted transport rates at different locations is small in the early experimental stages and with time increases. Thus, the pattern of spatial variation of total transport rate that was observed during experiments of the present study (see fig. 6.8) is adequately reproduced for low shear stress values and not so satisfying for high exerted shear forces.

7.5.2 Comparison between predicted and measured fractional dimensionless transport rate W^*_i

The good performance of the proposed model is verified by the results of the comparison between predicted and measured fractional dimensionless transport rates, which is shown in fig. 7.21. The values of W^*_i that were determined from measurements of the fractional content in bed surface F_i andt he fractional transport rate $q_{bi,}$ which was taken at 20 different time points during the five experiments that were performed with different water discharges and movable bed length of 12 m, are plotted in this figure. Thus, each individual point on fig. 7.21 represents the determined value (either predicted or measured) of W^*_i for a given time point and the exerted flow strength 12 m downstream from the flume inlet. In the same figure, the solid black line represents the line of the perfect agreement between experimental measurements and model predictions.
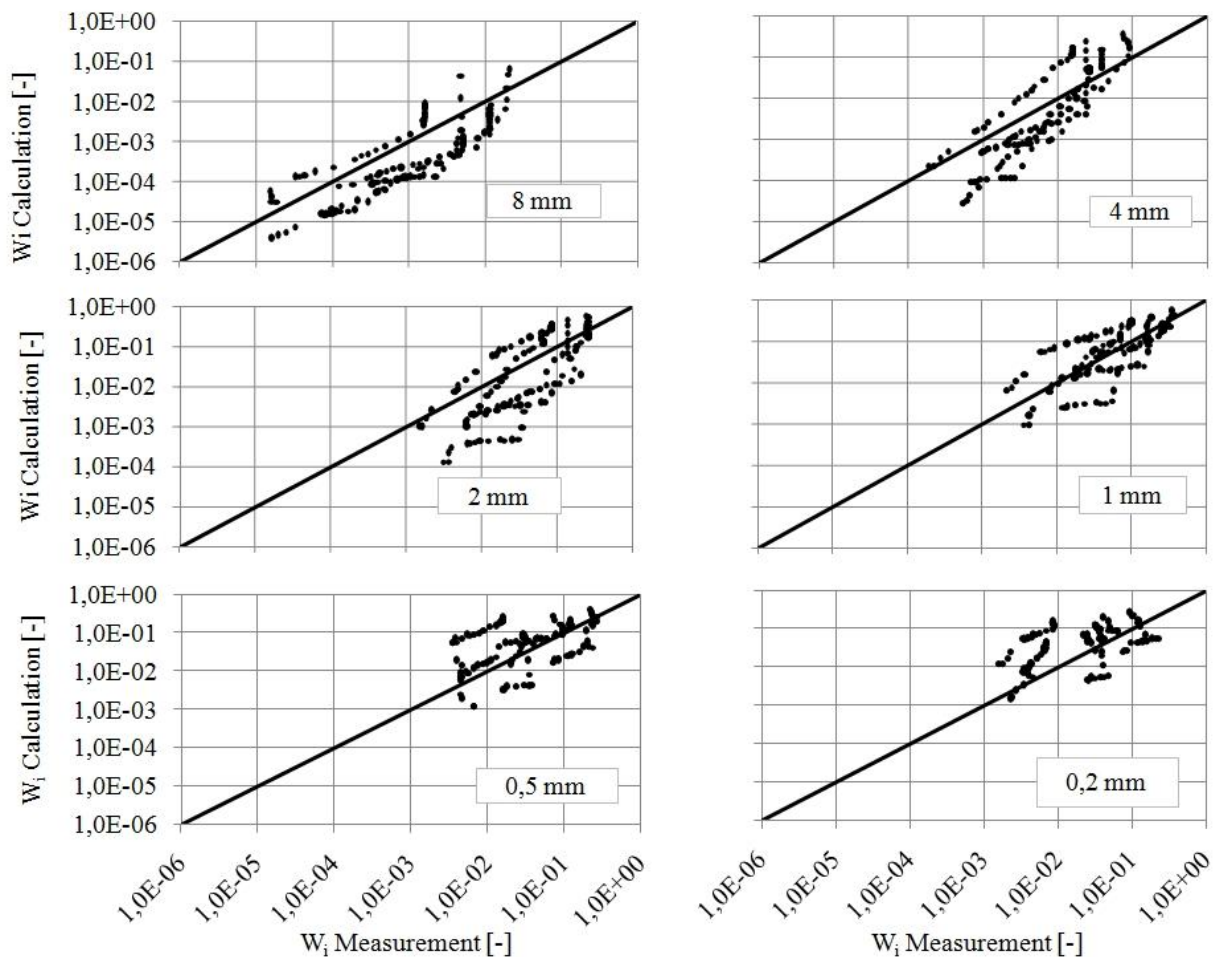
Fig. 7.21 Comparison between predicted and determined from experimental results values of dimensionless transport rater W^*_i for all grain classes (movable bed length 12 m).

Fig. 7.21 shows that the agreement between the predictions and the measurements is valid for all grain classes that were contained in the employed sediment mixture. This shows that the good performance of the model regarding the total transport rate was not a coincidence. It proves that the individual fractional transport rates of all grain classes were predicted with accuracy. Thus, the sum of the correctly predicted fractional transport rates led to the correct prediction of total transport rate.

It must be noted that the model appears to slightly underpredict the grain mobility of the three coarser grain classes. However, the overall agreement between predictions and measurements remains adequate.

The fine agreement between the experimental measurements and the model predictions is further illustrated in fig. 7.22. This figure shows the variation of fractional dimensionless transport rate W^*_i with absolute grain size d_i at different time points during the experiment that was performed with movable bed length of 4 m and flow discharge of 100 l/s. The $W^*_i - d_i$ distribution was transformed with progressing time and hence bed surface coarsening accordingly to the pattern that was observed experimentally and is described in section 6.7.1. This is verified from the obvious similarity between fig. 7.22 and fig. 6.21.
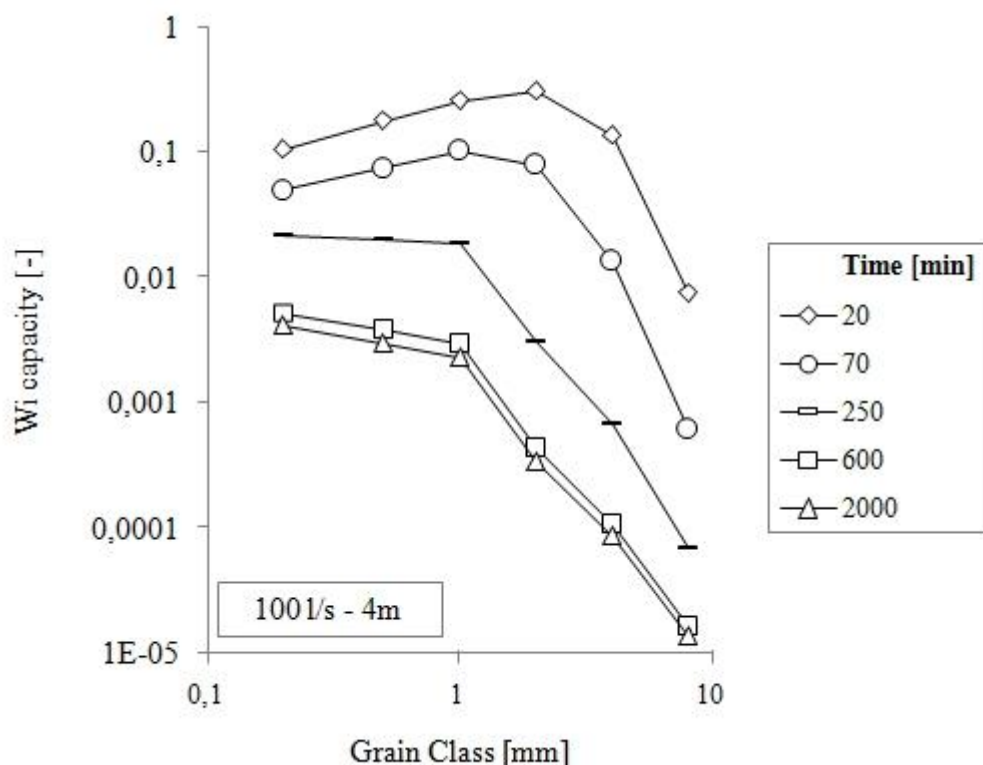
Fig. 7.22 Variation of dimensionless fractional transport rate W^*_i with progressing time as predicted by the proposed transport model for the experimental run performed with water discharge of 100 l/s and flume length of 4 m

7.5.3   Comparison between predicted and measured median grain size of transported material d_{50tr}

The upper diagram in fig. 7.23 shows the values of median grain size of transported material that were determined by sieve analysis of samples of eroded material taken at different time points during the five experiments which were conducted by using different water discharge that movable bed length of 12 m. The lower diagram of the same figure shows the median grain size of transported material that was predicted by the proposed model when the appropriate, i.e. the one measured at the given time point, grain size distribution of bed surface and exerted shear stress was used as input data.
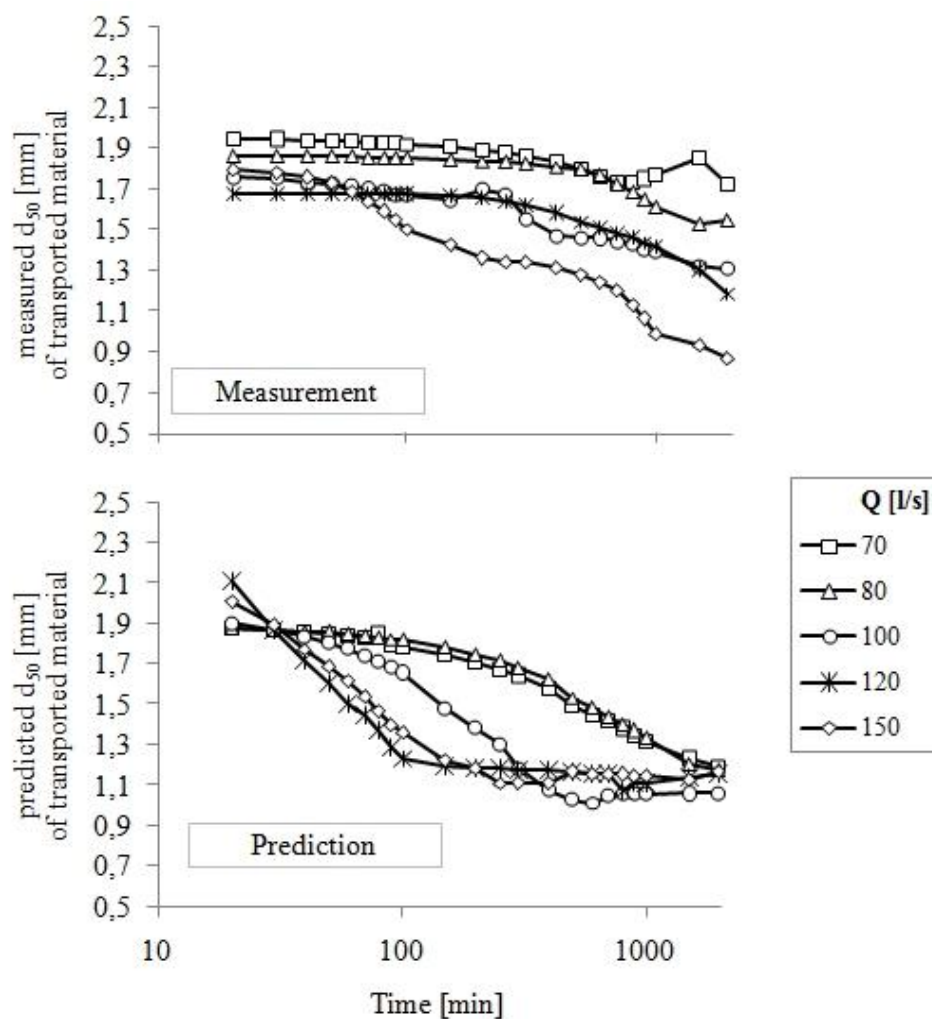
Fig. 7.23 Comparison between predicted and measured temporal variation of median grain size of transported material. (movable bed length 12 m).

The comparison of the two diagrams shows that the model was able to reproduce the observed fining of transported material. Furthermore, the reduction of the predicted d_{50} of transported material was smaller when the exerted flow strength was reduced, something that is in agreement with the experimental observations. Finally, the

calculated d_{50} of transported material varied within a range from 2,1 mm to 1,1 mm which is in very good agreement with the observed variation that lied between 2,0 mm and 0,9 mm.

Fig. 7.23 shows that the model predicted a considerably faster reduction of the median grain size of the transported material than the one observed during the experiments. The measured d_{50} of transported material showed a continuous reduction even when the d_{50} of bed surface stopped increasing, while the proposed model predicted a bedload discharge of constant grain size distribution when the bed surface had reached its maximum degree of coarsening under a given exerted flow strength. Furthermore, the model predicts a larger reduction of the median grain size of bedload than the one observed, especially when the flow strength is reduced.

The correct prediction of the bedload gradation depends on an efficient estimation of fractional transport rates q_{bi}. The calculation of the latter is based on the exerted shear stress τ, the fractional reference shear stresses τ_{ri} and the fractional content of each individual grain class in bed surface F_i. In chapter 6.2 was shown that the exerted flow strength remained invariant throughout each individual experiment due to the observed parallel bed degradation and the regulation of the downstream hydraulic boundary conditions, which kept the water depth constant. Thus, the proposed model reproduced the temporal variation of the fractional transport rates and consequently of the bedload gradation by adjusting the fractional reference shear stresses to the progressive coarsening of bed surface. The hiding function that is responsible for the estimation of fractional reference shear stresses utilizes the parameters d_{50s}, d_{50o} and the exerted shear stress τ. The median grain size of the parent bed material d_{50o} and the shear stress was the same throughout the experiments and thus cannot affect the predicted temporal variation of bedload d_{50}. Hence, the bed surface grain size distribution is the parameter that controls the variation of the predicted fractional transport rates and consequently the predicted bedload gradation when the bed surface becomes coarser and the shear stress remains constant.

The deviation between predicted and measured temporal variation of bedload composition is caused by the quality of the bed surface gradation data that were used for the development of the proposed model. The root of the problem is probably errors in the determination of bed surface grain size distribution as well as by changes in the bed surface gradation which either could not be detected by the applied image analysis method or are not taken into account by the statistical parameter of median grain size that is involved in the herein developed hiding function. For example a small variation of the content of fines in the bed surface is very difficult to be detected by means of image analysis and at the same time even if it is detected it might not influence essentially the median grain size d_{50} rather smaller characteristic grain sizes like the diameter d_{16}. However such a small change in the content of fines might affect

considerably the bed stability and consequently control the grain size distribution of the transported material. This case will be a possible shortcoming of the proposed model.

Despite the deviation between the predicted and measured temporal variation of bedload median grain size, the proposed model was able to capture and reproduce the essential transient changes in the composition of the transported bed material, i.e. the process of fining and the range within which the median grain size of bedload varied. The correct qualitatively and to a large extent quantitatively prediction of the observed transient changes in the bedload gradation is significant because older surface based transport models were not able to yield predictions of the same accuracy under the given hydraulic and sedimentological boundary conditions.

Hunziker (1995) simulated the experimental run I/5 that was conducted by Gessler. The investigation of Gessler focused on the entrainment threshold of sediment mixtures and involved experiments that employed the same configuration as the one of the present study. Hunziker reports that he had to employ the equation of Iwagaki (1956) for the estimation of the critical dimensionless shear stress, modifying thus the hiding function of his model, in order to achieve a good agreement between predicted and measured bed surface gradation. Furthermore the simulation reproduced rotational erosion instead of parallel bed degradation that is reported by Gessler.

The model of Wilcock & Crowe (2003) was also not able to reproduce the observed fining of bedload when the bed surface became progressively coarser. Fig. 7.24 shows the temporal variation of mean grain size of transported material as predicted by the model of Wilcock & Crowe (2003) for five different water discharges and length of movable bed 12m.
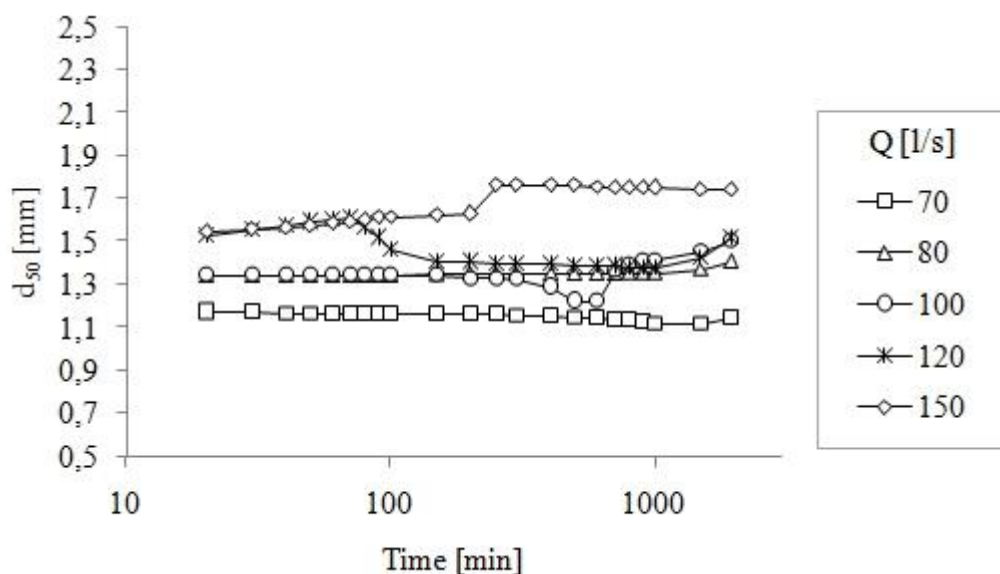

Fig. 7.24 Predicted temporal variation of median grain size of transported material by model Wilcock & Crowe (2003).

Fig. 7.24 shows that the model of Wilcock & Crowe predicted that the median grain size of transported material will not change over time or even it will become slightly coarser as time progresses and consequently the bed surface becomes coarser. Furthermore the predicted transport median grain size increased with increasing flow strength. Thus the model fails to reproduce the observations regarding the temporal variation of bedload grain size even qualitatively.

7.6   Chapter summary

- The fractional reference shear stress at different stages of bed surface coarsening was estimated by employing the method that is described by Parker et al. (1982a) and was followed also by Wilcock & Crowe (2003).

- The estimated values of fractional reference shear stress revealed a variation pattern with progressive coarsening that was very close to the one that was based on analysis of the observed transient changes in fractional mobility during the individual experimental runs, which however was not quantified.

- The appropriate mathematical transformations allowed for a collapse of the individual fractional distributions of reference shear stress at different stages of the under investigation phenomenon.

- The discussion on the structure of the already published hiding functions that are incorporated in previous surface based transport models showed that the herein documented variation pattern of reference shear stress could not be reproduced by a hiding function of the classical form (based only on the associated with median grain size of bed surface d_{50s} relative grain size d_i/d_{50s}).

- The mathematical expression that was employed for the description of the observed τ_{ri} variation during the formation procedure of a finally static armor layer incorporated implicitly the degree of armoring d_{50s}/d_{50o} by taking into account additionally the associated with the median grain size of parent bed material d_{50o} relative grain size d_i/d_{50o}.

- The mathematical expression that was derived from the data set which was obtained during the present study was modified in order to be applied also for different types of sediment mixtures.

- The concept of the modification was based on theoretical considerations and was accomplished with use of the data set that was published by Wilcock et al. (2001).

- The estimation of excess shear stress τ/τ_{ri} with application of the proposed hiding function for the estimation of τ_{ri} resulted in a consistent collapse of estimated fractional mobility values, for both employed data sets, in a data cloud with a clearly defined trend.

- This trend was adequately described by the $W^{*}_{i} - \tau/\tau_{ri}$ that is incorporated in the transport model of Wilcock & Crowe (2003).

- The proposed transport model was tested against the data that were used for its derivation. The comparison between measurements and predictions showed that the model is able to capture with satisfactory accuracy all the transient changes in bed-load transport rate and composition during the gradual formation of a finally static armor layer.

8. Validation of proposed transport model

8.1 Comparison with experimental results of Curran & Wilcock (2005)

Almost all investigations in sediment feed flumes were conducted with sediment supply that had the same composition with the sub-surface bed material. However, it is recognized that the bed-load can be finer than the sub-surface bed material. Curran & Wilcock (2005) published experimental results from a study during which the feed transport rate became progressively finer and larger from run to run.

8.1.1 Description of experimental conditions and results

The experiments were performed with the same water discharge, which was approximately 47 l/s. They consisted of two segments. In the first segment that lasted at least 80 minutes, the sediment feed was identical to the parent bed material. As soon as the system achieved a steady state, indicated by stable transport rate equal to the feed rate, the second experimental segment began. During the second part of the experiments the gravel feed rate was held constant at 112 g/s m while the sand feed rate was increased from run to run, ranging between 54 and 684 g/s m (in the first segment the sand feed rate was 18 g/s m). The experimental conditions are given in table 8.1

Table 8.1   Experimental conditions in the study of Curran & Wilcock (2005)

Run	Water discharge	Sand feed rate	Gravel feed rate	Total feed rate	% Sand in feed	d_{50} transport	d_{50} bed sub-surface
	(m^3/sm)	(gr/sm)	(gr/sm)	(gr/sm)	(%)	(mm)	(mm)
6	0,0465	180	112	292	62	1,53	
7	0,0470	94	112	206	46	4,90	
8	0,0481	284	112	396	72	1,29	
9	0,0465	258	112	360	70	1,34	17,09
10	0,0465	803	0	803	100	0,95	
11	0,0470	684	112	796	86	1,08	
12	0,0470	36	224	260	14	17,09	

The second experimental segment was stopped as soon as a new equilibrium had been established, indicated again by a stable transport rate equal with the feed rate.

The results of the study are summarized in table 8.2. Curran & Wilcock (2005) and Curran (2007) did not publish the grain size distributions of bed surface that was measured in the experiments. They rather provided the sand content only, as well as the composition of sand and gravel material used for creation of the sand-gravel mixture initially placed in the flume. Thus, the median grain size that is shown in table 8.2 was calculated by the given data. Despite the increase in total transport rate, the channel did not respond by trying to increase its transport capacity through aggradation and the associated increase of bed slope. This is what the classical approach of Lane 1955 demands, considering that the water discharge was held constant from run. Contrary, as the sediment feed median grain size became smaller, the channel bed degraded and the slope was reduced although the transport rate increased. Furthermore the bed surface became finer as the sand content in bed-load increased. This response can be attributed only to the progressive reduction of the bed-load grain size. The observed response of the bed to different feed conditions is shown in fig. 8.1
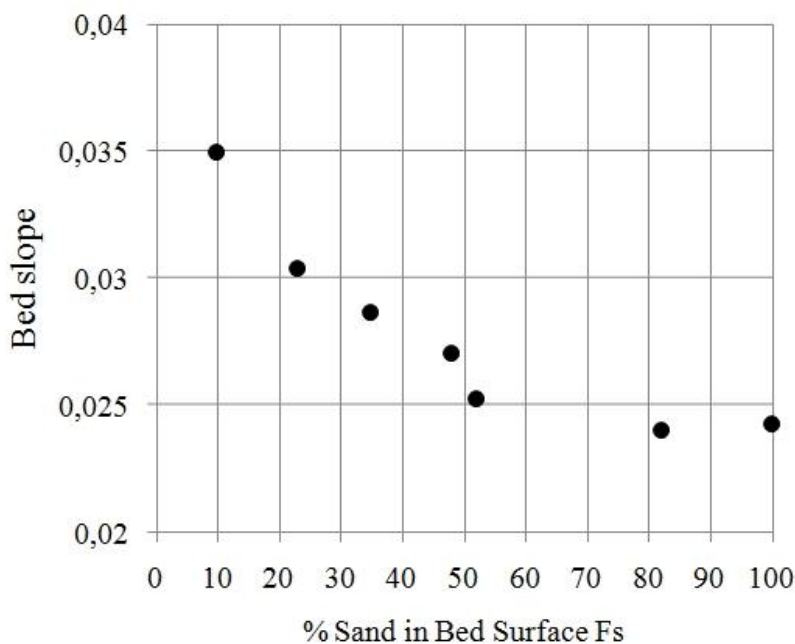
Fig. 8.1 Reduction of bed slope with increase in sand content of bed surface as it was observed in experiments of Curran & Wilcock (2005). The increase in sand content of bed surface is associated with reduced feed grain size and increased feed rate.

Based on these results, Curran & Wilcock (2005) arrived at the conclusion that an increase in sand content either in bed surface or in sediment supply renders the gravel fractions more mobile. The same gravel transport rate was transported by lower shear

stress, provided that the sand content increased. This finding was in good agreement with previous investigations performed under different boundary conditions, e.g. Ikeda & Iseya (1988) and Jackson & Beschta (1983).

Table 8.2   Experimental results in the study of Curran & Wilcock (2005)

Run	Established equilibrium bed slope	Wall-corrected shear stress	Proportion of sand in bed surface	d_{50} bed surface
	(-)	(Pa)	(%)	(mm)
6	0,0287	17,88	35	12,51
7	0,0304	19,00	23	16,01
8	0,0252	14,31	52	1,9
9	0,0271	15,90	48	3,69
10	0,0243	12,95	98	0,97
11	0,0240	12,41	82	1,13
12	0,0350	20,50	10	17,51

8.1.2   Comparison between predictions of the suggested model and experimental results

The transport model that is proposed in the present study was tested against the results of the experimental investigation of Curran & Wilcock (2005). The measured equilibrium bed slope and observed grain size distribution of bed surface were used as input data and the total bed-load transport rate and grain size distribution of transported material were computed by applying the herein developed model. The comparison between model predictions and experimental measurements is presented herein.

Fig. 8.2 shows the comparison between predicted and measured total, sand and gravel transport rates. A good agreement between model estimations and measurements is apparent. The total transport rate, represented by solid circles in fig. 8.2, was slightly overestimated by the model. The predicted sand transport rates were slightly smaller than the measured for low sand feed rates. Contrary, they were larger than the measured at high sand feed rates. The gravel transport rates were above the line of perfect agreement with one exception which was observed at the experiment with the

highest feed sand content of 86 % and accordingly the highest bed surface sand content (82 %).
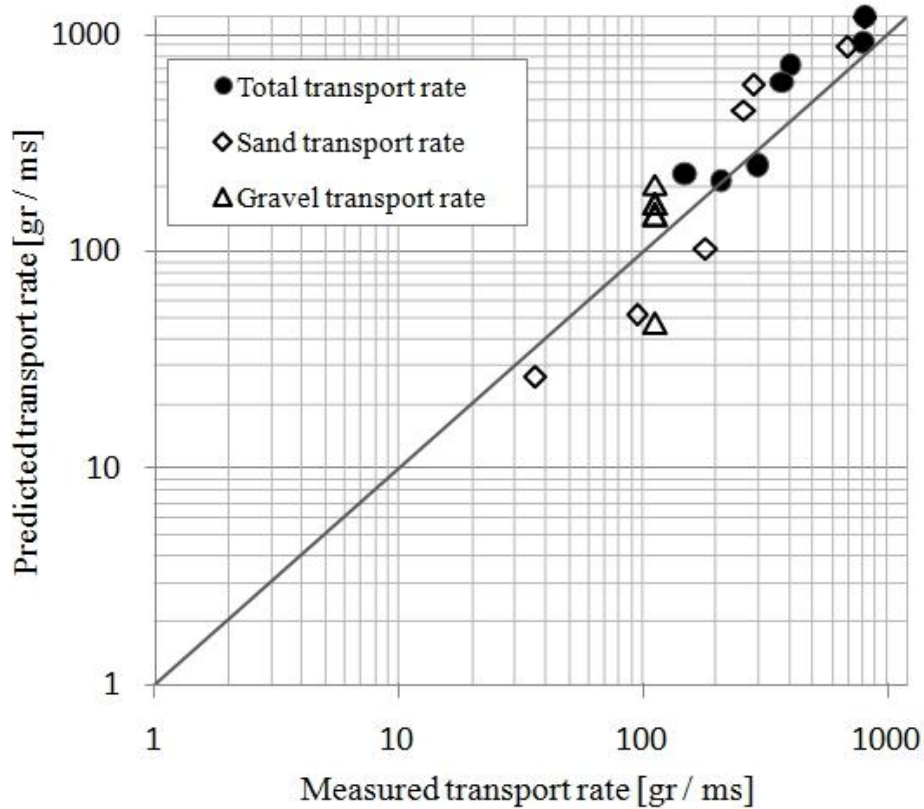
Fig. 8.2 Comparison between predicted and measured total, sand and gravel transport rates

The measured and predicted total, sand and gravel transport rates against the shear stress that was exerted when the equilibrium condition had been established at the end of the second segment of the experiments is shown in fig. 8.3 a-c. The model was able to capture all the observed trends of variation of transport rate with flow strength. The predicted sum of the transport rates of the fractions belonging to the sand size range increased as the bed slope and consequently the exerted shear stress decreased. Simultaneously, the predicted gravel transported rates showed a very small variation with flow strength, except the extreme case of very high sand content in the sediment feed. Even in that case the predicted gravel transport rate of 46 gr / s m was close to the measured gravel transport rate of 112 gr / s m.
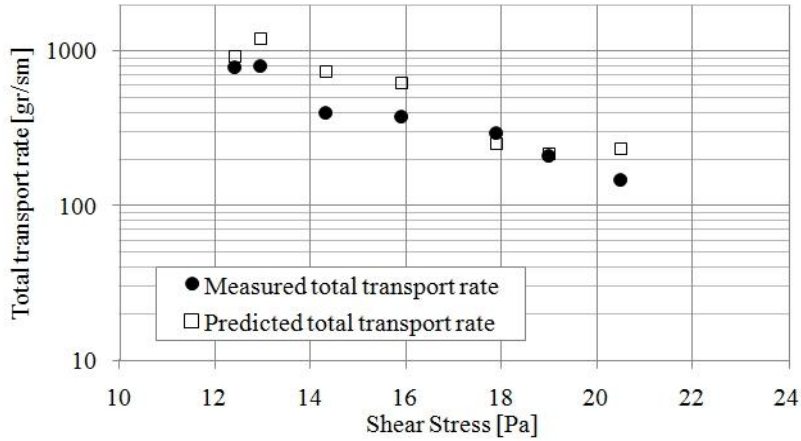
Fig. 8.3a Variation of predicted and measured total transport rates with shear stress
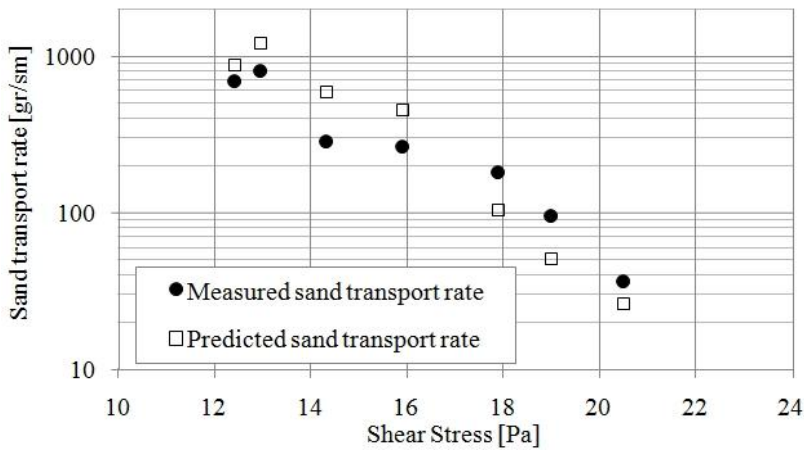
Fig. 8.3b Variation of predicted and measured sand transport rates with shear stress
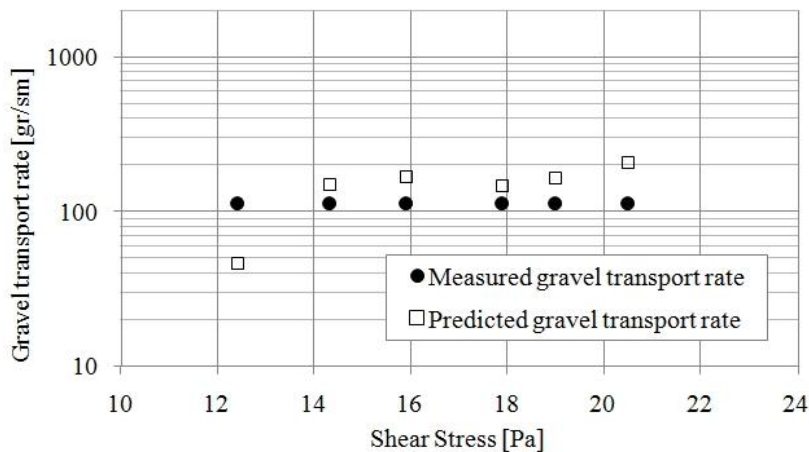
Fig. 8.3c Variation of predicted and measured gravel transport rates with shear stress

Thus, the model was able to reproduce the main experimental result that the same gravel amount may be transported even under lower shear stress, as long as the sand content of bed surface increases.

The median grain size of transported material observed in the experiments, as well as the median grain size of bed-load predicted from the model against the sand content of bed surface are plotted in fig. 8.4. The suggested model was able to reproduce sufficiently the observed decrease in the grain size of transported material with increased sand content of bed surface accurately.
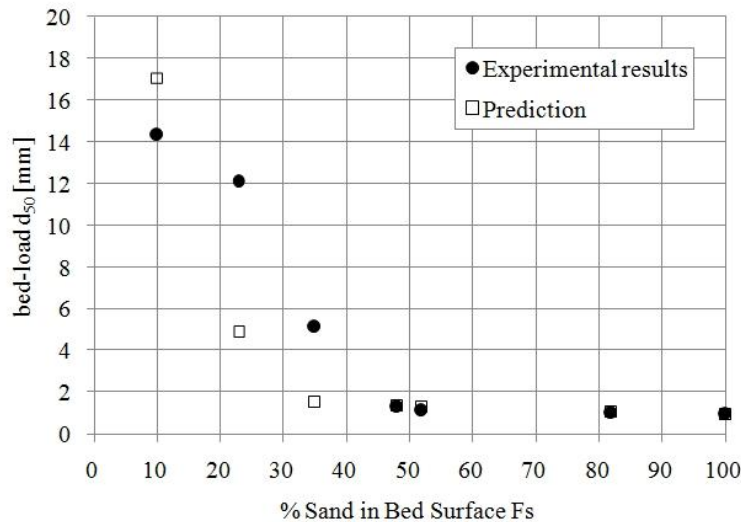
Fig. 8.4   Comparison between predicted and measured median grain size of bed-load, for different sand contents of bed surface

8.2   Comparison with experimental results of Dietrich et al. (1989)

8.2.1   Description of experimental conditions and results

Dietrich et al. 1989 presented the results of three experiments in order to support the hypothesis that bed surface coarsening is the response of a gravel-bed river system when the sediment supply from upstream is less than the ability of the flow to transport that load. The experiments were performed in a 7,5 m long and 0,3 m wide flume. Sediment was fed at the flume inlet by hand or conveyor belt at rates that varied from run to run and were progressively reduced from 29 gr /s m in the first run to 10,2 gr / s m in the second and 1,2 gr / s m in the third experimental run. The water discharge was kept constant in the three experimental runs (60 l/s m). Bed and water surface slope as well as bed surface texture were free to adjust to a new equilibrium for each value of imposed sediment loading. The experimental conditions, as well as the experimental results are summarized in table 8.3. The grain size distribution of the parent bed material and the sediment supply were almost identical and are shown in fig. 8.5. In the same figure the median grain size of bed surface d_{50s} that was determined at the end of each experimental run is shown.

Table 8.3   Experimental conditions and results in the study of Dietrich et al. (1989)

Run	Sediment feed rate	d_{50} sediment feed	d_{50} initial bed	Established equilibrium bed slope	Shear stress	d_{50} bed surface
	(gr / s m)	(mm)	(mm)	(-)	(Pa)	(mm)
1	29,0			0,0052	5,2	3,7
2	10,2	3,6	4,15	0,0046	4,7	4,3
3	2,9			0,0035	3,9	4,8

The experiments of Dietrich et al. (1989) showed that when the grain size distribution of the sediment feed remains constant and is almost the same with the grain size distribution of the sub-surface material, then an increase of transport is associated with an increase of the bed slope and a reduction of the bed surface grain size. The median grain size of the bed surface approaches that of the sub-surface material at high transport rates, while at low bed-load transport rates the bed surface is coarser than the sub-surface bed material. The degree of coarsening increases with decreasing transport rate.
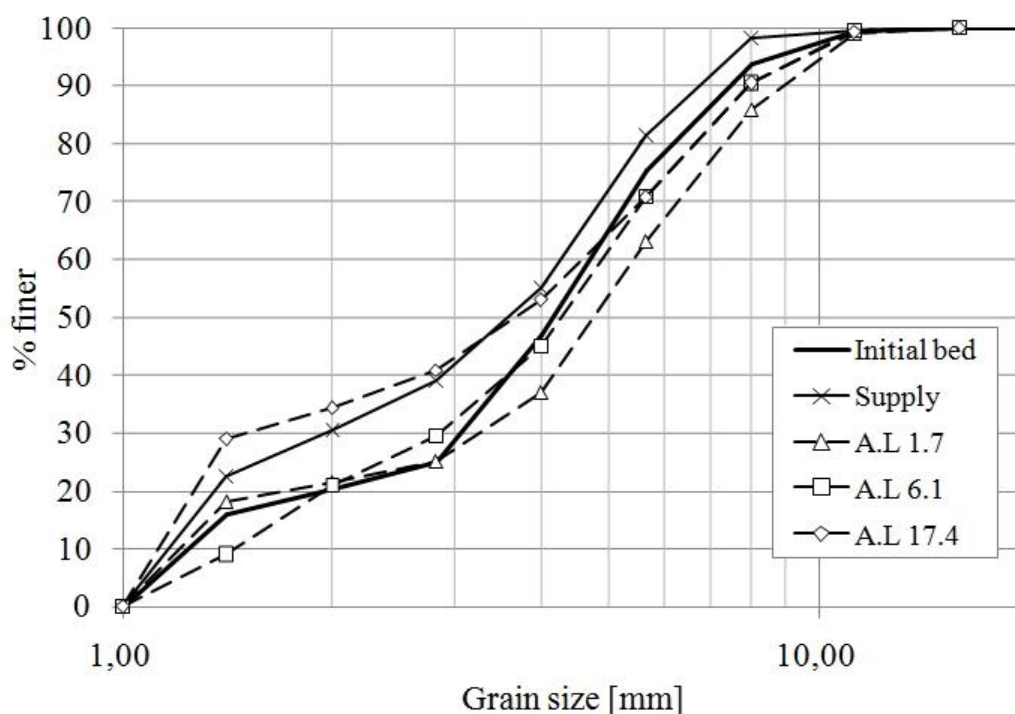
Fig. 8.5   Grain size distribution of parent bed material, sediment supply and bed surface at the end of each individual experimental run in the investigation of Dietrich et al. (1989)

8.2.2 Comparison between predictions of the suggested model and experimental results of Dietrich et al. (1989)

The predictive ability of the proposed transport model was tested by comparing the experimental results of Dietrich et al. (1989) with the predictions of the model regarding the total transport rates and the grain size distribution of the transported material. The predicted as well as the measured total transport rates are plotted in fig. 8.6 against the observed median grain size of bed surface in the three experimental runs of the investigation of Dietrich. The agreement between predicted and measured transport rates is very good. This shows that the model is able to reproduce the observed reduction in transport rate with bed surface coarsening and reduction in exerted flow strength.
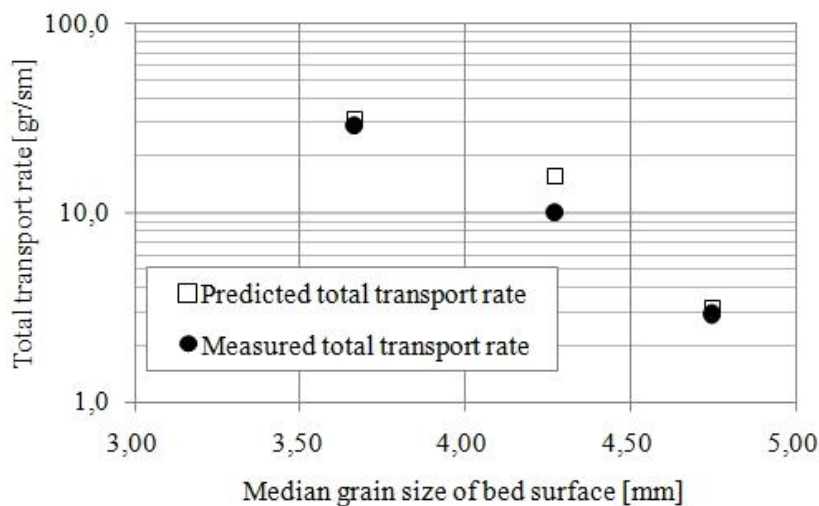
Fig. 8.6   Comparison between measured and predicted total transport rates in the experiments of Dietrich et al. (1989)

Fig. 8.7 shows the predicted fractional transport rates q_{bi} as well as the fractional transport rates that were measured during the experiments of Dietrich et al. (1989). The predicted fractional transport rates generally followed the trend that characterized the variation of measured fractional transport rates with grain size d_i. Exception was the prediction of q_{bi} for grains with size smaller than 4 mm in the second experimental run. The predicted fractional transport rates of these grain classes showed a considerable smaller variation with grain size than the observed fractional transport rates. A possible reason for this deviation might be an erroneous estimation of the fractional content of these grain sizes. This argument is supported by the observation that the deviation occurs in the second run while in the first and third the model is able to predict the variation of q_{bi} with d_i adequately.
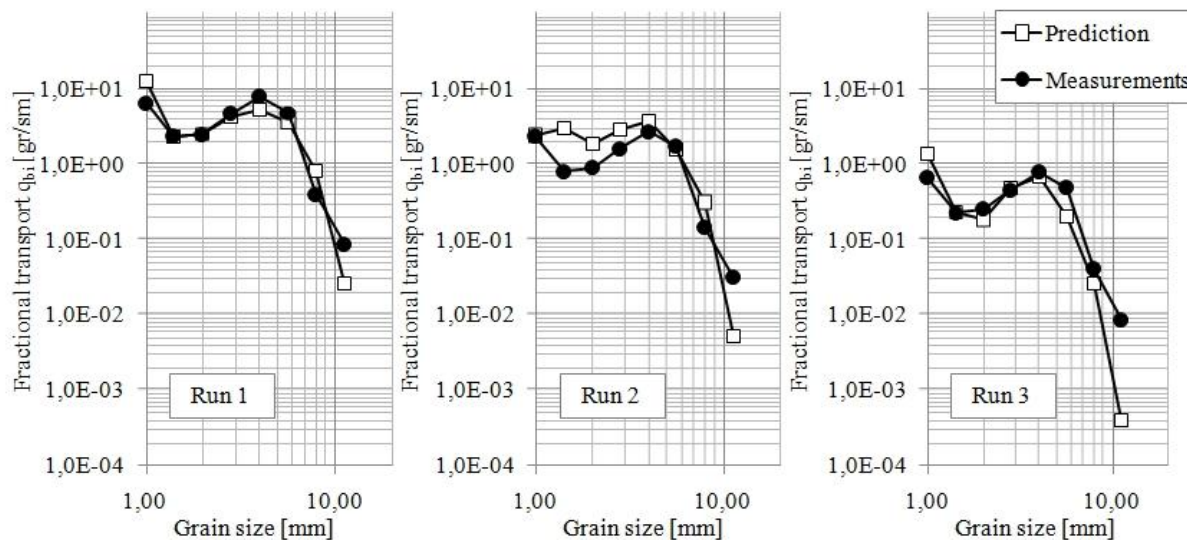
Fig. 8.7   Comparison between measured and predicted fractional transport rates q_{bi} in the experiments of Dietrich et al. (1989)

Furthermore, the proposed transport model slightly over predicted the fractional transport rates of fine grain classes ($d_i < 4$ mm) and in accordance under predicted the fractional transport rates of coarse grain classes ($d_i \geq 4$mm). This is better illustrated in fig. 8.8. In this figure are plotted the measured (solid circles) and the predicted (empty squares) median grain sizes of transported material in the three experimental runs of Dietrich. The predicted d_{50} of transported material was in all experiments smaller than the measured.
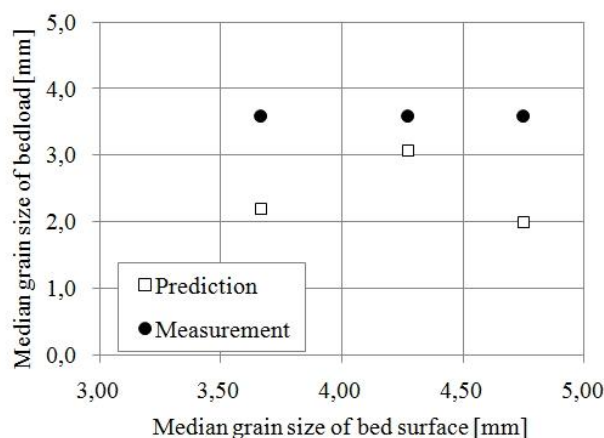

Fig. 8.8   Comparison between measured and predicted median grain size of transported material d_{50tr} in the experiments of Dietrich et al. (1989)

An important observation however, is that the predicted values of median grain size of transported material did not show any increasing or reducing trend with increasing median grain size of bed surface and accordingly declining total transport rate. Thus it can be concluded that the model might need further tuning but the proposed model logic is able to reproduce the experimental observations of Dietrich et al. (1989).

8.3 Comparison with field measurements of Kuhnle (1992)

Kuhnle measured the bed-load discharge of eight size fractions on Goodwin Creek during a wide range of different flow events. The maximum exerted shear stress that was documented was in excess of seven times the critical value. The study area is briefly described in section 2.4.1.1 while in figure 2.7 the grain size distribution of transported material during different flow events is shown. The measurements of Kuhnle showed that the transported material became coarser with increasing exerted flow strength.

The predictions of the proposed model are herein compared to the field measurements in Goodwin Creek that were taken by Kuhnle. In fig. 8.9 are plotted the predicted total transport rates against the measured on the field total transport rates. The agreement between predictions and measurements is very good for high transport rates, but becomes worse when the transport rate is reduced, i.e. when the exerted shear stress becomes lower.
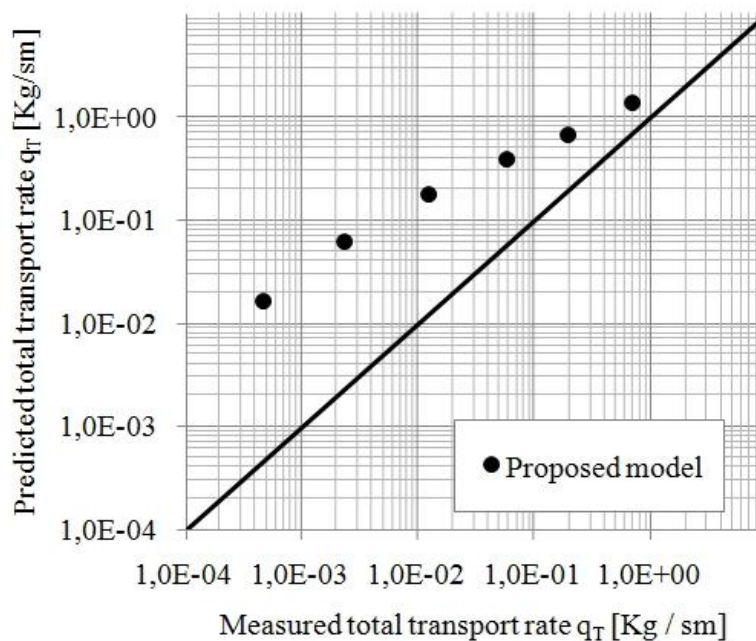
Fig. 8.9   Comparison between measured and predicted median grain size of transported material d_{50tr} in the experiments of Dietrich et al. (1989)

The fractional transport rates that were predicted by the proposed model are plotted against absolute grain size d_i for the six different flow events that are reported by Kuhnle in fig. 8.10. Next to them the fractional transport rates that were measured from Kuhnle are also plotted. As expected the agreement is good when the shear stress is high but becomes poorer with reducing flow strength. Generally, the measured transport rates show a larger reduction with reducing flow strength than the predicted (the spaces between the plotted lines are larger for the measured than the predicted),

something that is also shown by the fact that the points in fig. 8.8 are not parallel displaced relative to the line of perfect agreement, rather the distance is increasing with reducing flow strength.
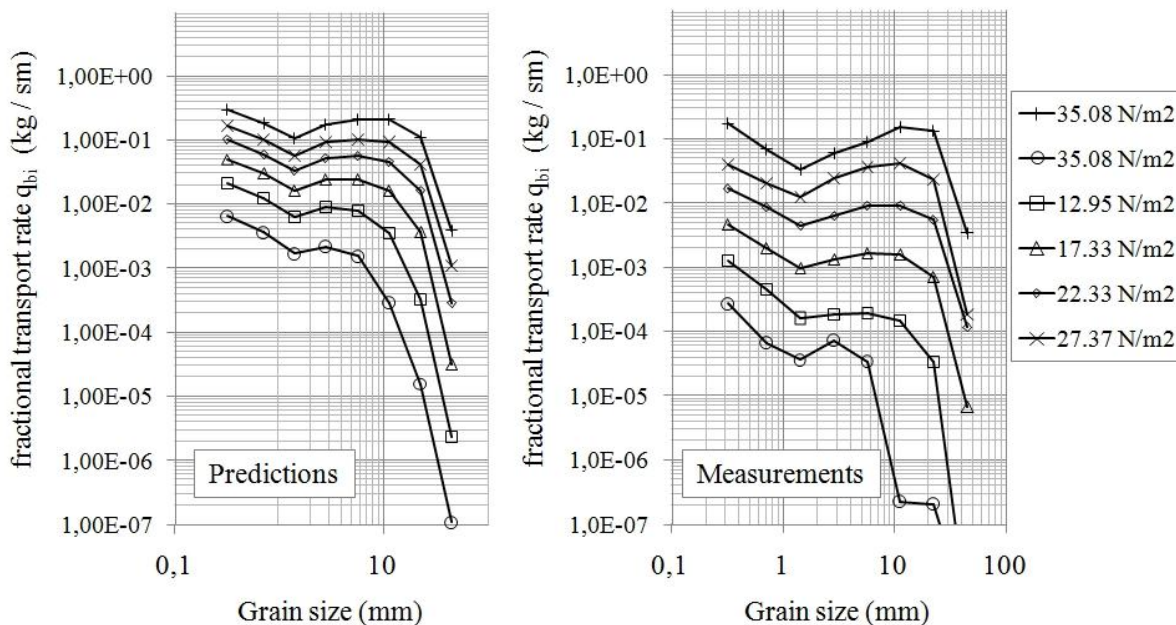

Fig. 8.10 Comparison between measured and predicted median grain size of transported material d_{50tr} in the experiments of Dietrich et al. (1989)

The predicted against the measured median grain sizes of transported material are plotted in fig. 8.11. The proposed model was able to reproduce the coarsening of transported material with increasing flow strength. However, the agreement this time was poor at high flow events and became better when the bed-load discharge was small.
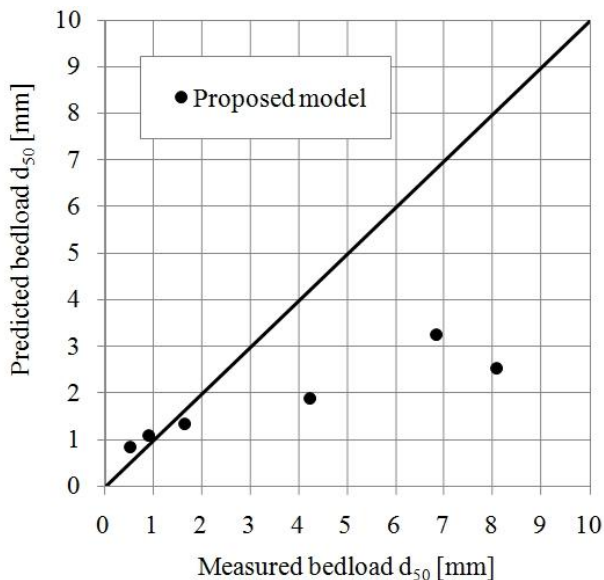
Fig. 8.11 Comparison between measured and predicted median grain size of transported material d_{50tr} in the experiments of Dietrich et al. (1989)

Kuhnle (1992 & 2007) showed that the agreement between measured transport rates in Goodwin Creek and the predictions of several published transport relations is poor. In the paper that was published in 2007, Kuhnle compared his field measurements with the results of three surface based transport models, i.e. the transport model of Parker (1990), Wu et al. (2000) and Wilcock and Crowe (2003). The results that were presented by Kuhnle (2007) regarding the performance of the three transport models are presented in table 8.4 and are further expanded with the performance of the proposed model. The predicted values were compared with the measured for the six different flow events that are reported by Kuhnle. The minimum, maximum and average percent differences between measurement & predictions are shown in table 8.4.

Table 8.4 Percent differences between measured & predicted q_{bT} and d_{50tr} in Goodwin Creek (taken from Kuhnle (2007) and expanded with results of the proposed model)

Model	% differences between measurement & prediction of q_{bT} $$100 \frac{\left| q_{bT\,meas.} - q_{bT\,pred.} \right|}{q_{bT\,meas.}}$$				% differences between measurement & prediction of d_{50tr} $$100 \frac{\left| d_{50tr\,meas.} - d_{50tr\,pred.} \right|}{d_{50tr\,meas.}}$$			
	P	**WC**	**W**	**PM**	**P**	**WC**	**W**	**PM**
Min.	208	329	8	89	7	11	1	18
Max.	3291	13970	93	3435	29	408	78	68
Mean	1235	3930	56	1346	16	154	43	46

Where   P   is for model of Parker (1990)
           WC is for model of Wilcock and Crowe (2003)
           W   is for model of Wu et al. (2000)
           PM is for proposed model

As far as the prediction of bed-load transport rate is concerned, the model of Wu et al. predicted transport rates that were closer to the measurements than the predictions of the other three tested models. The proposed model predicted almost the same transport rates with the model of Parker, while the model of Wilcock & Crowe predicted transport rates that showed the largest deviations from the measurements. The model of Parker predicted better the median grain size of transported material, while the proposed model showed almost the same behavior with the transport model of

Wu et al. The predictions of Wilcock & Crowe (2003) showed the largest deviations from the field measurements.

A reason for this poor agreement between measurements and model predictions might be that Kuhnle (1992) has published only one grain size distribution for the bed surface. According to the classical approach, at higher shear stresses, i.e. higher bed-load discharges, the bed surface is finer than during flow events that are characterized by low shear forces. Thus, it sounds logical to assume that during the field measurements of Kuhnle the bed surface did not have exactly the same composition regardless of the exerted shear stress, especially during such a wide range of flow events. It must be noted that the development of the model of Wu et al. (2000) was partly based on data of Kuhnle (Kuhnle (1993)) and thus shows a better reaction when the bed surface remains invariant during flow events of varying flow intensity.

8.4   Comparison with experimental results of Gessler (1961)

In terms of his investigation on incipient motion of sediment mixtures, Gessler (1961) performed experiments with the same configuration as that of the experiments of the present study. He used however a bed material with considerable finer grain size distribution. The proposed model is tested herein against the experimental results of Gessler. This test is useful because it will show the performance of the model when the parent bed material is considerably finer than that employed in the present study.

The experiments of Gessler are shortly described in section 3.2. Unfortunately Gessler did not publish the whole data set of measurements that he performed during his experimental runs. However, he published one figure that showed the grain size distribution of the armor layer at the end of experimental run I/5 as well as the grain size distribution of transported material at different time intervals after experiment incision. Thus the knowledge of parent bed material's and final bed surface grain size distribution as well as of exerted shear stress during Gessler's experimental run I/5, allows for prediction of transport rate and grain size distribution of transported material at the beginning as well as at the end of that experiment. Consequently the predictions of the proposed model are directly compared with the experimental observations of Gessler.

Fig. 8.12 shows the grain size distributions of parent bed material that Gessler employed. Additionally is also shown the grain size distribution of armor layer at the end of the experiment. The method that was used for finding this grain size distribution was area-by-weight with use of wax as adhesive. Therefore the originally published gradation curve has been converted to its equivalent volume-by-weight grain size distribution. The method that was used for this conversion is the same with the

one employed in the present study, which is described in section 5.3.6.4. The grain size distribution of transported material, which was determined by sieve analysis of samples taken 2,5 hours and 74 hours after the beginning of the experiment respectively, representing thus the initial and final composition of transported material is plotted in the same figure. Finally fig. 8.11 shows the grain size distribution of transported material that was predicted by the proposed model when the bed surface was unarmored, i.e. $d_{50s}/d_{50o} = 1$ and when the bed surface had attained its maximum degree of armoring which is determined by the given measured final armor layer.
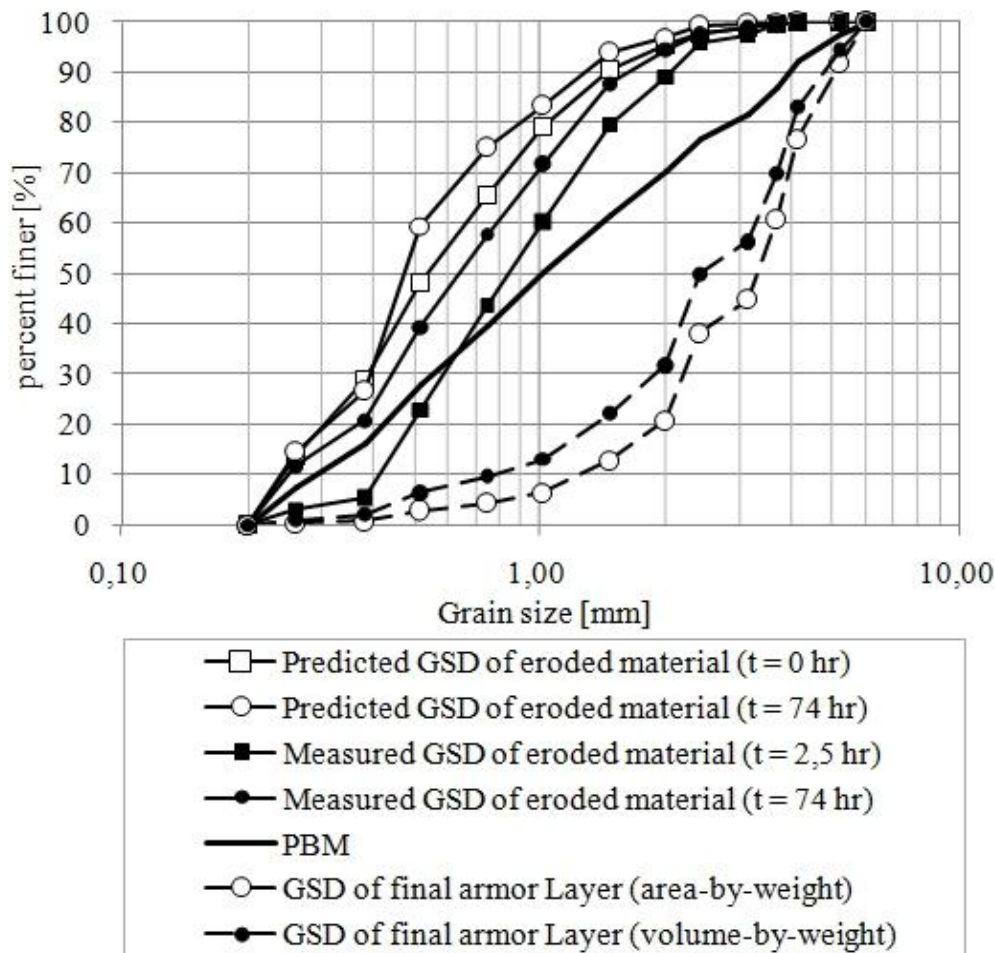
Fig. 8.12 Comparison between measured and predicted grain size distribution of transported material at the beginning and at the end of experimental run I/5 in the investigation of Gessler (1961)

The proposed model predicted a finer grain size distribution of transported material than that determined from experimental measurements both at the beginning as well as at the end of the experiment. However, it was able to reproduce the observed fining of transported material, although the tested sediment was considerably finer than that employed for the derivation of the model.

8.5 Chapter summary

The herein developed transport model was tested against measurements collected during equilibrium experiments that were performed under different conditions of sediment supply. Specifically, the model predictions were compared with the experimental results of the study of Curran & Wilcock (2005) on influence of sand content in bed-load transport of sand-gravel mixtures, as well as with the experimental results of the study of Dietrich et al. (1989) on response of bed surface to varying sediment feed rate, when the composition of sediment supply remains constant and is identical with the substrate material gradation. In addition the predictions of the proposed transport model were tested against the field measurements of Kuhnle (1992) in Goodwin Creek, USA. Finally, the observations of Gessler (1961) during one of his experiments on variation of transported material with progressive coarsening of bed surface were compared with the predictions of the model. The main results of the comparison between model predictions and measurements are herein summarized.

- The model was able to predict with very good accuracy the fractional transport rates that were measured during the experiments of Curran & Wilcock. The main success was that the model was able to predict that the gravel transport rate remained invariant while the sand transport rate increased from run to run under the given bed surface and bed slope equilibrium conditions. This shows that the incorporated hiding function is able to reproduce the effect of sand content in gravel transport rates that has been observed by many various researchers in the past.

- In the case of the experiments of Dietrich et al. (1989), the model predicted with high accuracy the total transport rates that were measured in the laboratory. The predicted median grain size of transported material was underestimated by the model, a deviation that is briefly discussed in the following chapter. Nonetheless the model predictions as far as the d_{50} of transported material did not show any tendency to increase or decrease from run to run, something that was one of the main imposed constraints.

- The model predictions of total transport rate deviated from the field measurements of Kuhnle (1992) in Goodwin Creek for low flow events. However, the predictions of the proposed model were considerably closer to the measurements than those of the model proposed by Wilcock & Crowe (2003), although both models employ the same $W^*_i - \tau/\tau_{ri}$ relation. This shows that the new hiding function predicted more accurate reference shear stress values. The deviations might be attributed to the fact that Kuhnle published only one measurement of bed surface grain size distribution which was used to describe the bed condition during a wide range of flow events. This contradicts the classical approach which supports that the bed

surface tends to be coarser during low bed-load activity and contrary is finer during events characterized by high transport rate. Finally the model was able to reproduce adequately the observed fining of transported material with reduction of flow intensity.

- The proposed model reproduced adequately the observed fining of transported material during the evolution of a static armor layers in one of the experiments of Gessler (1961). This test was important because the employed parent bed material by Gessler had a considerably higher sand content than that in the parent bed material that was employed in the present study.

9.   Conclusions

9.1   Short description of the objectives of the study and the employed methodology

The present study had two objectives.

- The first objective was to document the transient changes that occur during non-equilibrium bed-load transport of sediment mixtures under zero sediment feed conditions.

- The second objective was to develop a transport model that would be able to predict with accuracy the non-equilibrium processes.

In order to accomplish these two objectives, 15 experimental runs were performed, which allowed for a detailed determination of the spatial and temporal variation of fractional transport rates during the transformation of an initially unarmored bed surface to a stable armor layer, i.e. during the evolution of a finally static armor layer, under varying exerted shear stress. The spatial variation was determined by measuring the fractional bed-load discharge at three different locations along the flume. The temporal variation was documented by sampling at regular time intervals the eroded material and conducting a customary sieve analysis. Additionally, the spatial and temporal variation of bed surface grain size distribution was documented by employing an appropriate non-intrusive method, which was based on processing of plan view photos of bed surface during ongoing experiments. Hence, the obtained data set contained time series of fractional transport rates at different locations along the flume fully coupled with the corresponding bed surface gradation at a given time.

9.2   Main results of the experimental investigation

The results of the experiments are presented in detail in chapter 6. A short summary is provided herein.

- The constraint upstream sedimentological boundary condition had as result the coarsening of bed surface and decline of measured transport rate as time progressed. Thus, the state of equilibrium, which was defined by no motion due to the imposed sediment starved supply, was approached gradually.
- The measurements of transport rate at three different locations along the flume showed that the bed-load discharge increased in the downstream direction almost linearly. This was verified by optical observations during the experiments as well

as by the measured almost parallel bed degradation, which is clear evidence of increase of transport rate with distance.

- The decline of transport rate was associated with a progressive fining of the eroded material. In particular, the transport rate of sand grain fractions showed a considerably smaller reduction with bed surface coarsening when compared to the temporal variation of measured transport rate of gravel grain fractions.

9.3 Compatibility of herein obtained data set with previously published results

The trends that characterized the collected data (for example the two phased temporal variation of transport rates, the almost linear increase of transport rate with distance from flume inlet and the progressive fining of transported material) are also met in data sets that were obtained during previous studies that employed the same experimental arrangement. Furthermore they obeyed to a general trend that appears to characterize bed-load transport regardless of the employed sediment feed configuration, i.e. the increase of the ratio d_{50tr} / d_{50s} (i.e. median grain size of transported material to median grain size of bed surface) with increasing bed-load activity.

9.4 On the necessity of employment of a surface based transport model for accurate reproduction of non-equilibrium transport of sediment mixtures.

The analysis of the experimentally obtained data set highlighted the necessity of employment of a surface based transport model in order to predict with accuracy the observed, driven by disequilibrium, transient changes in grain size distribution and transport rate of eroded material. The already published surface based transport models have been based on the logical consideration that the grains contained on the surface layer are immediately available for entrainment into motion because they are directly exposed to the forces exerted by the flow. Consequently, the prediction of instantaneous fractional transport rates during transient conditions should account of the current fractional content of each individual grain class on bed surface (instead of the availability of each grain class in the substrate bed material). The herein obtained data set allowed for a direct comparison of fractional transport rates at different locations either at the same time point or when the bed surface had achieved the same degree of coarsening. The comparison showed that the measured fractional transport rates at different locations along the flume were almost equal when the degree of coarsening was used as discretization scale (i.e. the fractional transport rates q_{bi} measured 4 m downstream of the flume inlet when $d_{50s,\,4m}/d_{50o} = a$, was almost the

same with q_{bi} 12 m downstream the flume inlet when $d_{50s,\ 12m}/d_{50o} = a$. This result provides for first time (to the knowledge of the author) a sound argument, based on experimental measurements taken during an ongoing disequilibrium procedure, that supports the logical consideration upon which is based the development of surface-based bed-load transport predictors and justifies their employment for accounting of transient conditions.

9.5   Variation pattern of fractional reference shear stress with bed surface coarsening.

The second objective of the present work was to develop a transport model that would be capable to capture the observed transient adjustments between bed surface gradation and fractional transport rates. The so far published transport models consist of two main structural modules. The first one is a hiding function which allows for determination of reference (a surrogate for critical) shear stress of each individual grain fraction. The second structural module is the functional relation among grain mobility W^{*}_i and excess shear stress, where the latter is defined as the difference between exerted average bed shear stress and fractional reference shear stress.

The detailed documentation of the observed variation of fractional transport rates in combination with the knowledge of bed surface gradation during ongoing experiments provided the opportunity to interrelate the transient changes in fractional mobility to the required adjustments of reference shear stress for each individual grain class. This was possible only because the average bed shear stress was assumed to remain constant throughout each experimental run. This assumption was supported by the observed parallel degradation of bed elevation, the adjustment of water level during experiments in order to keep the water depth constant and the lack of bed forms. Considering that the exerted flow strength remained constant, the observed transient changes in fractional mobility could be attributed solely in variation of reference shear stress with progressive bed surface coarsening, as long as the influence of fractional content of each grain class had been neutralized (being incorporated in the determination of fractional mobility).

Having as theoretical background the above considerations, the experimental results revealed that the reference shear stress of all grain classes increased with progressive surface armoring. Moreover, the gravel grains exhibited a considerably larger reference shear stress variation when the bed surface became gradually coarser than the sand grains. In addition, the increase was almost equivalent for all gravel particles regardless of their absolute size d_i, contrary to the sand grains, which showed a size depending behavior as far as the increase of reference shear stress with bed armoring is concerned. The derivation of the abovementioned variation pattern of fractional

reference shear stress was based on the analysis of mutual adjustments among bed surface and transported material. Later on it was verified when the reference shear stress of each individual grain class was directly determined (quantified) from the experimental measurements.

9.6 Physical mechanism that governs grain stability during progressive bed surface coarsening.

The variation of fractional reference shear stress during the evolution of a coarse surface layer was attributed to alteration of hiding/-exposure conditions for each individual grain class. The employed parent bed material had a high sand content and thus during the initial stages the bed surface could be characterized as matrix supported. On the contrary, at the final stages the sand content in bed surface was considerably reduced and the latter was framework supported. Based on optical observations of bed surface structure during ongoing experiments as well as on theoretical considerations it was assumed that the transformation of bed surface from matrix to framework supported affected more the gravel grains than the sand grains. The size depending variation of reference shear stress within the sand size range was attributed to the fact that the larger proportion of fine sand grains within the active layer zone is always protected by other particles regardless of the degree of armoring. On the contrary, the impact of bed surface coarsening on reference shear stress of large particles is stronger because these grains tend to find easier locations that offer an increased protection from re-entrainment and at the same time the increased roughness of bed surface due to progressive formation of a coarse armor layer affects directly their displacement length.

9.7 New dynamic hiding function

9.7.1 Development procedure of new hiding function

The experimentally derived data set was further processed in order to estimate the fractional reference shear stress of each individual grain class at different stages of bed surface armoring. After the required mathematical transformations for the nondimensionalization of the involved physical quantities, a new dynamic hiding was developed, which allows for prediction of the fractional reference shear stress during ongoing non-equilibrium bed-load events. The development of the new hiding function was based initially on the data collected during the present study. The experimental runs, that are herein described, were performed with only one sand-gravel sediment mixture, which was characterized by a high sand content. In order to

expand the validity of the proposed hiding function also on different types of sediment mixtures, the initially proposed equations were modified and fitted on the data set that was published by Wilcock et al. (2001). The modification was based on the theoretical consideration that when the sand content of parent bed material is low, the particles with grain size smaller than the median diameter of substrate material will belong in the gravel size range and therefore they will suffer an almost equivalent reference shear stress increase regardless of their grain size.

9.7.2   Comparison with previously published hiding functions

The herein proposed hiding function shares some common elements with other hiding functions, especially that proposed by Wilcock & Crowe (2003). At the same time is able to adjust to gradually changing armoring conditions, being thus dynamic.

9.7.2.1 Similarities with older hiding functions

- The new hiding function predicts a higher reference shear stress τ_{ri} for particles with diameter smaller than the median grain size of bed surface d_{50s} and reduces the τ_{ri} value of grain classes coarser than d_{50s}, relative to the τ_{ri} value that these particles would have if the belonged to an uniform population. From this point of view the proposed hiding function acts in accordance with the previously published functions.

- The new hiding function is characterized by two limbs with different slope, when plotted in a log-log diagram. The limb with the milder slope is responsible for the calculation of τ_{ri} value of fine ($d_i < d_{50s}$) grain classes, while the limb with the steep slope is responsible for the calculation of the τ_{ri} values of coarse ($d_i > d_{50s}$) grain classes. This two-part trend is also met in the hiding functions that were implemented in the transport models of Proffitt & Sutherland (1983) and Wilcock & Crowe (2003).

- The slope of the limb that is responsible for the prediction of the τri value of coarse particles ($d_i/d_{50s} > 1$) is similar to that of the hiding function of Wilcock & Crowe (2003).

- The reference shears stress $\tau_{r50s,}$ which is associated with d_{50s}, appears to increase gradually when the bed surface becomes progressively coarser. This finding is in good agreement with the observation of Wilcock & Crowe (2003) that τ_{r50s} was increased when the sand content in bed surface was reduced because the reduction in sand content of bed surface is clearly associated with the evolution of the armor layer.

9.7.2.2 Innovation of proposed hiding function

The proposed hiding function is called dynamic, meaning that it does not remain the same under all circumstances but it changes obeying to a low, when the bed surface becomes progressively coarser. The response of the hiding function to alteration of bed surface gradation consists of the systematic variation in the slope of the limb that is responsible for the prediction of τ_{ri} value of grains with diameter smaller than d_{50s}. The degree of armoring d_{50s}/d_{50o} for a given parent bed material with median grain size d_{50o} is taken into account implicitly, by incorporating into the hiding function not only the relative grain size d_i/d_{50s}, but the relative grain size d_i/d_{50o} too. The dynamic character of the hiding function is degenerated when the coarseness of parent bed material (which is adequately described by its sand content) becomes larger.

The previously published hiding functions are given by a single predictive relation. This strict mathematic definition results in conservation of a certain fractional distribution of reference shear stress regardless of the armoring condition of bed surface. For example a single predictive relation enforces that the reference shear stress of particles with diameter $d_i = 0,5$ mm will be 1,5 times (randomly chosen proportion for reasons of simplicity) larger than the reference shear stress of particles with diameter $d_i = 1$ mm, regardless of the composition of the parent bed material or bed surface. The herein developed hiding function adjusts this proportionality in terms of the type of sediment mixture of parent bed material and the actual bed surface gradation during ongoing non-equilibrium bed-load transport events. Thus, the new hiding function regulates specifically the reference shear stress of relatively fine grain classes with respect to the sand content of parent bed material and armoring condition of bed surface, while for the relatively coarse particles the proposed function is described by a single defined curve, i.e. the proportionality in reference shear stress among coarse grain classes is considered to remain constant when the bed surface becomes progressively coarser.

9.8 W^*_i-τ/τ_{ri} relation of the proposed transport model

The excess shear stress τ/τ_{ri} that corresponded to each fractional transport rate measurement was found by estimating the fractional reference shear stress τ_{ri} by means of the newly developed hiding function. The similarity collapse of the calculated fractional mobility values W^*_i when plotted against excess shear stress on a data cloud with clearly defined trend was satisfactory. The same procedure was repeated also for the measurements that are included in the data set of Wilcock et al. (2001). The similarity collapse was again very good. The functional relationship between W^*_i and τ/τ_{ri} that is incorporated in the transport model of Wilcock & Crowe (2003) was employed also in the herein developed non-equilibrium transport model.

This good agreement between measurements collected during an ongoing disequilibrium procedure and measurements collected when the equilibrium condition had been already established shows that non-equilibrium transport can be approached as a time series of individual equilibrium events, as long as they are short in duration and confined in a finite movable bed length. Prerequisites for this good agreement are that the estimated fractional mobility has been associated to the fractional content in bed surface and finally that a suitable hiding function has been employed for the estimation of excess shear stress These temporal or spatial discretized events differ from each other in the imposed boundary conditions. These boundary conditions might be the exerted flow strength, or might concern the sediment supply or the bed surface gradation.

9.9   Performance of proposed transport model

The choice of an appropriate W^*_i-τ/τ_{ri} relation completed the development of a transport model, the derivation of which was primarily based on a data set obtained from non-equilibrium experiments. The proposed model was tested initially against the data that were used for its development, in order to check its ability to capture the observed transient changes during the disequilibrium procedure of formation of a finally static armor layer. The model was able to reproduce with satisfactory accuracy the observed two phased temporal variation as well as the observed spatial lag of fractional transport rates. In addition the model was able to predict the gradual adjustment of transported material's grain size distribution to progressive bed surface coarsening. The proposed bed-load predictor was able to follow also the observed transient changes in one of Gessler's experiments. Gessler (1961) employed a considerably sandier sediment mixture during his experimental study on static armoring. Thus, the good agreement between model predictions and experimental measurements increases the reliability of the proposed model also for sediment mixtures finer than the one employed in the current study.

The model was also tested against measurements collected in the experimental studies of Curran & Wilcock (2005) and Diettrich et al. (1989). These experimental investigations were chosen because they are characterized by different sedimentological boundary conditions and they describe the required mutual adjustments between bed-load transport and bed surface gradations that are necessary for the establishment of equilibrium transport under these conditions.

In the study of Curran & Wilcock the sediment supply was increased from run to run. The increase in sediment supply occurred due to increased sand content in the feed material while the gravel feed rate was kept constant. Therefore the equilibrium transported load became also finer from run to run. The proposed model was applied

directly, i.e. the composition and transport rate of transported material was predicted under the given for each experimental run bed surface gradation and established equilibrium slope. The agreement between measurements and model predictions was very good. The model was able to predict both the increased sand content as well as the constant gravel content in transported material from run to run. When compared to the predictions made by the model of Wilcock & Crowe (2003) (presented by Curran & Wilcock (2005), the latter could not predict the constant gravel transport rate and reproduced a progressive increase in gravel transport rate when the sand content increased. Considering that the two models, i.e. the herein developed and the Wilcock & Crowe model, differ only in the hiding function, this provides an additional supporting argument for the implemented attitude toward variation of reference shear stress of fine grains.

Consequently the model was tested against the experimental measurements collected during the study of Diettrich et al. (1989). This study was chosen because the supply composition was kept constant from run to run and varied only the feed rate. The varying sediment supply caused the response of the bed surface, which coarsened as the sediment load became lower. The proposed model was applied again directly. The predicted transport rates were almost the same with the measured during the experiments. The predicted median grain size of transported material was slightly finer than the experimentally determined. However the predicted d_{50} of transported material did not show any variation when the bed surface coarsened and the transport rate became lower from run to run, which was the main imposed boundary condition. The deviation between the predicted and measured d_{50} of transport material might be attributed to a slight dependence of reference shear stress of coarse particles upon armoring condition, which is not taken into account from the proposed model.

Finally the proposed model was tested against the field measurements of Kuhnle (1992). The model predictions and measurements in the field of fractional transport rates showed satisfactory agreement, although the deviations were considerably than the previous cases. These deviations may be attributed to the fact that the bed surface was described by only one grain size distribution for a wide range of flow events. Although the question of persistence of armor layers during high flow events has not been cleared out yet, according to the classical approach the bed surface should show at least a slight variation when the bed-load activity changes. Considering the sensibility of the proposed transport model to bed surface changes, it can be assumed that the observed differences between predictions and measurements might be actually smaller if the bed surface is coarser at low flow events and finer at high flow events, than the one given by Kuhnle, something that is a logical assumption. In addition, the model was able to reproduce the observed coarsening of transported material with increasing flow strength.

9.10 Application procedure of proposed transport model

The direct application of the proposed model reauires:

1. Calculation of associated with the median grain size of bed surface d_{50s} dimensionless reference shear stress τ^*_{r50s}

$$\tau^*_{r50s} = 0{,}018 + \frac{0{,}014}{1 + \exp\left(14{,}5 - 14\dfrac{d_{50s}}{d_{50o}}\right)}$$

where: d_{50o} is the median grain size of parent bed material

2. Calculation of associated with the median grain size of bed surface d50s reference shear stress τr50s

$$\tau_{r50s} = \tau^*_{r50s}(s-1)\rho g d_{50s}$$

where: s   is the submerged specific gravity of sediment
ρ is water density
g   is gravitational acceleration
d_i is size of ith grain class

3. Calculation of parameters ai and bi (that will be used subsequently for the calculation of fractional reference shear stress τ_{ri})

$$a_i = \begin{cases} 0{,}61\left(\dfrac{d_i}{d_{50o}}\right)^{(-0{,}1+0{,}5\exp(-44\exp(-22\,f_{so}))} & ,\dfrac{d_i}{d_{50o}} \leq 1 \\[4mm] 0{,}59\left(\dfrac{d_i}{d_{50o}}\right)^{0{,}45} & ,\dfrac{d_i}{d_{50o}} > 1 \end{cases}$$

$$b_i = \begin{cases} 0{,}44\left(\dfrac{d_i}{d_{50o}}\right)^{(-0{,}6-0{,}82\exp(-30\exp(-22\,f_{so}))} & ,\dfrac{d_i}{d_{50o}} \leq 1 \\[4mm] 0{,}45\left(\dfrac{d_i}{d_{50o}}\right)^{0{,}68} & ,\dfrac{d_i}{d_{50o}} > 1 \end{cases}$$

where: d_i is the diameter of ith grain class
f_{so} is the sand content of parent bed material

4. <u>Calculation of fractional reference shear stress τ_{ri}</u>

$$\frac{\tau_{ri}}{\tau_{r50s}} = a_i\, e^{b_i \frac{d_i}{d_{50s}}}$$

where: a_i, b_i are parameters that have been previously calculated

5. <u>Calculation of excess shear stress φ_i</u>

$$\varphi_i = \frac{\tau}{\tau_{ri}}$$

where: τ is exerted average bed shear stress

6. <u>Calculation of fractional dimensionless transport rate W^*_i</u>

$$W_i^* = \begin{cases} 0{,}002\varphi_i^{7,5} & ,\quad \varphi_i < 1{,}35 \\[2mm] 14\left(1 - \dfrac{0{,}894}{\varphi_i^{0,5}}\right)^{4,5} & ,\quad \varphi_i \geq 1{,}35 \end{cases}$$

7. <u>Calculation of fractional transport rate q_{bi} in m³/s m</u>

$$W_i^* = \frac{(s-1)g q_{bi}}{F_i u_*^3}$$

where: q_{bi} is volumetric transport rate per unit width of ith grain class
            F_i is fractional content of ith grain class in bed surface

References

Ackers, P.; White, W.R. (1973): Sediment transport: a new approach and analysis. Journal Hydraulic Engineering, ASCE, Vol. 99, No. 11, 2041–2060.

Ahrens, J.P. (2000): The fall-velocity equation. Journal of the Waterways, Harbors and Coastal Engineering Division, Vol. 126, No. 2, pp. 99–102.

Anastasi, G. (1984): Geschiebeanalysen im Felde unter Berücksichtigung von Grobkomponenten. Mitteilungen der Versuchsanstalt für Wasserbau, Hydrologie und Glaziologie, Nr. 70, ETH, Zürich.

Andrews, E. D.; Erman, D.C. (1986): Persistence in the size distribution of surficial bed material during an extreme snowmelt flood. Water Resources Research, AGU, Vol. 2, No. 2, pp. 191–197.

Andrews, E. D.; Parker, G. (1987): Formation of a coarse surface layer as the response to gravel mobility. In: Thorne, C.R.; Bathurst, J.C.; Hey, R.D. (Eds). Sediment Transport in Gravel-bed Rivers, John Wiley & Sons, Chichester, pp. 269–325.

Ashida, K.; Michiue, M. (1972): Study on hydraulic resistance and bedload transport rate in alluvial streams. in: Transcripts of the Japan Society for Civil Engineers, pp. 59–69.

Ashworth, P.J.; Ferguson, R.I. (1989): Size selective entrainment of bedload in gravel bed streams. Water Resources Research, AGU, Vol. 25, No. 4, pp. 627–634.

Bagnold, R.A. (1966): An approach to the sediment transport problem from general physics. Tech. Rep. 422-I. US Geological Survey professional paper.

Baker, R.E. (1986): Local scour at bridge piers in non-uniform sediments. Report No. 402, School of Engineering, University of Auckland, Auckland, New Zealand.

Bell, R.G., Sutherland, A.J. (1983): Non-equilibrium bed load transport by steady flows. Journal Hydraulic Engineering, ASCE, Vol. 109, No. 3, pp. 351–367.

Buffington, J.M.; Montgomery, D.R. (1997): A systematic analysis of eight decades of incipient motion studies, with special reference to gravel-bedded rivers. Water Resources Research, AGU, Vol. 33, pp. 1993–2029.

Bui, M.D.; Rutschmann, P. (2006): A 3D Numerical Model of Graded Sediment Transport in Nonequilibrium Condition, ed. Piasecki, M.; et al.: Proceedings of the7th International Conference on Hydroscience and Engineering (ICHE-2006).

Butler, J.B.; Lane, S.N.; Chandler, J.H. (2001): Automated extraction of grain-size data for gravel surfaces using digital image processing. Journal of Hydraulic Research, IAHR, Vol. 39, No. 5, pp. 519-529.

Carling, P.A. (1988): The concept of dominant discharge applied to two gravel-bed streams in relation to channel stability thresholds, Earth Surface Processes and Landforms, Vol. 13, No. 4, pp. 355–367.

Carling, P.A. (1989): Bedload transport in two gravel-bedded streams, Earth Surface Processes Landforms, Vol. 14, No. 1, pp. 27-39.

Chin, C.O. (1985): Stream bed armouring. Rep. No. 403, School of Engineering, University of Auckland, Auckland, New Zealand.

Chin, C.O.; Melville, B.W.; Raudkivi, A.J. (1994): Stream bed armouring. Journal Hydraulic Engineering, ASCE, Vol. 120, No. 8, pp. 899–918.

Cheng, N.S. (1997): Simplified settling velocity formula for sediment particle. Journal Hydraulic Engineering, ASCE, Vol. 123, No. 2, pp. 149–152.

Church, M.A.; McLean, D.G.; Wolcott, .JF. (1987): River bed gravel: sampling and analysis. In: Thorne, C.R.; Bathurst, J.C.; Hey, R.D. (Eds). Sediment Transport in Gravel-bed Rivers, John Wiley & Sons, Chichester, pp. 43–88.

Church, M.; Wolcott, J. F. ; Fletcher, W.K. (1991): A test of equal mobility in fluvial sediment transport: Behavior of the sand fraction, Water Resources Research, AGU, Vol. 27, No. 11, pp. 2941–2951.

Crowder, D.W.; Diplas, P. (1997): Sampling Heterogeneous Deposits in Gravel-Bed Streams. Journal Hydraulic Engineering, ASCE, Vol. 123, No. 12, pp. 1106-1117.

Curran, J.C. (2007): The decrease in shear stress and increase in transport rates subsequent to an increase in sand supply to a gravel-bed channel. Sedimentary Geology, Vol. 202, No. 3, pp. 572-280.

Curran, J.C.; Wilcock, P.R. (2005): The effect of sand supply on transport rates in a gravel bed channel. Journal Hydraulic Engineering, ASCE, Vol. 131, No. 11, pp. 961-967.

Day, T.J. (1980): A Study of the Transport of Graded Sediments. Report IT190, Hydraulic Research Station,wallingford, 10 pp.

Dietrich, W.E. (1982): Settling velocity of natural particles: Water Resources Research, AGU, Vol. 18, No. 6, pp. 1615-1626.

Dietrich, W.E.; Kirchner, J.W.; Ikeda, H.; Iseya, F. (1989): Sediment supply and the development of the coarse surface layer in gravel-bedded rivers, Nature, Vol. 340, 215–217.

Diplas, P. (1987): Bedload transport in gravel-bed streams. Journal Hydraulic Engineering, ASCE, Vol. 113, No. 3, pp. 277–292.

Diplas, P.; Dancey, C. L.; Celik, A. O.; Valyrakis, M.; Greer, K.; Akar, T. (2008): The role of impulse on the initiation of particle movement under turbulent flow conditions. Science, Vol. 322, No.5902, pp. 717-720.

Diplas, P.; Fripp, J.B. (1992): Properties of various sediment sampling procedures. Journal Hydraulic Engineering, ASCE, Vol. 118, No. 7, pp. 955-970.

Diplas, P.; Parker, G. (1992): Deposition and removal of fines in gravel-bed streams. in Billi, P., Hey, R. D., Thorne, C. R. and Tacconi, P. (Eds), Dynamics of Gravel-bed Rivers, Wiley, Chichester, 313-329.

Diplas, P.; Shaheen, H. (2008): Bed Load Transport and Streambed Structure in Gravel Streams. Chapter 11, Gravel Bed Rivers VI - From Process Understanding to River Restoration, ed. Habersack H. Elsevier, pp. 291-312.

Diplas, P.; Sutherland, A.J. (1988): Sampling techniques for gravel sized sediments. Journal Hydraulic Engineering, ASCE, Vol. 114 , No. 5, pp. 484-501.

Dittrich, A. (1998): Wechselwirkung Morphologie/Strömung naturnaher Fließgewässer. Mitteilungen des Instituts für Wasserwirtschaft und Kulturtechnik, Heft 198, Universität Karlsruhe (TH), Karlsruhe.

Drake, T.G.; Shreve, R.L.; Dietrich, W.E.; Whiting, P.J.; Leopold, L.B. (1988): Bedload transport of fine gravel observed by motion picture photography. Journal of Fluid Mechanics. Vol. 192, pp.193-217.

DuBoys, P. (1879): Le Rohne et les Rivieres a Lit Affouillable. Annales des Pontes et Chausses Series 5, Vol. 18, pp. 141–195.

Efthymiou, N. (2008): Abschätzung der Sohloberflächenkornzusammensetzung von digitalen Photoaufnahmen, Fachtagung Gewässermorphologie & EU-WRRL, 24.-25.7.2008, Wallgau, Berichte des Lehrstuhls und der Versuchsanstalt für Wasserbau und Wasserwirtschaft der Technischen Universität München, Band Nr. 122, pp. 204-212.

Efthymiou, N.; Rutschmann, P. (2009): Estimation of grain size distribution by image analysis, 33rd IAHR Congress: Water Engineering for a Sustainable Environment, 9.- 14.2009, Vancouver, British Columbia, Canada, International Association of Hydraulic Engineering & Research (IAHR), pp.131-138.

Egiazaroff, I.V. (1965): Calculation of non-uniform sediment concentrations. Journal Hydraulics Division, ASCE, Vol. 91, No. 4, pp. 225-248.

Einstein, H.A. (1934): Der hydraulische oder Profil-Radius. Schweizerische Bauzeitung, Band 103, Nr. 8, pp. 89-91.

Einstein, H.A. (1950): The bed load function for sediment transportation in open channels. Technical Bulletin 1026, U.S. Department of Agriculture, Soil Conservation Service, Washington, DC.

Engelund, F.; Hansen, E. (1972): A monograph on sediment transport in alluvial streams, 3rd Ed., Technical Press, Copenhagen, Denmark.

Ettema, R. (1984): Sampling armor-layer sediments. Journal Hydraulic Engineering, ASCE, Vol. 110, No. 7, pp. 992-996.

Fehr, R. (1987a): Geschiebeanalysen in Gebirgsflüssen. Umrechnung und Vergleich von verschiedenen Analyseverfahren. Mitteilungen der Versuchsanstalt für Wasserbau, Hydrologie und Glaziologie, No. 92, ETH, Zürich, Switzerland 139 pp.

Fehr, R. (1987b): Einfache Bestimmung der Korngrössenverteilung von Geschiebematerial mit Hilfe der Linienzahlanalyse. Schweizer Ingenieur und Architekt, Vol. 105, pp. 1104-1109.

Ferguson, R.I.; Prestegaard, K.L.; Ashworth, P.J. (1989): Influence of sand on hydraulics and gravel transport in a braided gravel bed river. Water Resources Research, AGU, Vol. 25, pp. 635–643.

Fraccarollo, L.; Marion, A. (1995): Statistical approach to bed-material surface sampling. Journal Hydraulic Engineering, ASCE, Vol. 121, No. 7, pp. 640-545.

Gessler, J. (1965): Der Geschiebetriebbeginn bei Mischungen untersucht an natürlichen Abpflästerungserscheinungen in Kanälen. Diss. Nr. 3711, Mitteilungen der Versuchsanstalt für Wasserbau und Erdbau, No. 69, ETH, Zürich, Switzerland.

Gessler, J. (1970): Self-Stabilizing Tendencies of Alluvial Channels. Journal of the Waterways, Harbors and Coastal Engineering Division, Vol. 96, No. 2, pp. 235-249.

Gomez, B. (1983): Temporal variations in bedload transport rates: the effect of progressive bed-armouring, Earth Surface Processes and Landforms, Vol. 8, No. 1, pp. 41-54.

Gomez, B. (1984): Typology of segregated (armoured/paved surfaces: some comments. Earth Surface Processes and Landforms, Vol. 9, No. 1, pp. 19-24.

Graf, W.H. (1971): Hydraulics of sediment transport, McGraw-Hill, New York, USA, 524 pp.

Grünzner M.; Rutschmann P. (2009): Initial motion of exposed grains − High resolution LES of Experiments by Fenton and Abbott, 33rd IAHR Congress: Water Engineering for a Sustainable Environment, 9.-14.2009, Vancouver, British Columbia, Canada, International Association of Hydraulic Engineering & Research (IAHR), pp.6344-6351.

Guy H. P.; Rathbun R. E.; Richardson E.V. (1967): Recirculation and sand-feed type flume experiments. Journal Hydraulic Division, ASCE, Vol. 93, No. 5, pp. 97-114.

Günter, A. (1971): Die kritische mittlere Sohlenschubspannung bei Geschiebe-mischungen unter Berücksichtigung der Deckschichtbildung und der turbulenz-bedingten Sohlschubspannungsschwankungen. Diss. Nr. 4649, Mitteilungen der Versuchsanstalt für Wasserbau, Hydrologie und Glaziologie, No. 3, ETH, Zürich, Switzerland.

Harrison, A.S. (1971): Report on special investigations of bed sediment segregation in a degrading bed. Report Series No. 33, University of California, Institute of Engineering Research, Issue No. 1, Berkeley, CA, USA.

Haschenburger, J.K.; Wilcock, P.R. (2003): Partial transport in a natural gravel bed channel. Water Resources Research, AGU, Vol. 39, No. 1, pp. 1020-1029.

Hassan, M.A.; Church, M. (2000): Experiments on surface structure and partial sediment transport. Water Resources Research, AGU, Vol. 36 , No. 7, pp. 1885 – 1895.

Haynes, H.; Pender, G. (2007): Stress history effects on graded bed stability. Journal Hydraulic Engineering, ASCE, Vol. 33, No. 4, pp. 343-349.

Hey, R.D.; Thorne, C.R. (1983): Accuracy of surface samples from gravel bed material. Journal Hydraulic Engineering, ASCE, Vol. 109, No. 6, pp. 842-851.

Hunziker, R.P. (1995): Fraktionsweiser Geschiebetransport. Mitteilungen der Versuchsanstalt für Wasserbau, Hydrologie und Glaziologie, No. 138, ETH, Zürich, Switzerland.

Hunziker, R.P.; Jaeggi, M.N.R. (2002): Grain sorting processes. Journal Hydraulic Engineering, ASCE, Vol. 128, No. 12, pp.1060-1068.

Ikeda, H. (1984): Flume experiments on the superior mobility of sediment mixtures, Ann. Rep. Inst. Geosci., Vol. 10, Univ. of Tsukuba, Tsukuba, Japan. pp. 53-56.

Ikeda, H.; Iseya, F. (1988): Experimental study of heterogeneous sediment transport. Environmental Research Center Paper No. 12, Univ. of Tsukuba, Tsukuba, Japan.

Jackson, W. L.; Beschta R. L. (1982): A model of two-phase bedload transport in an Oregon coast range stream, Earth Surface Processes and Landforms, Vol. 7, No. 6, pp. 517-527.

Jackson, W. L.; Beschta R. L. (1984): Influences of increased sand delivery on the morphology of sand and gravel channels, J. Am. Water Resour. Assoc., Vol. 20, No. 4, pp. 527–533.

Jäggi, M.N.R. (1984): Abflussberechnung in kiesführenden Flüssen. Wasserwirtschaft, 24. Jg., Heft 5, pp. 263-267.

Jain, S.C. (1990): Armor or pavement. Journal Hydraulic Engineering, ASCE, Vol. 116, No. 3, pp. 436-440.

Jimenez, J.A.; O.S. Madsen (2003): A simple formula to estimate the settling velocity of natural sediments. Journal Waterways, Port, Coastal and Ocean Engineering, ASCE, Vol. 129, No. 2, pp. 70-78.

Kellerhals, R.; Bray, D.I., (1971): Sampling procedures for coarse fluvial sediments. Journal Hydraulics Division, ASCE, Vol. 97, 1165–1180.

King, J.G.; Emmett, W.W.; Whiting, P.J.; Kenworthy, R.P.; Barry, J.J. (2004): Sediment transport data and related information for selected coarse-bed streams and rivers in Idaho. U.S. Forest Service Technical Report RMRS-GTR-131, 26 pp.

Knauss, J. (1996): Argolische Studien: Alte Straßen - alte Wasserbauten. Talsperre von Mykene; Flußumleitung von Tiryns; Hydra von Lerna; Küstenpass Anigraia, Berichte des Lehrstuhls und der Versuchsanstalt für Wasserbau und Wasserwirtschaft der Technischen Universität München, Band Nr. 77.

Komar P. D. (1987): Selective gravel entrainment and the empirical evaluation of flow competence. Sedimentology, Vol. 34, No. 6, pp. 1165-1176.

Komar P. D.; Li, Z. (1988): Applications of grain pivoting and sliding analyses to selective entrainment of gravel and to flow competence evaluations. Sedimentology, Vol. 35, No. 4, pp. 681-695.

Komar, P.D.; Shih, S. (1992): Equal mobility versus changing bed load grain sizes in gravel-bed stream. In: Billi, P.; Hey, R.D; Thorne, C.R;.Tacconi, P. (eds.), Dynamics of Gravel-bed Rivers, John Wiley & Sons., Chichester, pp. 73–93.

Kuhnle, R.A. (1989): Bed-surface size changes in gravel-bed channel, Journal Hydraulic Engineering, ASCE, Vol. 115, No. 6, pp. 731– 743.

Kuhnle, R.A. (1992): Fractional transport rates of bedload on Goodwin Creek. In: Billi, P.; Hey, R.D; Thorne, C.R;.Tacconi, P. (eds.), Dynamics of Gravel-bed Rivers, John Wiley & Sons., Chichester, pp. 141– 155

Kuhnle, R.A. (2007): Prediction of Bed Load Transport on Small Gravel-Bed Streams. In: Proceedings 7th International Conference on Hydroscience & Engineering, 10 pp.

Lamberti, A.; Paris, E. (1992): Analysis of armouring processes through laboratory experiments. In: Billi, P.; Hey, R.D; Thorne, C.R;.Tacconi, P. (eds.), Dynamics of Gravel-bed Rivers, John Wiley & Sons., Chichester, pp. 227-250.

Lane, E.W. (1955): Design of stable channels. Transactions of the American Society of Civil Engineers, 120, pp. 1234–1260.

Laronne J. B.; Reid I.; Yitshak Y.; Frostick L.E., (1994): The non-layering of gravel streambeds under ephemeral flow regimes. Journal Hydrology, vol. 159, Issues 1-4, pp. 353-363.

Laronne, J.B.; Reid, I, (1993): Very high rates of bedload sediment transport by ephemeral desert streams. Nature, Vol. 366, pp. 148–150.

Leopold LB. (1992): The sediment size that determines channel morphology. In: Billi, P.; Hey, R.D; Thorne, C.R;.Tacconi, P. (eds.), Dynamics of Gravel-bed Rivers, John Wiley & Sons., Chichester, pp. 297–311.

Lisle T.E. (1989): Sediment transport and resulting deposition in spawning gravels, north coastal California. Water Resources Research, AGU, Vol. 25, No. 6, pp. 1303-1319.

Lisle T.E. (1995): Particle size variations between bed load and bed material in natural gravel bed channels. Water Resources Research, AGU, Vol. 31. No.. 4, pp. 1107-1118.

Lisle, T.E.; Iseya, F.; Ikeda, H. (1993): Response of a channel with alternative bars to a decrease in supply of mixed-size bed load: A flume experiment. Water Resources Research, AGU, Vol. 29, pp. 3623– 3629.

Lisle, T.E.; Madej, M.A. (1992): Spatial variation in armouring in a channel with high sediment supply, In: Billi, P.; Hey, R.D; Thorne, C.R;.Tacconi, P. (eds.), Dynamics of Gravel-bed Rivers, John Wiley & Sons., Chichester, pp. 277– 293.

Lisle, T.E., Nelson,M.N., Pitlick, J., (2000): Variability of bed mobility in natural, gravel-bed channels and adjustments to sediment load at local and reach scales. Water Resources Research, AGU, Vol. 36, No. 12, pp. 3743–4755.

Little W.C.; Mayer P.G. (1976): Stability of Channel Beds by Armouring. Journal Hydraulic Division, ASCE, Vol. 102, No. 11, pp. 1647-1661

Malcherek A. (2006): Sedimenttransport und Morphodynamik. Institut fuer Wasserwesen der Universitaet der Bundeswehr Muenchenm Fakultaet fuer Bauingenieur- und Vermessungswesen, München-Neubiberg, Gernany, 190 pp.

Mao L.; Cooper, J.R.; Frostick L.E. (2009): Armour layer development during sediment starvation and recirculation flume experiments. 33rd IAHR Congress: Water Engineering for a Sustainable Environment, 9.-14.2009, Vancouver, British Columbia, Canada, International Association of Hydraulic Engineering & Research (IAHR).

Marion, A.; Faccarollo L. (1997): New conversion model for areal sampling of fluvial sediments. Journal Hydraulic Engineering, ASCE, Vol. 123, No. 12, pp. 1148-1151.

Meyer-Peter, E.; Müller, R. (1948): Formulas for bed-load transport. Proceedings, 2nd Congress International Association for Hydraulic Research, Stockholm, Sweden, pp. 39–64.

Milhous, R.T. (1973): Sediment transport in a gravel-bottomed stream, Ph.D. thesis, Oreg. State Univ., Corvallis.

Miller, M.C.; McCave, I.N.; Komar, P.D. (1977): Threshold of sediment motion under unidirectional currents. Sedimentology, Vol. 24, No. 4, pp. 507–527.

Misri, R. L., R. J. Garde, K. G. Ranga Raju, (1984): Bed load transport of coarse nonuniform sediment. Journal Hydraulic Engineering, ASCE, Vol. 110, No. 3, pp. 312-328

Mosconi C.E. (1988): River bed variations and evolution of armor layers. PhD thesis, University of Iowa, Iowa, USA

Ockelford, A.M. (2011): The impact of stress history on non cohesive sediment bed stability and bed structure. PhD thesis, University of Glasgow.

Paintal, A.S. (1971): A stochastic model for bed load transport. Journal Hydraulic Research, IAHR, vol. 9, No. 4, pp. 527–553.

Paris E. (1991): Time – space bed load evolution in static armoring. Proc., Int. Seminar on Grain Sorting, Ascona, Mitteilungen der Versuchsanstalt für Wasserbau, Hydrologie und Glaziologie, Nr. 117, ETH, Zürich, Switzerland, pp. 193-206.

Parker, G. (1990): Surface-based bedload transport relation for gravel rivers. Journal Hydraulic Research, IAHR, vol. 28, No. 4, pp. 417–436.

Parker G. (2008): Transport of gravel and sediment mixtures. In: Garcia, M.(ed.) Sedimentation Engineering: Processes, Measurements, Modeling, and Practice (Manual 110), ASCE, 1132 pp.

Parker, G.; Dhamotharan, S.; Stefan, H. (1982b): Model experiments on mobile, paved gravel bed streams, Water Resources Research, AGU, Vol. 18, No. 5, pp. 1395–1408.

Parker G.; Klingeman, P.C. (1982): On why gravel bed streams are paved. Water Resources Research, AGU, Vol. 18, No. 5, pp. 1409–1433.

Parker, G.; Klingeman, P.C.; McLean, D.G. (1982a): Bed load and size distribution in paved gravel-bed streams, Journal Hydraulic Engineering, ASCE, Vol. 108, No. 4, pp. 544–571.

Parker, G.; Toro-Escobar, C.M. (2002): Equal mobility of gravel in streams: The remains of the day. Water Resources Research, AGU, Vol. 38, No. 11, pp. 1264-1272.

Parker, G.; Wilcock, P.R. (1993): Sediment feed and recirculating flumes: A fundamental difference, Journal Hydraulic Engineering, ASCE, Vol. 119, No. 11, pp. 1192– 1204.

Pender, G.; Hoey, T.B.; Fuller, C.; Mcewan, I.K. (2001): Selective bedload transport during the degradation of a well sorted graded sediment bed. Journal of Hydraulic Research, IAHR, vol. 39, No. 3, pp. 269-277.

Petrie, J.; Diplas, P. (2000): Statistical approach to sediment sampling accuracy, Water Resources Research, AGU, Vol. 36, No. 2, pp. 597-605.

Phillips, B.C., Sutherland, A.J. (1989): Spatial lag effects in bed load sediment transport. Journal of Hydraulic Research, IAHR, Vol. 27, No. 1, pp. 115–133.

Powell, D.M. (1998): Patterns and processes of sediment sorting in gravel-bed rivers. Progress in Physical Geography. Vol. 22, pp. 1 – 32.

Powell, D.M.; Reid, I.; Laronne, J.B. (2001): Evolution of bed load grain size distribution with increasing flow strength and the effect of flow duration on the caliber of bed load sediment yield in ephemeral gravel bed rivers. Water Resources Research, AGU, Vol. 37, No. 5, pp. 1463–1474.

Proffitt, G.T. (1980): Selective transport and armouring of non-uniform alluvial sediments. Report no. 80/22, Department of Civil Engineering, University of Canterbury, Christchurch, New Zealand.

Proffitt, G. T.; Sutherland, A. J. (1983): Transport of non-uniform sediments. Journal of Hydraulic Research, IAHR, Vol. 21, No. 1,pp. 33–43.

Raudkivi, A.J. (1991): Loose boundary hydraulics. 4th Edition. Balkema, Rotterdam, Netherlands.

Reid, I.; Frostick, L.E.; Layman, J.T. (1985): The incidence and nature of bedload transport during flood flows in coarse-grained alluvial channels. Earth Surface Processes and Landforms, Vol. 13, No. 1, pp. 33–44.

Reid, I.; Powell, D.M.; Laronne, J.B. (1996): Prediction of bed-load transport by desert flash floods. Journal Hydraulic Engineering, ASCE, Vol. 122, No. 3, pp. 170–172.

Rosato, A.; Strandburg, K.J.; Prinz, F.; Swendsen, R.H. (1987): Why the Brazil nuts are on top: size segregation of particulate matter by shaking. Phs. Rev. Lett., Vol. 58, No. 10, pp. 1038-1040.

Schöberl, F. (1979): Zur Frage der Gefälllsausbildung beim Selbststabilisierungs-prozess von erodierenden Flußstrecken. Diss. Institut für Konstruktiven Wasser- und Tunnelbau, Universität Innsbruck, Innsbruck, Austria.

Schöberl, F. (1981): Abpflasterungs- und Selbststabilisierungsvermögen erodierter Gerinne. Österreichische Wasserwirtschaft, Jg. 33, Heft 7/8, pp. 180-186.

Schöberl, F. (1992): Prediction methods for grain size distribution and armour layer stability. Proc., Int. Seminar on Grain Sorting, Ascona, Mitteilungen der Versuchsanstalt für Wasserbau, Hydrologie und Glaziologie, Nr. 117, ETH, Zürich, Switzerland, pp. 251-271.

Shields, A. (1936): Anwendung der Aehnlichkeitsmechanik und der Turbulenz Forschung auf die Geschiebebewegung. Mitteilungen der Preussische Versuchsanstalt für Wasserbau und Schiffbau, Berlin, Germany, No. 26.

Simon, A.; Thorne, C. R. (1996): Channel adjustment of an unstable coarse-grained stream: Opposing trends of boundary and critical shear stress, and the applicability of extremal hypotheses, Earth Surf Processes Landforms, 21, 155–180, 1996.

Smith R. D.; R. C. Sidle and P.E. Porter, (1993): "Effects of bedload transport of experimental removal of woody debris from a forest gravel-bed stream", Earth Surface Processes Landforms, 18, 455-468.

Southard J. (2006): An Introduction to Fluid Motions, Sediment Transport, and Current-generated Sedimentary Structures. MIT OpenCourseWare, http://ocw.mit.edu/courses/earth-atmospheric-and-planetary-sciences/

Strobl, Th.; Zunic, F. (2006): Wasserbau: Aktuelle Grundlagen - Neue Entwicklungen. Berlin u.a.: Springer, XVI, 604 p.

Sutherland, A.J. (1987): Static armour layers by selective erosion. Sediment Transport in Gravel-Bed Rivers. C.R. Thorne et al., Wiley, Chichester, pp. 243-60.

Suzuki, K.; Kato, K. (1991): Mobile bed armouring of bed surface in a steep slope river with gravel and sand mixture. Proc., Int. Workshop on Fluvial Hydraulics of Mountain Regions, Trento, Lecture Notes in Earth Sciences No. 37, Springer Verlag, Berlin, pp. 393–404.

Suzuki, K.; Hano, A. (1992): Grain size change of bed surface layer and sediment discharge of an equilibrium river bed. Proc., Int. Seminar on Grain Sorting, Ascona, Mitteilungen der Versuchsanstalt für Wasserbau, Hydrologie und Glaziologie, Nr. 117, ETH, Zürich, Switzerland.

Tait, S.J.; Willetts, B.B.; Maizels, J.K. (1992): Laboratory observations of bed armouring and changes in bedload composition. In: Billi, P.; Hey, R.D; Thorne, C.R;.Tacconi, P. (eds.), Dynamics of Gravel-bed Rivers, John Wiley & Sons., Chichester, pp. 205-225.

van Rijn, L.C. (1984): Sediment transport, Part II: Suspended load transport. Journal Hydraulic Engineering, ASCE, Vol. 110, No. 11, pp. 1613–1641.

Vanoni, V.A.; Brooks, N.H. (1957): Laboratory studies of the roughness and suspended load of alluvial streams. Sedimentation Laboratory, California Institute of Technology, Pasadena, California, U. S. A.

Venditti, J.G.; Dietrich W.E.; Nelson P.A.; Wydzga M.A.; Fadde J.; Sklar L. (2010): Mobilization of coarse surface layers in gravel bedded rivers by finer gravel bed load. Water Resources Research, AGU, Vol. 46, W07506, doi:10.1029/2009WR008329

Wathen, S. J.; Ferguson R. I.; Hoey T. B.; Werritty A. (1995): Unequal mobility of gravel and sand in weakly bimodal river sediments. Water Resources Research, AGU, Vol. 31, No. 8, pp. 2087–2096.

Whiting, P.J.; King, J.G. (2003): Surface particle sizes on armoured gravel streambeds: effects of supply and hydraulics. Earth Surf Processes Landforms, Vol. 28, No. 3, pp. 1459–1471.

Wilcock, P.R. (1988): Methods for estimating the critical shear stress of individual fractions in mixed-size sediment. Water Resources Research, AGU, Vol. 24, No. 7, pp. 1127-1135.

Wilcock P. R. (1992): Experimental investigation of the effect of mixture properties on transport dynamics. In: Billi, P.; Hey, R.D; Thorne, C.R;.Tacconi, P. (eds.), Dynamics of Gravel-bed Rivers, John Wiley & Sons., Chichester, pp. 109-139.

Wilcock, P.R. (1993): Critical shear stress of natural sediments. Journal Hydraulic Engineering, ASCE, Vol. 119, No. 4, pp. 491-505.

Wilcock, P.R. (1997): The components of fractional transport rate. Water Resources Research, AGU, Vol. 33, No. 1, pp. 247-258.

Wilcock P. R. (2004): Sediment Transport Seminar: Lecture notes. January 26-28, 2004, University of California at Berkeley, CA, USA. http://calm.geo.berkeley.edu/geomorph/wilcock/wilcock.html

Wilcock, P.R.; Crowe, J.C., (2003): Surface-based transport model for mixed-size sediment. Journal Hydraulic Engineering, ASCE, Vol. 129, No. 2, pp. 120–128.

Wilcock, P.R.; DeTemple B.T. (2005): Persistence of armor layers in gravel-bed streams, Geophys.Res. Lett., Vol. 32, L08402, 4 pp.

Wilcock, P.R.; Kenworthy S.T.; Crowe J.C. (2001): Experimental study of the transport of mixed sand and gravel. Water Resources Research, AGU, Vol. 37, No. 12, 3349– 3358.

Wilcock, P.R.; McArdell, B. W. (1993): Surface-based fractional transport rates: mobilization thresholds and partial transport of a sand-gravel sediment. Water Resources Research, AGU, Vol. 294, No. 4, pp. 1297–1312.

Wilcock, P.R.; McArdell, B. W. (1997): Partial transport of a sand/gravel sediment. Water Resources Research, AGU, Vol. 33, No. 1, pp. 235-245.

Wilcock, P.R.; Southard, J.B., (1988): Experimental study of incipient motion in mixed-size sediment. Water Resources Research, AGU, Vol. 24, No. 7, pp. 1137-1151.

Wilcock, P.R.; Southard, J.B., (1989): Bed-load transport of mixed-size sediment: fractional transport rates, bed forms, and the development of a coarse bed-surface layer. Water Resources Research, AGU, Vol. 25, No. 7, pp. 1629-1641.

Willi, W. (1966): Zur Frage der Sohlen erosion bei grossen Gefällen. Mitteilungen Versuchsanstalt für Wasserbau und Erdbau (VAWE), Nr. 68, E.T.H., Zürich, Switzerland.

Williams, G. P. (1970): Flume width and water depth effects in sediment transport experiments. U. S. Geological Survey, Professional Paper 562-H, 42 pp.

Wolman, M.G. (1953): A method of sampling coarse river bed material. Transactions of American Geophysical Union Vol. 35, No. 6, pp. 951-956.

Wong, M.; Parker, G. (2006): Reanalysis and correction of bed-load relation of Meyer-Peter and Müller using their own database. Journal Hydraulic Engineering, ASCE, 132, No. 11, pp. 1159–1168.

Wu, W.; Wang, S. S. Y.; Jia, Y. (2000): Nonuniform sediment transport in alluvial rivers. Journal Hydraulic Research, IAHR, Vol. 38, No. 6, pp. 427-434.

Yalin, M.S. (1992): River Mechanics. Pergamon Press, Oxford, 219 pp.

Yalin, M.S.; Karahan, E. (1979): Inception of sediment transport. Journal Hydraulics Division, ASCE, Vol. 105, No. 11, pp. 1433–1443.

Yalin, M. S; Scheuerlein, H. (1988): Friction factors in alluvial rivers. Berichte des Lehrstuhls und der Versuchsanstalt für Wasserbau und Wasserwirtschaft der Technischen Universität München, Band Nr. 59.

Yen, C.L.; Lee, K.T. (1995): Bed Topography and Sediment Sorting in Channel Bend with Un-steady Flow. Journal Hydraulic Engineering, ASCE, Vol. 121, No. 8, pp.591-599.

Zanke, U. (1977): Berechung der Sinkgeschwindigkeiten von sedimenten. Mitt. des Franzius-Instituts für Wasserbau, 46(243), Technical University Hannover, Hannover, Germany.

Appendix

The data set that was obtained during the experimental investigation is given in the present appendix. The transport rate values that are given herein were found after fitting power functions to the experimental data and do not correspond to the direct measurements.

The data set of Wilcock et al. (2001) was provided from the authors as an AGU electronic supplement in ftp://agu.org, directory "apend" (Username "anonymous", Password "guest").

Experimental run		A-1
Flume length	[m]	4
Water Discharge	[l/s]	70
Shear Stress	[Pa]	2,00

d_{50s}/d_{50o} [-]	Time [min]	q_{bi} [gr / s m]						F_i [%]						
		8 mm	4 mm	2 mm	1 mm	0,5 mm	0,2 mm	16 mm	8 mm	4 mm	2 mm	1 mm	0,5 mm	0,2 mm
1,0	0	2,5E-03	9,7E-03	6,7E-02	1,5E-01	2,9E-02	8,6E-03	1,0	33,7	14,4	14,4	17,4	10,7	9,5
1,1	37	2,5E-03	9,7E-03	6,7E-02	1,5E-01	2,9E-02	8,6E-03	1,3	33,4	14,2	13,2	16,1	9,8	8,7
1,2	182	1,3E-03	5,5E-03	4,0E-02	9,1E-02	1,9E-02	6,2E-03	1,5	33,8	14,3	13,8	16,2	9,7	6,6
1,3	367	5,8E-04	2,7E-03	2,1E-02	4,7E-02	1,2E-02	4,1E-03	1,8	36,1	15,1	14,6	15,7	9,8	5,9
1,4	515	3,5E-04	1,7E-03	1,4E-02	3,1E-02	8,9E-03	3,2E-03	1,4	37,9	15,7	14,9	14,7	9,7	4,9
1,5	624	2,4E-04	1,2E-03	1,1E-02	2,3E-02	7,2E-03	2,6E-03	1,7	39,4	16,2	14,9	13,9	9,4	4,7
1,6	790	1,8E-04	9,7E-04	8,6E-03	1,8E-02	6,1E-03	2,3E-03	1,9	39,2	17,2	14,2	12,9	9,8	3,9
1,7	1018	1,4E-04	7,8E-04	7,1E-03	1,5E-02	5,3E-03	2,0E-03	1,7	41,5	18,4	14,3	11,7	9,1	3,1
1,8	1235	1,1E-04	6,3E-04	5,9E-03	1,3E-02	4,6E-03	1,8E-03	2,4	42,1	19,1	14,1	11,2	9,1	2,7
1,9	1615	8,1E-05	4,7E-04	4,5E-03	9,6E-03	3,8E-03	1,5E-03	3,1	43,9	19,2	15,1	10,4	9,5	1,7
2,0	2345	4,7E-05	3,0E-04	3,0E-03	6,2E-03	2,7E-03	1,2E-03	3,3	46,3	19,5	12,8	12,2	8,4	2,1
2,1	2847	3,7E-05	2,4E-04	2,5E-03	5,1E-03	2,4E-03	1,0E-03	3,4	45,1	20,2	10,5	12,4	7,5	1,5

Experimental run			A-2
Flume length	[m]		4
Water Discharge	[l/s]		80
Shear Stress	[Pa]		2,29

d_{50s}/d_{50o} [-]	Time [min]	q_{bi} [gr / s m]						F_i [%]						
		8 mm	4 mm	2 mm	1 mm	0,5 mm	0,2 mm	16 mm	8 mm	4 mm	2 mm	1 mm	0,5 mm	0,2 mm
1,0	0	5,1E-03	1,8E-02	1,2E-01	2,6E-01	6,7E-02	1,9E-02	1,0	33,7	14,4	14,4	17,4	10,7	9,5
1,1	29	5,1E-03	1,8E-02	1,2E-01	2,6E-01	6,7E-02	1,9E-02	1,3	33,4	14,0	13,9	16,7	9,6	7,8
1,2	169	1,9E-03	6,6E-03	4,8E-02	1,0E-01	3,0E-02	9,5E-03	1,3	34,6	14,7	14,0	15,9	9,2	6,2
1,3	318	1,0E-03	3,5E-03	2,6E-02	5,6E-02	1,6E-02	5,6E-03	1,3	35,8	15,3	14,2	15,1	9,3	5,6
1,4	467	6,9E-04	2,4E-03	1,8E-02	3,9E-02	1,1E-02	4,1E-03	1,3	37,0	16,0	14,3	14,2	9,3	4,9
1,5	618	5,2E-04	1,8E-03	1,4E-02	2,9E-02	8,5E-03	3,2E-03	1,3	38,3	16,6	14,4	13,4	9,4	4,2
1,6	770	4,2E-04	1,4E-03	1,1E-02	2,4E-02	6,8E-03	2,6E-03	1,3	39,5	17,3	14,6	12,6	9,5	3,6
1,7	923	3,5E-04	1,2E-03	9,6E-03	2,0E-02	5,8E-03	2,4E-03	1,3	40,8	18,0	14,7	11,7	9,5	2,9
1,8	1153	2,9E-04	1,0E-03	8,0E-03	1,7E-02	6,5E-03	3,0E-03	1,7	43,2	18,5	14,6	11,2	9,5	2,3
1,9	1457	2,3E-04	7,7E-04	6,3E-03	1,3E-02	7,5E-03	3,8E-03	1,9	43,9	18,9	14,2	10,9	8,4	1,8
2,0	2197	1,5E-04	5,1E-04	4,3E-03	9,0E-03	9,5E-03	5,6E-03	2,7	44,2	18,4	12,3	11,8	7,9	1,9
2,1	2646	3,6E-05	1,2E-04	1,0E-03	2,1E-03	2,8E-03	1,7E-03	3,1	44,8	18,1	11,1	11,9	7,8	2,1

Experimental run		A-3
Flume length	[m]	4
Water Discharge	[l/s]	100
Shear Stress	[Pa]	3,05

d_{50s}/d_{50o} [-]	Time [min]	q_{bi} [gr / s m]						F_i [%]						
		8 mm	4 mm	2 mm	1 mm	0,5 mm	0,2 mm	16 mm	8 mm	4 mm	2 mm	1 mm	0,5 mm	0,2 mm
1,0	0	3,4E-02	9,9E-02	5,0E-01	7,4E-01	1,1E-01	4,6E-02	1,0	33,7	14,4	14,4	17,4	10,7	9,5
1,1	22	3,4E-02	9,9E-02	5,0E-01	7,4E-01	1,1E-01	4,6E-02	0,9	33,4	14,3	14,2	17,1	9,0	7,3
1,2	55	1,4E-02	4,6E-02	2,3E-01	3,6E-01	6,5E-02	2,6E-02	1,2	35,1	14,9	13,9	16,9	8,9	6,8
1,3	90	7,8E-03	2,4E-02	1,2E-01	1,9E-01	4,0E-02	1,8E-02	1,3	35,9	15,1	13,4	16,3	8,2	6,2
1,4	125	5,5E-03	1,6E-02	8,3E-02	1,3E-01	3,0E-02	1,4E-02	1,3	36,9	15,9	12,9	15,5	7,9	5,9
1,5	161	4,0E-03	1,1E-02	5,7E-02	9,4E-02	2,3E-02	1,1E-02	1,5	38,5	16,7	12,2	15,2	7,5	5,6
1,6	197	3,1E-03	8,7E-03	4,4E-02	7,3E-02	1,9E-02	9,7E-03	1,5	40,3	17,6	11,5	14,8	7,1	5,3
1,7	233	2,6E-03	7,1E-03	3,6E-02	6,0E-02	1,6E-02	8,6E-03	1,5	41,6	18,3	11,1	14,4	6,8	5,0
1,8	269	2,2E-03	5,8E-03	2,9E-02	5,0E-02	1,4E-02	7,7E-03	1,6	42,9	18,9	10,7	14,0	6,4	4,7
1,9	309	1,8E-03	4,9E-03	2,4E-02	4,2E-02	1,2E-02	6,9E-03	1,6	44,3	19,5	10,3	13,6	6,0	4,4
2,0	396	1,4E-03	3,5E-03	1,8E-02	3,1E-02	9,8E-03	5,7E-03	1,7	45,9	19,9	10,0	12,7	5,3	3,9
2,4	1465	2,9E-04	6,5E-04	3,2E-03	6,1E-03	2,8E-03	2,1E-03	2,4	53,5	19,5	9,6	9,3	3,1	2,6

Experimental run			A-4											
Flume length	[m]		4											
Water Discharge	[l/s]		120											
Shear Stress	[Pa]		3,24											

d_{50s}/d_{50o} [-]	Time [min]	q_{bi} [gr / s m]						F_i [%]						
		8 mm	4 mm	2 mm	1 mm	0,5 mm	0,2 mm	16 mm	8 mm	4 mm	2 mm	1 mm	0,5 mm	0,2 mm
1,0	0	8,0E-02	1,5E-01	4,0E-01	7,8E-01	2,5E-01	1,1E-01	1,0	33,7	14,4	14,4	17,4	10,7	9,5
1,2	39	8,0E-02	1,5E-01	4,0E-01	7,8E-01	2,5E-01	1,1E-01	1,4	34,5	13,6	13,4	17,8	8,7	6,0
1,3	57	5,3E-02	9,2E-02	3,4E-01	6,6E-01	2,1E-01	9,9E-02	2,6	37,5	13,5	13,3	18,2	8,5	5,5
1,4	71	3,9E-02	6,6E-02	2,5E-01	4,8E-01	1,7E-01	8,2E-02	2,9	38,7	13,4	13,0	18,4	8,3	5,1
1,5	76	3,6E-02	6,1E-02	2,3E-01	4,4E-01	1,6E-01	7,7E-02	2,9	40,0	13,8	12,5	17,8	8,3	4,9
1,6	81	3,3E-02	5,5E-02	2,1E-01	4,0E-01	1,4E-01	7,3E-02	2,9	41,3	14,1	11,9	17,1	8,2	4,6
1,8	86	3,1E-02	5,1E-02	1,9E-01	3,7E-01	1,4E-01	7,0E-02	2,8	42,5	14,5	11,4	16,4	8,1	4,3
1,9	90	2,8E-02	4,7E-02	1,8E-01	3,4E-01	1,3E-01	6,6E-02	2,8	43,7	14,8	10,8	15,8	8,0	4,1
2,0	95	2,7E-02	4,4E-02	1,6E-01	3,2E-01	1,2E-01	6,4E-02	2,8	44,9	15,2	10,3	15,1	8,0	3,8
2,2	120	2,1E-02	3,4E-02	1,3E-01	2,5E-01	9,8E-02	5,4E-02	2,7	47,3	15,8	9,3	13,9	7,8	3,4
2,4	1905	2,1E-02	3,4E-02	1,3E-01	2,5E-01	9,8E-02	5,4E-02	1,5	53,8	16,0	8,7	9,3	5,0	5,2

Experimental run		A-5
Flume length	[m]	4
Water Discharge	[l/s]	150
Shear Stress	[Pa]	3,44

d_{50s}/d_{50}		q_{bi} [gr / s m]						F_i [%]						
o [-]	Time [min]	8 mm	4 mm	2 mm	1 mm	0,5 mm	0,2 mm	16 mm	8 mm	4 mm	2 mm	1 mm	0,5 mm	0,2 mm
1,0	0	1,2E-01	2,5E-01	6,2E-01	1,0E+00	3,9E-01	2,4E-01	1,0	33,7	14,4	14,4	17,4	10,7	9,5
1,3	35	1,2E-01	2,5E-01	6,2E-01	1,0E+00	3,9E-01	2,4E-01	2,4	34,9	16,5	12,9	19	6,0	6,0
1,4	50	7,3E-02	1,4E-01	3,8E-01	6,5E-01	3,9E-01	2,4E-01	2,9	35,6	17,7	12,5	20	4,7	5,6
1,5	69	4,7E-02	9,1E-02	2,6E-01	4,5E-01	3,9E-01	2,4E-01	3,3	36,6	18,7	12,2	20,7	3,4	5,1
1,6	100	2,8E-02	5,2E-02	1,6E-01	2,9E-01	3,4E-01	2,2E-01	3,3	38,8	18,2	12,3	19,6	3,3	4,5
1,7	127	2,2E-02	4,0E-02	1,2E-01	2,3E-01	2,7E-01	1,9E-01	3,3	40,7	17,8	12,5	18,5	3,3	3,9
1,9	153	1,6E-02	2,8E-02	9,2E-02	1,8E-01	2,1E-01	1,5E-01	3,3	42,5	17,3	12,7	17,5	3,3	3,4
2,0	175	1,3E-02	2,4E-02	7,9E-02	1,6E-01	1,9E-01	1,4E-01	3,3	44,0	17/0	12,8	16,7	3,3	3,0
2,1	196	1,1E-02	2,0E-02	6,7E-02	1,3E-01	1,6E-01	1,2E-01	3,3	45,5	16,6	13,0	15,9	3,2	2,5
2,3	269	7,0E-03	1,2E-02	4,5E-02	9,3E-02	1,1E-01	9,2E-02	3,3	49,2	15,7	13,3	13,8	3,2	1,4
2,5	2388	2,2E-03	2,1E-03	6,2E-03	1,4E-02	2,5E-02	2,1E-02	2,4	58,8	16,8	8,8	9,5	2,4	1,2

Experimental run		B-1
Flume length	[m]	8
Water Discharge	[l/s]	70
Shear Stress	[Pa]	2,00

d_{50s}/d_{50o} [-]	Time [min]	q_{bi} [gr / s m]						F_i [%]						
		8 mm	4 mm	2 mm	1 mm	0,5 mm	0,2 mm	16 mm	8 mm	4 mm	2 mm	1 mm	0,5 mm	0,2 mm
1,0	0	4,0E-03	4,9E-03	5,4E-02	1,2E-01	2,0E-02	1,3E-02	1,0	33,7	14,4	14,4	17,4	10,7	9,5
1,1	178	4,0E-03	4,9E-03	5,4E-02	1,2E-01	2,0E-02	1,3E-02	1,2	33,9	14,2	13,9	15,9	9,5	8,7
1,2	453	1,4E-03	2,2E-03	2,5E-02	5,4E-02	1,3E-02	8,0E-03	2,4	36,4	13,5	16,4	16,3	10,9	6,1
1,3	692	7,6E-04	1,4E-03	1,6E-02	3,4E-02	1,1E-02	6,1E-03	2,8	35,7	14,7	15,7	15,1	11,0	4,3
1,4	915	5,0E-04	1,0E-03	1,1E-02	2,4E-02	8,9E-03	5,1E-03	2,9	36,7	14,6	16,1	13,4	11,1	3,4
1,5	1345	3,5E-04	7,7E-04	8,6E-03	1,9E-02	7,7E-03	4,3E-03	3,1	37,9	16,7	14,1	14,5	11,9	2,7
1,6	1928	2,0E-04	5,1E-04	5,7E-03	1,2E-02	6,2E-03	3,4E-03	2,7	39,4	16,5	13,1	13,8	11,7	2,4
1,7	2746	1,1E-04	3,1E-04	3,5E-03	7,5E-03	4,7E-03	2,5E-03	3,6	39,4	19,0	14,0	13,0	9,9	1,3
1,8	4459	3,6E-05	1,1E-04	1,2E-03	2,5E-03	1,6E-03	8,5E-04	3,1	41,2	19,6	13,7	13,1	7,8	1,3

Experimental run		B-2
Flume length	[m]	8
Water Discharge	[l/s]	80
Shear Stress	[Pa]	2,50

d_{50s}/d_{50o} [-]	Time [min]	q_{bi} [gr / s m]						F_i [%]						
		8 mm	4 mm	2 mm	1 mm	0,5 mm	0,2 mm	16 mm	8 mm	4 mm	2 mm	1 mm	0,5 mm	0,2 mm
1,0	0	3,0E-03	9,3E-03	5,8E-02	1,3E-01	6,3E-02	2,2E-02	1,0	33,7	14,4	14,4	17,4	10,7	9,5
1,1	154	3,0E-03	9,3E-03	5,8E-02	1,3E-01	6,3E-02	2,2E-02	1,3	33,9	14,9	14,2	16,9	9,9	8,4
1,2	399	9,2E-04	3,7E-03	3,9E-02	9,0E-02	2,6E-02	8,1E-03	1,2	34,7	14,7	14,1	15,5	10,1	5,5
1,3	641	2,7E-04	1,5E-03	2,6E-02	6,2E-02	1,5E-02	4,1E-03	1,1	37,1	15,2	14,1	15,1	10,6	4,5
1,4	877	2,3E-04	1,2E-03	2,0E-02	4,9E-02	1,9E-02	5,4E-03	1,0	38,6	15,7	14,2	14,4	11,2	3,6
1,5	1196	2,6E-04	1,0E-03	1,6E-02	3,9E-02	1,8E-02	6,3E-03	1,1	39,7	16,3	14,3	13,8	11,5	2,8
1,6	1752	3,1E-04	6,9E-04	1,1E-02	2,9E-02	1,6E-02	6,9E-03	1,9	40,1	17,3	14,2	13,3	11,3	2,0

Experimental run   B-3
Flume length [m]   8
Water Discharge [l/s]   100
Shear Stress [Pa]   2,75

d_{50s}/d_{50o} [-]	Time [min]	q_{bi} [gr / s m]						F_i [%]						
		8 mm	4 mm	2 mm	1 mm	0,5 mm	0,2 mm	16 mm	8 mm	4 mm	2 mm	1 mm	0,5 mm	0,2 mm
1,0	0	3,2E-02	5,2E-02	2,7E-01	5,6E-01	1,0E-01	3,3E-02	1,0	33,7	14,4	14,4	17,4	10,7	9,5
1,1	32	3,2E-02	5,2E-02	2,7E-01	5,6E-01	1,0E-01	3,3E-02	1,2	33,8	14,3	14,2	16,6	9,9	8,2
1,2	84	2,8E-02	5,2E-02	2,7E-01	5,6E-01	1,0E-01	3,3E-02	1,2	34,8	14,6	14,1	16,1	9,4	6,4
1,3	134	1,7E-02	3,7E-02	2,0E-01	4,2E-01	8,8E-02	3,1E-02	1,4	36,4	15,2	13,8	16,1	8,8	5,8
1,4	184	1,1E-02	2,4E-02	1,3E-01	2,9E-01	7,1E-02	2,8E-02	1,3	37,9	15,6	13,7	15,5	8,7	5,3
1,5	232	8,3E-03	1,8E-02	1,0E-01	2,2E-01	6,1E-02	2,6E-02	1,5	39,5	16,1	13,2	14,8	8,6	4,9
1,6	280	6,6E-03	1,4E-02	8,0E-02	1,7E-01	5,4E-02	2,5E-02	1,6	40,8	16,6	13,1	14,4	8,5	4,4
1,7	336	5,4E-03	1,1E-02	6,5E-02	1,4E-01	4,8E-02	2,4E-02	1,6	42,1	16,9	12,9	14	8,2	4,1
1,8	397	4,3E-03	9,0E-03	5,2E-02	1,2E-01	4,3E-02	2,3E-02	1,7	43,4	17,1	12,6	13,6	7,8	3,8
1,9	461	3,6E-03	7,5E-03	4,4E-02	9,8E-02	3,9E-02	2,2E-02	1,8	44,7	17,2	12,3	13,3	7,2	3,6
2,0	560	2,9E-03	5,9E-03	3,5E-02	7,8E-02	3,4E-02	2,1E-02	1,7	46,1	17,3	11,7	12,8	6,3	3,2
2,3	1739	4,5E-04	8,4E-04	5,5E-03	1,3E-02	1,3E-02	1,4E-02	2,3	50,7	18,2	10,7	11,0	4,5	2,6

		q_{bi} [gr / s m]						F_i [%]						
d_{50s}/d_{50o} [-]	Time [min]	8 mm	4 mm	2 mm	1 mm	0,5 mm	0,2 mm	16 mm	8 mm	4 mm	2 mm	1 mm	0,5 mm	0,2 mm
1,0	0	7,9E-02	1,8E-01	5,7E-01	6,9E-01	1,4E-01	5,6E-02	1,0	33,7	14,4	14,4	17,4	10,7	9,5
1,1	20	7,9E-02	1,8E-01	5,7E-01	6,9E-01	1,4E-01	5,6E-02	0,9	34,0	14,2	14	17,2	9,2	8,4
1,2	30	7,9E-02	1,8E-01	5,7E-01	6,9E-01	1,4E-01	5,6E-02	1,1	34,9	14,2	13,7	17	8,5	6,2
1,3	35	7,9E-02	1,8E-01	5,7E-01	6,9E-01	1,4E-01	5,6E-02	1,1	37,9	14,6	13,7	17,2	8,5	6,3
1,4	42	7,9E-02	1,8E-01	5,7E-01	6,9E-01	1,4E-01	5,6E-02	1,0	39,4	14,4	12,8	17,1	7,7	5,7
1,5	52	7,9E-02	1,8E-01	5,7E-01	6,9E-01	1,4E-01	5,6E-02	1,0	40,9	14,5	12,6	17,1	7,3	5,4
1,6	61	7,5E-02	1,8E-01	5,7E-01	6,9E-01	1,4E-01	5,6E-02	0,9	42,3	14,6	12,3	17,2	7,0	5,1
1,7	70	6,5E-02	1,6E-01	5,6E-01	6,9E-01	1,3E-01	5,5E-02	0,8	43,7	14,7	12,1	17,2	6,7	4,8
1,8	82	5,3E-02	1,3E-01	4,7E-01	5,9E-01	1,2E-01	5,0E-02	1,1	44,4	15,7	12	16,2	6,3	4,3
1,9	96	4,3E-02	1,1E-01	3,9E-01	5,1E-01	1,1E-01	4,5E-02	1,5	45,1	16,9	11,8	15,1	5,8	3,7
2,0	339	8,8E-03	2,1E-02	9,0E-02	1,6E-01	6,0E-02	2,5E-02	1,4	46,2	18,1	11,3	13,6	5,3	3,2
2,3	1725	1,1E-03	2,4E-03	1,3E-02	3,3E-02	5,7E-02	3,3E-02	1,4	52,1	18,0	9,1	10,7	4,4	3,8

Experimental run   B-4
Flume length   [m]   8
Water Discharge   [l/s]   120
Shear Stress   [Pa]   3,22

Experimental run			B-5
Flume length	[m]		8
Water Discharge	[l/s]		150
Shear Stress	[Pa]		3,48

d_{50s}/d_{50o} [-]	Time [min]	q_{bi} [gr / s m]						F_i [%]						
		8 mm	4 mm	2 mm	1 mm	0,5 mm	0,2 mm	16 mm	8 mm	4 mm	2 mm	1 mm	0,5 mm	0,2 mm
1,0	0	1,3E-01	3,0E-01	8,7E-01	1,4E+00	3,9E-01	1,4E-01	1,0	33,7	14,4	14,4	17,4	10,7	9,5
1,1	20	1,3E-01	3,0E-01	8,7E-01	1,4E+00	3,9E-01	1,4E-01	1,1	33,9	14,2	13,8	17	8,5	8,7
1,2	30	1,3E-01	3,0E-01	8,7E-01	1,4E+00	3,9E-01	1,4E-01	1,5	34,6	14,7	13,6	17,5	8,5	7,8
1,3	34	1,3E-01	3,0E-01	8,7E-01	1,4E+00	3,9E-01	1,4E-01	2,1	35,7	14,5	14,1	17,0	7,2	6,3
1,4	38	1,3E-01	3,0E-01	8,7E-01	1,4E+00	3,9E-01	1,4E-01	3,4	36,8	14,6	14,4	17,1	6,6	5,4
1,5	45	1,3E-01	3,0E-01	8,7E-01	1,4E+00	3,9E-01	1,3E-01	4,4	37,4	14,7	13,7	17,1	6,2	5,1
1,6	54	1,3E-01	2,9E-01	8,3E-01	1,4E+00	3,8E-01	1,2E-01	5,0	38,2	14,8	13,7	17,1	5,6	4,8
1,7	63	1,2E-01	2,5E-01	7,1E-01	1,2E+00	3,4E-01	1,1E-01	5,5	38,9	14,9	13,7	17,2	5,1	4,4
1,8	82	7,5E-02	1,5E-01	4,6E-01	8,1E-01	2,5E-01	9,1E-02	5,9	39,7	15,1	13,4	17	4,7	4,0
1,9	112	4,7E-02	9,5E-02	2,9E-01	5,4E-01	1,9E-01	7,7E-02	6,3	40,6	15,4	13,0	16,7	4,5	3,5
2,0	160	2,5E-02	4,9E-02	1,6E-01	3,2E-01	1,2E-01	6,2E-02	6,1	41,5	15,7	12,3	16,3	4,2	2,8
2,4	1310	5,3E-03	5,6E-03	1,6E-02	3,3E-02	1,9E-02	1,8E-02	5,7	50,3	17,1	10,2	12,4	3,0	1,4

Experimental run		C-1
Flume length	[m]	12
Water Discharge	[l/s]	70
Shear Stress	[Pa]	2,20

d_{50s}/d_{50o} [-]	Time [min]	q_{bi} [gr / s m]						F_i [%]						
		8 mm	4 mm	2 mm	1 mm	0,5 mm	0,2 mm	16 mm	8 mm	4 mm	2 mm	1 mm	0,5 mm	0,2 mm
1,0	0	6,5E-03	1,9E-02	4,8E-02	6,8E-02	1,6E-02	3,0E-03	1,0	33,7	14,4	14,4	17,4	10,7	9,5
1,1	292	6,5E-03	1,9E-02	4,8E-02	6,8E-02	1,6E-02	3,0E-03	1,2	32,8	15,7	14,2	16,0	10,2	7,8
1,2	832	1,7E-03	7,9E-03	2,2E-02	3,1E-02	8,3E-03	1,8E-03	1,5	33,3	14,8	12,3	15,7	12,2	7,2
1,3	1435	9,1E-04	5,2E-03	1,5E-02	2,1E-02	5,9E-03	1,4E-03	1,9	35,0	16,0	16,1	16,3	9,7	4,2
1,4	1926	5,2E-04	3,7E-03	1,0E-02	1,5E-02	4,5E-03	1,1E-03	1,8	36,2	17,4	15,2	15,2	10,9	3,4
1,5	2709	3,4E-04	2,8E-03	8,1E-03	1,2E-02	3,7E-03	9,7E-04	1,4	39,8	16,9	13,8	16,7	8,0	3,7
1,6	3587	2,6E-04	2,3E-03	6,8E-03	1,0E-02	3,1E-03	8,7E-04	1,6	43,4	19,7	15,5	17,2	8,9	2,7
1,7	4564	2,0E-04	1,9E-03	5,7E-03	8,4E-03	2,7E-03	7,7E-04	1,7	42,0	21,0	12,2	16,9	6,7	2,5
1,8	5335	1,4E-04	1,6E-03	4,6E-03	6,9E-03	2,3E-03	6,8E-04	1,6	44,3	21,8	13,5	15,4	5,4	2,5
1,9	6104	1,0E-04	1,3E-03	3,9E-03	5,9E-03	2,0E-03	6,2E-04	1,9	42,4	21,1	11,2	14,1	4,4	2,9
2,0	6978	8,5E-05	1,2E-03	3,5E-03	5,2E-03	1,8E-03	5,7E-04	2,1	47,3	23,2	11,7	15,1	3,9	2,6
2,1	8058	6,6E-05	9,8E-04	3,0E-03	4,5E-03	1,6E-03	5,2E-04	2,4	48,1	24,3	10,2	14,3	2,1	2,5

		q_{bi} [gr / s m]						F_i [%]						

Experimental run   C-2
Flume length [m] 12
Water Discharge [l/s] 80
Shear Stress [Pa] 2,32

d_{50s}/d_{50o} [-]	Time [min]	8 mm	4 mm	2 mm	1 mm	0,5 mm	0,2 mm	16 mm	8 mm	4 mm	2 mm	1 mm	0,5 mm	0,2 mm
1,0	0	6,8E-03	2,3E-02	1,2E-01	1,7E-01	1,7E-02	6,9E-03	1,0	33,7	14,4	14,4	17,4	10,7	9,5
1,1	270	6,8E-03	2,3E-02	1,2E-01	1,7E-01	1,7E-02	6,9E-03	1,2	33,7	14,4	14,2	17,1	9,6	7,8
1,2	717	1,6E-03	7,6E-03	3,6E-02	5,7E-02	9,3E-03	3,2E-03	1,7	34,5	15,2	14,7	16,2	10,3	5,5
1,3	1201	7,0E-04	4,5E-03	2,0E-02	3,3E-02	6,8E-03	2,2E-03	1,8	35,6	16,0	15	15,8	10,8	4,5
1,4	1758	3,5E-04	2,8E-03	1,2E-02	2,1E-02	5,3E-03	1,6E-03	1,7	37,1	16,7	14,7	15,9	10,3	3,6
1,5	2354	2,0E-04	2,0E-03	8,4E-03	1,5E-02	4,4E-03	1,2E-03	1,4	38,7	17,5	14,1	16,0	9,5	2,7
1,6	3069	1,5E-04	1,6E-03	6,5E-03	1,2E-02	3,8E-03	1,0E-03	1,3	40,2	18,2	13,5	16,0	8,5	2,2
1,7	3939	1,2E-04	1,3E-03	5,1E-03	9,3E-03	3,3E-03	8,7E-04	1,5	41,5	19,0	12,9	15,5	7,3	2,3
1,8	4810	8,8E-05	9,4E-04	3,6E-03	6,9E-03	2,8E-03	7,1E-04	1,7	42,7	19,8	12,3	15,1	6,1	2,3
1,9	5720	8,5E-05	7,5E-04	2,9E-03	5,5E-03	2,5E-03	6,1E-04	1,9	43,9	20,6	11,7	14,6	4,9	2,4
2,0	6658	9,0E-05	6,4E-04	2,4E-03	4,6E-03	2,3E-03	5,4E-04	2,2	45,2	21,5	11,0	14,1	3,6	2,5
2,1	7986	9,6E-05	5,2E-04	1,9E-03	3,8E-03	2,0E-03	4,7E-04	2,3	46,0	22,0	10,6	13,8	2,8	2,5

Experimental run		C-3
Flume length	[m]	12
Water Discharge	[l/s]	100
Shear Stress	[Pa]	3,09

d_{50s}/d_{50o} [-]	Time [min]	q_{bi} [gr / s m]						F_i [%]						
		8 mm	4 mm	2 mm	1 mm	0,5 mm	0,2 mm	16 mm	8 mm	4 mm	2 mm	1 mm	0,5 mm	0,2 mm
1,0	0	5,0E-02	6,9E-02	4,3E-01	5,5E-01	1,4E-01	2,7E-02	1,0	33,7	14,4	14,4	17,4	10,7	9,5
1,1	60	5,0E-02	6,9E-02	4,3E-01	5,5E-01	1,4E-01	2,7E-02	1,4	34,0	14,2	14,1	16,4	9,7	8,4
1,2	157	2,9E-02	4,8E-02	3,1E-01	4,4E-01	1,2E-01	2,5E-02	1,5	35,3	14,6	14,4	15,8	10,6	5,3
1,3	251	1,1E-02	2,5E-02	1,6E-01	2,4E-01	7,8E-02	2,0E-02	1,6	36,6	15,0	14,8	15,1	11,5	4,2
1,4	324	6,5E-03	1,8E-02	1,2E-01	1,8E-01	6,2E-02	1,7E-02	1,8	37,9	15,4	14,8	14,5	11,8	3,6
1,5	374	4,8E-03	1,4E-02	9,5E-02	1,5E-01	5,4E-02	1,6E-02	1,9	39,2	15,7	14,5	14,1	11,3	3,3
1,6	420	3,6E-03	1,2E-02	8,0E-02	1,3E-01	4,8E-02	1,5E-02	2,1	40,4	16,0	14,1	13,6	10,7	3,1
1,7	461	3,0E-03	1,1E-02	7,1E-02	1,2E-01	4,5E-02	1,5E-02	2,3	41,6	16,2	13,7	13,2	10,1	2,9
1,8	501	2,4E-03	9,3E-03	6,2E-02	1,0E-01	4,1E-02	1,4E-02	2,5	42,8	16,5	13,2	12,8	9,4	2,8
1,9	539	2,1E-03	8,5E-03	5,7E-02	9,6E-02	3,8E-02	1,4E-02	2,7	43,9	16,7	12,8	12,4	8,8	2,7
2,0	600	1,7E-03	7,2E-03	4,9E-02	8,3E-02	3,4E-02	1,3E-02	2,4	45,1	17,1	12,2	11,7	7,8	2,5
2,3	1753	4,8E-04	1,6E-03	9,2E-03	1,4E-02	8,7E-03	6,4E-03	2,9	52,1	18,3	11,1	8,9	4,6	2,1

Experimental run			C-4
Flume length	[m]		12
Water Discharge	[l/s]		120
Shear Stress	[Pa]		2,91

d_{50s}/d_{50o} [-]	Time [min]	q_{bi} [gr / s m]						F_i [%]						
		8 mm	4 mm	2 mm	1 mm	0,5 mm	0,2 mm	16 mm	8 mm	4 mm	2 mm	1 mm	0,5 mm	0,2 mm
1,0	0	2,8E-02	5,4E-02	3,1E-01	4,9E-01	9,3E-02	4,3E-02	1,0	33,7	14,4	14,4	17,4	10,7	9,5
1,1	20	2,8E-02	5,4E-02	3,1E-01	4,9E-01	9,3E-02	4,3E-02	1,3	34,1	13,9	13,8	18,0	9,2	7,3
1,2	31	2,8E-02	5,4E-02	3,1E-01	4,9E-01	9,3E-02	4,3E-02	1,3	35,4	13,9	13,8	18,7	7,5	6,0
1,3	49	2,8E-02	5,4E-02	3,1E-01	4,9E-01	9,3E-02	4,3E-02	1,3	37,9	13,9	13,8	19,7	6,6	5,4
1,4	65	2,8E-02	5,4E-02	3,1E-01	4,9E-01	9,3E-02	4,3E-02	1,3	39,4	13,9	13,8	20,6	5,7	4,9
1,5	78	2,8E-02	5,4E-02	3,1E-01	4,9E-01	9,3E-02	4,3E-02	1,5	40,5	14,2	12,8	20,6	5,9	4,6
1,6	91	2,8E-02	5,4E-02	3,1E-01	4,9E-01	9,3E-02	4,3E-02	1,9	41,3	14,8	11,2	20,0	6,7	4,2
1,7	114	2,4E-02	4,8E-02	2,8E-01	4,5E-01	8,8E-02	3,7E-02	2,2	42,1	15,3	9,7	19,4	7,4	3,9
1,8	234	1,1E-02	2,3E-02	1,3E-01	2,3E-01	5,8E-02	1,3E-02	2,4	43,1	15,8	8,7	18,7	7,6	3,6
1,9	485	4,7E-03	1,1E-02	6,4E-02	1,2E-01	3,8E-02	1,3E-02	2,3	44,3	16,1	8,7	17,8	7,3	3,4
2,0	879	2,4E-03	5,8E-03	3,5E-02	7,1E-02	2,7E-02	1,2E-02	2,1	45,7	16,7	8,6	16,4	6,8	2,9
2,3	1945	1,0E-03	2,6E-03	1,6E-02	3,5E-02	1,7E-02	1,1E-02	2,0	51,3	18,1	8,3	12,7	5,3	1,8

Experimental run		C-5
Flume length	[m]	12
Water Discharge	[l/s]	150
Shear Stress	[Pa]	3,40

d_{50s}/d_{50o} [-]	Time [min]	q_{bi} [gr / s m]						F_i [%]						
		8 mm	4 mm	2 mm	1 mm	0,5 mm	0,2 mm	16 mm	8 mm	4 mm	2 mm	1 mm	0,5 mm	0,2 mm
1,0	0	1,3E-01	1,7E-01	6,1E-01	1,1E+00	3,4E-01	1,0E-01	1,0	33,7	14,4	14,4	17,4	10,7	9,5
1,1	25	1,3E-01	1,7E-01	6,1E-01	1,1E+00	3,4E-01	1,0E-01	1,1	34,9	12,7	14,1	18,5	8,7	6,2
1,2	59	1,3E-01	1,7E-01	6,1E-01	1,1E+00	3,4E-01	1,0E-01	0,7	39,2	11,1	14,4	20,9	8,1	5,2
1,3	76	9,2E-02	1,3E-01	5,6E-01	1,0E+00	3,3E-01	1,0E-01	0,8	40,4	11,2	14,3	20,8	7,7	4,8
1,4	90	7,0E-02	9,9E-02	4,6E-01	8,6E-01	3,0E-01	9,9E-02	1,1	41,0	11,8	14,1	20,0	7,4	4,6
1,5	105	5,7E-02	7,9E-02	3,9E-01	7,5E-01	2,7E-01	9,4E-02	1,3	41,7	12,4	13,9	19,3	7,1	4,3
1,6	120	4,8E-02	6,7E-02	3,5E-01	6,7E-01	2,5E-01	8,9E-02	1,6	42,4	13	13,6	18,5	6,8	4,0
1,7	136	4,0E-02	5,4E-02	3,0E-01	5,9E-01	2,3E-01	8,5E-02	1,9	43,0	13,7	13,4	17,7	6,5	3,8
1,8	152	3,2E-02	4,2E-02	2,5E-01	5,1E-01	2,2E-01	8,1E-02	2,2	43,7	14,3	13,2	16,9	6,2	3,5
1,9	169	2,9E-02	3,9E-02	2,3E-01	4,6E-01	2,1E-01	7,8E-02	2,5	44,5	15,0	12,9	16,0	5,9	3,2
2,0	196	2,4E-02	3,4E-02	1,9E-01	3,9E-01	1,9E-01	7,3E-02	2,4	45,3	16,2	12,5	14,6	5,3	2,7
2,5	2401	4,6E-03	4,6E-03	1,9E-02	4,8E-02	5,5E-02	3,3E-02	2,5	56,7	17,3	8,5	9,7	3,2	2,0

List of figures

278

List of tables

List of symbols

Latin symbols

a	[mm]	Longest axis of the particle
a	[-]	Constant that takes a value near unity (estimation of grain settling velocity Dittrich 1982)
A_b	[m^2]	Wetted area associated with the bed
a_i	[-]	Parameter for the calculation of fractional reference shear stress τ_{ri}
A_m	[m^2]	Wetted area associated with the whole cross-section
$a_{n\,i\,(n\,=\,1\text{-}4)}$		Parameters that regulate the variation of τ_{ri}/τ_{r50s} with d_i/d_s according to the value of relative grain size d_i/d_{50o}. Their value varies with sand content of parent bed material
A_s	[m^2]	Sampling area
A_w	[m^2]	Wetted area associated with the wall
B	[mm]	Intermediate axis of the particle eq. 5.10
b	[-]	Parameter for determining the variation of τ_{ri} with relative grain size d_i/d_{s50} (exponent in wilcock & Crowe hiding function)
b_i	[-]	Parameter for the calculation of fractional reference shear stress τ_{ri}
$b_{n\,i\,(n\,=\,1\text{-}4)}$	[-]	Parameters that regulate the variation of τ_{ri}/τ_{r50s} with d_i/d_s according to the value of relative grain size d_i/d_{50o}. Their value varies with sand content of parent bed material
c	[mm]	Shortest axis of the particle
C	[-]	Constant found by integrating Eq. 5.25
c_1	[-]	Function of b (degree of coarsening) and the ratio $\tau^*_{r50s,d50s/d50o=1}/\tau^*_{r50s,d50s/d50o=b}$
c_2	[-]	Function of b, the ratio $\tau^*_{r50s,d50s/d50o=1}/\tau^*_{r50s,d50s/d50o=b}$ and the ratio a_1/a_2 which in turn depends on absolute grain size d_i.
C_1	[-]	Constant, which is function of the angle of repose of the granular material for calculation of Coulomb resistance force
C_2	[-]	Constant for calculation of lift force
C_3	[-]	Constant, which is a function of boundary Reynolds number for calculation of drag force
CSF	[-]	Corey shape factor
d	[mm]	Grain size of bed material
D	[m]	Square sieve opening
D_*	[-]	Dimensionless grain size
d_{50s}	[mm]	Median grain size of the armor layer
d_{50o}	[mm]	Median grain of parent bed material
$d_{50s(max)}$	[mm]	d_{50} of the coarsest armor layer that can be developed by a given sediment mixture (when the exerted shear stress by the flow reaches a certain upper limit value)
d_i	[mm]	Mean grain size of ith grain class

d_g	[mm]	Geometric mean size
d_m	[mm]	Mean size of grains belonging to the sediment mixture
d_{max}	[mm]	Coarsest grain size contained in the parent bed material and at the same time in the armor layer
d_{ms}	[mm]	Arithmetic mean grain size of the armor layer
d_{mo}	[mm]	Median grain size of parent bed material
$d_{ms(max)}$	[mm]	Geometric mean grain size of the coarsest grain size that the parent bed material can develop
D_s	[mm]	Wax penetration depth
d_u	[mm]	Scaling grain size (profit Sutherland transport model)
d_{90*}	[-]	Dimensionless parameter
d_{sg}	[mm]	Geometric mean size of the bed material in the bed surface
$E_V[\overline{D}_i]$	[mm]	Arithmetic mean diameter of the volumetric sample
$E_A\left[\overline{D}_i^{-1}\right]$	[mm]	Arithmetic mean diameter of the areal sample
f		Denotes a functional relation
f_1		Denotes a functional relation
f_b	[-]	Darcy-Weisbach friction factor for the bed sub-area
F_D	[N]	Drag force
F_d	[-]	Froude number when calculated with use of the maximum flow velocity for the steepest possible slope
F_G	[N]	Submerged weight
f_i	[-]	Fractional content of ith grain class
F_i	[-]	Content of ith grain class in bed surface material
F_L	[N]	Lift force
f_m	[-]	Darcy-Weisbach friction factor for the whole cross section
F_R	[N]	Coulomb resistance force
F_s	[-]	Sand content on bed surface
f_{so}	[-]	Sand content of parent bed material
f_w	[-]	Darcy-Weisbach friction factor for the wall sub-area
G		Denotes functional relation
g	[m/s^2]	Gravitational acceleration (g = 9,81 m/s^2)
g_b	[Kg/s/m]	Total weight transport rate per unit width
$q^*_{bdms,i}$	[-]	Fractional dimensionless bed-load transport rate related to mean grain size of bed surface
g^*_{bi}	[-]	Dimensionless weight transport rate per unit width
g_o		Denotes hiding function
h	[m]	Depth of flow
J	[-]	Energy slope
m	[-]	Exponent that adjusts variation of mobility with increase in shear stress

M_o	[Nm]	Overturning moment due to to F_D and F_{Rx}, when a grain is in a state of incipient motion
M_R	[Nm]	Resisting moment due to F_L and F_G, when a grain is in a state of incipient motion
N	[-]	Number of grain-size fractions
P	[-]	Powers value of roundness
p_b	[m]	Wetted perimeter associated with the bed
p_i	[-]	Content of ith grain class in transported material
$p_{in}(i)$	[-]	Fractional content of ith grain class in the mixture entering the system
$p_{out}(i)$	[-]	Fractional content of ith grain class in the mixture leaving the system
$P_{d50s(max)}$	[-]	Relative weight of the distribution corresponding to the d_{50} of the armor layer at the limiting shear stress condition $d_{50s(max)}$
p_m	[m]	Wetted perimeter associated with the whole cross-section
p_w	[m]	Wetted perimeter associated with the wall
$p(V\text{-}W)_i$	[-]	Percentage of ith fraction obtained from volume-by-weight
$p(A\text{-}W)_i$	[-]	Percentage of ith fraction obtained from area-by-weight
$p_i^{a\text{-}w}$	[-]	Fraction of the ith fraction in the area-by-weight distribution
$p_{i,0}$	[-]	Fraction of the ith fraction in the volume-by-weight distribution
$p_{v,0}$	[-]	Porosity
$p_i^{s\text{-}a}$	[-]	Percentage of ith fraction in surface by area frequency distribution
$p_{i,0}$	[-]	Percentage of total volume occupied by particles of the ith fraction
$p_{i,\infty}$	[-]	Porosity
q_b	[m³/s/m]	Bed-load transport rate
q_b^*	[-]	Dimensionless bed-load transport rate or Einstein transport parameter
q_{bi}	[m³/s/m]	Fractional volumetric bed-load transport per unit width
q_{bi}^*	[-]	Dimensionless bed-load transport rate per unit width per unit fraction content
$q_{b\ in}$	[m³/s/m]	Bed-load discharge entering the system
$q_{b\ out}$	[m³/s/m]	Bed-load discharge leaving the system
$q_{bi\ in}$	[m³/s/m]	Bed-load discharge of ith grain class entering the system
$q_{bi\ out}$	[m³/s/m]	Bed-load discharge of ith grain class leaving the system
q_{bT}	[m³/s/m]	Total bed-load discharge per unit width
R_1	[-]	Parameter accounting for the effect of grain size and density
R_2	[-]	Parameter accounting for the effect of grain shape
R_3	[-]	Parameter accounting for the effect of grain roundness
Re^*	[-]	Boundary Reynolds number related to grain size d
Re_i^*	[-]	Particle Reynolds number corresponding to i^{th} grain class
Re_m	[-]	Reynolds number for the whole cross-section

Re_w	[-]	Reynolds number for the wall sub-area
r_h	[m]	Hydraulic radius
r_{hb}	[m]	Bed hydraulic radius
r_{hm}	[m]	Whole cross-section hydraulic radius
r_{hw}	[m]	Wall hydraulic radius
s	[-]	Ratio of sediment to water density, submerged specific gravity of sediment
S	[-]	Limiting slope eq. 3.6 Schoeberl method
t	[min]	Time
u_*	[m/s]	Shear velocity
v	[m²/s]	Kinematic viscosity of the fluid ($v = 1{,}16 \ 10^{-6}$ m²/s)
v_m	[m/s]	Velocity in the whole cross section
v_w	[m/s]	Velocity in the wall sub-area
w_*	[-]	Dimensionless grain settling velocity
W^*_i	[-]	Einstein bed-load parameter, i.e. the dimensionless volumetric transport rate per unit width
W^*r	[-]	Reference value of dimensionless transport rate
W_i		Weight of the ith fraction in the areal sample
w_s	[m/s]	Grain settling velocity
W_{tot}	[N]	Total weight of the areal sample
x	[m]	Distance from the flume inlet

Greek symbols

α	[-]	Parameter that is incorporated in the hiding function of Hunziker
$α_g$	[-]	Parameter determined by the grain size distribution of parent bed material used to describe the shape of the grading curve
$γ_s$	[KN/m³]	Specific weight of the sediment
$γ_w$	[KN/m³]	Specific weight of water ($γ_w = 10$ KN/m³)
δ	[-]	Kronecker operator (it is assumed that Di>Dj when j>i)
ε	[-]	Relative roughness number
$ε_i$		Exposure correction of fractional Shields stress
μ	[Kg/ms]	Viscosity of the fluid
ρ	[Kg/m³]	Fluid density ($ρ = 1000$ Kg/m³)
$ρ_s$	[Kg/m³]	Sediment density ($ρ_s = 2650$ Kg/m³)
τ	[N/m²]	Exerted average boundary shear stress
$τ_c$	[N/m²]	Critical shear stress for entrainment of grain

τ_{ci}	[N/m^2]	Critical shear stress of particle with size d$_i$
τ_{cm}	[N/m^2]	Critical shear stress of particle with size d$_m$
τ_{ri}	[N/m^2]	Reference shear stress related to ith grain class
τ_{r50s}	[N/m^2]	Reference shear stress related to d$_{50}$ of bed surface material
τ^*	[-]	Dimensionless shear stress or Shields parameter
τ^*_c	[-]	Dimensionless critical shear stress
τ^*_{ci}	[-]	Dimensionless critical shear stress related to grain size d$_i$
τ^*_{ce}	[-]	Critical dimensionless shear stress for incipient motion for uniform bed material
τ^*_{cm}	[-]	Dimensionless critical shear stress related to geometrical mean grain size d$_m$
τ^*_i	[-]	Dimensionless shear stress (Shields stress) related to ith grain class
τ^*_{mo}	[-]	Dimensionless shear stress related to mean size of substrate
τ^*_{50s}	[-]	Dimensionless shear stress related to d50 of bed surface material
τ^*_{ri}	[-]	Dimensionless reference shear stress of ith grain class
τ^*_{r50s}	[-]	Dimensionless reference shear stress related to d$_{50}$ of bed surface material
τ'^*_{ms}	[-]	Corrected for side wall effects and bedform drag dimensionless shear stress related to mean grain size of bed surface
σ_g	[-]	Geometric standard deviation of sediment mixture grain sizes
σ_φ	[-]	Standard deviation of the surface material on the φ-scale
$\sigma_{\varphi0}$		Functional relation of the form $\sigma_{\varphi0} = \sigma_{\varphi0}(\varphi_{sg0})$ which is defined in fig.4.8
φ	[^{o}]	Angle of repose of the granular material
φ_i		Hiding correction (Hunziker model)
φ_i	[-]	Fractional excess shear stress
φ_{sg0}	[-]	Normalized dimensionless shear stress referred to d$_{sg}$ of bed surface, expresses the intensity of the flow
ω		Straining function for adaptation to mixtures of arbitrary composition
ω_0		Functional relation of the form $\omega_0 = \omega_0(\varphi_{sg0})$ which is defined in fig.4.8